A STUDY OF THE EFFECT OF ADDITIONAL RADICALS ON IGNITION AND FLAME PROPAGATION

by

JOHN ERNEST ORRIN, B.Sc.

July 1980

A thesis submitted for the degree of Doctor of Philosophy of the University of London, and for the Diploma of Imperial College

Department of Chemical Engineering
and Chemical Technology
Imperial College of Science and Technology
London S.W.7.

ABSTRACT

The importance of injected radicals in facilitating ignition and increasing flame propagation rates in lean methane-air mixtures is studied. Limits of ignitability and burning velocities are recorded using time-resolved schlieren and C_2 emission spectroscopy following the injection of high velocity jets of specific radicals from a plasma plug igniter. The primary objective is to design ignition plugs for successful combustion of very lean mixtures in internal combustion engines.

Major contributions to the improvements in flame characteristics are found from both chemical and fluid dynamic properties of the jet. Either effect can be fostered by changes in plug geometry and plasma medium as found by the use of hydrogen, nitrogen and argon plasma feedstocks. The results show that hydrogen plasmas are more effective in igniting lean methane-air mixtures than nitrogen plasmas which in turn are more effective than argon plasmas.

A fine line resonance absorption technique for the hydroxyl radical was developed to monitor the chemical effects. These are most prominent with plasmas containing H atoms where high levels of chemical reactivity enable sub-limit mixtures to be ignited and burnt, lead to rapid transition from an expanding plasma plume to a propagating flame and give rise to considerably increased burning velocities. Measured hydroxyl concentrations for these flames are higher than for less reactive plasmas and the flame structure appears to be modified. This is similar to that predicted by detailed computations on simulated hydrogen plasma jet ignition.

The fluid mechanics determines jet penetration and the initial (convoluted) flame surface area which for plasmas of low chemical reactivity (nitrogen and argon) lead to high turbulent burning velocities. The two effects - chemical and fluid dynamic - are complementary since flame convolutions tend to laminarise at a rate which increases with laminar burning velocity and hence chemical reactivity of the initial plasma.

ACKNOWLEDGEMENTS

I acknowledge with gratitude the encouragement and guidance given by Professor F. J. Weinberg throughout this work and for the help and time spent by Dr. I. M. Vince in the many constructive discussions. I would also like to thank Professor A. G. Gaydon, FRS, and Dr. M. C. Carabine for their advice on the spectroscopic and chemical kinetic sections of the thesis.

My thanks are also due to the Departmental technical staff, in particular Mr. C. Smith and Mr. K. Grose (glassblowers); Mr. M. Dix and Mr. D. Wood (electronic workshop), and Mr. I. Drummond (analytical services).

I am grateful to Mrs. T. Wright for typing the manuscript and Mr. B. Stallard for tracing the diagrams.

Last but not least, I would like to thank the Science Research Council for financing me and to my parents and Mr. and Mrs. D. Branch for their continued interest and support throughout this work.

I N D E X

		Page
CHAPTER 1	INTRODUCTION	
1.1	The Practical Objectives.	15
1.2	The Approach to these Objectives.	19
	(a) The Generation of Radicals "In Situ" within a Flame.	21
	(b) The Generation followed by the Injection of Radicals.	21
CHAPTER 2	THE PRODUCTION AND DETECTION OF ATOMS AND RADICALS	
2.1	Methods for Producing Atoms and Radicals.	23
	(a) Thermal Methods:	23
	(1) Shock Tubes.	24
	(2) Heated Filaments.	27
	(b) Photochemical Methods:	28
	(1) Flash Photolysis.	28
	(2) Indirect Photolysis.	29
	(3) Direct Photolysis.	29
	(c) Electrical Discharge Methods:	32
	(1) Low Frequency Discharge.	33
	(2) Intermittent Capacitive Discharge.	35
	(3) High Frequency Discharge.	36
	(4) The Mechanism of Dissociation by an Electric Discharge.	37
	(5) Generation of Radicals "In Situ" within a Flame by an Electrical Discharge or Electrical Field.	38

Index (Continued)

		Page
CHAPTER 2 (Contd.)		
2.2	The Decay of Atom and Radical Concentrations following Injection into the Unburnt Gases.	39
	(a) Calculation of Hydrogen Atom Decay.	39
2.3	Methods of Detection and Measurement of Atoms and Radicals in the Gas Phase.	41
	(a) Probe Methods.	42
	(b) Spectroscopic Methods.	42
CHAPTER 3	PRELIMINARY EXPERIMENTS ON RADICAL GENERATION AND MEASUREMENT	
3.1	The Use of Heated Tungsten for Producing Hydrogen Atoms.	44
3.2	The Use of Electric Fields.	46
3.3	High Frequency Discharges.	48
3.4	The Use of Calorimetric Methods for the Detection of Hydrogen Atoms.	48
3.5	The Use of Mass Spectrometry.	49
CHAPTER 4	THE DEVELOPMENT OF THE OH RESONANCE ABSORPTION TECHNIQUE	
4.1	Reasons for the Use of the OH Radical.	53
4.2	The Theory of Absorption Spectroscopy.	56
4.3	The Method.	68
4.4	Experimental:	68
	(a) The Optics.	70
	(b) The Burners.	70
	(c) The Light Source.	71
	(1) The Hollow Cathode Lamp.	72
	The Mechanism of Excitation in a Hollow Cathode.	73

Index (Continued) Page

CHAPTER 4 (Contd)

(d) Signal Processing. 74

4.5 Results and Conclusions. 75

(a) Selection of the Hollow Cathode Lamp. 75

(b) The Spectra. 80

(c) The Calibration Curves. 82

CHAPTER 5 THE APPARATUS FOR PLASMA JET IGNITION STUDIES

5.1 The Combustion Vessel. 83

5.2 The Plasma Jet Spark Plug. 89

5.3 The Plasma Jet Ignition Circuit. 91

5.4 Laser Schlieren/Shadowgraphy System. 94

5.5 High Speed Cinephotography. 96

5.6 Operation. 96

CHAPTER 6 THE APPLICATION OF THE SPECTROSCOPIC TECHNIQUES TO PLASMA JET IGNITION STUDIES

6.1 The OH Resonance Absorption Technique. 99

(a) Experimental: 99

(1) The Optics. 99

(2) The Signal Processing. 102

(b) Limitations and Errors in the Method. 103

6.2 The C_2 Emission Method. 104

(a) The Theory. 105

(b) Experimental. 107

(c) The Calibration. 109

(d) Limitations and Errors in the Method. 112

CHAPTER 7 PLASMA JET IGNITION - AN EXAMINATION OF THE MECHANISMS

7.1 Effects due to Adiabatic Compression. 114

Index (Continued) Page

CHAPTER 7 (Contd)

7.2 Effects of Long-Range Ultraviolet Radiation. 115

7.3 The Fluid Dynamic Properties of the Plasma Jet. 118

(a) Results and Discussion. 119

(1) Plasma Jet Discharging into Air. 119

(2) Plasma Jet Igniting a Methane-Air mixture. 127

(3) Summary. 128

7.4 Conclusions on the Contributory Mechanisms. 131

CHAPTER 8 THE INCENDIVITY OF THE PLASMA JET

8.1 Experimental. 133

8.2 Results. 134

(a) Variation of Incendivity with Applied Energy. 134

(1) Nitrogen and Argon Plasmas. 139

(2) Hydrogen Plasmas. 139

(b) Variation of Incendivity with Plasma Gas Flow Rate. 140

8.3 Discussion of Results. 140

(a) General. 140

(b) Hydrogen Plasmas. 141

(c) Nitrogen and Argon Plasmas. 141

(1) Calculation of the Fractional Plasma Energy Content. 141

(2) Extension of Limits by Turbulence. 143

(3) Energy Balance during Ignition. 145

(a) Theory - Spark Ignition. 145

(b) Nitrogen Plasma Jet Ignition, Calculation of Plasma Source Energy Densities and Mean Plasma Plume Temperatures for a Nitrogen Plasma. 147 149

Index (Continued) Page

CHAPTER 8 (Contd)

8.4 Conclusions on the Incend ivity of the Plasma Jet. 151

CHAPTER 9 RATES OF FLAME PROPAGATION

9.1 (a) Burning Velocities in methane-air mixtures following Spark Ignition. 154

(b) Burning Velocities in methane-air mixtures following plasma jet ignition. 154

9.2 The Methods used to Measure Flame Areas. 157

(a) The Use of Schlieren Records. 157

(b) The Use of C_2 Emission Spectroscopy. 159

9.3 Calculation of Burning Velocities from Measured Flame Areas. 159

9.4 Results and Discussion. 161

(a) Spark Ignition. 161

(b) Argon Plasmas. 166

(c) Nitrogen Plasmas. 168

(d) Hydrogen Plasmas. 168

Calculations to Evaluate the Importance of Turbulence. 171

CHAPTER 10 RESULTS AND DISCUSSION OF THE OH RESONANCE ABSORPTION MEASUREMENTS

10.1 Flame Growth (1st Stage Ignition). 175

(a) Results. 175

(1) Hydrogen Plasmas. 175

(2) Argon Plasmas. 176

(3) Nitrogen Plasmas. 177

(b) Kinetic Analyses of the Peak Values and Decay of Hydroxyl Concentration during the pre-ignition stage of a nitrogen plasma. 181

Index (Continued) Page

CHAPTER 10 (Contd)

(1) Peak Hydroxyl Concentration, $[OH]_{max}$. 181

(2) Decay of Hydroxyl Concentration from the Peak Value. 181

10.2 Development of the Flame Front. 185

(1) Calculated Hydroxyl Radical Concentrations. 187

(i) The Method. 187

(ii) The Results. 187

(a) Argon Plasmas. 192

(b) Nitrogen Plasmas. 193

(c) Hydrogen Plasmas. 194

(2) Evidence for the Change in Flame Structure. 194

(3) Variation with Position of OH Beam. 198

(a) Vertical Distance from Plug. 198

(b) Horizontal Distance from Plug. 201

(c) Hydroxyl Radical Concentrations and Plasma Source Energy Densities. 204

10.3 Relationship between Hydroxyl Concentration and Flame Properties. 204

Computer Studies on the Effects of H Atom Injection from the Plasma. 207

CHAPTER 11 CONCLUSIONS AND SUGGESTIONS FOR FUTURE WORK 212

LIST OF FIGURES

		Page
Figure (1)	Performance characteristics of S.I. Internal Combustion Engine.	18
Figure (2)	Equilibrium hydrogen atom concentrations.	25
Figure (3)	Potential energy curve for hydrogen.	31
Figure (4)	Rate of hydrogen atom recombination.	40
Figure (5)	Reaction chamber, molecular beam sampler and mass spectrometer.	50
Figure (6)	Detection of hydrogen atoms.	52
Figure (7)	Typical spectral line.	58
Figures (8)(9)	Calibration curve.	60, 64
Figures (10)(11)	Emission spectrum of OH electronic transition.	65, 66
Figure (12)	Apparatus for resonance absorption technique.	69
Figure (13)	Operating characteristics for Bismuth hollow cathode lamp.	77
Figures (14)(15)	Operating characteristics of Argon and Water Vapour hollow cathode lamp.	78, 79
Figure (16)	Bismuth emission and OH absorption line profiles.	81
Figure (17)	Combustion vessel.	87
Figure (18)	Flow system.	88
Figure (19)	Plasma jet.	90
Figure (20)	Plasma jet ignition circuit.	92
Figure (21)	Laser schlieren and C_2 emission system.	95
Figure (22)	The apparatus.	98

List of Figures (Continued) Page

Figure (23)	The OH resonance absorption technique.	100
Figure (24)	C_2 emission detection system.	108
Figure (25)	C_2 emission intensity calibration.	110
Figure (26)	Flame areas and C_2 emission.	111
Figure (27)	Focussing system.	117
Figure (28)	Definition of symbols.	123
Figure (29)	Axial and radial distances for a nitrogen plasma.	124
Figure (30)	Axial and radial distances for a hydrogen plasma.	125
Figure (31)	Axial and radial distances for an argon plasma.	126
Figure (32)	A nitrogen plasma igniting a methane-air mixture.	129
Figure (33)	A hydrogen plasma : (1) Discharging into air; (2) Igniting a methane-air mixture.	130
Figure (34)	Variation of equivalence ratio with stored plasma energy.	135
Figure (35)	Variation of equivalence ratio with stored plasma energy (hydrogen).	136
Figure (36)	Variation of equivalence ratio with stored plasma energy (nitrogen).	137
Figure (37)	Variation of equivalence ratio with stored plasma energy (argon).	138
Figure (38)	Fractional plasma energy content.	142
Figure (39)	Energy balance for a nitrogen or argon plasma igniting a methane-air mixture.	144
Figure (40)	Plasma plume energy densities for a nitrogen plasma.	150

List of Figures (Continued)

		Page
Figure (41)	Rates of flame propagation of plasma ignited flames (from the literature).	155
Figure (42)	Mean radius vs. time for hydrogen and argon plasmas and spark ignition of a methane-air mixture.	162
Figure (43)	Burning velocity measurements for plasmas igniting a methane-air mixture.	163
Figure (44)	Burning velocity against flame radius.	164
Figure (45)	Burning velocities for hydrogen plasmas igniting a methane-air mixture.	172
Figure (46)	Plasma source energy densities and burning velocities against time for a hydrogen and nitrogen plasma igniting a methane-air mixture.	173
Figure (47)	Burning velocities and hydroxyl concentration for plasmas igniting a methane-air mixture.	179
Figure (48)	OH concentrations, plasma source energy densities and temperatures for a nitrogen plasma pre-igniting a methane-air mixture.	182
Figure (49)	$1/[OH]$ vs. time for the decay during the pre-ignition period by a nitrogen plasma.	184
Figure (50)	$[OH]_{EXPERIMENTAL} - [OH]_{CALCULATED}$ for plasmas igniting a methane-air mixture.	195
Figure (51)	OH concentrations from resonance absorption measurements for a hydrogen plasma igniting a methane-air mixture.	199

List of Figures (Continued)

		Page
Figure (52)	Variation of $[OH]_{EXPERIMENTAL} - [OH]_{CALCULATED}$ with position for hydrogen plasmas igniting a methane-air mixture.	200
Figure (53)	Maximum OH resonance absorption vs. radial distance for hydrogen and nitrogen plasma jets igniting a methane-air mixture.	202
Figure (54)	Time for $[OH]_{INITIAL}$ against radial distance of OH diagnostic beam.	203
Figure (55)	Plasma source energy densities and $X_{OH(EXPERIMENTAL)} - X_{OH(CALCULATED)}$ against time for a hydrogen plasma igniting a methane-air mixture.	205
Figure (56)	Burning velocities and OH concentrations for a hydrogen plasma near the lower ignitability limit.	206
Figure (57)	Concentration profiles (computed) through a methane-air flame.	208
Figure (58)	Concentration profiles (computed) through a hydrogen plasma ignited methane-air flame.	210
Figure (59)	Plasma plug designs.	220

LIST OF PLATES

		Page
Plate (1)	Burner for the injection of hydrogen atoms from heated tungsten foil.	45
Plate (2)	The application of electric fields to methane-air flames.	47
Plate (3)	The apparatus.	84
Plate (4)	(A) The plasma jet. (B) Cylindrical combustion vessels.	86
Plate (5)	(A) OH beam "target". (B) Apparatus for OH resonance absorption studies.	101
Plate (6)	Nitrogen plasma discharging into air.	120
Plate (7)	Hydrogen plasma discharging into air.	121
Plate (8)	Argon plasma discharging into air.	122
Plate (9)	Spark ignition for C_2 emission calibration.	165
Plate (10)	Argon plasma igniting methane-air mixture.	167
Plate (11)	Nitrogen plasma igniting methane-air mixture.	169
Plate (12)	Hydrogen plasma igniting methane-air mixture.	170
Plate (13)	OH resonance absorption oscillograms for a nitrogen plasma igniting methane-air.	180
Plate (14)	Example of "zone" method for determination of calculated hydroxyl values.	188
Plate (15)	OH resonance absorption oscillograms for a hydrogen plasma igniting methane-air (1).	196
Plate (16)	OH resonance absorption oscillograms for a hydrogen plasma igniting methane-air (2).	197

CHAPTER I

INTRODUCTION

1.1 The Practical Objectives

Since the beginning of this Century, two quite separate fields of interest have promoted the study of ignition and flame propagation. Firstly, the prevention of explosions in mines and factories requires an understanding of the behaviour of potential ignition sources such as electrical discharges, incandescent solids and flames. In assessing the incendive properties of these localised ignition sources, use is made of minimum ignition energies and minimum ignition temperatures, values of which are well documented throughout the literature (for example, see refs.(1) and (2)).

The subject of ignition of gases by sparks has been in doubt for a considerable length of time. The main problem was in determining whether the effect of an electric spark was purely thermal or whether ionization produced by the spark had a dominating role in producing active species. This question remains unanswered even today although our knowledge of ignition has advanced significantly. For example, it has been recognised that apart from quenching effects of the electrodes, the minimum ignition energy will depend on the relative proportion of energy retained in the capacitive and inductive components of the spark and how effectively these interact with the size and shape of electrodes and width of spark gap to give the optimum rate of energy release (3,4). Also for capacitance sparks, the importance of the frequency of the oscillatory discharge on its igniting ability has been investigated (5). For lean propane-air mixtures, a maximum igniting ability was found at a frequency of 100 kHz and it was concluded that the discharge frequency rather than the spark duration was the predominant factor in ignition by a capacitance spark. More recently, initiation and subsequent propagation of flame

fronts by the breakdown, arc and glow discharge phases of a spark have been investigated by time resolved interferometry (6). In these studies, the breakdown phase (Duration 1 to 10 nS) was found to control the ignition process up to about 1 mS due to its high energy transfer producing very high temperatures and radical concentrations (H, O, C and N).

Similarly, for ignition of a flammable gas by a hot solid, the geometry, size and material of the heating element and duration of contact have all been found important in determining the minimum temperature at which spontaneous combustion occurs. The smaller the heated object, the higher the temperature required to enable it to cause ignition whilst quartz surfaces have been found more effective than those of Nickel which are in turn more effective than those of Platinum. This was found to be due to the different catalytic effects which these promoted.

Allied to these studies on ignition, the continuous search for more effective fire extinguishing and explosion preventing substances has revealed new facets of information concerning the mechanism of flame propagation.

The second area in which a study of ignition and flame propagation is regarded essential is that of internal combustion engines and burner systems. With imminent and future shortages of fossil fuels and concern over concentration levels of combustion generated pollutants, the need exists to design these systems to operate with higher efficiency and lower emissions. One such example where considerable improvements could be made is in the case of the spark ignition internal combustion engine. For reliable and efficient operation using a standard (electronic or otherwise) ignition system, air to fuel ratios near to stoichiometric are required (air : fuel $\simeq$ 14.5 : 1). Operation with lean mixtures - ($>$ About 18:1 Air : fuel ratio) results in misfire preventing the optimum specific thermal efficiencies and lowest overall pollutant emission concentrations being attained.

The increase in specific thermal efficiency with increasing air to fuel ratios can be illustrated by consideration of the expression for the thermal efficiency, η of a four stroke Otto engine operating under ideal conditions namely,

$$\eta = 1 - \frac{1}{R^{(\gamma-1)}} \qquad (1)$$

where R is the compression ratio and γ is the ratio of specific heats $(\frac{C_p}{C_v})$ of the working fluid.

For a given compression ratio, the value of γ and consequently the thermal efficiency, increases as the mixture becomes leaner. This is shown in Fig.(1) which also shows the general trend of pollutant emissions (CO, hydrocarbon and NO_x) as a function of air:fuel ratio for a conventional four stroke engine. It can be seen (Fig.(1)) that the concentration of hydrocarbons decreases as the air to fuel ratio is increased until the onset of misfire (air to fuel ratio about 17 to 1) which causes the hydrocarbon concentration to increase. Under these weak mixture conditions, a longer duration, inductive type discharge has been found to be more successful at preventing engine misfire than a shorter duration capacitive type spark. Similarly, the concentration of CO which is controlled by the water gas equilibrium reaction decreases as the air to fuel ratio increases. Leaner mixtures (higher O_2 concentration) provide high OH concentrations thereby increasing the forward rate of the reaction

$$CO + OH \rightleftharpoons CO_2 + H \qquad (2)$$

which increases the rate of decay of the CO concentration.

The concentration of oxides of nitrogen (NO_x), which is strongly dependent on flame temperature, reaches a maximum just on the lean side of stoichiometric as a consequence of the Zeldovich reaction mechanism. Like the concentrations of CO and hydrocarbons, the NO_x concentration could be drastically reduced by operating with very lean mixtures.

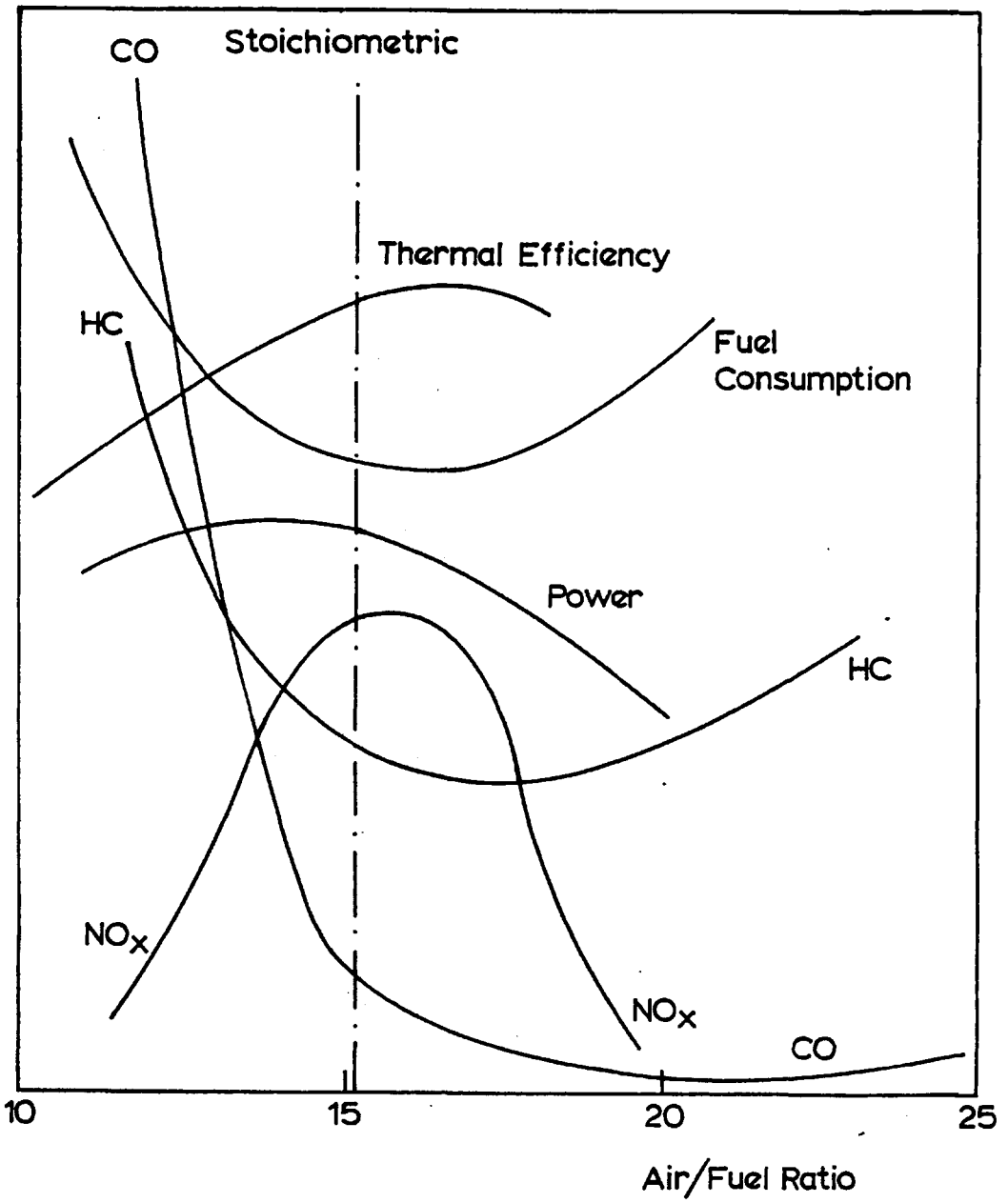

CO
Stoichiometric
Thermal Efficiency
HC
Fuel
Consumption
Power
HC
NOx
NOx
CO
10
15
20
25
Air/Fuel Ratio

FIG (1)

Clearly in the interest of both high thermal efficiency and low pollutant emissions, the optimum operating air to fuel ratio must be in the range of about 17 : 1 to 25 : 1. To prevent engine misfire at these lean mixtures a more effective ignition source than a conventional spark is required. Also, because of the very low rates of laminar flame propagation in these mixtures the ignition source must be capable of increasing the overall rate of burning throughout the entire charge within the cylinder. This could be achieved either chemically by diffusion of radicals or fluid dynamically by pre-turbulization producing a multi-ignition source throughout the charge to be burnt. The pre-chamber or torch ignition concept attempts to fulfill this requirement (7,8,9,10).

A more effective ignition source than the standard surface discharge igniter would also be desirable for re-lighting at high altitudes in aircraft gas turbines. In this context, the possibility of using continuous arc plasma jets to increase flame reaction rates, stability and throughput whilst lowering pollutant emissions has been considered (11,12). A similar requirement arises for the efficient premixed combustion of high throughputs of very low calorific value fuels in a furnace or boiler system.

1.2 The Approach to These Objectives

To achieve ignition and increased rates of flame propagation in very lean mixtures using the smallest fraction of power (typically 1% of the total energy release of the flame) from an external source, the most efficient mode of coupling of energy from source to flame must be employed. The addition of thermal energy to raise temperatures and increase reaction rates in hydrocarbon-air mixtures is clearly inadequate except in certain combustion designs which employ recirculation of product gas enthalpy back to the unburnt gases (e.g. spouted bed and Swiss Roll

burners, bluff bodies etc. (13,14)). On the other hand, if the diffusional (chainbranching) properties of ignition and flame propagation are invoked, reaction rates could be enhanced by generating a non-Boltzman distribution of atoms or radicals which could initiate and promote specific combustion reactions at lower translational temperatures. The results of some recent computational studies have in fact shown this to be true. For example, (15) for a homogeneous very lean methane-air mixture with $\phi = 0.5$, a 1% initial radical concentration would lead to ignition at a 300 K difference in initial temperature (1200 K) compared to the situation with zero initial radical concentration (1500 K). For equal initial temperatures, the time for chemical ignition was reduced by increasing the initial radical concentration although the maximum radical concentrations achieved during combustion were similar for all cases. Clearly, there is a limit to which high initial temperatures can be replaced by high initial radical concentrations above which little is to be gained. This is because of the proportionately higher rates of third body recombination reactions which would merely raise the initial temperature to the ignition temperature without initiating the same proportion of chain propagation or chain branching reactions.

Similar computations have been performed on the sequence of events following an ignition at the axis of a cylinder or centre of a sphere in a 60% hydrogen-air mixture (16,17). It was found that for a constant total energy, ignition was facilitated by increasing the proportion supplied as hydrogen atoms rather than thermal energy.

It would be expected that the addition of hydrogen atoms becomes particularly important for lean hydrogen or hydrocarbon-air flames which are deficient in these species compared with stoichiometric of fuel rich flames. Also for systems which are not highly mixed, an advantage is gained by the high diffusion coefficient of the H atom compared with other reactive species such as O, OH, N and CH_3.

By considering the high energy spark ignition of a hydrocarbon-air mixture at or slightly below the lower flammability limit, it is observed in many cases that the external ignition source appears to support a localised flame which fails to propagate any distance from the source. In this situation, both heat transfer by conduction and diffusion of atoms and radicals from the source help maintain the temperature and concentration profiles characteristic of a flame. By "Spreading" this source of energy and radicals, combustion could be initiated throughout the entire volume to be burnt and to do this one of the following two approaches can be taken.

(a) The Generation of Radicals "In Situ" Within a Flame

This will be discussed in Chapter 2, Section 2.1(c) and Chapter 3, Section 3.2 which describes the preliminary work done in investigating the feasibility of this method. Although this approach has the advantage that "Mixing" of the radicals generated becomes unnecessary, the magnitude of the effects and the mechanisms responsible for them of this type of augmentation are hard to assess.

(b) The Generation followed by the Injection of Radicals

This was the main line of approach taken in the present research. The methods available for the generation of atoms and radicals were examined (Chapter 2, Section 2.1) and the problems associated with the mixing of these with the unburnt gases or flame are discussed (Chapter 2, Section 2.2).

A high energy, capacitive discharge plasma plug which had the facility to control the plasma media (and hence the radicals generated) was chosen for the main study. This was primarily used to generate hydrogen atoms (thought to be the most effective at initiating combustion reactions) from molecular hydrogen, nitrogen atoms from molecular nitrogen and thermally hot argon atoms (an inert and therefore likely to be the

least effective) from high purity argon. Some experiments were also performed using methane as a source of hydrogen atoms.

The high discharge pressures within the plasma plug were employed for injection of these radicals into the unburnt gases at sonic velocities thereby reducing losses by radical recombination whilst dismissing the mixing problem (Chapter 2, Section 2.2).

To examine in more detail the role of atoms and radicals, a review was made of the analytical methods currently available for their detection and estimation (Chapter 2, Section 2.3). Of these methods, absorption spectroscopy was considered the most suitable and a fine line resonance absorption technique was developed to follow the growth and decay of OH radicals (which quickly came to equilibrium with other radicals), following the injection of H, N and Ar atoms from the plug into lean methane-air mixtures. In this way, the dependence of the combustion characteristics (limits of ignitability and burning velocities) on radical concentrations could be investigated.

CHAPTER 2

THE PRODUCTION AND DETECTION OF ATOMS AND RADICALS

2.1 Methods for Producing Atoms and Radicals

Chemically highly reactive atoms and free radicals can be generated by supplying sufficient energy to the parent molecules to cause dissociation. This energy can take a wide range of different forms including thermal, photochemical, electrical discharge and radiolysis. The use of radiolysis was discounted since it is known to produce only very low yields of atoms and radicals.

For the present purpose, it would have been desirable to generate high concentrations of atoms or radicals in the ground electronic state with a well defined translational temperature. This is usually not possible and a wide variety of other reactive by-products are also formed which include ions, electrons, metastables, and radicals in various electronic, vibrational and rotational states.

The thermal, photochemical and electrical discharge methods are described below and the preliminary experiments which were carried out in connection with these methods are described in Chapter 3.

(a) Thermal Methods

For a given temperature, the yield of atoms or radicals produced increases with decreasing dissociation energy of the parent molecule. The dissociation energies of some common diatomic and triatomic molecules are listed below (18,1).

	Dissociation Energy	
	kcal/mole	Electron Volts
Hydrogen	103.25	4.48
Oxygen	117.97	5.12
Nitrogen	225.1	9.76
$H + OH \rightleftharpoons H_2\ O$	114.6	4.97
$H + O \rightleftharpoons O\ H$	104.3	4.53

For hydrogen, calculations were made of the equilibrium hydrogen atom concentrations as a function of temperature for total pressures equal to 0.1, 1 and 10 atmospheres and the results are shown in Fig.(2). This shows the rapid increase of hydrogen atom concentration with temperature over the range 2,000 K to 3,000 K (pressure 1 atmosphere) and the corresponding fall in the increase of atom concentration with temperature at higher temperatures. Similar curves to these are obtained for other diatomic molecular gases for which the fractional equilibrium atom concentration, x, is given by

$$\frac{x^2}{1 - x} = \frac{Kp(T)}{p}$$

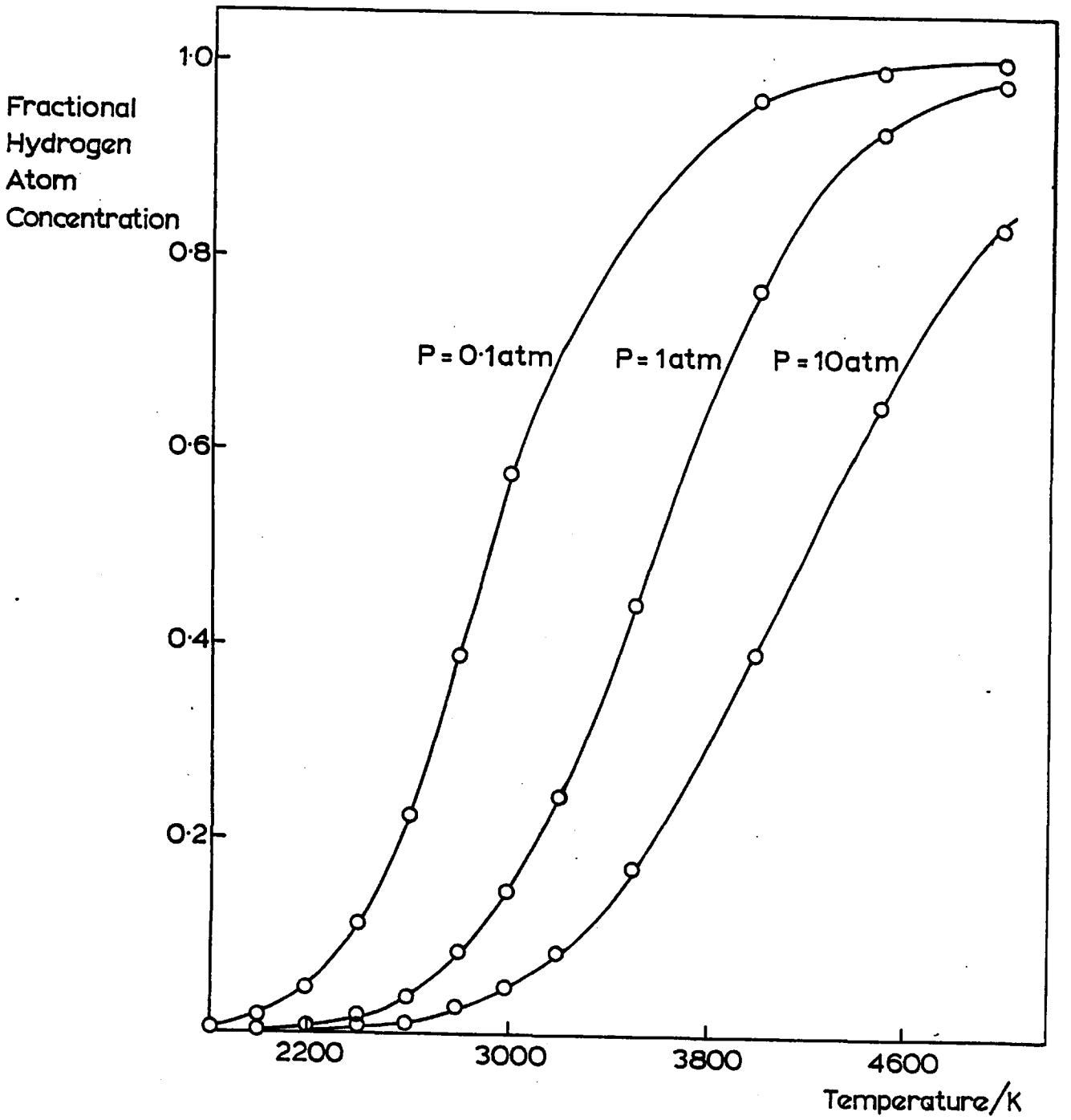
where $Kp(T)$ is the equilibrium constant at constant pressure and P is the total pressure.

The most common methods of supplying heat are (1) Enclosing the reaction vessel in a furnace, (2) Use of an electrically heated filament and (3) Subjecting the parent gas to a shock wave. The use of a furnace or electrically heated filament is usually confined to gases with fairly low dissociation energies (e.g. H_2) since temperatures in excess of about 2,000 K are difficult to attain. Shock tubes, on the other hand, can be used to obtain very high transient concentrations of atoms and radicals and have been widely used in chemical kinetic studies (19).

(1) Shock Tubes

A shock wave caused by the sudden bursting of a diaphram adiabatically compresses the gas through which it passes producing a rapid rise in temperature. For monatomic gases, temperatures as high as 18,000K can be obtained with slightly lower temperatures for diatomics.

The application of a shock wave to a flammable mixture would produce very high radical concentrations which could play an important part in



FIG(2)

EQUILIBRIUM HYDROGEN ATOM CONCENTRATIONS AGAINST TEMPERATURE $H_2 \rightleftharpoons 2H$

initiating a detonation within the mixture. Clearly a detonation (for example, stabilised in a combustion chamber) would be an alternative method for obtaining an increased rate of propagation of the combustion wave in the same mixture (50).

It is worth mentioning here some of the shock tube kinetic studies done on the H_2/O_2 ignition process which are relevant to the present research (20,21,22,23). In these, the initial heating period by the shock wave is in the order of microseconds and the chemical reactions that follow have been studied spectroscopically (20,21) up to times 10^{-5} to 10^{-3} of a second after passage of the shock front and subsequent thermal relaxation of the shocked gases. Measurements of the shock velocities serve to relate the immediate post-shock temperatures and pressures with the pre-shock conditions whilst OH, O and H absorption and I.R. emission from water vapour are some of the spectroscopic techniques which have been used to follow the exponential growth and gradual decay of intermediates during chemical reaction.

In studies of this kind, two interesting types of behaviour have been reported concerning the mechanism of ignition. For temperatures above 1100 K (20,21) a single induction period, τ_1, was observed at the end of which there was a single increase in OH absorption simultaneously with a pressure rise and the relationship

$$\tau_1 \left[O_2\right] = \text{constant}$$

was found. For temperatures below 1100 K, the first appearance of OH absorption after the induction period τ_1 was not accompanied by a pressure rise. Only after a longer induction period τ_2 after which there was a second rise in OH that a pressure rise occurred. In this case, no correlation between τ_2 and $\left[O_2\right]$ could be found but instead it was observed that

$$\tau_2 \left[H_2\right] = \text{constant.}$$

These results have been explained by examination of the individual elementary reactions for the H_2/O_2 system since during the early stages of the induction period, the radical concentrations are low and the consumption of reactants is very small. For this reason, only the elementary steps which are first order in the radical concentration need to be considered and in this way some useful information has been gained on these reactions (for example, see references 20 and 23).

These observations on the two separate induction periods for ignition resemble the nitrogen plasma jet ignition of methane-air mixtures found in the present research (discussed in Chapter 7). The induction periods in this case are much longer and other mechanisms as well as the reaction kinetics need to be taken into consideration to account for this two induction period phenomena.

(2) Heated Filaments

The use of a high temperature electrically heated filament for thermal dissociation has been confined to gases which do not appreciably chemically attack the filament. This excludes the dissociation of molecular oxygen by this method whilst attempts to dissociate nitrogen have failed due to its relatively large dissociation energy (24). On the other hand, it was first shown by Langmuir (25) that hydrogen could be successfully dissociated at low pressures by a high temperature (2,500 k) tungsten filament and since then the mechanisms of atomization of hydrogen by heated tungsten have been examined (26,27,28,29). This method was later applied to the study of atomic hydrogen with acetylene over the pressure range 1 to 15 torr using an isothermal calorimeter for the measurement of hydrogen atom concentration (30). In a reaction tube, 18 mm in diameter, the distance from the filament to the detector 73 mm and the temperature of the tungsten filament 1700 $\pm$ 50°C, the following results for the partial pressures of hydrogen atoms, P_H were obtained by these authors:

Pressure (mm Hg)	P_H (mm x 10^3 Hg)	Flow Rate cc/min
1.15	4.62	40
5.64	6.02	200
8.75	7.25	360
12.9	8.77	400

In a more recent study with the tungsten filament at 1600 k, the concentration of hydrogen atoms detected by electron spin resonance spectroscopy was found to be about 4 x 10^{-2} torr at a total hydrogen pressure of 100 torr (31). The yield was found to decrease with increasing pressure and hydrogen atoms could just be detected at total pressures as high as 500 torr.

(b) Photochemical Methods

The methods which employ light as a source of energy for producing atoms and radicals can be classed under the 3 main headings of (1) Flash Photolysis, (2) Direct Photolysis and (3) Indirect Photolysis. Since the present research is directed towards the production of simple atoms or radicals (e.g. H and O) for initiation of combustion reactions, the photochemical methods relevant only to the production of these species have been considered.

(1) Flash Photolysis

Flash photolysis has been widely used to produce high, transient concentrations of atoms and radicals (32,33,34,35). A single, intense flash was obtained by discharging a bank of capacitors (2,000 to 5,000 Joules) which generates reactive species in the vicinity of the flash. The growth and decay of these species over the period of several hundreds of milliseconds after the strong flash was then followed by absorption spectroscopy using a second smaller flash (70 Joules) triggered at a pre-set time after the first flash. High temperatures were avoided by diluting the reactants with a large excess of an inert gas which prevented

the temperature rising more than a few degrees.

(2) Indirect Photolysis

Indirect methods of photolysis can be used to produce both hydrogen and oxygen atoms (36). For example, H atoms and CHO radicals are produced in the primary step in the photolysis of formaldehyde or hydrogen sulphide used as a photolytic source of hydrogen atoms:

$$H_2S + h_\upsilon \longrightarrow H(^2S_{1/2}) + HS$$

In the case of the photolysis of hydrogen iodide by

$$HI(^1\Sigma^+) + h_\upsilon \ (\lambda = 2537\ \text{Å}) \longrightarrow H(^2S_{1/2}) + I(^2P_{3/2})$$

translationally "hot" hydrogen atoms are produced due to the light hydrogen atom taking an appreciable fraction of the excess photochemical energy. Similarly, oxygen atoms in different electronic states (depending on the wavelength of incident radiation) are produced by the photolysis of NO_2.

The last example of photochemical dissociation is that of photo-sensitised decomposition. If a mixture of hydrogen and mercury is irradiated with the 2537 Å mercury resonance radiation, mercury atoms are excited to the 6^3P_1 state which are collisionally quenched by hydrogen molecules, the latter acquiring excess of its dissociation energy. By a similar mechanism, hydrogen atoms have been obtained by the mercury photo-sensitised decomposition of paraffin hydrocarbons.

Although these indirect photochemical methods provide some very interesting possibilities as atom and radical sources, it would ultimately be very difficult to apply these to any practical combustion system. For this reason, they were not considered further.

(3) Direct Photolysis

By direct photolysis, a very low steady state concentration of atoms and radicals can be maintained by continuous irradiation. For a diatomic

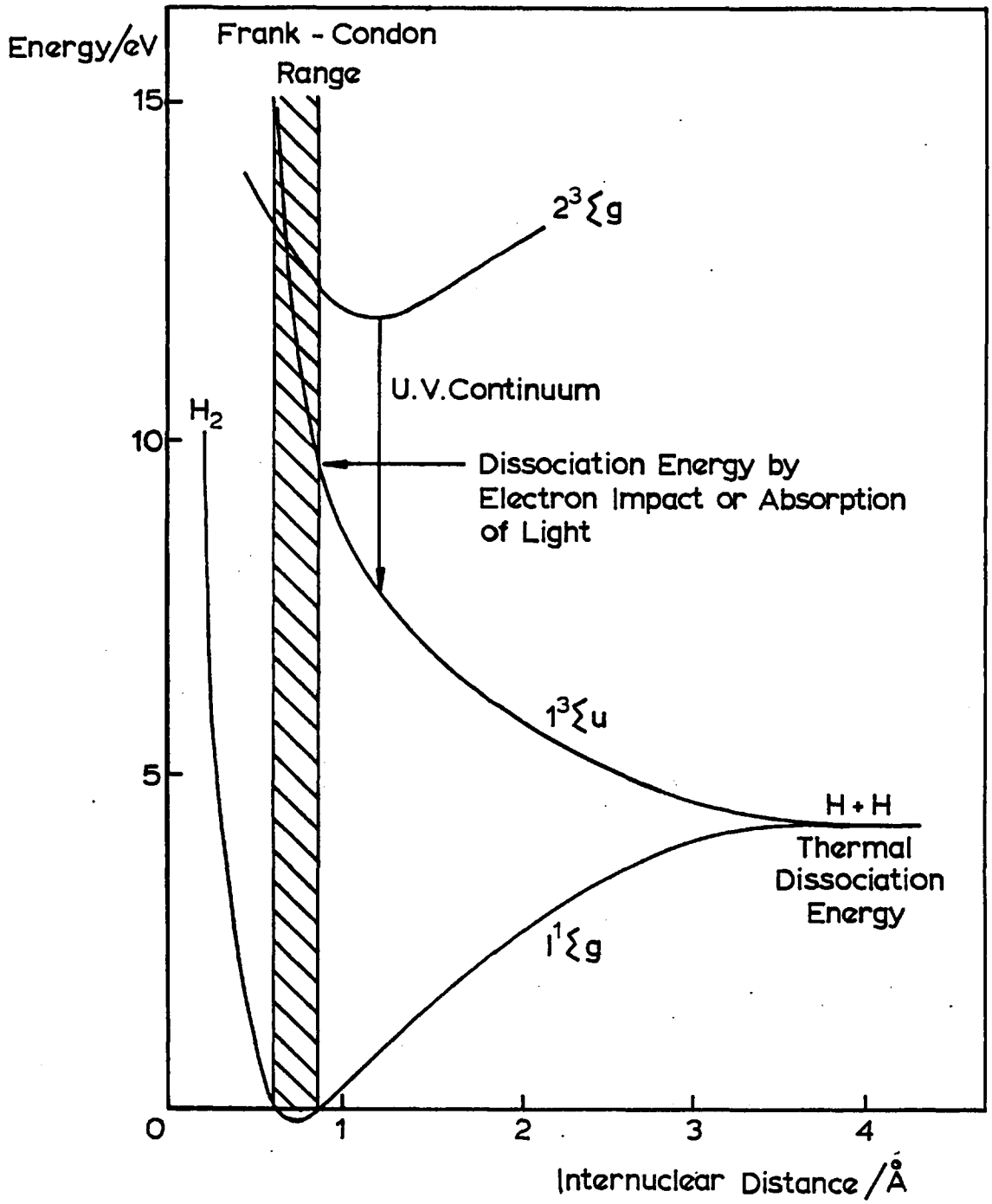
molecule, absorption of radiation in the visible or ultraviolet region of the spectrum results in excitation to a higher electronic state. According to the Frank-Condon principle, the most probable transitions are those in which the internuclear distance remains constant and therefore the absorption spectrum of the molecule will be determined by the relative positions of the potential energy curves and the requirement of certain spectroscopic rules (37). In the case of hydrogen, the upper state is a repulsive one (see Fig.(3)) and therefore the region of maximum absorption in the continuum will correspond to an energy considerably greater than that required to produce dissociation. Although the longest wavelength (i.e. smallest energy) which can be absorbed is that required to reach the dissociation limit of the upper curve (Fig.(3)), in practice because of the Frank-Condon principle, the intensity of the continuous absorption falls off long before this limit is reached. Therefore continuous absorption occurs only in the extreme vacuum-ultraviolet region where experimental difficulties are usually too great for this method to be used.

The Schumann oxygen continuum, on the other hand, starts at 1754 Å and by using a lamp with a quartz or lithium fluoride window, the direct photolysis of oxygen can be used as a source of atoms. The mechanism is that of direct dissociation which leads to one excited and one ground state atom:

$$O_2(^3\Sigma g^-) + h\upsilon \longrightarrow O_2(^3\Sigma u^-)$$

$$\longrightarrow O(^1D) + O(^3P)$$

The direct photochemical dissociation of oxygen for the initiation and enhancement of combustion reactions has been studied recently with a particular emphasis towards practical applications such as the extension of the ignition limits in aircraft gas turbines and ramjets (38). It



FIG(3)

POTENTIAL ENERGY CURVE FOR HYDROGEN

has been reported that "minute" energy pulses (10 μJ) of vacuum ultraviolet radiation (1450 Å $< \lambda <$ 1800 Å) have ignited fuel-air mixtures flowing at high velocities ($0 < M < 1$) in a combustion system. In this work, the design of the lamp (which was, for example, a high pressure Xenon lamp fitted with Lithium fluoride windows) was optimised to maximise the output of vacuum ultraviolet radiation in the required spectral region for the photodissociation of oxygen. By doing this, input energies of less than one joule to the source lamp have produced the required radiant intensity for ignition (generating about 10^{14} oxygen atoms cm^{-3}).

(c) Electrical Discharge Methods

The third important method of generating atoms or radicals is by an electrical discharge or plasma. Since these may at the same time as generating dissociation products emit sufficient radiation to cause photodissociation within their vicinity, the relative importance of each of these two mechanisms for ignition and augmentation of combustion needed to be examined. Since for the main study in this research a capacitor discharge plasma jet plug (described in detail in Chapter 5, Section 5.2) was chosen for generating atoms and radicals, it was necessary to examine the photochemical effects associated with this particular plasma jet (39). The use of this plug has enabled increased rates of flame propagation particularly when the plasma produced contains hydrogen atoms (40). It was also noted however, by high speed photography of a plasma jet ignition, that the duration of the plasma luminosity in the visible corresponded with the enhanced rates of flame propagation. This seems to suggest that ultraviolet radiation from the plasma (causing photodissociation within the unburnt mixture) may have an equal, if not more important, influence on the initiation of combustion reactions than that of the diffusion of hydrogen atoms (i.e. whether this influence is based on the mean free path of a photon of the appropriate wavelength or

that relevant to the diffusion of hydrogen atoms).

The set of experiments which were carried out to examine the photochemical effects produced by the plasma plug are described in Chapter 7. These concluded that the atoms and radicals generated by the electrical discharge in the plasma plug play a predominant role in initiating and enhancing combustion reactions and for this reason the methods of atom and radical generation by electrical discharges is considered in more detail.

Electrical discharges fall into one of the two general categories of electrode and electrodeless discharges both of which can be operated continuously (e.g. an arc) or intermittently (e.g. a spark). Some of the more important properties of these discharges relevant to atom and radical generation are described here with more detail being found in references (41), (42) and (43).

(1) Low Frequency Discharge

The best known example of a low frequency electrode discharge is that of the Woods tube which has been used extensively for the production of H, O, OH and N atoms at low pressures (44,45). This consists of a U tube 1 to 2 metres long with an electrode and molecular gas inlet situated at each end and the outlet for the dissociated species placed at the centre of the tube. For hydrogen at a pressure of about 0.5 mm Hg, discharge currents of about 0.1 ampere were drawn when the electrodes were maintained at a potential of about 2 kV and the effect of hydrogen atom yield on flow rate and power input has been studied (see (45)). Although these types of discharges are associated with relatively low power density (due to the high volume of gas between the electrodes) and contamination of the plasma by the electrode material, they were commonly used for some of the early work done with atomic flames (46).

At high pressures (i.e. atmospheric pressure) these conditions are no longer suitable because of the high breakdown voltages required and

the fact that the discharge tends to contract to a very narrow channel with very high energy concentration (transition from a low pressure glow to a high pressure arc discharge). For these reasons, it has been necessary to use continuous arc or intermittent spark (as used in this research) plasma jets for atom and radical generation at atmospheric pressure.

D.C. or low frequency arc plasma jets are usually designed with an anode/cathode separation of around 5 mm and operate with discharge currents of typically $10 - 10^3$ A at applied operating voltages of $10 - 10^2$ V. When used as atom and radical sources, the main problems encountered are those of arc instability and non-uniform heating of the molecular gas. Several different designs based on a tungsten nozzle anode shielded with an inert gas to reduce chemical attack and a water cooled coaxial cathode can be found in the literature (47,48,49). Improvement in the uniformity of heating by the arc can be achieved by magnetic rotation of the arc around the cathode. This also induces swirl and turbulence in the gas to be dissociated and as a result of its angular momentum causes the jet to expand considerably on leaving the nozzle thereby improving the mixing of the dissociated species with the outside gas (50).

Plasma jets of this type have been used to improve the stability and throughput of methane-air mixtures in a flame tube (51). The reactive species OH, O, H and N were generated by the addition of H_2O, O_2, CH_4 or N_2 to the inert carrier gas, argon. All of these were found to improve the maximum throughput which could be achieved when compared with argon alone with nitrogen being the most effective. For nitrogen plus argon as the carrier gas, an increase in the throughput of almost 700% was achieved compared to that with no augmentation. In this case, the amount of electrical power added was equivalent to typically 10% of the chemical energy flux (or equivalent to an increase of approximately 116°C

in the final temperature which would be expected to produce less than a doubling in reaction rate if equilibriated). In this study, it was concluded that the effectiveness of nitrogen was due to its large dissociation energy (N atoms then producing other atoms and radicals important in flame propagation) and to the generation of energetic and long lived molecular fragments (see, for example, reference (52)). This does not contradict the approach and conclusions of the present research (see Chapter 11), since for a highly stirred system such as this, the large diffusion coefficient of the hydrogen atom is no longer of such importance.

From a practical viewpoint, all of the D.C. or low frequency arc plasma jets so far described have certain drawbacks. Firstly, they require an inert gas supply although recently certain designs have made this superfluous. Secondly, they require a high voltage pulse to initiate the arc which under certain conditions can become unstable. Lastly, they are clearly only suitable for continuous operation (i.e. unsuitable for intermittent applications such as within a combustion chamber of an internal combustion engine).

(2) Intermittent Capacitive Discharge

The other type of electrical discharge which is well suited for atmospheric pressure operation is that of the intermittent (i.e. spark) capacitive type discharge. When discharges with energies of typically 0.5 J (per spark) are confined to a cavity of small volume (e.g. 30 mm^3), a jet of plasma is produced. These have been used with success as sources of ignition in spark ignition internal combustion engines in a number of studies (53,54,55,56). In these, the atoms and radicals produced in the plasma originate from the gas within the cavity which is identical to that of the unburnt mixture. Therefore for operation with lean mixtures, high concentrations of N atoms (with some O, H, CH_3, etc.) are generated since the cavity gas is mainly air. On the other hand, by

including a gas inlet tube to the cavity, the cavity gas and consequently the specific atoms and free radicals produced by the discharge could be controlled.

This was first studied by examining the growth of lean methane-air flames in a constant volume bomb by various plasmas (40). In this, the most effective gas for the cavity was found to be hydrocarbons generally, which produced flame propagation rates corresponding to an approximately 50 fold increase in reaction rate. This was thought to be due to the high concentration of hydrogen atoms produced by the high temperature pyrolysis of these gases. Other studies by these authors have examined the fluid dynamic aspects as well as the chemical effects produced by the plasma jets and will be referred to throughout this thesis (57,58).

(3) High Frequency Discharge

The last group of electrical discharges suitable for the production of dissociated species are those of the high frequency, electrodeless type. These have mainly superseded the low frequency electrode type for use in kinetic flow tube studies (59,60,61,62) since there is no contamination of the plasma by the electrode materials. For radio-frequency discharges, power from a radiofrequency oscillator (output of a few hundred Watts, frequency 1-20 MHz) is coupled to a discharge tube via a plate or coil electrode (see Plate 2). However, to sustain a discharge at atmospheric pressure (63), high operating power levels are required (e.g. 2 to 3 kW) and difficulties are encountered with the discharge spreading due to stray fields.

These problems are mainly overcome using microwave energy (> 100 MHz) supplied from a magnetron power source. These units are commercially available and with the use of a resonant cavity enable energy to be very effectively coupled from the source to the discharge. In this way, very intense localised discharges of high energy concentration can be obtained which are extremely suitable as atom and radical sources. With careful

tuning of the cavity, the discharge can be maintained at pressures up to atmospheric pressure for incident power levels as low as 50 W.

The chemical synthesis of free radicals produced in N_2, H_2, O_2, air and CH_4 microwave glow discharges has been studied in some detail (64). Relationships were found to exist between the radical yield and the discharge variables of electric field strength, contact time and pressure. Also, it was found that the emission spectrum of the microwave glow was far more extensive than that of a 60 cps flow discharge indicating increased molecular excitation.

On the other hand (65), from measurements of hydrogen atom concentrations produced by nearly identical microwave discharges at atmospheric pressure, it was concluded that at these higher pressures, the discharge became a very inefficient source of atoms. Even though the microwave power delivered to the cavity was approximately five times that needed to dissociate the total hydrogen flow, levels of dissociation of only 0.01% were found.

(4) The Mechanism of Dissociation by an Electric Discharge

Molecular dissociation in an electric discharge at low gas pressures occurs primarily by electron impact. At a pressure of about 1 torr, the electron temperature within the discharge (i.e. typically 50,000 k) is considerably higher than the gas temperature which is usually no higher than 500 k. As the pressure is increased, the electron temperature and gas temperature tend to equalise (66), until at atmospheric pressure, dissociation occurs via a complex interaction of electrons, ions, atoms and molecules (i.e. the mechanism of dissociation becomes partly thermal in nature).

The theory relating to these processes is fairly well known for the case of simple diatomic gases (67). For hydrogen, dissociation by electron collisions requires an energy of 8.8 ($\pm$0.2) eV compared to 4.4 eV for ordinary thermal dissociation. This is due to dissociation

occurring mainly by direct excitation to the lowest repulsive state $^1\Sigma^+_g \longrightarrow {}^3\Sigma_u^+$ and to a lesser extent via the process $^1\Sigma^+_g \longrightarrow {}^3\Sigma^+_g$ where after emission, $^3\Sigma^+_g$ falls to $^3\Sigma_u^+$ and dissociates (see Fig.(3)). The dissociation mechanisms of N_2 and O_2 are slightly more complicated and can be found throughout the literature (68,18).

(5) Generation of Radicals "In Situ" within a Flame by an Electrical Discharge or Electrical Field

The augmentation of combustion by electrical discharges has been studied in some detail by a number of separate workers (e.g. 69,70,46, 47,50). The main problem is that the discharge tends to contract within the flame to a very narrow channel of very high energy concentration. Attempts to spread the discharge include varying the flow pattern, inducing turbulence, extending the discharge-gas contact, seeding the reactants, radiofrequency discharges and rotating the arc by a magnetic field. All of these methods, apart from increasing the product enthalpy of the flame, generate a wide variety of atoms and free radicals in an uncontrolled fashion "In Situ" throughout the flame.

Clearly the question arises as to whether D.C./A.C./H.F. or microwave fields could augment combustion using the flame front as a source of electrons and ions. The deflection of a flame caused by a D.C. or low frequency field is well known and can be explained by non-chemical phenomena such as the "Ionic Wind" effect (50). On the other hand, high frequency fields (> 1 MHz) should not cause these effects since the amplitude of ion oscillations would be smaller than the flame front thickness. Therefore, the displacement of a "floating" lean methane-air flame caused by the presence of a 7 MHz, 0-4,000 Volt (R.M.S.) field has been attributed to vibrational excitation of reactant molecules or radicals causing increased flame reaction rates (71). On this basis, the possibility of using microwave energy to increase flame propagation

rates in spark ignition internal combustion engines operating with lean mixtures has been examined (72).

In spite of a theoretical analysis on electron-neutral gas energy exchanges in high frequency fields (73), the actual magnitude of the increase in burning velocity caused by these fields is still in considerable doubt. For this reason it was thought worthwhile to carry out some preliminary experiments to look at the feasibility of using this method for enhancing flame propagation rates and these are described in Chapter 3.

2.2 The Decay of Atom and Radical Concentrations following Injection into the Unburnt Gases

The main problem which is encountered when reactive species are injected from a source into a flammable mixture is that associated with atom or radical recombination reactions. At atmospheric pressure, these are primarily homogeneous gas-phase reactions such as:

$$H + H + M \xrightarrow[k_1]{} H_2 + M \qquad (1)$$

$$H + OH + M \xrightarrow[k_2]{} H_2O + M \qquad (2)$$

where $k_1 \simeq 9.2 \times 10^{16} \times T^{-0.6}$ l^2 $mole^{-2}$ s^{-1} and $k_2 \simeq 6 \times 10^{10}$ l^2 $mole^{-2}$ s^{-1} at 2,000 K.

(a) Calculation of Hydrogen Atom Decay

Calculations were made of the decay of hydrogen atom concentration with time by reaction (1) above at temperatures of 3000K, 1,000K, 1500 K and 2,000 K at atmospheric pressure and the results are shown in Fig.(4). These were calculating using the recombination rate equation with $M = H_2$, that is

$$-\frac{d[H]}{dt} = k_1 [H]^2 [H_2]$$

which when integrated gives

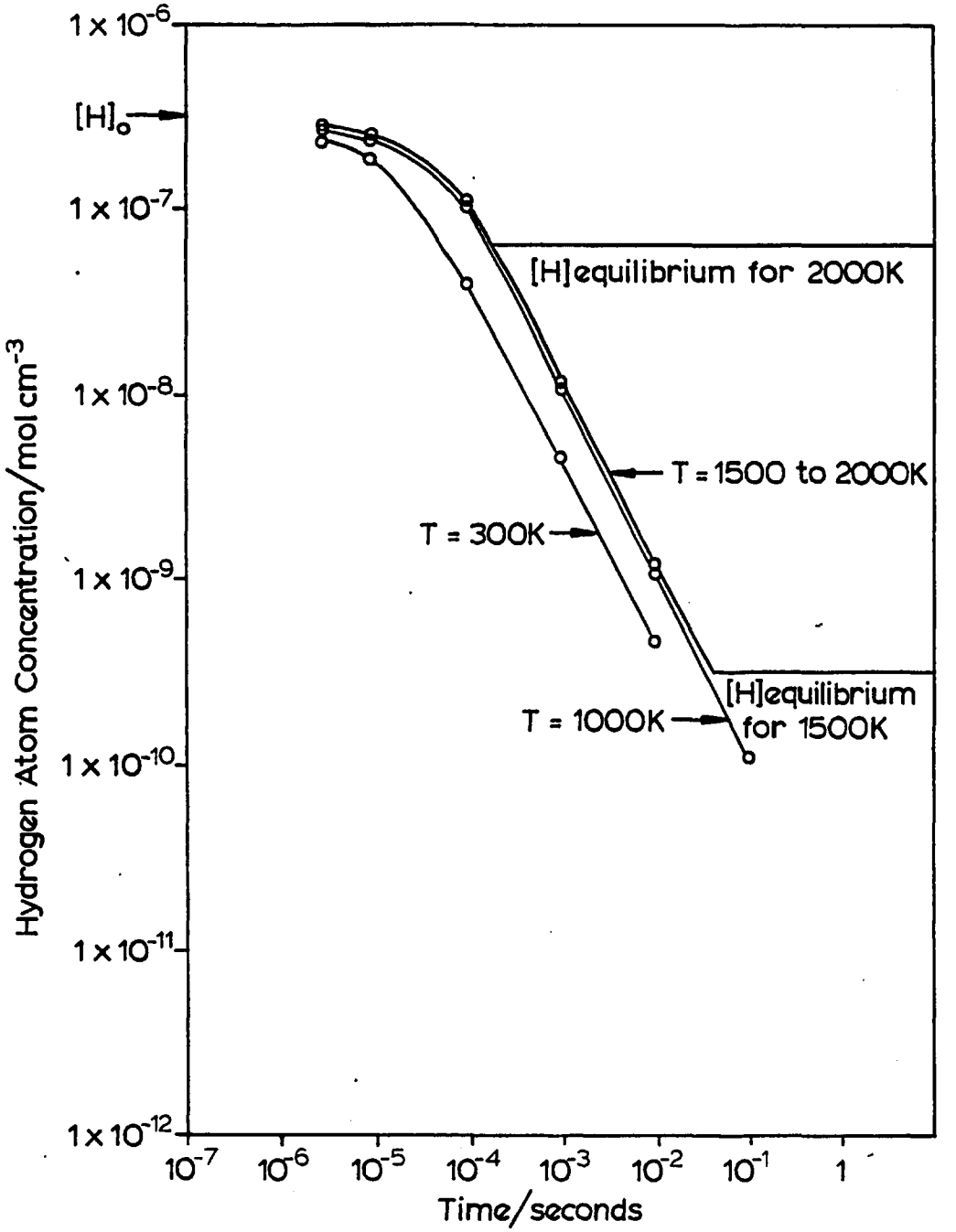


FIG. (4)

RATE OF HYDROGEN ATOM RECOMBINATION

$H + H + H_2 \xrightarrow[K_1]{} 2H_2, K_1 = 9{\cdot}2 \times 10^{16} \times T^{-0{\cdot}6}$

$$\frac{1}{[H]} = k_1 [H_2] t + \frac{1}{[H]_o}$$

where t = time and the subscript o denotes the initial conditions. For the calculations shown in Fig.(4), the following initial conditions were used:

$$[H_2] = 5 \times 10^{-5} \text{ mol cm}^{-3}$$

$$[H]_o = 5 \times 10^{-7} \text{ mol cm}^{-3}$$

(1% dissociated)

Clearly this example is oversimplified since for a high velocity plasma being ejected from a cavity, the recombination reactions would not be proceeding in a constant temperature environment. It does, however, illustrate the magnitude of the times required for a particular hydrogen atom concentration to decay to the equilibrium values at four different constant temperatures.

Less important are the heterogeneous recombination reactions on a surface, details of which can be found in references (74) and (75). For high temperatures and pressures, the rate of recombination varies with the square of the pressure with metals in general being more effective surfaces for recombination than quartz or plastics.

2.3 Methods of Detection and Measurement of Atoms and Radicals in the Gas Phase

Methods used for the detection and estimation of atom and radical concentrations are based either on the mass, spectra or chemical reactivity of the measured species. These fall into the general categories of probe and spectroscopic techniques both of which can be further classified as direct or indirect. Probe techniques include such methods as (1) Calorimetry, (2) Mass Spectrometry, (3) Colorimetry, (4) Wrede Harteck gauge and (5) Scavenger probe sampling. These are capable of point by

by point measurements although they suffer the disadvantage of creating an aerodynamic, chemical and thermal disturbance within the test region. Spectroscopic techniques on the other hand do not disrupt the test space although an integrated measurement along the beam axis is obtained which makes the interpretation slightly more complex. These include methods such as (1) Emission, (2) Absorption, (3) Flame photometry, (4) Resonance Fluorescence, (5)Electron Spin resonance and (6) Laser magnetic resonance.

In practice, all of the above methods can measure relative atom or radical concentrations accurately but few measure absolute concentrations reliably. Initially, all of the available techniques were examined for use with an atom or radical source and combustion system and some preliminary experiments, which are described in Chapter 3, were undertaken to help assess the relative merits of each method.

(a) Probe Methods

The calorimetric and mass spectrometric techniques which were examined experimentally are described in Chapter 3. For the reasons discussed above and in Chapter 3, these methods were later discontinued in favour of a spectroscopic technique which is described in detail in Chapter 4.

(b) Spectroscopic Methods

Basically the apparatus required is common to all emission, absorption, resonance fluorescence, and photometric spectroscopic methods. The use of electron spin resonance for the present research was thought unsuitable in spite of its high sensitivity (81), because of the low spatial resolution associated with a gas phase resonant cavity. Also the more recent analytical techniques (e.g. laser magnetic resonance) are more suited to extremely low atom or radical concentrations and the complexity and expense would certainly not justify their use for this research. Similarly, resonance fluorescence spectroscopy (82,83,84) is used for the very low concentration range (e.g. 10^{10} particles cm^{-3})

where linear relationships exist between the fluorescence signal and the concentration of fluorescing species. With this method, extreme care is required for calibration since small changes in temperature or composition affect the fluorescent intensity. Likewise, the strength of emission (46,85) is not always clearly related to the concentration of emitting species in the lower excitational state since the emission is strongly dependent on the temperature and mode of excitation (e.g. chemiluminescence). Also considered unsuitable were the indirect photometric methods of detection (86) such as those based on Li and Na emission since these are more applicable to a study of the post flame region of the flame.

Absorption spectroscopy, on the other hand, enables quantitative concentrations of ground state absorbing atoms or radicals to be made over a fairly wide range of temperature, irrespective of changes in foreign gas composition and excitation phenomena. For these reasons, it was decided to use absorption spectroscopy to monitor atom and radical concentrations. This method is also well suited to the study of the transient behaviour of a plasma jet ignited flame.

CHAPTER 3

PRELIMINARY EXPERIMENTS ON RADICAL GENERATION AND MEASUREMENT

Some of the methods for atom and radical generation and detection described in Chapter 2 suggested that some preliminary experiments would be desirable. From these experiments the best methods for the generation and detection of atoms and radicals could be chosen for the more detailed study of the effect of additional radicals on ignition and flame propagation which is described in subsequent chapters.

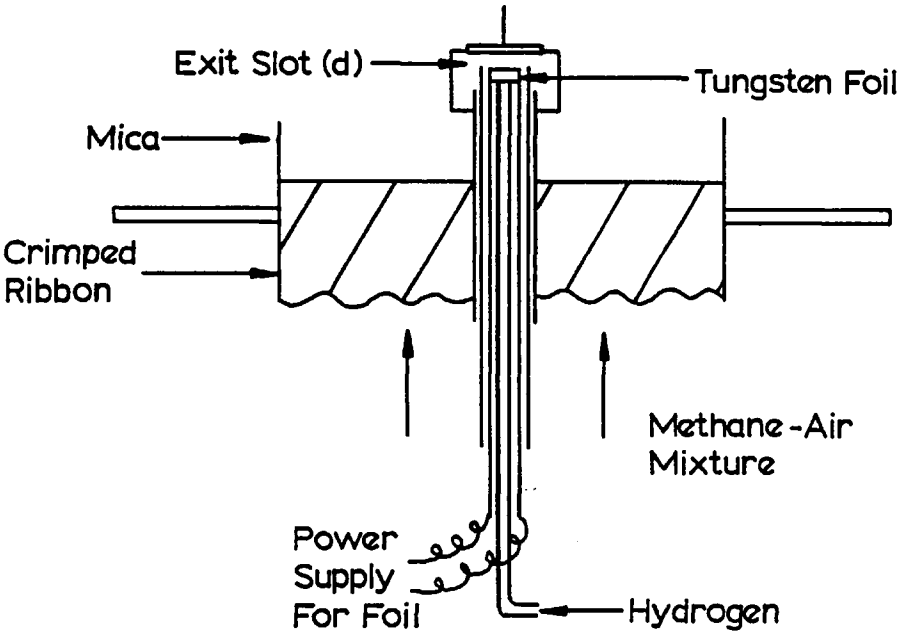
3.1 The Use of Heated Tungsten for producing Hydrogen Atoms

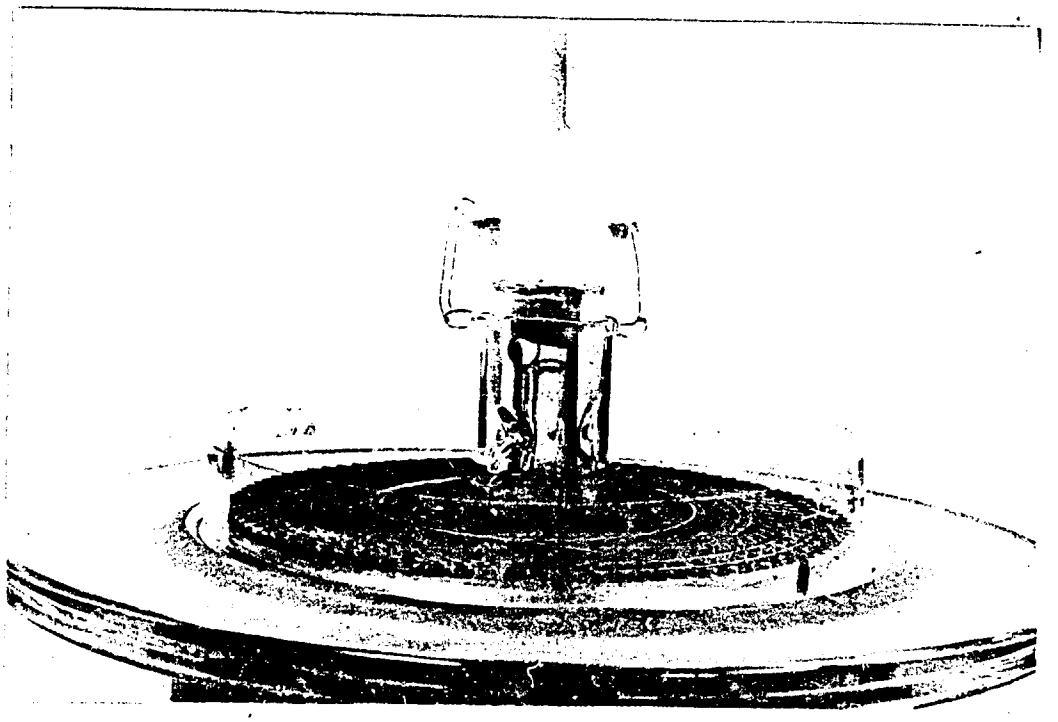
In view of the success with which molecular hydrogen could be dissociated by heated tungsten filaments over the pressure range 1 to 500 torr as described in Chapter 2, Section 2.1(a), it was decided to attempt hydrogen atom production at atmospheric pressure by this method. A series of experiments using different diameter tungsten filaments heated in a stream of hydrogen showed by using mass spectrometric analysis (see Section 3.5) that a detectable concentration of hydrogen atoms survived a few m.m. from the filament at a pressure of 370 torr. It would be expected that at lower gas pressures (e.g. 10 torr), the lower overall rates of hydrogen atom gas phase recombination reactions would have enabled similar concentrations of hydrogen atoms to survive probably 10 to 15 cms from the filament.

To provide a larger area of contact of molecular hydrogen with heated tungsten and to incorporate this method into a burner system, the inverted flame burner shown in Plate 1 was constructed. An inverted flame was necessary since it was anticipated that combustion would start immediately after injection of hydrogen atoms from the filament into the unburnt mixture and this would act as a stabilization point for the

PLATE (1)

BURNER FOR THE INJECTION OF HYDROGEN ATOMS FROM HEATED TUNGSTEN FOIL.





flame. The inner tube from which the hydrogen atoms were injected was constructed from quartz to lower the rates of hydrogen atom surface recombination reactions and the flow velocity of hydrogen and hydrogen atoms horizontally into the unburnt methane-air mixture below the flame could be varied by adjustment of the exit slot, (d). In this way, the importance of the hydrogen atom could be assessed by looking for additional flame stabilization due to hydrogen atoms surviving and producing an additional effect to hydrogen molecules in the flame.

Although thermal methods of atom and radical production have the advantage of not simultaneously generating high concentrations of reactive by-products, this method was later discontinued because a better method became available.

3.2 The Use of Electric Fields

Several different experiments were carried out on an approximately stoichiometric methane-air flame supported on a glass nozzle burner. D.C./A.C./H.F. and microwave fields were applied to the flame using different electrode configurations, some of which are shown in Plate 2. In some experiments, the flames were seeded with CsCl in an attempt to draw Cs^+ ions into the unburnt gases where reactive species could be produced by dissociative ionic recombination reactions such as:

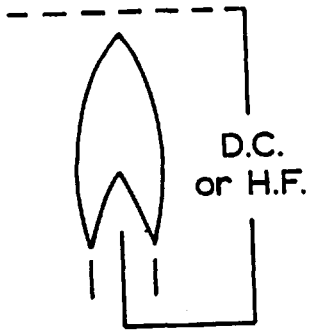
$$Cs^+ + e^- + H_2 \longrightarrow C_s + H + H$$

None of these experiments produced any observable increase in burning velocity although one of the most interesting was that of a R.F. field (Plate 2(D)). In this, a slight haziness was observed in the preheat zone with the applied field. In the case of microwave energy (2,450 MHz, Absorbed Power about 40 W), no change in flame shape was noticed when the resonant cavity was viewed from above (Plate 2(E)), and it was therefore concluded that the effects caused by electric fields on flame reaction rates would be too small to be of practical use.

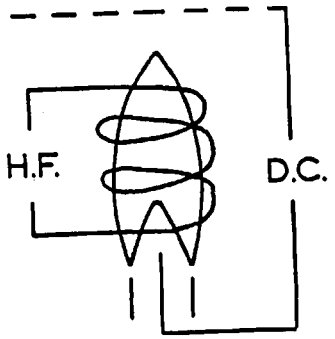
PLATE (2)

THE APPLICATION OF ELECTRIC FIELDS TO METHANE-AIR FLAMES.

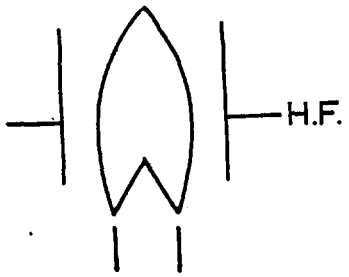
(A)



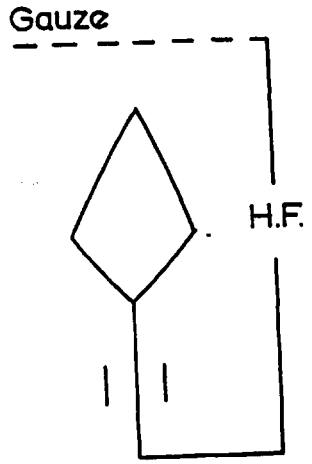
(B)



(C)

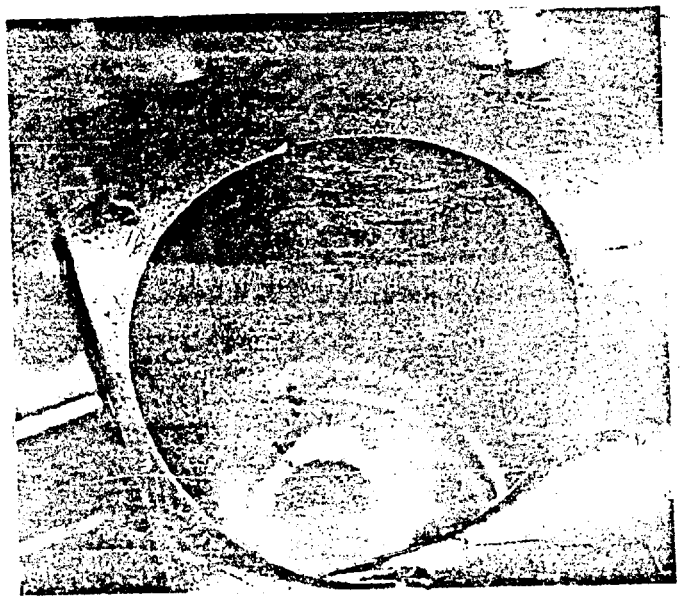


(D)



D.C. = Direct Current
H.F. = High Frequency

(E) Microwave



3.3 High Frequency Discharges

In this research, the production of hydrogen atoms at atmospheric pressure using microwave energy was attempted under similar conditions to those described in Chapter 2, Section 2.1. Power from a 200 W, 2,450 MHz microwave generat[or] (Microtron 2) was supplied to an Evenson 1/4 wave type resonant cavity surrounding a 1 cm O.D. quartz discharge tube. A gas flow of a mixture of argon plus 1 to 5% hydrogen was maintained through the discharge tube at one end of which was a sampling probe for mass spectrometric analysis (see Section 3.5) of the product gases leaving the discharge. With the discharge cavity situated 11 to 15 cms from the sampling probe, hydrogen atoms could not be detected and it was concluded that the concentration of these species had fallen below the detection limits of the mass spectrometer.

In general, the application of electrodeless discharges to combustion systems suffers certain drawbacks. These include the cost and complexity of equipment, the size and bulky nature of the resonant cavity or exciting coil and the instabilities of these discharges when operated at atmospheric pressure. It was therefore decided that the capacitive discharge plasma plug which will be described in Chapter 5, Section 5.2, should be used for the main study in the present research.

3.4 The Use of Calorimetric Methods for the Detection of Hydrogen Atoms

A catalytic probe, non-catalytic probe and isothermal calorimeter were constructed for the detection of hydrogen atoms from a thermal source (tungsten wire). The probes were constructed from 0.2 mm Pt/Pt 13% Rh wire; the junction of one probe being left bare (on which H atoms recombined) and the other coated with a non-catalytic coating for measuring temperature (76). The isothermal calorimeter which consisted of a 3 cm length of 0.002" diameter Pt wire spot welded to 1 mm diameter

tungsten rods formed one arm of a self-balancing Kelvin bridge (30). Both these techniques were easy to construct and use although they suffered the following disadvantages:

(1) The methods were non-specific.

(2) The catalytic activity of a particular surface was not always reproducible.

(3) The method had a low overall sensitivity since in detecting very small concentrations of H atoms in a hot gas (e.g. 800K), the heat liberated by recombination was very much smaller than the heat transferred to the wire by convection.

3.5 The Use of Mass Spectrometry

A molecular beam and mass spectrometer system as shown in Fig.(5) was later used to overcome some of the disadvantages associated with the calorimetric methods (77,78,79,80). Molecular beam gas sampling by 3-stage differential pumping enabled a collision free sample to be transferred from the test region (pressure up to one atmosphere) to the detector chamber (pressure 10^{-6} to 10^{-8} torr) of a quadrupole mass spectrometer (Extranuclear Laboratories, Emba II). The three basic units of the mass spectrometer, that is the ionizer, mass analyser and ion detector had been designed to achieve maximum sensitivity (detecting 1 in 10^6), this being later increased by modulation of the molecular beam using a piezoelectric chopper and processing the signal by phase sensitive detection.

During the early stages of the research, this unit was used to detect H atoms produced by a thermal method (heated tungsten wire) and a microwave discharge. Dissociative ionization of molecular hydrogen in the ionizer (which would otherwise swamp the contribution to the signal of H atoms) was prevented by operating this unit with low electron energies (i.e. in between the appearance potential of H and H_2). With this unit, hydrogen atoms could not be detected from the microwave

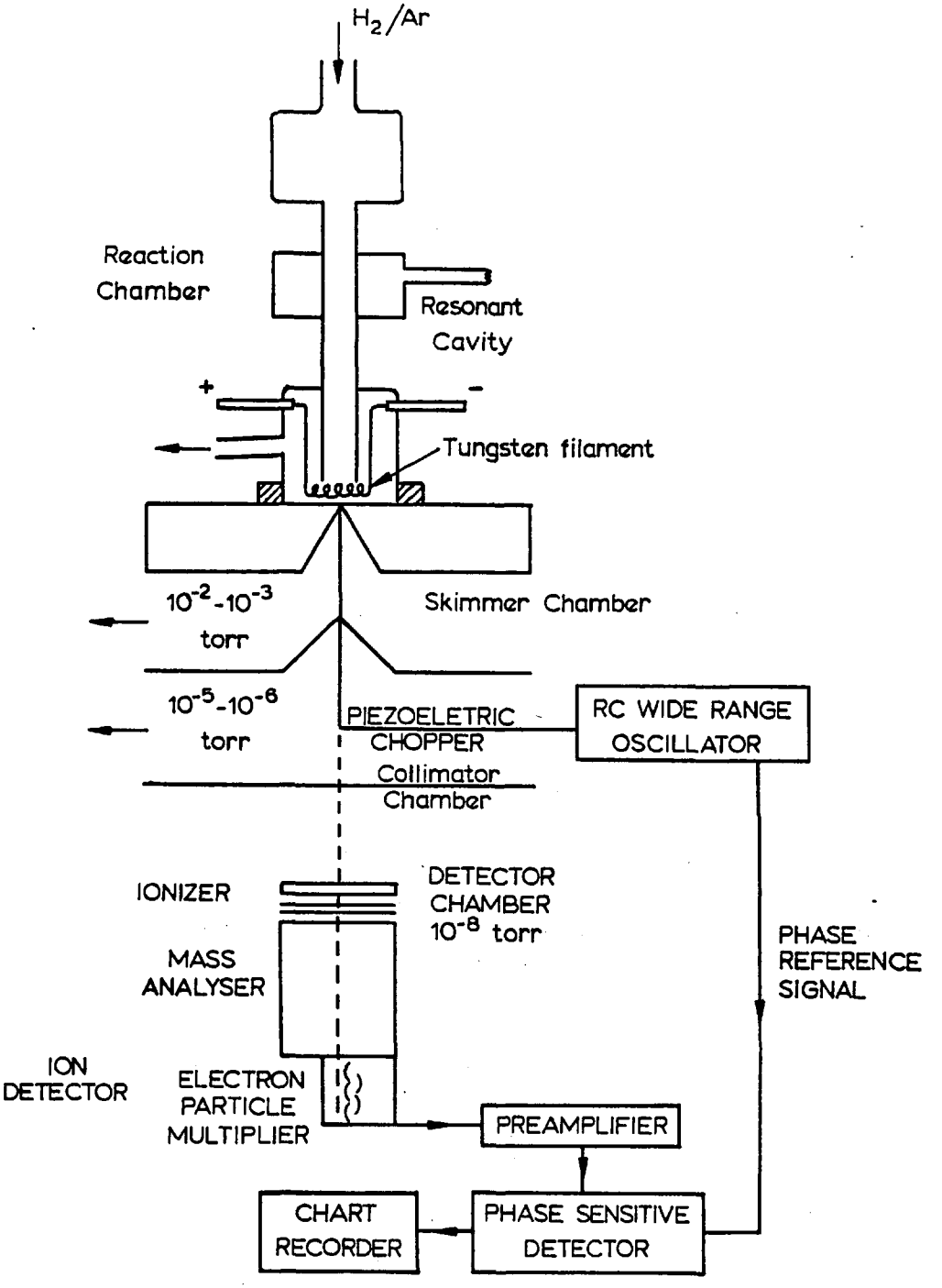


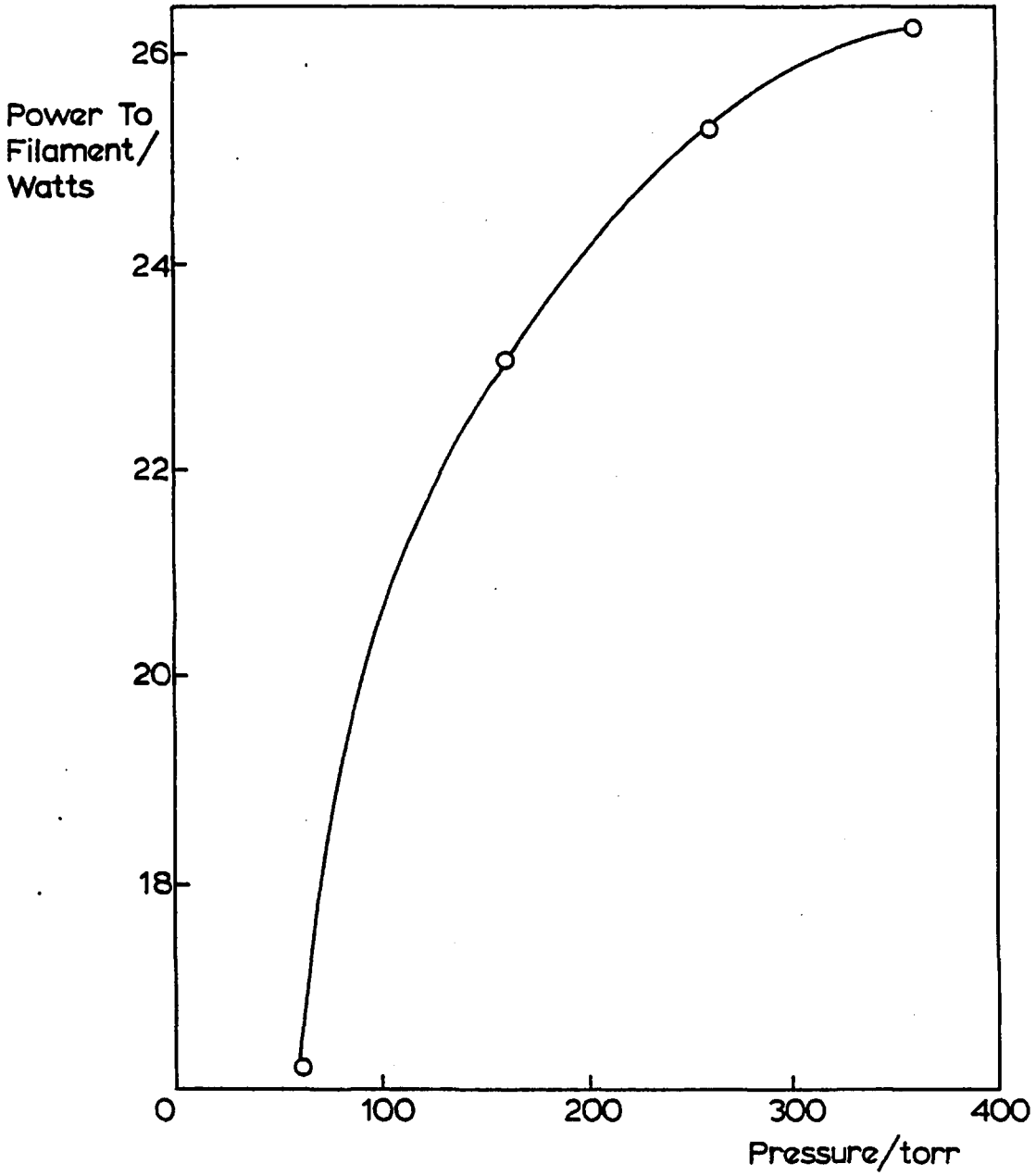
FIG. (5)

REACTION CHAMBER, MOLECULAR BEAM SAMPLER AND MASS SPECTROMETER.

discharge (see Section 3.3) although they were detected at pressures as high as 370 torr using the electrically heated tungsten wire positioned 3 to 4 mm above the sampling probe (see Section 3.1). As the pressure in the reaction vessel was increased from 70 to 370 torr, an increase in the electrical power to the filament was required to produce the same ion current (with manual setting at mass number 1) from the detector and the results are shown in Fig.(6).

This ion current corresponded to a hydrogen atom concentration of about 10^{14} atom cm^{-3}. At pressures greater than 370 torr, the increased rates of 3-body homogeneous recombination reactions together with the mass separation effects within the beam, prevented detection of H atoms.

Although the versatility of this unit for the detection of atoms and radicals over a wide mass range was appreciated, the method was later discontinued since it was anticipated that the sampling probe would cause a severe physical distortion of an expanding plasma ignited flame kernel. Also uncertainties exist in the calibration procedures for this method. For these reasons, the use of a spectroscopic method was considered more suitable than the probe methods which were examined and as described in Chapter 2, Section 2.3, absorption spectroscopy (see Chapter 4) was considered the most suitable of these spectroscopic techniques for studying plasma ignited flames.



FIG(6)

POWER REQUIRED TO HEAT TUNGSTEN FILAMENT FOR DETECTION OF H ATOMS BY MASS SPECTROMETER

CHAPTER 4

THE DEVELOPMENT OF THE OH RESONANCE ABSORPTION TECHNIQUES

4.1 Reasons for the use of the OH Radical

It is widely recognised that the OH radical is an important reaction intermediate in flames especially during the initial stages of combustion which are perhaps the most relevant to the ignition process. For example, during the initial stages of oxidation of a hydrocarbon RH, the most important reactive species are H, OH, O and R· and only the elementary reactions which are first order with respect to these need to be considered. In the case of methane oxidation, studies on low pressure CH_4-H_2-O_2-N_2O-Ar flames (87) have shown that

$$\frac{-d\,[CH_4]}{dt} = [CH_4]\,(k_1\,[H] + k_2\,[OH] + k_3\,[O]) \qquad (4.1)$$

where

$$k_1 = 2 \times 10^{11}\, e^{-\frac{11.5}{RT}}\ \ell\,mole^{-1}\,s^{-1}$$

$$k_2 = 3.5 \times 10^{11}\, e^{-\frac{9}{RT}}\ \ell\,mole^{-1}\,s^{-1}$$

and

$$k_3 = 2 \times 10^{9}\ \ell\,mole^{-1}\,s^{-1} \quad \text{at} \quad 1600\ K.$$

The reaction with oxygen atoms was regarded as unimportant (k_3 small) and for fuel rich flames with $\frac{[OH]}{[H]} = 0.06$ to 0.2, the attack by hydrogen atoms predominated. In lean mixtures $\frac{[OH]}{[H]}$ was about 40 times larger and the attack by OH radicals predominated. In a similar study (88), probe sampling of low pressure, flat, premixed flames of CH_4, C_2H_2 or C_3H_8 with O_2 and Ar showed from measurement of $\frac{-d\,[O_2]}{dt}$ and [H] that the reaction $H + O_2 \rightleftharpoons OH + O$ is primarily responsible

for the consumption of O_2.

Clearly during the initial stages, the reactive species, H, OH and O will be more or less equilibrated by a number of elementary radical molecule reactions. These reactions have been studied extensively in the post flame gases of hydrogen-air flames (89,90) in which it was usually possible to relate $[OH]$ quantitatively to the concentration of other reactive intermediate species, all of which have been found in concentrations much higher than that predicted from thermodynamic equilibrium considerations. For hydrogen rich flames (89), $[O]$ was considered too small to be of importance and equilibration between H and OH took place by the fast reaction

$$OH + H_2 \underset{}{\overset{k_1}{\rightleftharpoons}} H_2O + H \tag{4.2}$$

with

$$[H] = \frac{k_1 [OH] [H_2]}{[H_2O]}$$

Decay then proceeded via the slow 3 body recombination reactions:

$$H + OH + M \longrightarrow H_2O + M \tag{4.3}$$

and

$$H + H + M \longrightarrow H_2 + M \tag{4.4}$$

In lean mixtures (90), H and OH were equilibrated by the reactions

$$OH + H_2 \rightleftharpoons H_2O + H \tag{4.5}$$

$$H + O_2 \rightleftharpoons OH + O \tag{4.6}$$

and

$$O + H_2 \rightleftharpoons OH + H \tag{4.7}$$

with

$$[H] = \left(\frac{k_4}{k_5 k_6}\right) \left(\frac{[OH]^3}{[H_2O] [O_2]}\right) \tag{4.8}$$

Kinetic equilibration following injection of reactive species (e.g. H atoms) from a plasma into a methane-air mixture or flame will be controlled by reactions such as (4.5), (4.6) and (4.7) with competition from reactions (4.3) and (4.4). In this case, although a much larger reaction scheme must be considered, any increase in $[H]$, $[O]$ or $[CH_3]$ will quickly manifest itself as an increase in $[OH]$ which is being measured.

This is supported by some calculations (91), on the three stages of oxidation of methane (i.e. induction, methane consumption and CO oxidation) using detailed chemical reaction schemes. These have shown that during the induction period, the concentrations of H, O, OH, HO_2 and CH_3O remain in a quasi-steady state in the sense that the rates of creation and consumption are very nearly equal, although the concentrations change. The concentration of the methyl radical on the other hand, rises considerably since its rate of creation is very much faster than the rate at which it is consumed. This growth of CH_3 characterises the induction period which ends when the reaction rates become large enough to cause a rapid increase in temperature.

The concentration of OH continues to remain important throughout the subsequent methane consumption and CO oxidation stages. Once methane has been consumed, the four following reactions dominate the oxidation of CO above 2000 K.

$$CO + OH \longrightarrow CO_2 + H \qquad (4.9)$$

$$H + O_2 \longrightarrow OH + O \qquad (4.10)$$

$$O + H_2O \longrightarrow 2OH \qquad (4.11)$$

$$H + OH + M \longrightarrow H_2O + M \qquad (4.12)$$

As soon as all the C-H bonds have been broken, the radical concentrations begin to rise and since a steady state for O and H can

be assumed and reaction (4.11) omitted, the rate equation for OH becomes

$$\frac{d\,[OH]}{dt} = 2k_1\,[CO] \qquad (4.13)$$

Eventually, the radical concentrations become high enough for reaction (4.11) to become important and the $[OH]$ reaches a steady state value (well above the final equilibrium value) which is given by

$$[OH] = \frac{k_4\,[O_2]}{k_6\,[M]} \qquad (4.14)$$

Apart from the importance of the OH radical as a reactive intermediate in combustion reactions, its absorption spectrum lies in the accessible ultraviolet region, unlike that of H and O which lie in the experimentally difficult vacuum ultraviolet region. The other possibility was to measure CH_3 in absorption in the spectral region of about 216 nm using the same apparatus as that used for the OH measurements (92). However, initially, this may have posed additional problems to those of the OH absorption technique when applied to a study of plasma jet ignition especially in connection with the detection sensitivity.

4.2 The Theory of Absorption Spectroscopy

Theoretical relationships can be derived which enable the conversion of experimental absorption measurements to concentrations of absorbing species (93). These also exemplify the use of standard calibration curves which become essential when there is insufficient information on line profiles or temperatures to enable the direct calculation of absolute concentrations from light absorption measurements.

For a parallel beam of radiation with discrete line frequency, υ, and intensity $I^o(\upsilon)$, passing through a uniform gas layer of thickness L, the transmitted intensity, $I(\upsilon)$ is given by :

$$I_{(\upsilon)} = I^{o}_{(\upsilon)} \exp(-k_{\upsilon} L) \tag{4.15}$$

or

$$k_{\upsilon} = \ln\left(\frac{I^{o}_{(\upsilon)}}{I_{\upsilon}}\right) / L \tag{4.16}$$

where k_{υ} is the absorption coefficient at frequency υ ($k_{\upsilon} \geq 0$) and is independent of I_o and L.

The variation of k_{υ} with frequency for a typical absorption line profile is shown in Fig.(7) indicating quantities such as peak absorption coefficient, k_o and spectral half widths, Δ_{υ}. This line profile of k_{υ} as a function of frequency can be calculated if the effective line broadening parameters are known. For example, using the general expressions representing Gaussian and Lorentzian functions (94), the following Voigt expression can be derived:

$$k_{\upsilon} = Ca\,\beta_1 \int_{-\infty}^{\infty} \frac{e^{-y^2}}{a^2 + (w-y)^2}\, dy \tag{4.17}$$

where

$$y = \frac{x}{\beta_2}$$

$$w = \frac{(\upsilon - \upsilon_o)}{\beta_2}$$

and

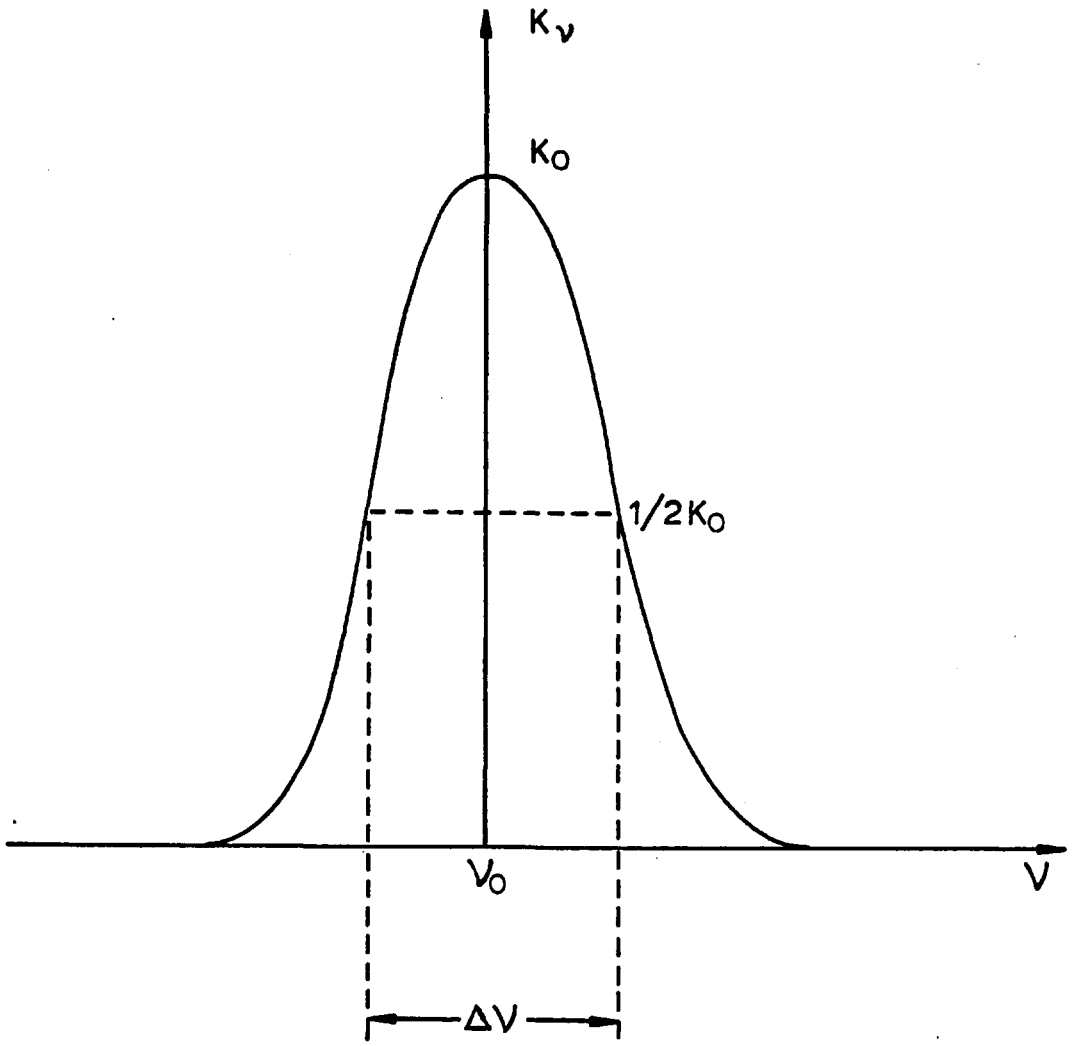
$$a = \frac{\beta_1}{\beta_2}$$

Since the constants β_1, β_2 and C can be related to the half-widths of the absorption profile:

$$\beta_1 = \frac{\Delta \upsilon_c}{2}, \qquad \beta_2 = \frac{\Delta \upsilon_D}{\sqrt{2 \ell n 2}}$$

and

$$C = \frac{2k'_o}{\Pi\, \Delta\upsilon_c}$$



FIG(7)

VARIATION OF ABSORPTION COEFFICIENT, K_ν, WITH FREQUENCY, ν, OF A TYPICAL SPECTRAL LINE.

where

$\Delta \upsilon_c$ = sum of Lorentzian type functions

$\Delta \upsilon_D$ = Doppler half-width

k'_o = peak absorption coefficient which would be obtained with an absorption line broadened only by the Doppler effect.

Substitution into equation (4.17) gives

$$k_\upsilon = \frac{k'_o a}{\pi} \int_{-\infty}^{\infty} \frac{e^{-y^2}}{a^2 + (w-y)^2} dy \qquad (4.18)$$

Equation (4.18) together with equation (4.15) can be used for theoretical calculations for the variation of light absorption with concentration similar to the experimentally determined curve shown in Fig.(8).

On the other hand, by integrating k_υ with respect to υ over the entire absorption line, a fundamental relationship between the integrated absorption coefficient, K, and the concentration of absorbing species in the lower excitational stage, Nj, can be used which is independent of the physical processes responsible for the broadening of the line. i.e.

$$K = \int_{line} k_\upsilon d_\upsilon = \frac{\pi e^2}{mc^2} \; fji \; Nj \qquad (4.19)$$

where e = charge of an electron

m = mass of an electron

c = speed of light in vacuo

fji = line oscillator strength

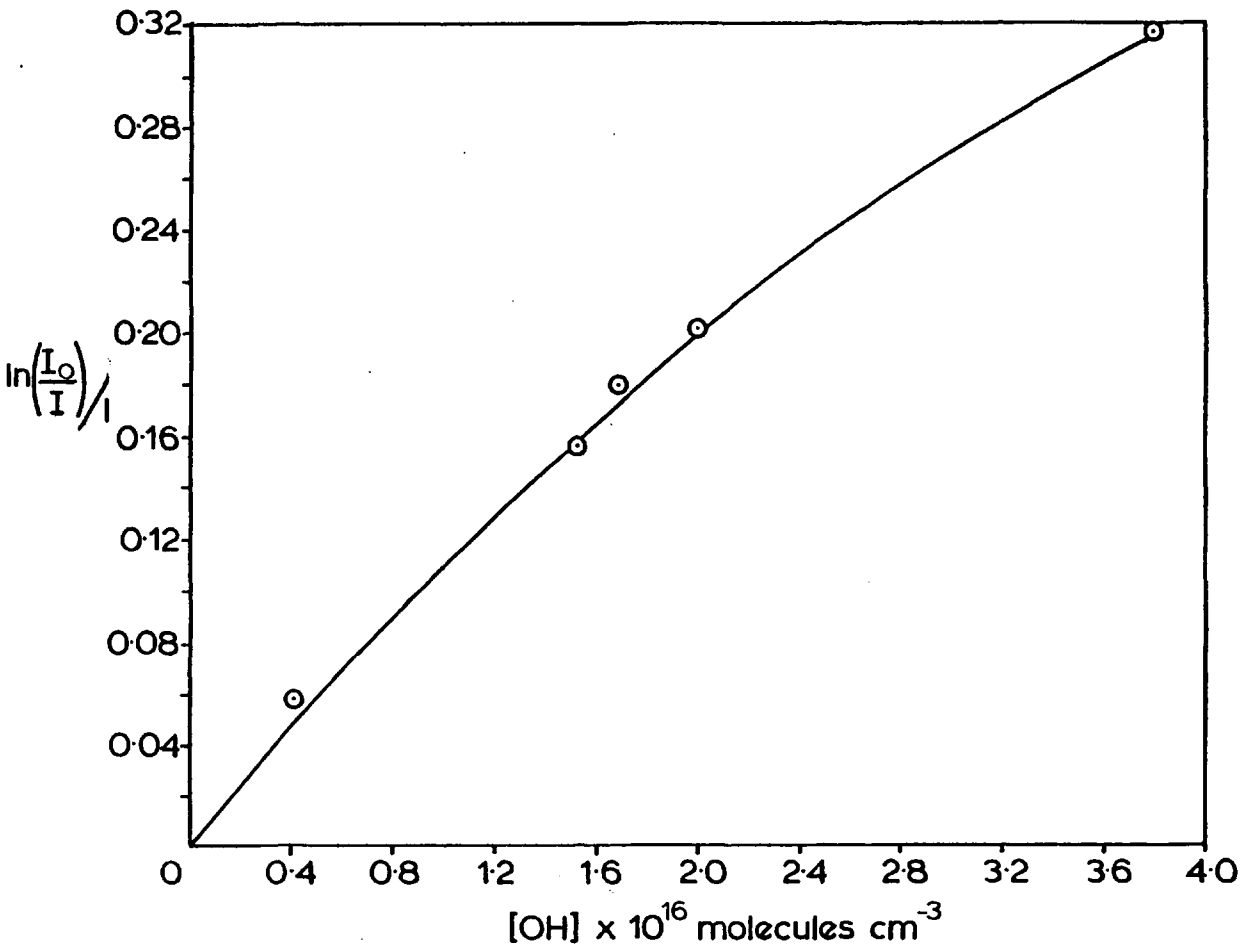


FIG. (8)

CALIBRATION CURVE (1) FOR THE OH RESONANCE ABSORPTION TECHNIQUE

However, in this research it would not have been possible to measure K for two reasons. Firstly, a spectrometer of extremely high resolving power would be required to record the absorption line profile. Secondly, it would have been extremely difficult to obtain this profile in the short duration associated with an expanding plasma jet ignited flame. For these reasons, only peak absorption measurements were taken, k_o corresponding to υ_o (Fig.7), which are related to the integrated absorption coefficient, K, and the half-width, $\Delta\upsilon$ by

$$k'_o = b \frac{2}{2\upsilon} K \tag{4.20}$$

where b depends on the type of broadening which prevails (95, 46). Its numerical value can range from $1/\pi$ for pressure (Lorentz) broadening to $(\ln \frac{2}{\pi})^{1/2}$ for Doppler broadening and can take intermediate values according to the $\frac{\Delta\upsilon L}{\Delta\upsilon D}$ values. If $\Delta\upsilon$ is independent of Nj (e.g. when there is no self absorption), then from equations (4.16), (4.19) and (4.20)

$$\ln \left(\frac{I^o(\upsilon_o)}{I_{(\upsilon_o)}}\right) = b \frac{2}{\Delta\upsilon} \frac{\pi e^2}{mc^2} fji\, Nj\, L \tag{4.21}$$

Often, it is convenient to express light absorption measurements in terms of the total absorption factor, A_T defined by :

$$A_T = \frac{\text{Absorbed Radiation Intensity}}{\text{Incident Radiation Intensity}} = \frac{\Delta I}{I_o} = \frac{I_o - I}{I} \tag{4.22}$$

since $I_o = \int I^o_\upsilon \, d\upsilon$ and $I = \int I_\upsilon \, d\upsilon$,

Equation (4.22) can be rewritten as

$$A_T = \frac{\int I^o_\upsilon \, d\upsilon - \int I^o_\upsilon \, e^{-k_\upsilon L} \, d\upsilon}{\int I^o_\upsilon \, d\upsilon} \tag{4.23}$$

Assuming I^{o}_{υ} is integrated over the same limits as k_{υ}, equation (4.23) becomes

$$A_T = \frac{\int I^{o}_{\upsilon} \, d\upsilon \int (1 - e^{-k_{\upsilon} L}) \, d\upsilon}{\int I^{o}_{\upsilon} \, d\upsilon} \tag{4.24}$$

or

$$A_T = \int (1 - e^{-k_{\upsilon} L}) \, d\upsilon \tag{4.25}$$

For a sharp source line (e.g. that emitted from a hollow cathode lamp), the limits of integration of Equation (4.25) differ by the width of the source line, $\Delta \upsilon_s$.

Approximating the usual Gaussian function by a triangular one, Equation (4.25) becomes

$$A_T = (1 - e^{d k'_o L}) \int_o \frac{\Delta \upsilon_s \sqrt{\pi}}{2 \sqrt{\ln 2}} \, d\upsilon \tag{4.26}$$

where

$k_{(\upsilon = 0)} = d k'_o$

d = a constant

For small $k'_o L$ (using the approximation $(1 - e^{-x}) = x$ for small values of x, equation (4.26) becomes

$$A_T = \frac{I_o - I}{I_o} = d k'_o L \, \frac{\Delta \upsilon \sqrt{\pi}}{2 \sqrt{\ln 2}} \tag{4.27}$$

Using equation (4.20) for a Doppler broadened line, i.e.

$$K = \frac{2 \sqrt{\ln 2}}{\sqrt{\pi} \, \Delta \upsilon} \, k'_o \tag{4.28}$$

and equation (4.19) relating K with Nj, equation (4.27) becomes

$$A_T = d \frac{\Delta \upsilon_s}{\Delta \upsilon_D} \frac{\pi e^2}{mc^2} fji\ Nj\ L \qquad (4.29)$$

that is, A_T varies linearly with Nj for a given path length L. At high values of $k'_o L$ (for strong absorption), the approximation $e^{-d k'_o L} = 0$ can be made and

$$A_T = \frac{\Delta \upsilon_s \sqrt{\pi}}{2 \sqrt{\ln 2}} \qquad (4.30)$$

i.e. the absorption reaches a constant value independent of Nj. This behaviour (A_T varying linearly with Nj for small $k'_o L$ and becoming independent of Nj at high values of $k'_o L$) is illustrated in Fig.(9), which shows the characteristic curvature of the graph of A_T against $[OH]$.

The theory which has been outlined so far is strictly for absorption by atoms but is also applicable to that of molecules or radicals such as OH. In this case, the strength of the electronic transition is dissipated over many individual lines corresponding to rotational and vibrational degrees of freedom. This results in the absorption intensity being generally less than that of atoms consequently lowering the ultimate sensitivity of the method (whilst reducing errors due to self absorption). This reduction in sensitivity is not so severe for the OH $A^2\Sigma^+ - X^2\Sigma$ resonance system (Figs.(10) and (11)) since the intensity is concentrated in a few lines of the (0,0) band with low values of k which are quite widely separated (96). Using equation (4.21), the concentration of OH in the rotational level i of the ground electronic state can be expressed as

$$[OH]_i = \frac{mc^2}{\pi e^2} \frac{2b}{\Delta \upsilon} \frac{1}{fji} \ln\left(\frac{I^o(\upsilon_o)}{I_{\upsilon_o}}\right) / L \qquad (4.31)$$

where fji is the line oscillator strength.

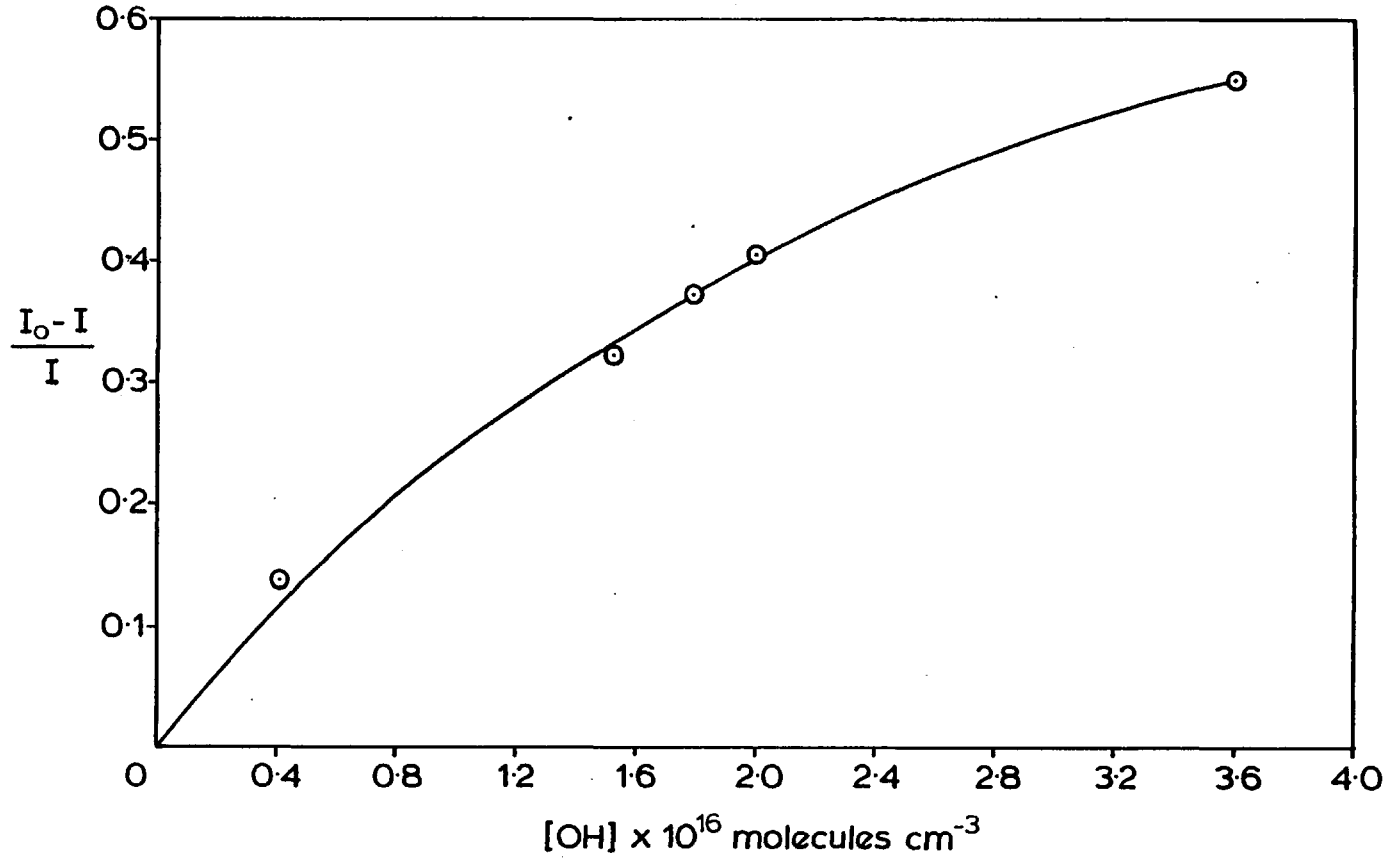


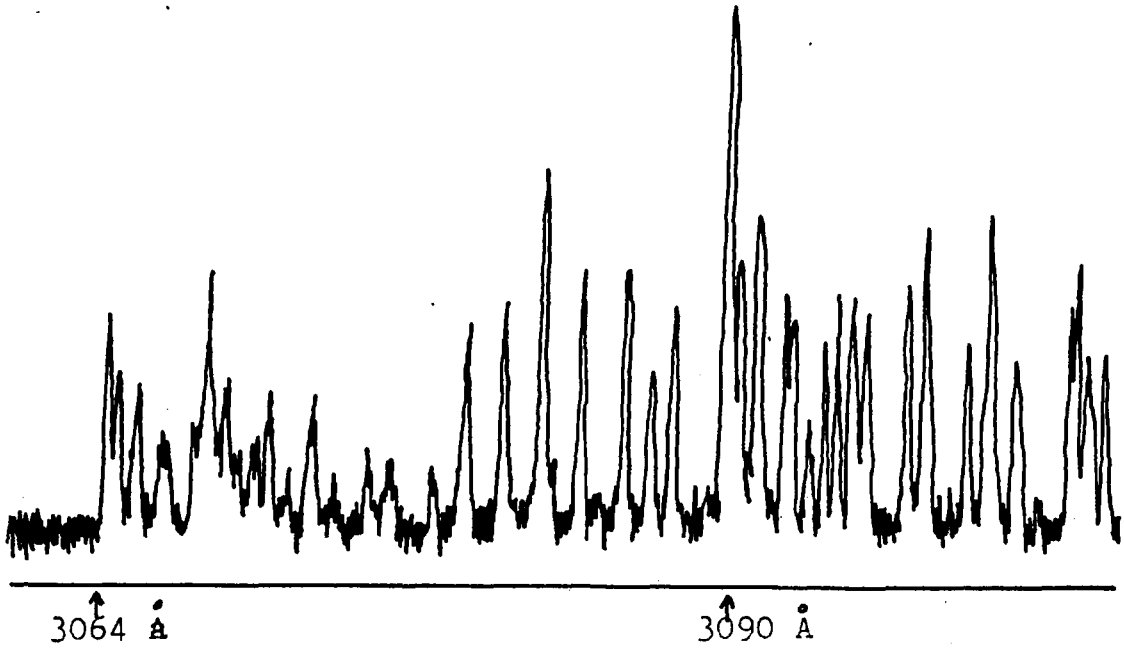
FIG. (9)

CALIBRATION CURVE (2) FOR THE OH RESONANCE ABSORPTION TECHNIQUE

FIG.(IO)

The Emission Spectrum of the $^2\Sigma^+-^2\Pi$ Transition of CH in the Spectral Region 3065-3105 Å Emitted from a Hollow Cathode Lamp.

(I) Pressure 0.7 torr



(2) Pressure 0.9 torr

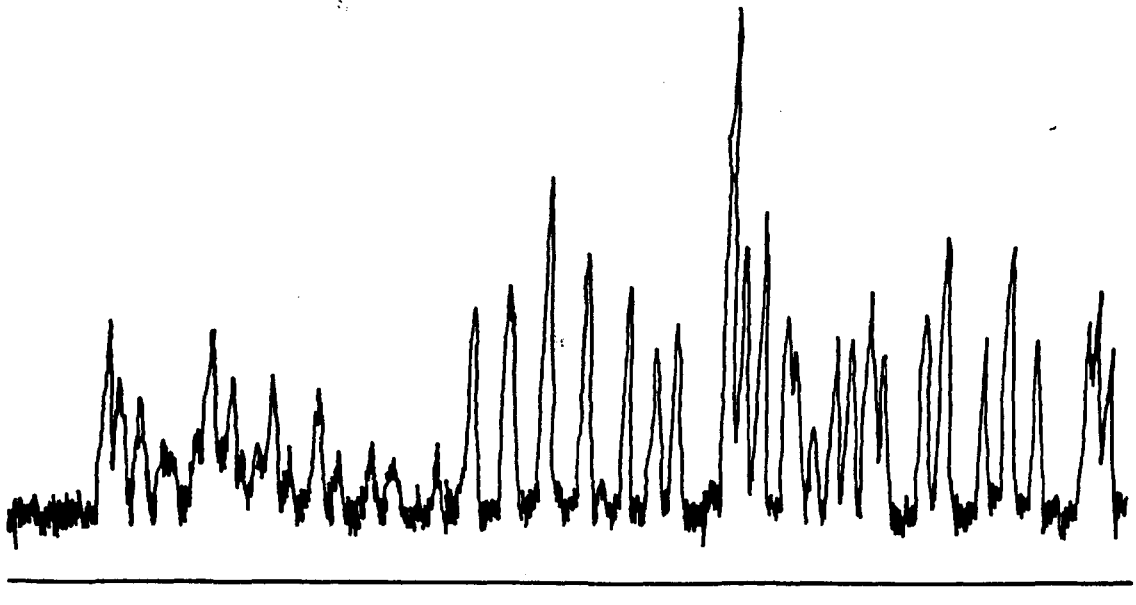
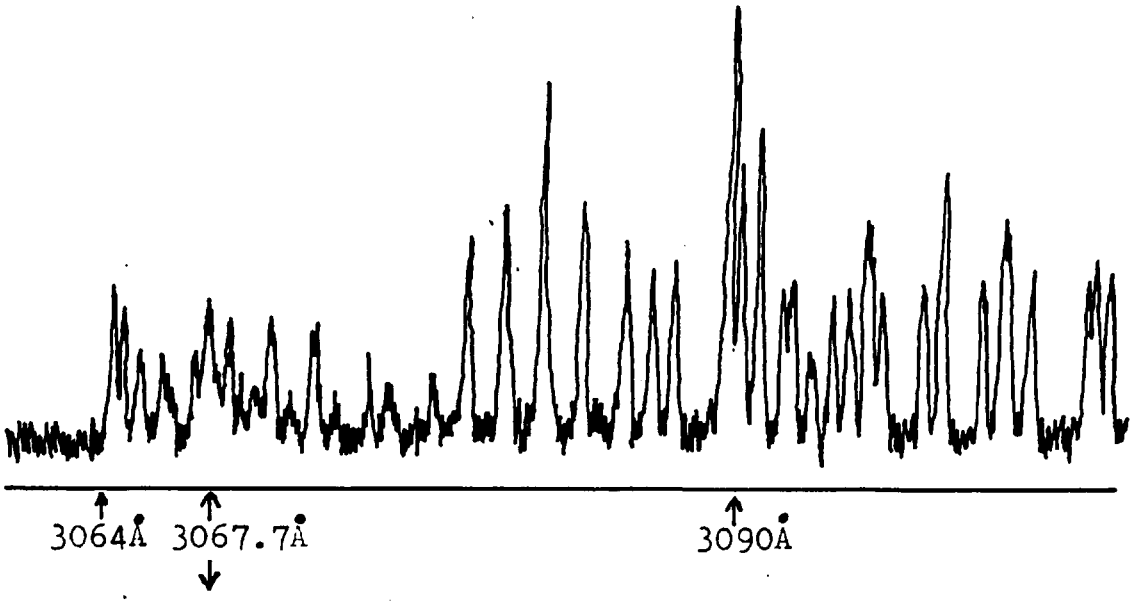
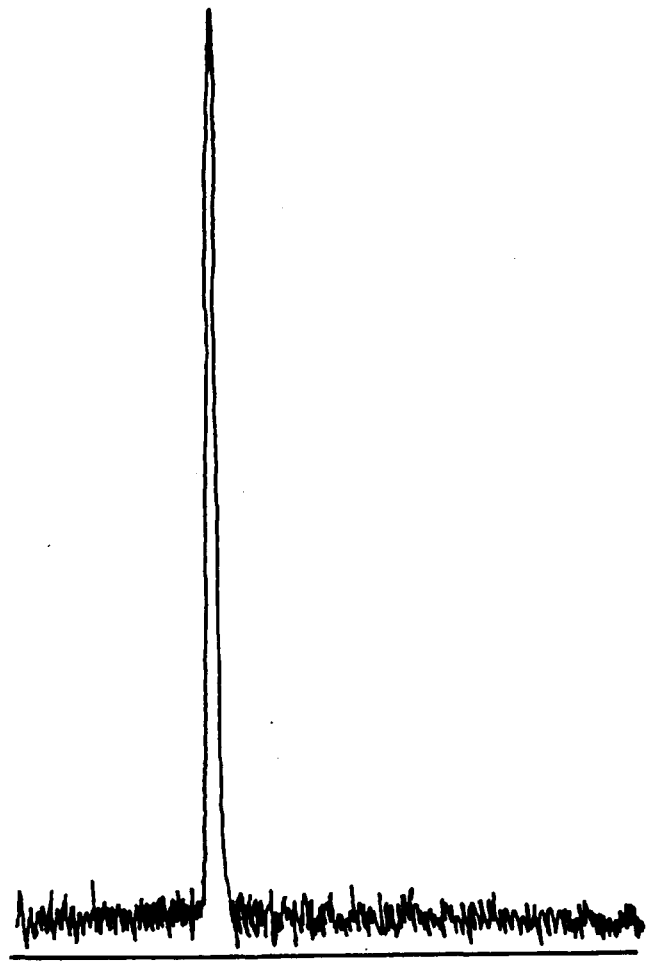


FIG.(II)

The Emission Spectrum of the $^2\Sigma^+ - ^2\pi$ Transition of OH in the Spectral Region 3065-3105 Å Emitted from a Hollow Cathode Lamp.

(3) Pressure I.0 torr.





The Bismuth Line at 3067.7 Å Emitted from a Hollow Cathode Lamp.

It can be shown, see ref.(89), that

$$f_{ji} = 3.07 \times 10^{-4} \frac{Ak}{(2J + 1)} \qquad (4.32)$$

where Ak is the relative transition probability and J is the rotational quantum number in the lower $^2\pi$ state. The total OH concentration in the $X^2\pi$ state, $[OH]$ is given by :

$$[OH] = [OH]_i \, (Q_{r,v}) \left[(2J + 1) \cdot \exp\left(\frac{-E_i}{RT}\right) \right]^{-1} \qquad (4.33)$$

where $Q_{r,v}$ is the rotation-vibration partition function and E_i is the rotational energy for level i.

Also

$$Q_{R,V} = \left(\frac{kT}{hcB}\right) \sum_h \exp\left(\frac{-E_n}{kT}\right) \qquad (4.34)$$

where k is the Boltzmann constant, h is Planck's constant, B is the rotational constant for OH, c is the velocity of light and E_n are the energies of the vibrational levels n.

From equations (4.31) and (4.33), we get

$$[OH] = \frac{mc^2}{\pi e^2} \frac{2b}{\Delta\upsilon} \ln\left(\frac{I^o_{(\upsilon o)}}{I_{\upsilon o}}\right) / L \times Q_{r,v} (\exp E_i/RT)^{-1} \times \frac{3.26 \times 10^3}{Ak} \qquad (4.35)$$

Equation (4.35) enables absolute concentrations of OH to be obtained directly from light absorption measurements if adequate information is available on parameters such as the absorption line profiles and line oscillator strengths. However, because of the uncertainties in these, the use of calibration curves of $\ln\left(\frac{I_o}{I}\right)/L$ against $[OH]$ (Fig.(8)) or A_T against $[OH]$ for a given L (Fig.(9))

became imperative for the interpretation of absorption measurements obtained from the plasma jet ignition studies.

4.3 The Method

In this method, a specific light source has been used which provides high sensitivity for measuring OH concentrations. This avoids the need to use a multiple reflection system which is usually necessary when a continuum light source such as a high pressure Xenon lamp is used (97). Such a multipass system would have been difficult to incorporate into the final configuration of apparatus used (see Plate (3)) and would have had an unacceptably lower spatial resolution than that of the discrete line source method developed in the present research. Also the method of interpretation of the measured quantities is somewhat easier for a discrete line source than with a continuum source especially if calibration curves are not used. For these reasons, a large part of this reasearch was devoted to optimising the specific light source with a discrete line frequency to provide a simple, reliable and sensitive method for monitoring OH concentrations of plasma ignited flames.

4.4 Experimental

The feasibility of the present method was first examined using a slightly modified atomic absorption spectrophotometer (described in Section (4.4(c)) after which the apparatus shown in Fig.(12) was constructed. The products of H_2-Air and CH_4-Air flames stabilised on porous plug burners were used as a source of OH for obtaining the calibration curves described in Section (4.5(c)). Later it was found that before the method could be successfully applied to a study of ignition by plasma jet, modifications to the method of signal processing became necessary and this is described in Section (4.4(d)).

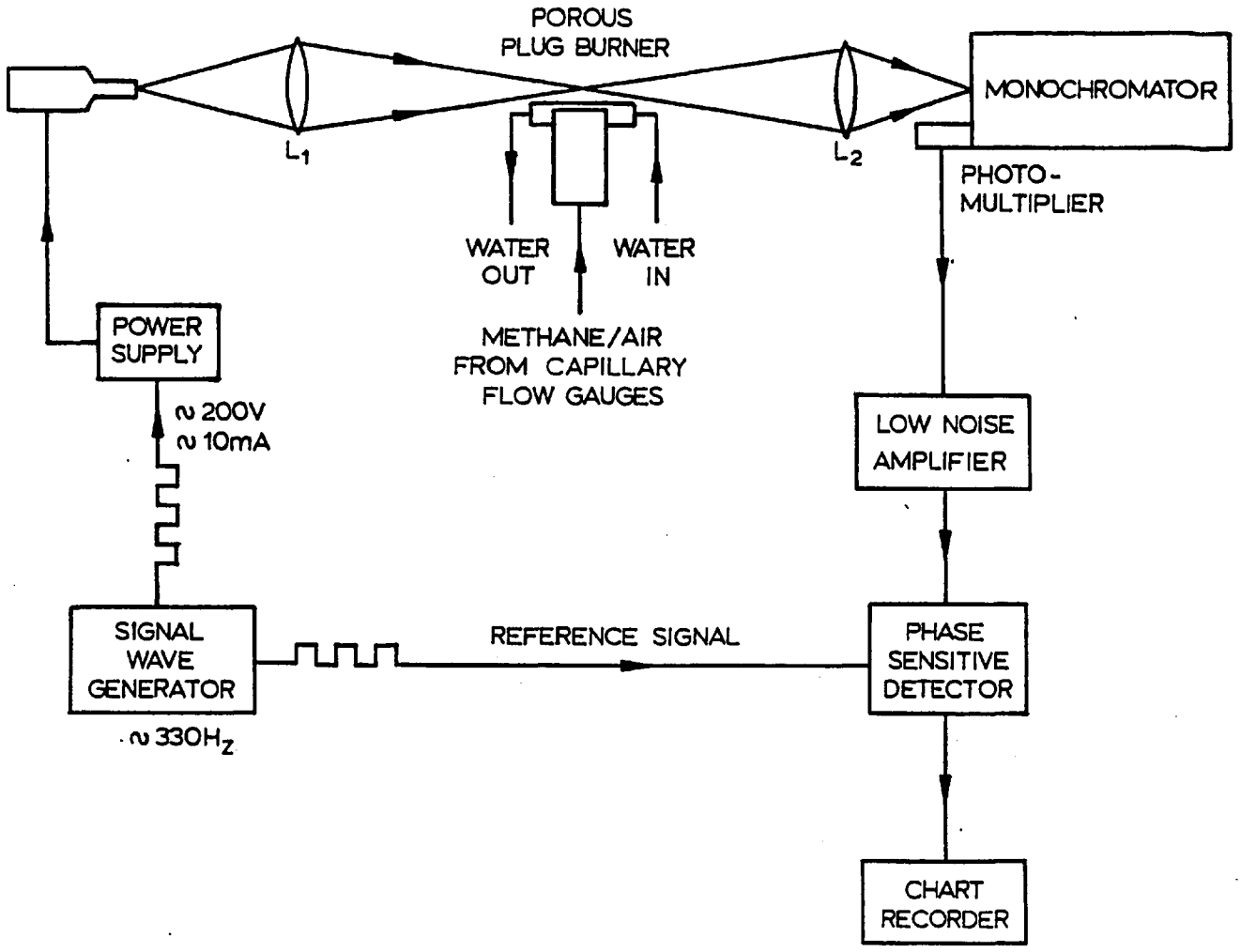


FIG. (12)

THE APPARATUS FOR THE OH RESONANCE ABSORPTION TECHNIQUE.

(a) The Optics

Referring to Fig.(12), light from the lamp (Section 4.4(c)) was brought to a focus by lens, L_1 (quartz - focal length 15 cms, diameter 3.2 cms) above the burner and refocussed by lens, L_2 (same specifications as lens L_1) onto the entrance slit of a 50 cms Ebert grating spectrometer (manufactured by the Jarrel-Ash Company, Model 82-000). The average width of the beam as it passed over the burner was about 2 mm. The resolution of the spectrometer was at least 0.2 Å in the first order using a 1180 grooves/mm grating and 10 μ slits. A single control calibrated in 2 μ units operated the adjustment of the entrance and exit slits between the limits of 5 and 400 μ. Throughout the work described in this thesis, a slit width of 65 μ was used with a grating blazed at 4000 Å.

(b) The Burners

Two water cooled porous plug burners (one 5 cms in diameter and the other 2.5 cms diameter) were used for stabilising premixed hydrogen-air and methane-air flames for the calibration measurements. Basically these consisted of (98,99) a pipe containing glass beads and capped at one end with a uniform porous plug through which the flammable mixture was forced. If the velocity of the mixture flowing from the plug is less than the normal burning velocity, the flame stabilises itself as a flat flame in close proximity to the porous plug. Since heat is transferred from the flame to the plug at a rate depending on the mass velocity of the gas, the final flame temperature and consequently the OH concentration could be varied independently of the mixture composition.

Two different flames and burner diameters were used to provide the widest possible variation of $\ln(\frac{I_o}{I})/L$ (α [OH]) values possible. Also edge effects due to the hot flame gases mixing with the surrounding cold air could be eliminated using the two burners of different diameters.

Alternatively, these edge effects (which were found to be almost negligible) could be eliminated by taking a second reading for each measurement with the beam slightly displaced from the central axis. Screening the flame with an inert gas to avoid an outer diffusion flame became unnecessary since throughout the calibration measurements only lean flames were used.

For each OH light absorption measurement, the flame temperature was measured at the same position within the flame using a thermocouple (for the methane-air flames) or Na-D line (for the hydrogen-air flames). In the case of the thermocouple temperature measurements, the thermocouple was positioned at the focus of the ultra-violet beam. This was achieved by slowing moving the thermocouple junction towards the focussed OH light beam (with the OH detection system in operation) until any further slight movement resulted in a large loss of light reaching the photomultiplier tube (and hence P.M. signal). This resulted in a small error since the temperature variation across the flame was about 50°C and the measured flame temperature would be slightly higher than the average temperature along the diagnostic beam. In spite of this, because of the high stability and uniformity associated with these flames, the use of porous plug burners enabled accurate calibration curves to be constructed which are described in Section (4.5(c)).

(c) The Light Source

The capabilities of the OH resonance absorption technique are, to a large extent, determined by the performance characteristics of the light source. As mentioned previously, a discrete line source which would provide high sensitivity for a small absorption path length through the flame was required. Light sources which exhibit this property include hollow cathode lamps, electrodeless discharge lamps and lasers. Although the use of a tunable dye laser has many advantages, the most important being that of providing high spatial resolution and ease of interpretation

of measured quantities, the need for frequency doubling of the laser radiation, complicates the use of this method. Similarly, electrodeless (e.g. microwave) low pressure discharges whilst being much simpler to construct, have certain drawbacks. The most serious of these concerns the difficulty in stabilising the output of microwave power from a magnetron valve source (94). This is due to the vary large changes of magnetron power with slight fluctuations in the voltage. For example, a power source operated from a supply voltage stablized to 0.1% would still give output fluctuations of several watts for a generator with 100 to 200 watts full power rating. Also very precise tuning of the resonant cavity to couple microwave power to the discharge is required initially and if this is later changed (by, for example, vibration) it may cause fluctuations in the output of light from the lamp.

The other disadvantage associated with the use of electrodeless discharges as light sources concerns the self absorption and line reversal of the emitted light from the discharge over certain operating pressure ranges. To avoid radiation from the emitting species in the hotter parts of the discharge passing through cooler regions (causing self absorption and line reversal), the length of the discharge region is limited to about 3 mm (100). Since pressure broadening of the emission line is reduced by operating the discharge at low pressure, the optimum operating pressure for these discharges has been shown to be about 3 torr.

The use of hollow cathode lamps as fine line sources avoids the disadvantages associated with the use of lasers or electrodeless discharges. The advantages include (1) low self absorption of resonance lines, (2) good stability with a high signal to noise ratio and (3) simplicity of design and operation.

(1) The Hollow Cathode Lamp

The attractive properties and simplicity of a hollow cathode lamp led to the idea that OH absorption measurements could be made using the

exact coincidence of a very narrow metallic resonance emission line from such a lamp with the OH $^2\Sigma^+ - ^2\Pi$ absorption spectrum. The best known coincidence of this type in atomic absorption spectrophotometry (in which it is regarded as a nuisance) is that of the Bismuth line at 3067.72 Å with the R_2 (10) line of OH. It was therefore decided that the preliminary work examining the use of this line for OH absorption measurements could be done using a commercial atomic absorption spectrophotometer.

With this in mind, a Perkin-Elmer Spectrophotometer was modified to enable OH absorption measurements to be made on a methane-air flame (absorption path length approximately 1.5 cms) stabilized on a glass nozzle burner. In this way, the absorption characteristics of several different metallic lines in the spectral region 3060-3100 Å were examined as a function of flame stoichiometry and position of the beam in the flame. The results are discussed in Section (4.5).

The Mechanism of Excitation in a Hollow Cathode

Since the design and operation of various hollow cathode lamps are described in detail in Ref.(94), only the more important aspects relevant to the present method are covered in this section.

A hollow cathode lamp consists of a sealed tube filled with an inert carrier gas at a pressure of a few torr. The discharge is struck between the anode and a hollow cylindrical cathode which is lined with the metal under consideration. At the operating pressure, the discharge concentrates in the hollow cathode giving high current densities and a low cathode-potential fall on the inner surface of the cathode. This is accompanied by a high concentration of ions which bombard the inner cathode surface giving a strong sputtering action and displacing metallic atoms from the cathode surface. These atoms are excited by second order collisions with the high concentration of inert gas atoms and ions to give

very intense emission spectra. At the operating current, this emission spectrum should be free from self absorption and line broadening factors (e.g. Stark and resonance broadening) and thereby produce extremely sharp lines ideal for resonance absorption spectroscopy.

(d) Signal Processing

The apparatus which was originally constructed (shown in Fig.(12)) employed a modulated light source with a phase sensitive detector (Brookdeal Model 411) using a reference waveform from a pulse generator which also controlled the modulation frequency. This method has been used previously for absorption spectroscopy (101) to almost eliminate any contribution to the signal due to the flame emission and to increase signal to noise levels. This is achieved by using a blocking capacitor in the output circuit which effectively eliminates the D.C. component of the photomultiplier output signal (due to the flame emission) but not the A.C. component (due to the signal by radiation from the lamp). The phase sensitive detector then compares this test signal (A.C.) with the reference signal to give a D.C. output which is proportional to the amplitude of that component of the test signal which is of the same frequency and phase as the reference signal. All frequencies other than that of the reference signal are rejected and consequently small variations in the absolute frequency become unimportant.

For the reasons discussed in Chapter 6, Section 6.1, it was necessary to discontinue this type of signal processing in favour of the D.C. mode of operation in which the lamp was operated continuously from a D.C. power source and the signal from the photomultiplier amplified directly using a Tetronix Type 1A7A amplifier (Fig.(22)). The output from the amplifier was then displayed on an oscilloscope screen and/or a chart recorder. Fortunately, the contribution to the signal due to the flame emission (i.e. the photomultiplier signal recorded with the lamp switched off) was negligible ($< 0.1\%$) for all of the plasma ignited flames and most of the calibration measurements.

4.5 Results and Conclusions

(a) Selection of the Hollow Cathode Lamp

Using the atomic absorption spectrophotometer and glass nozzle burner described in Section (4.3), absorption measurements were made on an approximately stoichiometric methane-air flame using a Bismuth hollow cathode lamp. With the detection system adjusted to the peak of the 3067.72 Å emission line, values of approximately 15% absorbance ($\Delta I/I_o$ x 100) were obtained when the beam traversed about 1.5 cms of the post-flame gases. To ensure that this was not caused by Schlieren-type deflections (46), other non-coincident lines at similar wavelengths (e.g. Al at 3082.16 Å) were examined and found to give values of 1 to 2% absorbance only.

Although the 3067.72 Å Bismuth line seemed quite adequate for OH absorption measurements, it was thought worthwhile to scan the spectral region (3060-3100 Å) for other spectral coincidences using different hollow cathode lamps. Clearly the depth of this study depended on the availability of the lamps and Appendix (1) shows the metallic lines which were examined. Strong absorbance (approximately 40%) was found at 3090.3 Å using a multi-element lamp (Cu, Co, Mn, Mo, Fe) and a lamp impurity such as Vanadium was thought to be responsible for this emission line. This was later supported by the fact that a Vanadium lamp gave similar absorption characteristics. However, a new Vanadium lamp gave no spectral emission line at 3090.3 Å indicating the older lamp contained an impurity which was absent in the new lamp. Only two possible explanations suggested themselves for the origin of this impurity. Firstly, it could have been a metal other than Vanadium with an emission line around 3090.3 Å coincident with the Q_1 7 rotational line of OH (e.g. Zirconium, Osmium or Tungsten). Some of these lines (e.g. Zirconium) were tried but without success. Secondly, it could be possible that the older Vanadium lamp had been manufactured containing a trace of water. This may have been introduced

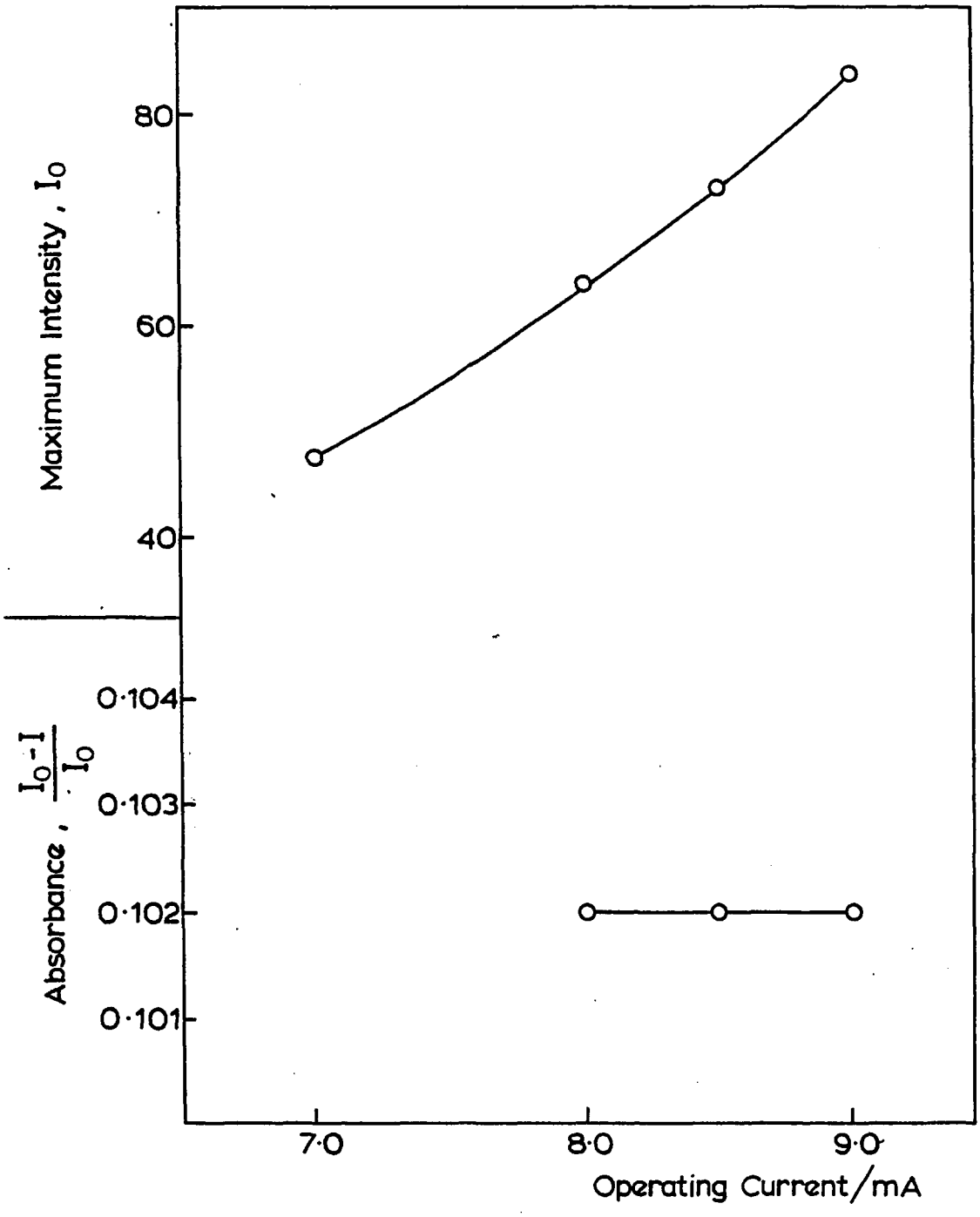
accidentally with the filler gas (for example, if the cylinders were nearly empty). The supposition that the impurity was water had to be assumed at this stage of the research because of the difficulty in continuing this investigation further (i.e. obtaining the more unusual metallic hollow cathode lamps giving emission lines around 3090 Å).

Since the older Vanadium lamps were at the end of their working life with low signal to noise levels, an OH emission hollow cathode lamp was constructed This was designed for a continuous flow of argon saturated with water vapour with high vacuum taps to seal the lamp as soon as the correct operating pressures were reached. However, in practice the lamp did not operate successfully with the high vacuum taps closed and the argon flow cut-off and for this reason the lamp was operated with a continuous flow.

The mechanism of excitation of OH in the lamp was similar to that of metals although obviously no sputtering action occurred. Hydroxyl radicals were produced in the vicinity of the inner cathode surface in a region of high electron and ion concentration and resonance radiation had little opportunity to undergo self absorption or line reversal by passing through cooler regions at the edge of the discharge.

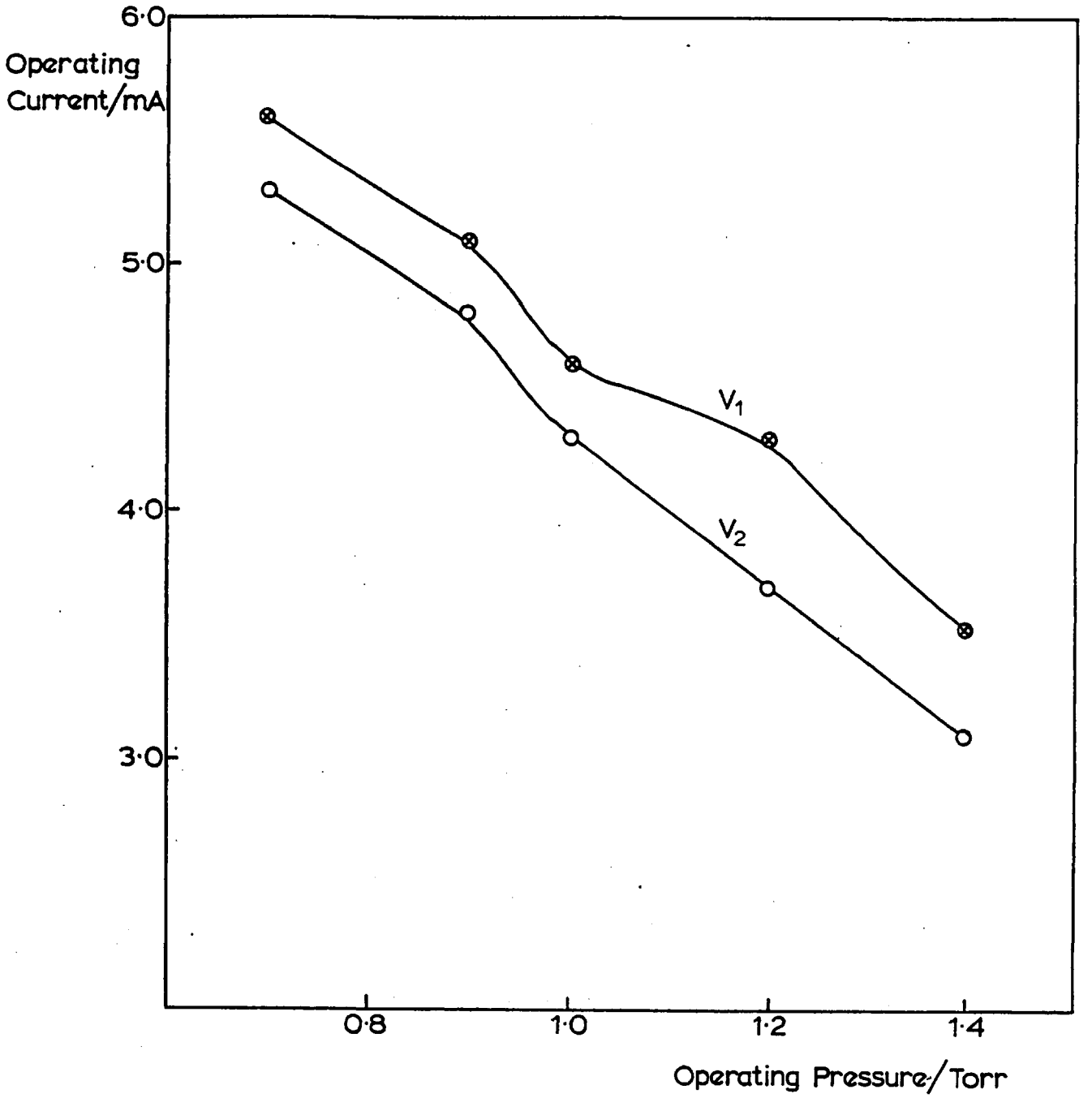
At the start of operation, the lamp was first flushed out with argon saturated with water vapour using the porous sinter (see Fig.(23)). The gas pressure was then reduced until the discharge struck and the operating pressure and flow conditions optimised by careful adjustment of valves (1), (2), (3) and (4) (Fig.(23)).

The results of a study of the operating characteristics of a Bismuth hollow cathode lamp and an OH emission hollow cathode lamp are shown in Figs.(13), (14) and (15). The almost linear variation of intensity, I_o, with operating current at constant pressure is shown in Fig.(13). This also shows the absorbance values obtained as a function of current using a hydrogen-air flame with constant $[OH]$ value over



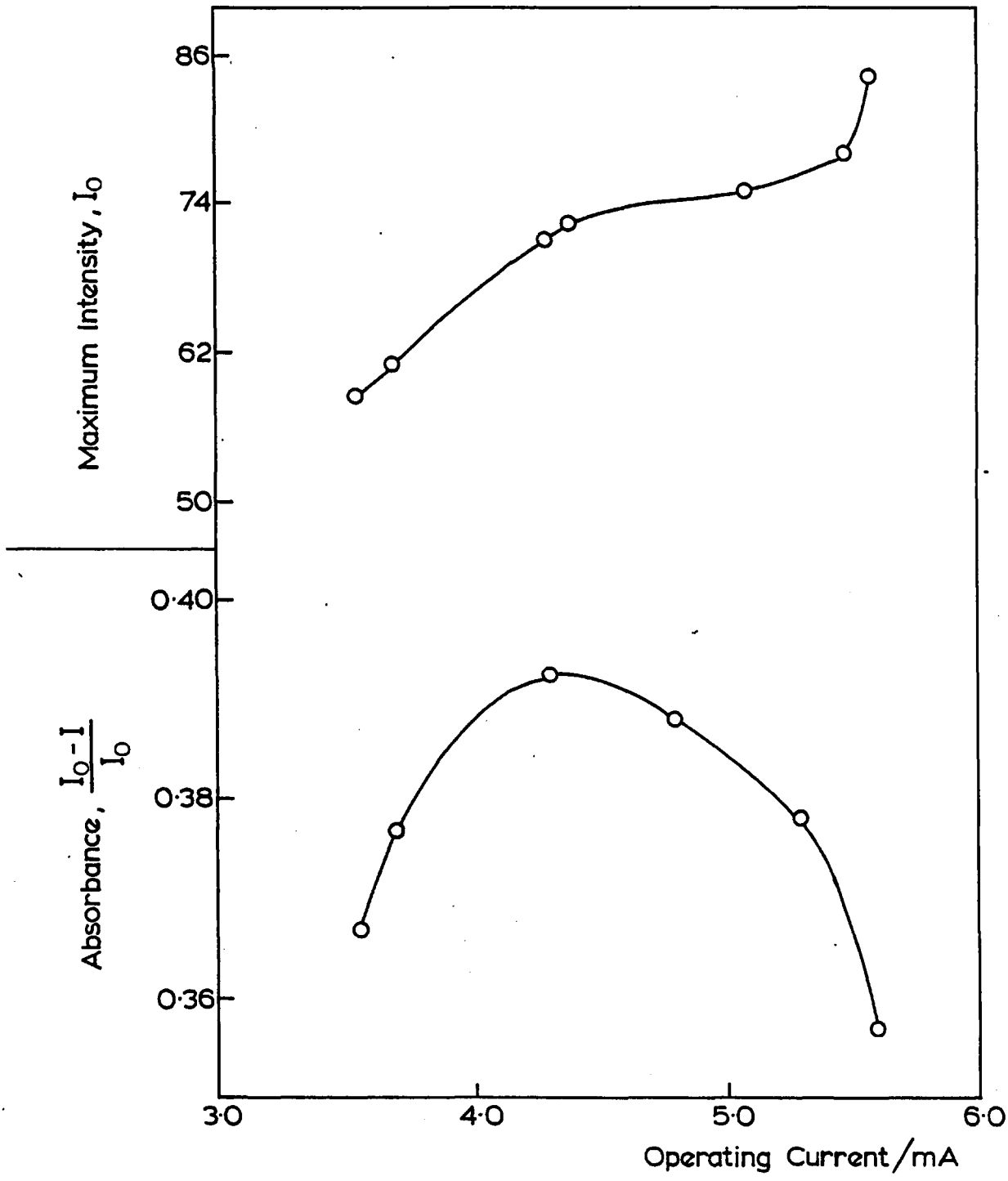
FIG(13)

MAXIMUM INTENSITY AND ABSORBANCE vs OPERATING CURRENT OF A BISMUTH HOLLOW CATHODE LAMP



FIG(14)

OPERATING CHARACTERISTICS OF THE HOLLOW CATHODE LAMP (ARGON AND WATER VAPOUR)



FIG(15)

MAXIMUM INTENSITY AND ABSORBANCE vs OPERATING CURRENT OF THE HOLLOW CATHODE LAMP (ARGON AND WATER VAPOUR)

the range studied. Consequently, the % absorption obtained for a fixed [OH] and path length is independent of the lamp intensity, indicating the absence of any self absorption.

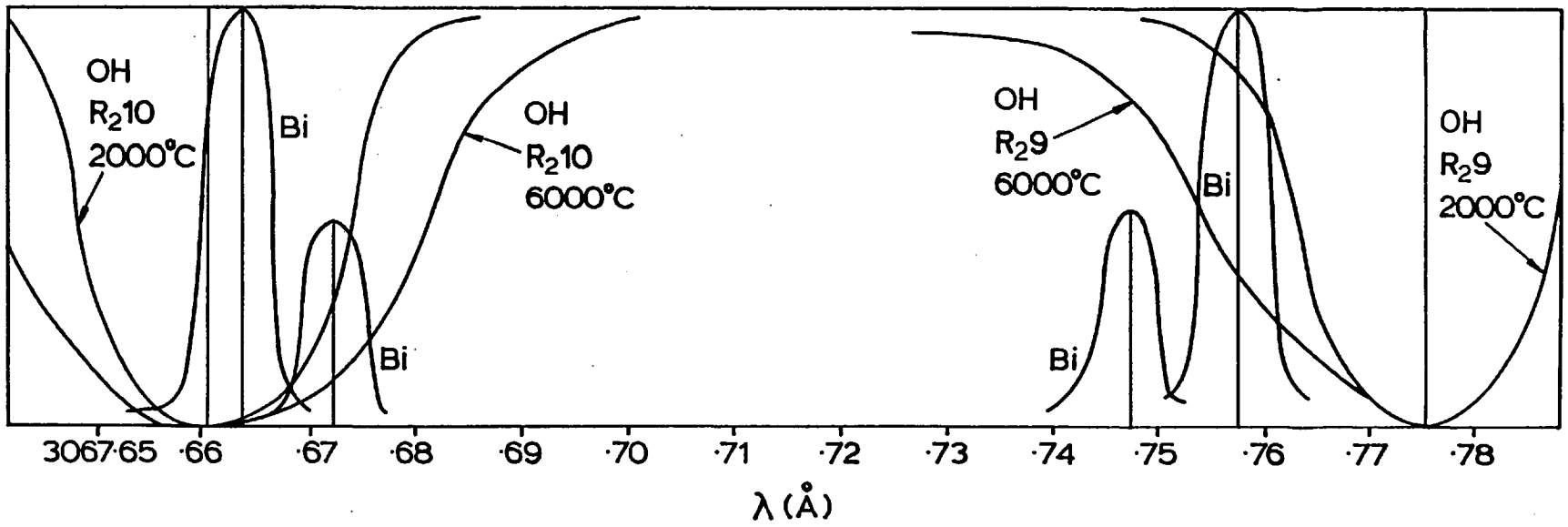
Figs.(14) and (15) refer to the OH emission hollow cathode lamp operated with a continuous flow of argon saturated with water vapour. The variation of discharge current with operating pressure (measured with a mercury manometer) for 2 arbitrary applied voltages, V_1 and V_2, is shown in Fig.(14). The irregularities in the two curves at a pressure of about 1 torr correspond to the transition where the discharge is drawn completely into the hollow cathode thereby minimising self absorption. This is also illustrated by Fig.(15), which shows maximum absorbance at an operating current of 4.4 mA and a pressure of about 1 torr. Clearly these are the optimum conditions at which to operate the lamp, even though the intensity is not a maximum there but at the beginning of a level plateau (upper curve Fig.(15)).

(b) The Spectra

Figs.(11) and (10) show the OH emission spectra for the argon/water vapour hollow cathode lamp at three different operating pressures together with the Bismuth line at 3067.72 Å obtained under identical conditions (i.e. the same (1) spectrometer slit width of 65 μ , (2) E.H.T. to the photomultiplier and (3) gain of the D.C. amplifier). Although the exact coincidence of the Bismuth line at 3067.7 Å with the R_2 10 line of OH is shown in Fig.(11), studies of the hyperfine structure of the Bismuth line have shown that it is in fact a multiplet consisting of six lines. This is illustrated in Fig.(16) which shows that approximately 80% of the light is absorbed by the R_2 10 line and the remainder by the R_2 9 line. This might have complicated the temperature dependence of the absorption characteristics very slightly since both the absorption and emission line widths change with temperature.

FIG. (16)

BISMUTH LINE (3067 Å) IN EMISSION AND $R_2(9)$, $R_2(10)$ LINES IN ABSORPTION



Two other pieces of information can also be obtained using the spectra shown in Figs.(10) and (11). Firstly, a comparison of the spectra emitted from the OH hollow cathode lamp at the three different operating pressures 0.7, 0.9 and 1.0 torr indicate the absence of any self absorption, since the relative intensities of lines do not change as the pressure changes. Secondly, using Fig.(11), the spectral band-width of the spectrometer can be measured from the Bismuth line width at half intensity. This is about 0.5 Å under the conditions used in the present experiment.

(c) The Calibration Curves

The calibration curves shown in Figs.(8) and (9) were constructed using premixed hydrogen-air and methane-air flames stabilised on the porous plug burners described in Section (4.3(b)). Using these flames, values of I and I_o were obtained at different positions in the flame for different mixture compositions and with different flow velocities of the unburnt gases. From these and the flame temperature measurements (see Section (4.3(b)), values of $\ln(\frac{I_o}{I})$ and A_T were related to the OH concentrations in the burnt products using thermodynamic data and previous experimental and computed values for OH concentrations in methane-air and hydrogen-air flames recorded in the literature (90,102,103,104, 105). These results were then used to interpret the OH oscillograms for plasma ignited flames described in later chapters.

CHAPTER 5

THE APPARATUS FOR PLASMA JET IGNITION STUDIES

The apparatus as shown in Plate (3) consists of the plasma jet igniter, the glass combustion vessel and the optical and spectroscopic layout. The Schlieren beam was designed to traverse the combustion vessel at right angles to the OH spectroscopic beam to record the position, geometry and size (and hence the effective path length) of the plasma ignited flame kernel at any given time for simultaneous spectroscopic measurements.

The combustion vessel, the plasma jet igniter and the optical layout is described in this chapter together with the method of operation of the complete apparatus (Section 5.6). The spectroscopic techniques (OH resonance absorption and C_2 emission) which were incorporated into this apparatus are described in more detail in Chapter 6.

5.1 The Combustion Vessel

Since it was decided to perform all of the plasma jet ignition work in a constant pressure environment, some of the early experiments with the plasma jet igniter were done with the porous plug burner described in Chapter 4, Section (4.3(b)) as opposed to a constant volume bomb. This was simply to avoid the pressure rise associated with combustion causing increased initial temperatures and thereby increasing the later stages of flame propagation.

In these early experiments, the plasma plug (positioned about 5 cms directly above the burner surface) was used to inject a jet of hot gas, atoms and radicals into a flowing flammable mixture issuing from the burner at a variable velocity. However, this was found later not to be particularly suitable because of entrainment of surrounding air causing a reduction of the equivalence ratio of the test mixture issuing from the burner.

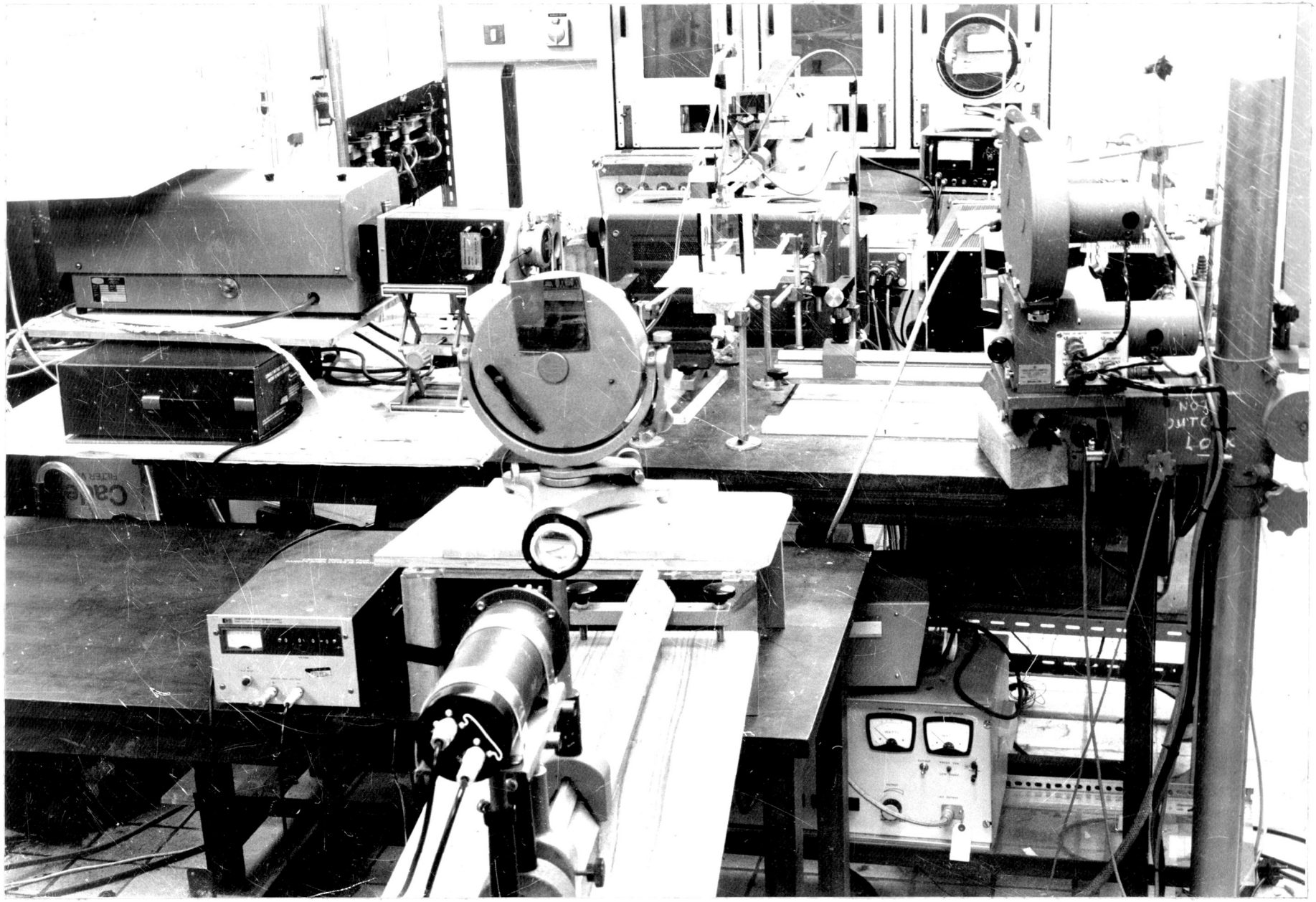


PLATE 3 THE APPARATUS

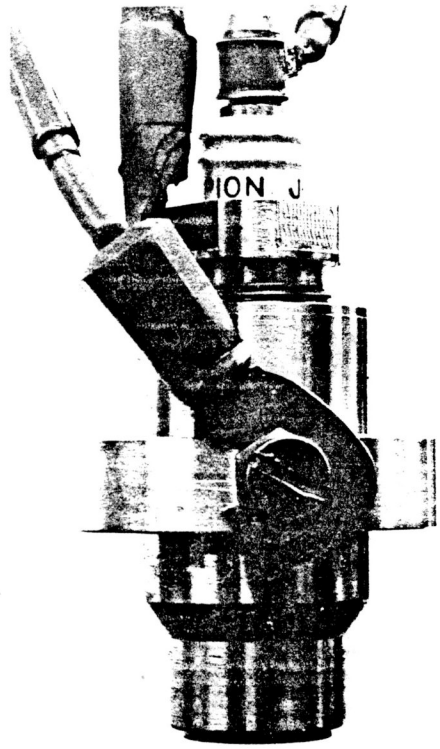
For this reason, the circular combustion vessels shown in Plate (4B) were constructed in the anticipation that the expanding flame would remain symmetrical throughout most of it's progression through the vessel, which may not have been so for rectangular or square-shaped geometries. However, it was found that with these circular vessels, too little of the expanding plasma plume and flame could be viewed with the optical beam. Therefore the rectangular-shaped combustion vessel shown in Fig.(17) and Plate (3) was used to obtain all the results described in this thesis.

The vessel (Fig.(17)), into which the plasma jet fires has a total internal volume of about 1260 cm^3. However, during the period in which measurements were taken, the flame kernel was confined to the top rectangular viewing section only (I.V. 960 cm^3). On two opposite sides of the vessel were mounted optically polished quartz windows 5 cms in diameter to allow transmission of the ultraviolet OH beam across the vessel (Chapter 6, Section 6.1(a)). Glass windows of thickness 0.5 mm made up the other set of opposite sides for the parallel beam of laser light (Fig.(21)).

During the experiments, the vessel was continuously purged with premixed methane and air at atmospheric pressure at a flow velocity of approximately 1 cm s^{-1} (metered by calibrated capill ary flow gauges - see Fig.(18)). The flow of methane and air to the vessel could be stopped immediately prior to firing the plasma jet by closing 2 valves and a drying column could be used either to dry the air from a compressor or by-passed using a 3-way valve.

The bottom section of the vessel contained glass beads to ensure good premixing of methane and air whilst preventing flash-back past the porous sinter which was also responsible for uniform flow through the vessel. A gauze was positioned across the top of the vessel to allow the escape of surplus methane-air mixture whilst preventing reverse flow of entrained air and consequent lowering of the equivalence ratio of the

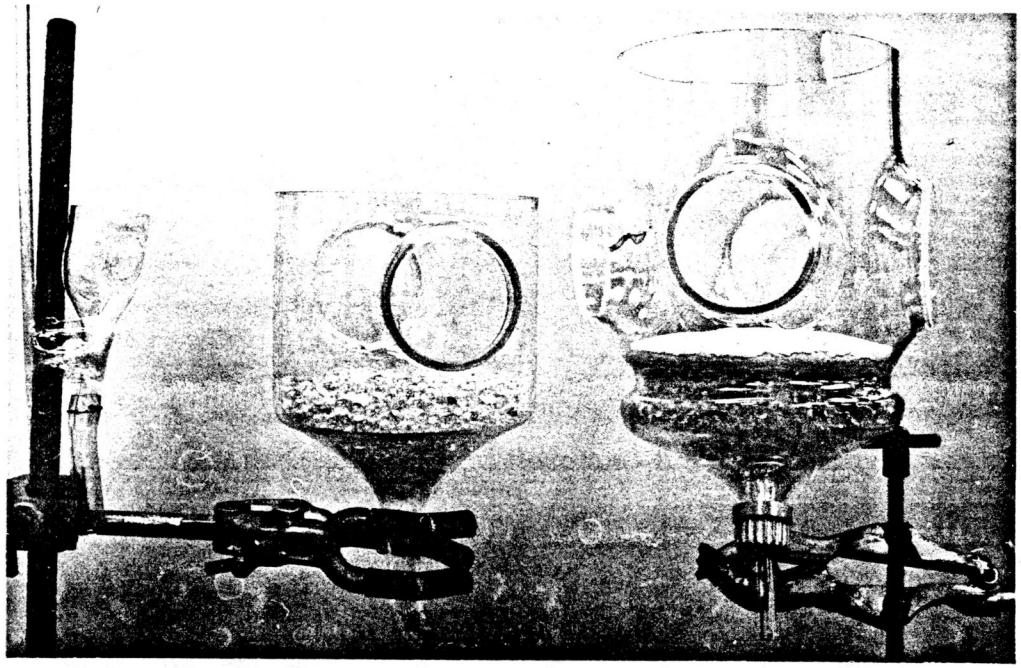
PLATE 4



A

THE PLASMA JET

B CYLINDRICAL COMBUSTION VESSELS



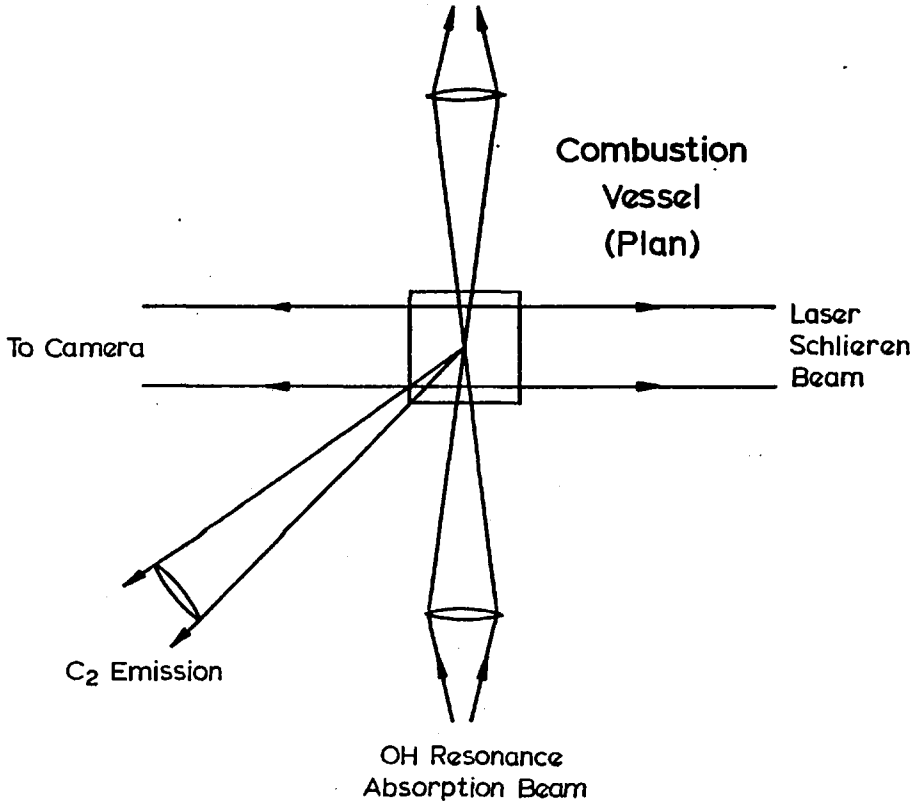
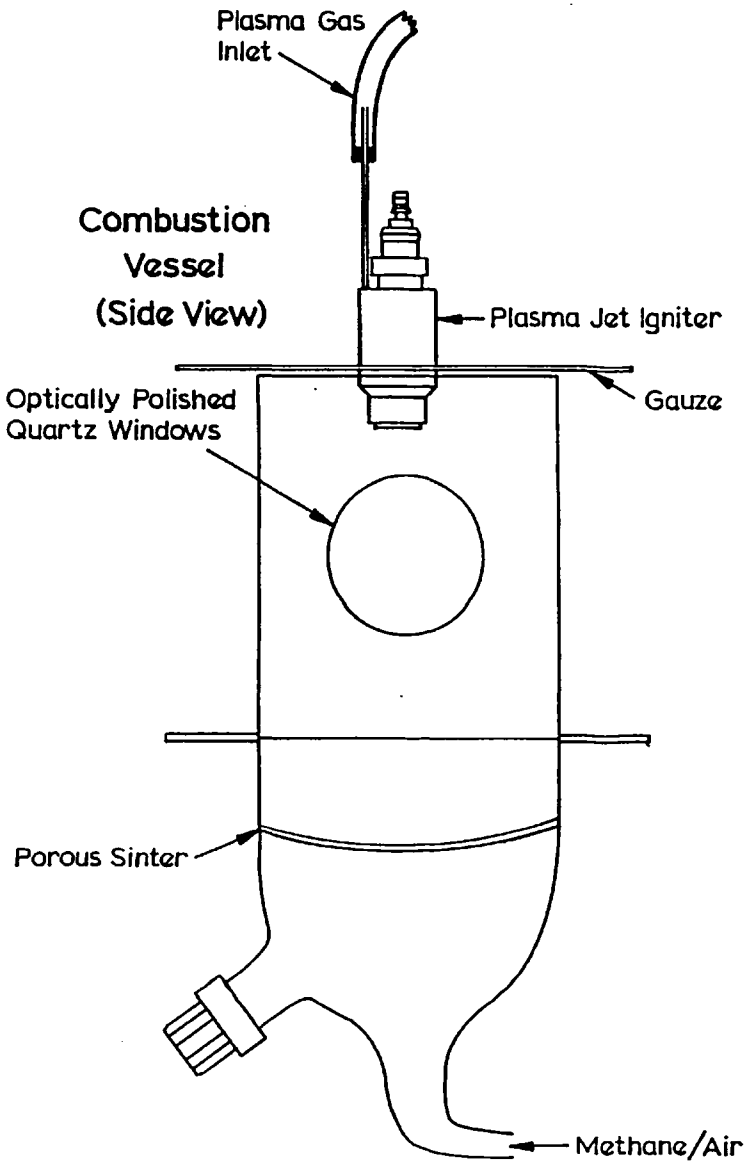


FIG. (17)

THE COMBUSTION VESSEL



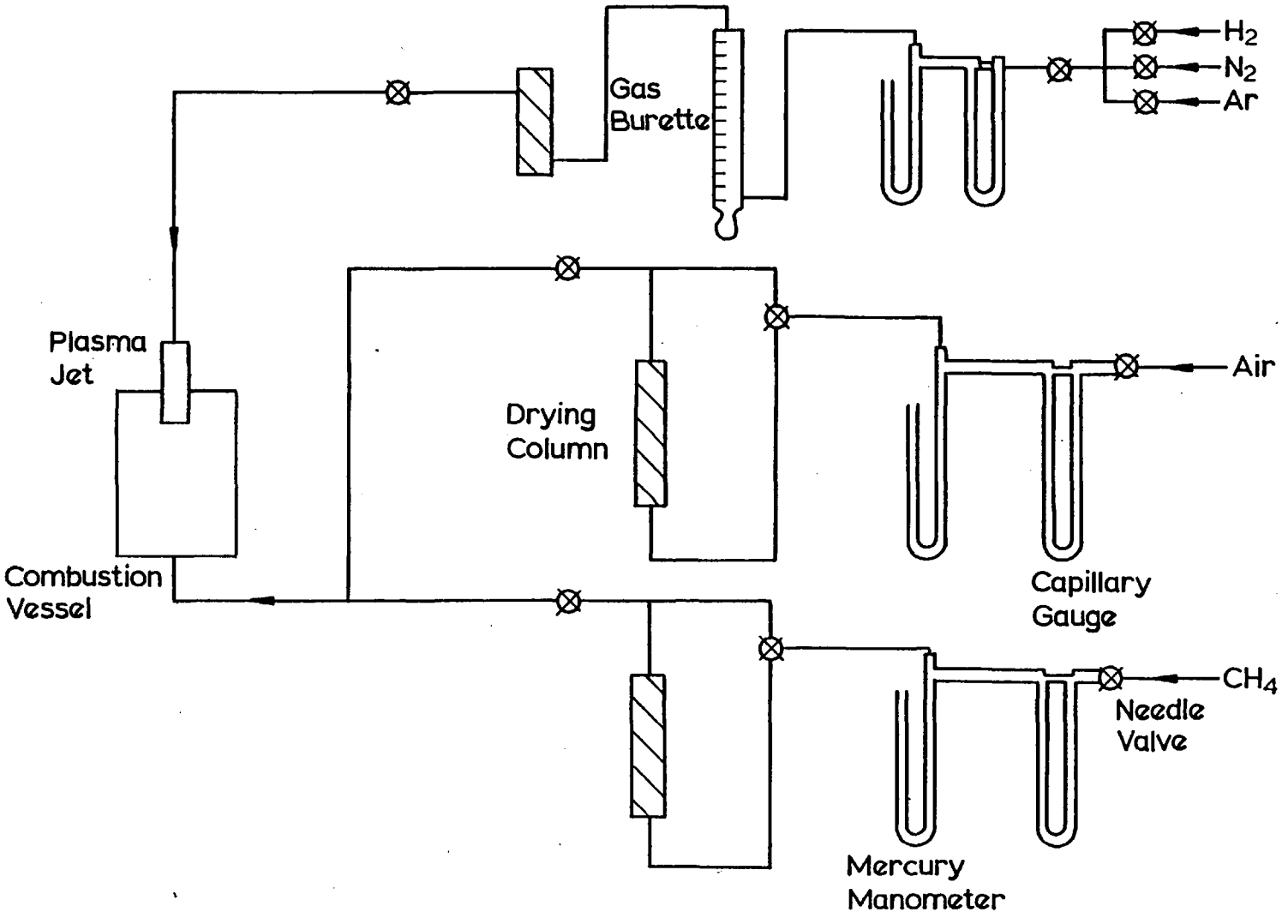


FIG. (18)

THE FLOW SYSTEM

reactant gases in the vessel. In practice, the gauze was found to exert quite an important influence on the ignition process. This was evidenced by an apparent increase in the minimum equivalence ratio, ϕ_{min} (see Chapter 8) which could be ignited by any given plasma when the gauze was removed.

5.2 The Plasma Jet Spark Plug

The plasma jet spark plug used throughout all the experiments was of the high energy, intermittent (capacitor discharge) type as shown in Fig.(19) and Plate (4A). Its design was based on the concept that if sufficient electrical energy is supplied to a small enough volume (i.e. cavity) in a short enough time, the temperature and pressure of the gas confined in that cavity increases extremely rapidly. The high cavity overpressure which results causes a jet of plasma to be ejected from the cavity at sonic velocity. Consequently, the fluid dynamic characteristics of the jet produced depend primarily on the cavity dimensions, the orifice size and the amount and rate of electrical energy supplied.

To enable a comparison to be made of the flame propagation rates of plasma ignited methane-air mixtures with those reported previously (40), an exact replica of the plug used by these authors was constructed. It consisted of a central electrode and procelain insulator of a Champion J-61Y spark plug extending into the teflon discharge cavity (Fig.(19)). The high energy spark (e.g. 500 mJ) then discharges between the central electrode and the outside stainless steel body of the plug and is thereby confined within the cylindrical teflon cavity of the following dimensions: Length 6.1 mm, diameter 2.4 mm and volume 28 mm^3. An orifice plate could be attached to the base of the plug by 3 small screws to restrict the size of the cavity exit. 1.2 mm, 1.6 mm, 2.0 mm and 2.4 mm diameter holes corresponded to the four different orifice plates made.

The gas within the cavity was maintained by an extremely small flow via the inlet tube and silica gel drying column. In spite of the small

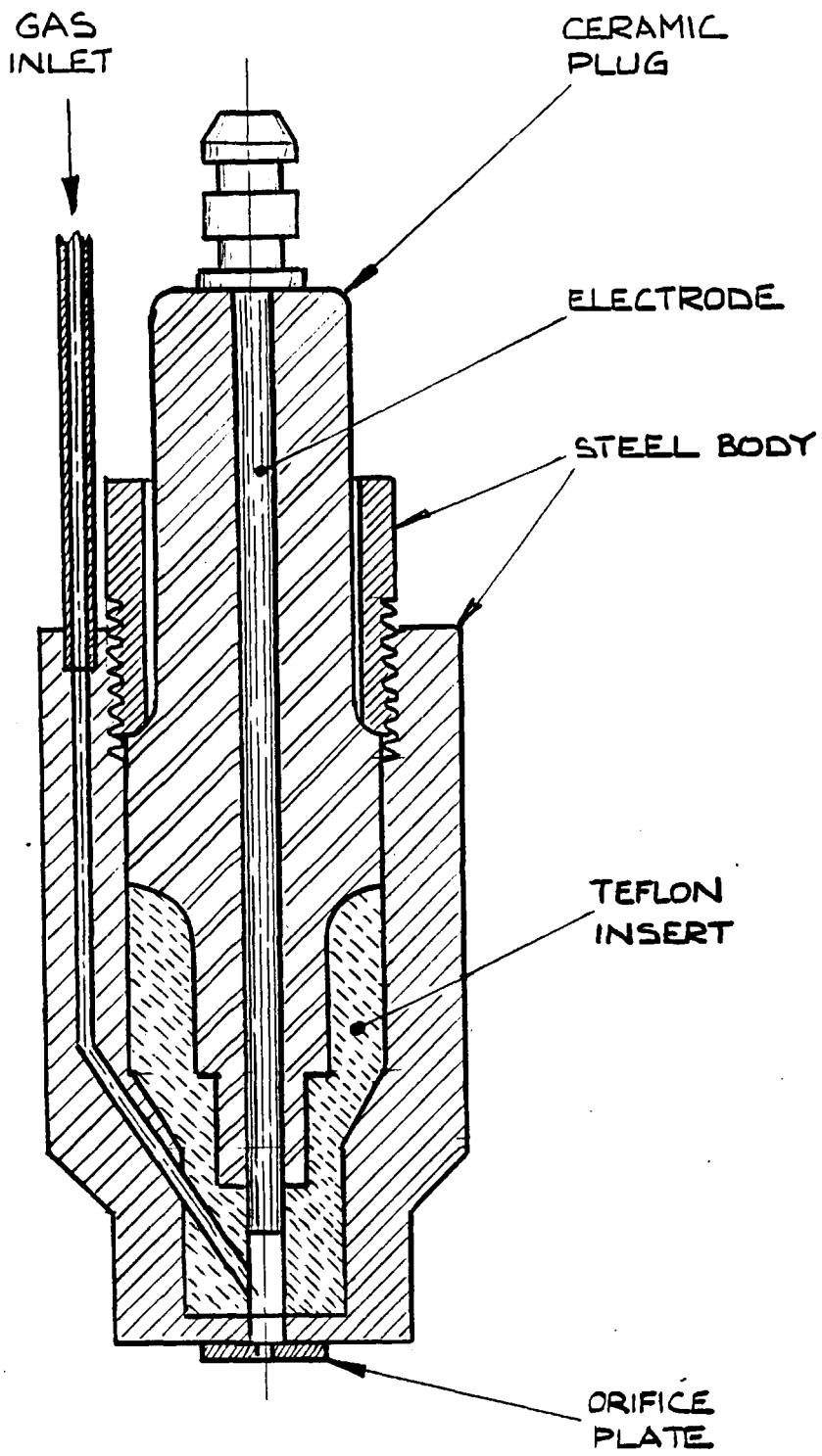


FIG. (19)

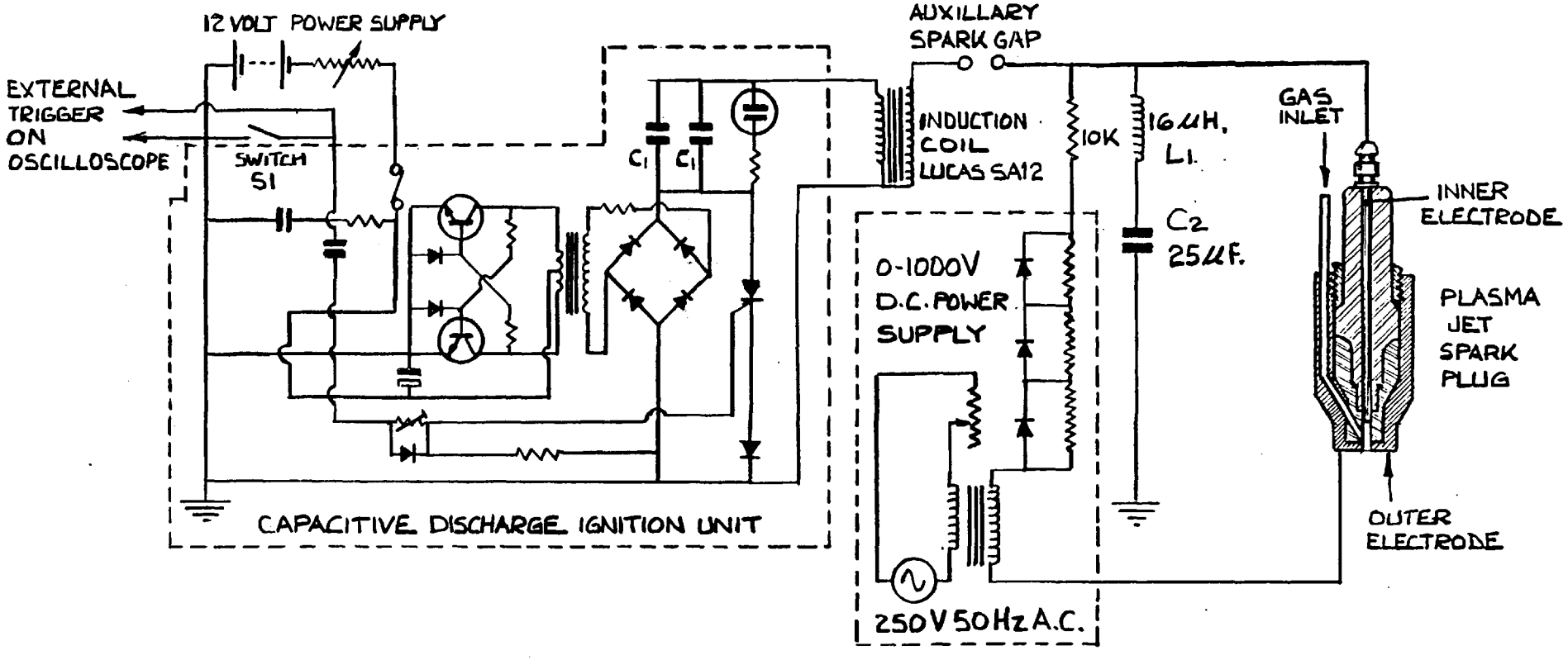
THE PLASMA JET

flow, corrections were made to the gas composition within the main combustion vessel to account for the overflow of test gas from the plasma cavity exit. This method of continuous flow of test gas was considered more suitable for the constant pressure combustion vessel used for the present experiments than the intermittent method of plasma gas feed by syringe used by the previous authors. This was because an equilibrium gas composition could be reached before the firing of the plug which would be more reproducible from experiment-to-experiment than an intermittent method of plasma gas injection into the cavity using a syringe.

5.3 The Plasma Jet Ignition Circuit

Electrical energy to the plasma jet sparking plug was provided by the electrical circuit shown in Fig.(20). This circuit consists of a 0-30 V, 10 A power supply, a capacitive discharge ignition unit (Stirling Sound) and Lucas induction coil to provide a high voltage trigger, an auxilliary gap and a 0-1000 V D.C. power supply with the main energy storage capacitors, C_2.

When switch, S_1, is depressed (contacts open) the trigger circuit of the capacitive discharge ignition unit operates whilst simultaneously applying 14 V across the external triggering connection of the storage oscilliscope to start spectroscopic measurements. The trigger circuit turns the thyristor (S.C.R.) on which short-circuits the output of the inverter and causes the capacitors, C_1, to discharge rapidly into the primary of the induction coil. The secondary winding then generates a high voltage pulse (in the region of 10 kV) which short-circuits the auxilliary spark gap necessary to isolate the main storage capacitors, C_2. Correct adjustment of the auxilliary spark gap length enabled the high voltage trigger to breakdown the main plasma cavity gap. Once breakdown occurred, the main storage capacitors, C_2 (25 uF charged to $\leq$ 1000 V) discharged simultaneously into the cavity generating the plasma. A 16 μhy



FIG(20) THE PLASMA JET IGNITION CIRCUIT

inductor protected the storage capacitor from the high voltage pulse which would otherwise prevent breakdown of the main gap.

The energy supplied to the cavity could be altered either by adjustment of the value of C_2 or the applied voltage across C_2. The latter was the most easily achieved and for a fixed value of 25 μF for C_2, the maximum stored energy available (limited by a maximum voltage of 1000 V of the D.C. power supply) was 12.5 J. The minimum stored energy which still produced a plasma was about 4.8 J depending on the test gas within the cavity. These values refer to the energy stored at C_2 of which 20 to 30% was dissipated within the cavity, the remainder being lost mainly by ohmic heating of the cables. The high voltage trigger contributed approximately 50 mJ to the energy deposited by virtue of C_2.

The duration of the discharge was a function of the capacitance, C_2, and inductance, L_1 (excluding resistance) of the circuit. Voltage reversal on C_2 caused the ignition circuit to discharge twice, although the second discharge could be avoided by placing a high voltage diode across C_2 in the present circuit. In this case, the current risetime, t_1, of the discharge is given by

$$t_1 = \pi/2 \sqrt{L_1 C_1} \tag{5.1}$$

and current fall time, t_2 (without voltage reversal on C_2) by

$$t_2 = \frac{L_1 I_o}{V_{ST}} \tag{5.2}$$

where the peak discharge current

$$I_o = V_o \sqrt{C_1 / L_1} \tag{5.3}$$

since

$$\frac{C_1 V_o^2}{2} = \frac{L_1 I_o^2}{2} \tag{5.4}$$

V_o = applied voltage across C_2, and V_{ST} = total sustaining voltage

of the discharge path.

For $C_2 = 25\,\mu$fd and $L_1 = 16\,\mu$hy values of $t_1 \simeq 30$ nS, $t_2 \simeq 300$ nS, $I_o = 750$ A ($V_o = 600$ V) are obtained for the duration of the discharge.

5.4 Laser Schlieren/Shadowgraphy System

The conventional z-shaped schlieren system shown in Fig.(21) was used in conjunction with high speed cinephotography. Light from a continuous 10 mW helium-neon laser (Scientifica Cook) was focussed by a short focal length lens onto a pinhole, the latter placed at the focal length of mirror M_1 of focal length 8', diameter 8". A second lens, L_2, ensured divergence of the light beam to fill mirror M_1. A second mirror, M_2, refocussed the parallel light beam which traversed the test region to produce a shadow of the test region in the plane of the camera. An additional lens, L_3, and filter ensured correct imaging and exposure of the test region.

Plate (6) shows a laser shadowgram of an expanding plasma plume in air. The white lines on this film indicate boundaries of hot and cold gas since markings correspond to 2nd derivatives of refractive index perpendicular to that part of the beam traversing the test region. The occurrence of fringes characteristic of the use of lasers were virtually eliminated by minimizing the amount of defocussing of the system (i.e. minimizing the distance of the film from the image plane of the test region). This also decreased the sensitivity to a level suitable for the present purpose. With the film in this position, the relative positions of markings closely reflect the relative positions of hot and cold boundaries.

This shadowgraphic system was easily converted to schlieren by positioning a knife at the focal point of mirror, M_2, and focussing the test object on the receptor. This was usually unnecessary since in

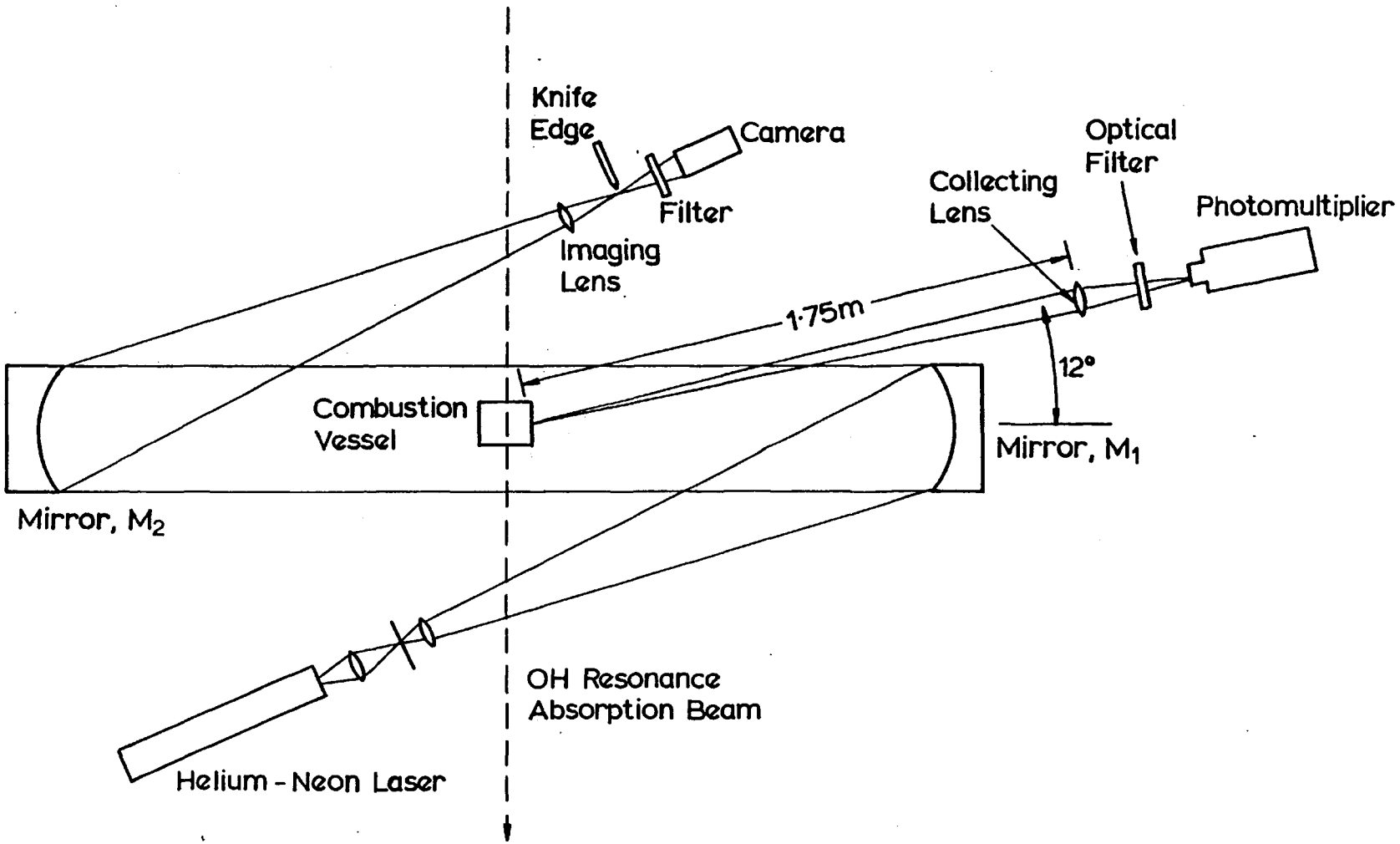


FIG. (21)

THE LASER SCHLIEREN AND C_2 EMISSION SYSTEM

practice it was found that for the present purpose, little was gained by the use of schlieren over shadowgraphy.

5.5 High Speed Cinephotography

High speed cinephotography enabled laser schlieren/shadow photographs to be taken during the duration of the expanding plasma plume and developing flame kernel. For this purpose, a Hitachi 16 mm high speed camera (Type 16 HM) was used with an advanced camera control system (Gordon Type GC 1026). This camera had a maximum framing rate of 10,000 frames per second.

The camera lens had been removed to allow laser light to fall directly on the film, the aperture being fully open. Once the laser schlieren/shadow system had been aligned, the camera was loaded with a 100 foot length of film and the camera and imaging lens adjusted so that an image of the test space just filled one frame. This was most easily achieved without the use of the viewfinder by viewing the film position from behind with the camera door open. The film used, which was found suitable for all framing rates, was Ilford Micro Neg. Pan Type 204 and Kodak Type 7231, 16 mm doubly perforated.

The camera control system used had the facility to trigger the plasma jet circuit (by opening a contact) once the camera was running at the pre-selected speed. This was particularly desirable since at the higher framing rates, approximately 1/3rd of the spool (30 to 40 feet of film) was used for attaining this speed. Unfortunately, interference from the plasma jet power supply in the form of electromagnetic radiation switched the camera to the "off" position preventing this "automatic switching" facility being used. For this reason, the plasma plug power supply was energized manually once the "running at speed" light showed on the camera control unit.

5.6 Operation

For simultaneous schlieren records, OH resonance absorption and

C_2 emission measurements (Chapter 6) of the plasma discharging into a flammable mixture, the following sequence of operations were performed.

(1) Adjustments were made to the OH resonance absorption beam to maximize the incident intensity, I_o, at the photomultiplier (see Chapter 6), i.e.

   (a) Adjustment of argon flow to light source (hollow cathode lamp or microwave discharge).

   (b) Adjustment of positions of lenses.

   (c) Adjustment of monochromator grating to ensure the wavelength corresponds to the peak of the rotational line.

   (d) Measurement of I_o.

(2) Adjustment of plasma plug position with respect to OH light beam using ground glass target (see Chapter 6).

(3) Adjustment of plasma gas and methane/air flow rates.

(4) Alignment of laser schlieren/shadow system.

(5) The camers was started and when running at speed, the plasma plug was fired. This simultaneously triggered the storage oscilloscope (see Fig.(22)) for spectroscopic measurements.

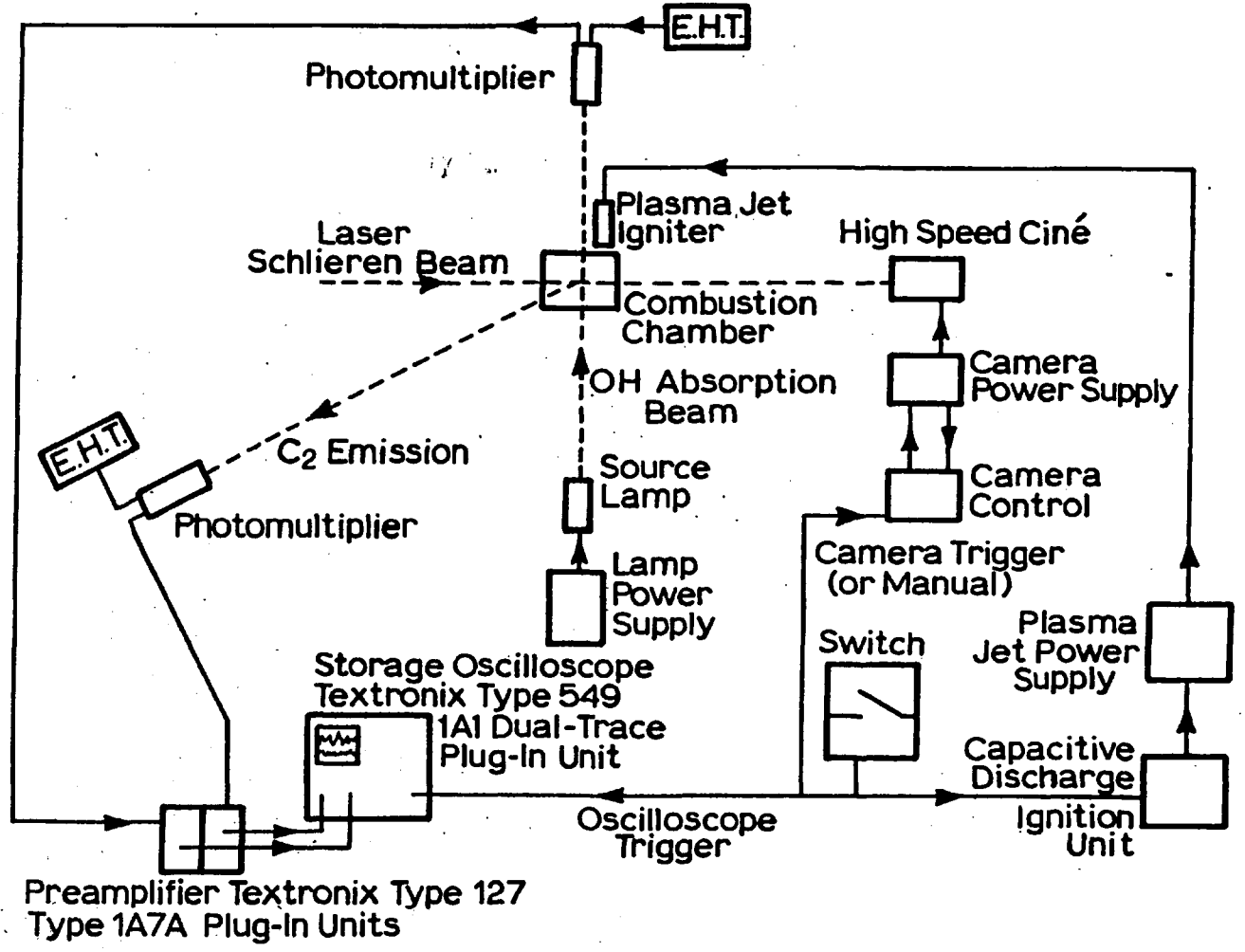


FIG. 22 THE APPARATUS

CHAPTER 6

THE APPLICATION OF THE SPECTROSCOPIC TECHNIQUES TO PLASMA JET IGNITION STUDIES

The integration of the two spectroscopic techniques into the plasma jet ignition apparatus (Chapter 5) is described in this chapter. The first part refers to the application of the OH resonance absorption spectroscopic technique discussed in Chapter 4 to the present study. In the second part, the C_2 emission method which was used for measuring the areas of plasma jet ignited flames is described.

6.1 The OH Resonance Absorption Technique

(a) Experimental

(1) The Optics

The apparatus used which is shown in Fig.(23) was basically the same as that described in Chapter 4. Light from the resonance lamp was focussed by lens, L_1, of focal length 15 cms to a point centrally placed in the combustion vessel. A second lens, L_2, of focal length 15 cms refocussed the light onto the slit of the 50 cms Ebert grating spectrometer. Access of ultraviolet light into and out of the combustion vessel was by 5 cms diameter optically polished quartz windows of thickness of about 1 mm which caused an approximately 10% reduction in light intensity reaching the spectrometer.

After adjustments had been made to the relative positions of the lamp, lenses, combustion vessel and spectrometer, the combustion vessel was fixed rigidly into position by tightening the hexagonal nuts in the supporting framework (see Plate (5B)). The position of the OH beam in relation to the plasma plug (and hence expanding flame kernel) could be adjusted by horizontal and vertical movement of the traverse (graduated in 2 mm divisions) which was fixed rigidly to both the plasma jet and

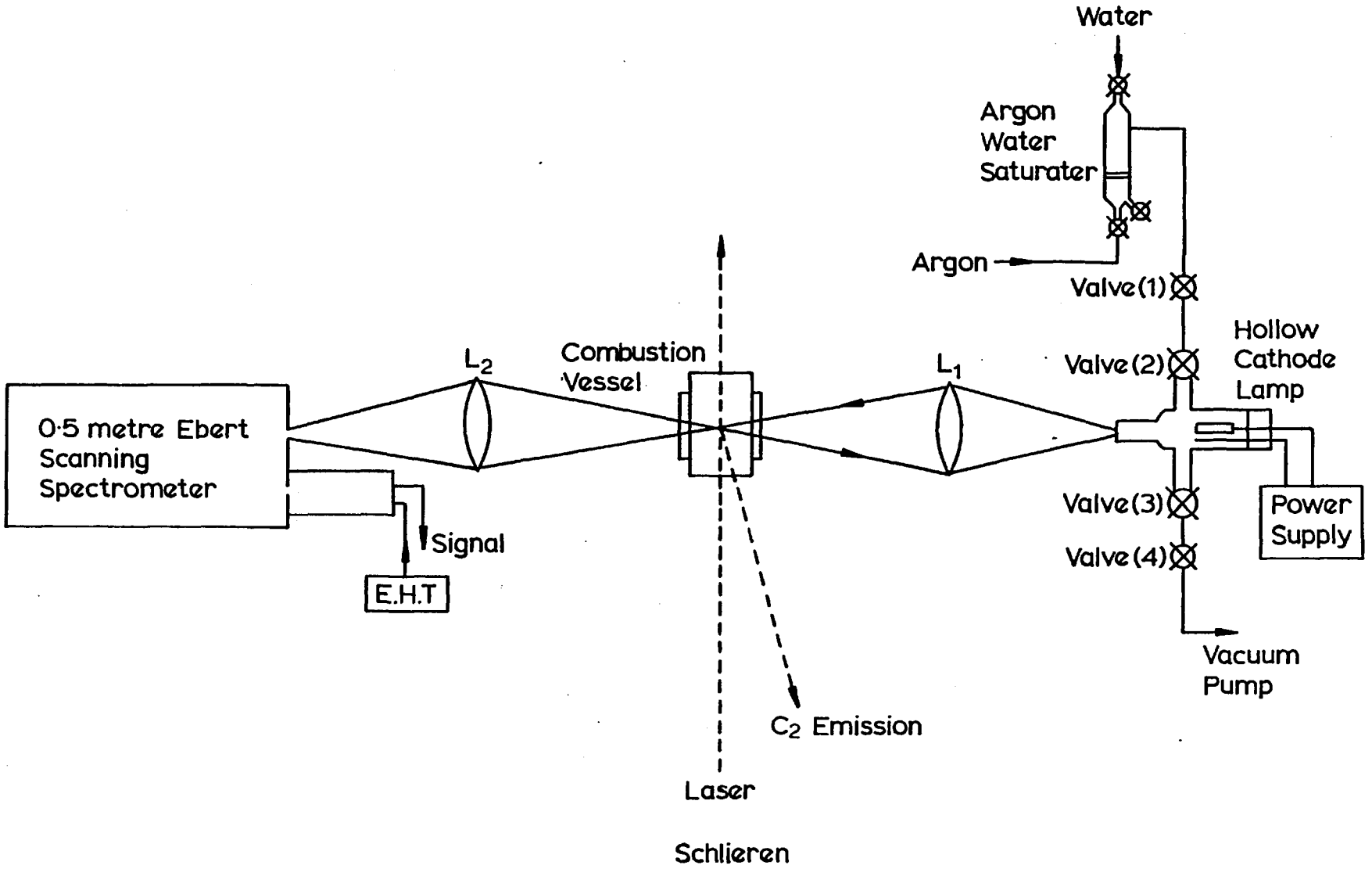
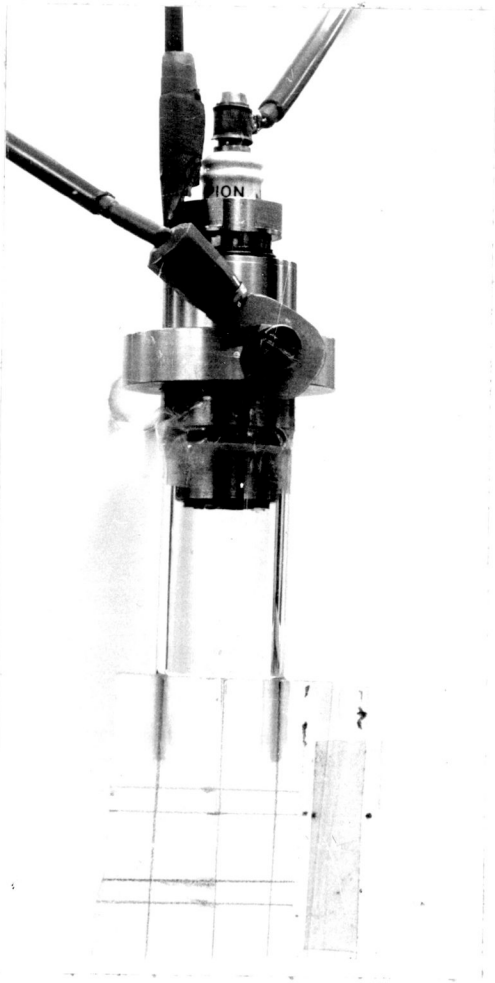


FIG. (23)

THE OH RESONANCE ABSORPTION TECHNIQUE

PLATE 5

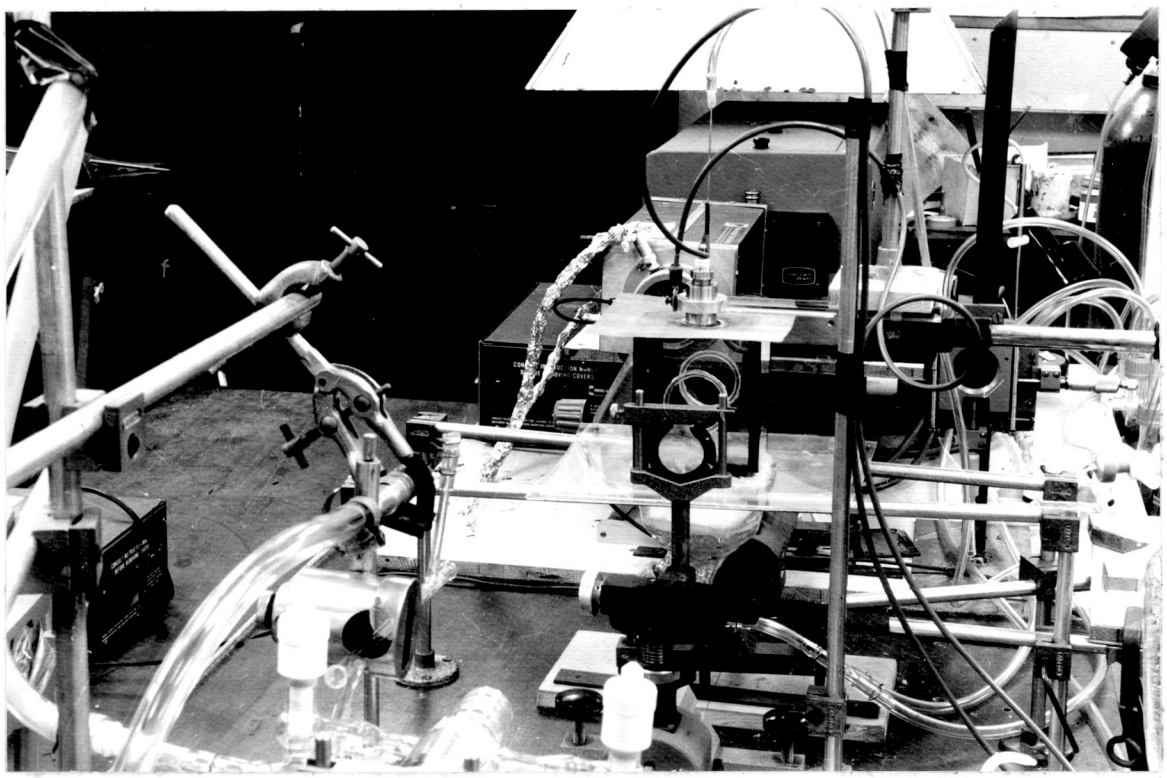


A

OH BEAM

"TARGET"

APPARATUS FOR OH ABSORPTION MEASUREMENTS



the supporting framework. To ensure that the beam was focussed in the right position relative to the plug prior to an experiment, use was made of a ground glass "target" which fitted onto the bottom of the plasma plug (see Plate (5A)). In this way, the exact position of the OH beam was known when analysing the shadow high speed cine photographs of the expanding flame.

(2) The Signal Processing

Although the method of modulating the light source and using phase sensitive detection as described in Section (4.3(d)), Chapter 4, was used initially, it was later discontinued for three reasons. The first concerned the interference in the form of electromagnetic radiation from the auxilliary spark gap (Fig.(20)) in the plasma jet power supply. This seriously affected the operation of the phase sensitive detector and low noise amplifier (Fig.(12)) and prevented OH measurements being taken up to 4 or 5 mS after the plasma firing. This problem was later solved by transferring these units to a screened room and by using screened coaxial cables from the photomultiplier outside the room to the signal processing units inside the screened room. The other major problems concerned the relatively high time constant of the phase sensitive detector (1 mS) which was available at that time and the high modulation frequency that was required during the early stages (1-5 mS) of OH absorption measurements. A phase sensitive detector with a lower time constant could have been used but the upper limit would still have been set by the modulation frequency of about 10 kHz above which the lamp could not be electronically modulated successfully.

However, as mentioned previously, the levels of OH emission from the plasma-ignited flames were much lower than anticipated and for this reason the D.C. mode of operation (Chapter 4, Section 4.3(d)) could be used. Also for simultaneous OH absorption and C_2 emission measurements, the dual trace facilities on the oscilloscope (Tektronix storage oscilloscope

Type 549 with a 1A1 Dual-Trace Plug-In unit) could be used with the external triggering for both traces obtained from the switch of the C.D.I. unit (see Fig.(22)). In practice though, slightly lower signal-to-noise levels were obtained using the dual trace than when a single trace was displayed on the oscilloscope (i.e. using only the Tektronix 1A7A amplifier).

(b) Limitations of and Errors in the Method

Apart from the interference associated with electromagnetic radiation from the auxilliary spark gap, two other sources of interference were present in these experiments. The first was that of strong magnetic fields caused by the high energy discharge in the plasma plug which directly affected the photomultiplier. This was later solved by screening the latter with a mumetal shield maintained at cathode potential. The second source of interference, due to the intense light from the plasma causing a "blinding effect" on the photomultiplier could not be eliminated. This occurred when measurements were made too near to the luminous plasma (i.e. with the beam focussed less than about 2 cms below the plug) which resulted in a photomultiplier signal at least an order of magnitude greater than the signal corresponding to that due to the radiation from the lamp. Since the duration of this effect was approximately the same as that of the luminosity in the visible from the plasma (i.e. approximately 5 mS), this became a major limitation of the present method. For example, for some of the low energy hydrogen plasmas, the flame was formed quite near to the plug (Chapter 7) and since the beam had to be focussed at a distance greater than about 2 cms from the plug, only the later stages of flame propagation (Chapter 10) could be recorded. It was at these later stages of flame propagation that it was suspected that the added radical concentrations would not be as large as during the early ignition stages. The problem of light emission from the plasma was also encountered during the C_2 emission measurements and this is described

in Section 6.2 of this chapter.

The ultimate accuracy of the OH resonance absorption method was determined primarily by the signal-to-noise levels of the trace recorded on the oscilloscope screen. This noise originated from sources such as the photomultiplier dark current and shot noise which caused fluctuations of around ± 1% (more in the case of the dual trace) in the measurements. This also determined the minimum OH concentration which could be detected since this required at least a 2% change in light intensity or $\ln(\frac{I_o}{I}) = 0.020$ which corresponded to $[OH] \simeq 1.6 \times 10^{15}$ radicals cm^{-3} for a 1 cm path length through the absorbing species.

These limits of accuracy could only have been avoided by using improved amplification of the photomultiplier signal to give higher signal to noise levels. This was illustrated by some earlier OH absorption traces obtained using modulation of the light source and phase sensitive detection in which the improved method of signal processing gave lower noise levels. However as already mentioned, this method was subject to considerable practical difficulties and in many cases the accuracy would then be limited by the measurement of the effective path lengths through the plasma ignited flames using the shadow cine photographs (Chapter 10).

6.2 The C_2 Emission Method

The C_2 emission method was used to measure the total flame areas of expanding plasma ignited methane-air flames. This was necessary because a distinction had to be made between the increased flame propagation rates due to turbulence originating from the expanding plume and those due to chemical enhancement by atoms and radicals generated in the plasma. For example, using the shadow photographs to measure flame propagation rates in the presence of small scale turbulence (i.e.during the early stages of the flame), only values for the effective turbulent burning

velocity, S_T, could be obtained. This was because it was usually not possible to measure the areas of all the tiny indentations and convolutions on the flame surface. The C_2 emission method, on the other hand permitted measurements of the total flame areas irrespective of flame shape and the scale of turbulence (106) so long as the flame structure was not modified by chemical effects. This enabled the evaluation of the laminar burning velocities, Su , which were required for the interpretation of the chemical augmentation effects which were thought to be particularly important during the early stages of the flame (i.e. when the turbulence intensity is also at its highest). This method of interpretation of the results using both the shadow photographs and the C_2 emission method will be dealt with in more detail in Chapter 9.

The alternative method of measuring total flame areas by using saturation currents (107) was also considered for the present study. However, it was anticipated that the high electric fields required would probably distort the plasma and that the additional electrons and ions produced by the latter would almost certainly cause interference during the most important early stage of the measurements. As mentioned below, the measurements obtained using the C_2 emission method were also not entirely free from interference by the plasma. In this case, the intense light from the plasma imposed certain limitations on the method, similar to those encountered for the OH resonance absorption technique.

(a) The Theory

The present method measures the emission intensity from electronically excited C_2 radicals which are known to be confined almost exclusively to the main reaction zone of hydrocarbon-air flames. The intensity of the C_2 emission varies considerably with equivalence ratio, becoming strongest with the very rich mixtures (46). Also the intensity is generally weaker with flames of saturated hydrocarbons than with flames of unsaturated

hydrocarbons and consequently the C_2 emission intensity is extremely weak for lean methane-air flames.

Although the C_2 generating reaction mechanism(s) are still in doubt, it is known that the concentration of C_2 in the main reaction zone of methane-air flames is extremely small in comparison to other atoms and free radicals. For this reason, the total C_2 emission intensity, I_{c_2}, is unaffected by self absorption and equal to :

$$I_{c_2} = Aij\ N_{c_2}\ h\upsilon\ \frac{g_i\ \exp(\frac{E_i}{kT})}{F(T)} \qquad (6.1)$$

where Aij is the overall transition probability,

N_{c_2} is the concentration of C_2 radicals in the ground electronic state,

h is Planck's constant

υ is the frequency

g_i is the statistical weight of the excited state,

E_i is the energy corresponding to the transition,

k is the Boltzmann constant,

T is the temperature,

and F(T) is the partition function.

Since I_{c_2} is proportional to N_{c_2} and the reaction zone volume, I_{c_2} becomes a unique function of the equivalence ratio, ϕ , only provided there are no chemical effects of injected radicals. This is because, firstly, N_{c_2} depends on the reaction zone gas composition, the reaction kinetics and the flame temperature all of which depend on ϕ (excluding flame quenching). Secondly, the characteristic laminar burning velocity, Su , and flame thickness, η , are related to ϕ for a given set of initial conditions of temperature and pressure. Therefore for any given size of laminar hydrocarbon-air flame, the total volume of reaction zone

(equal to the product of flame thickness and total flame area) will be determined by the value of the equivalence ratio, ϕ .

Another advantage that the absence of self absorption confers is that for a given flame area, the emission intensity is independent of flame shape. This applies to turbulent flame propagation (as during the early stages of plasma jet ignition) throughout the turbulence spectrum. Therefore, providing there is no self absorption, the fraction of the total radiation arriving at the detector (or collecting lens) depends on the solid angle that an elemental volume, dV (such as point A or B in Fig.(24)) subtends at the detector. With the use of a calibration curve for a given equivalence ratio, the radiation from the entire flame can then be related to the total flame area and this is described in the next section.

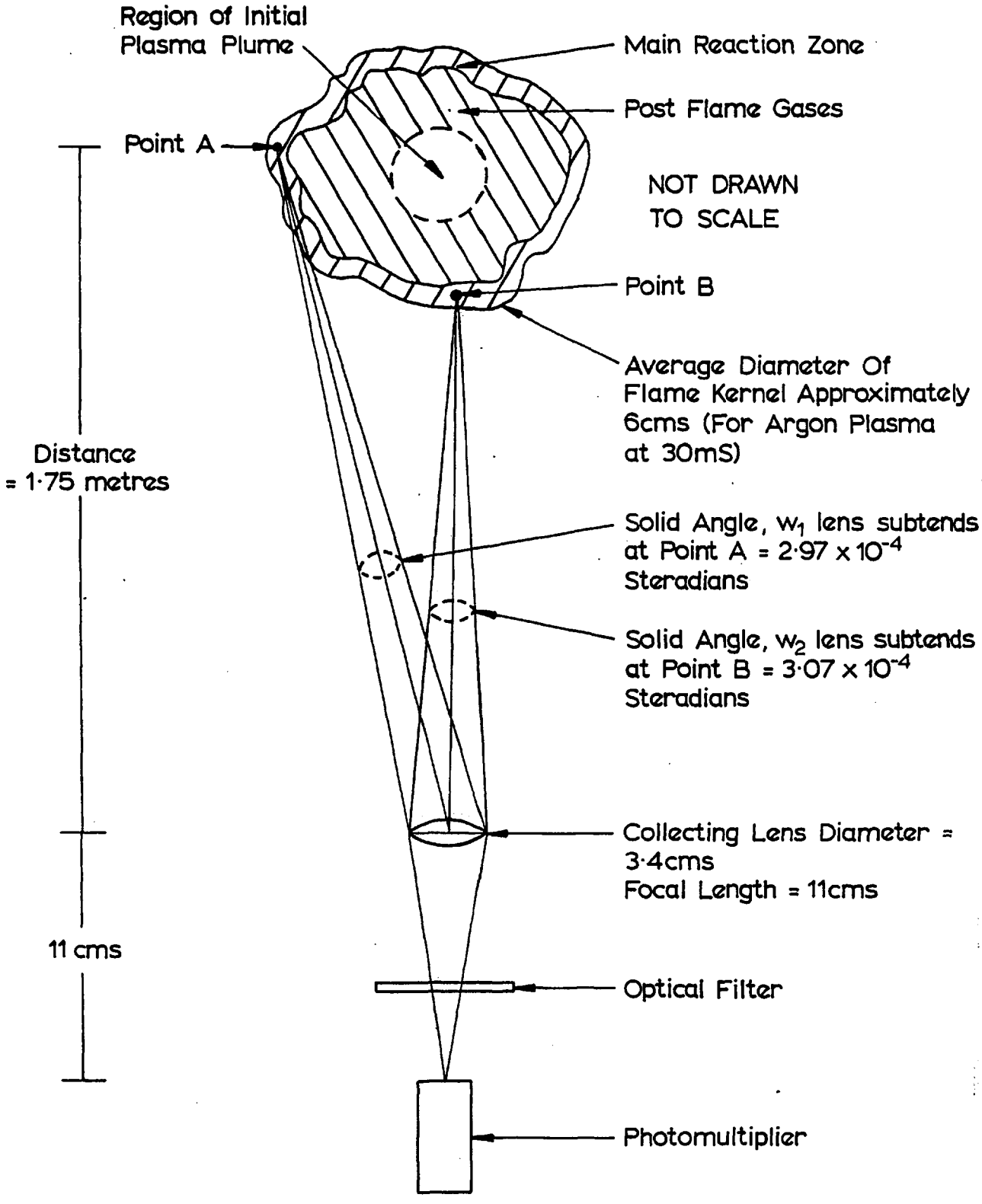
(b) Experimental

The C_2 detection system consisted of the following: (1) A photomultiplier (E.M.I. 9592A) and E.H.T. source; (2) a narrow band filter (Grubb Parsons with specifications: peak wavelength 515 nm; peak transmission 45%; bandwidth 5 nm and sidebands $< 0.1\%$); and (3) a 11 cms focal length collecting lens, as shown in Fig.(24).

In positioning the detection system, a distance from the collecting lens to the combustion vessel was chosen such as to ensure that the collecting lens subtended almost the same solid angle, w at all points in the flame. If the detection system was placed further away from the combustion vessel than this position, an unnecessary loss of photomultiplier signal resulted. As shown in Fig.(24), the optimum distance from the combustion vessel to the collecting lens was found to be 1.75 metres. The position of the photomultiplier was then adjusted to ensure that an image of the flame appeared on the photomultiplier cathode. This was achieved by placing a small quartz halogen lamp just below the plasma plug and focussing the image of this onto the cathode. The narrow band spectral

FIG. (24)

C_2 EMISSION DETECTION SYSTEM



filter was then positioned between the collecting lens and the photomultiplier and this served to isolate the (0,0) C_2 emission band head at 5156 Å from other radiation emitted by the flame.

(c) The Calibration

To derive total flame areas of plasma ignited methane-air flames from C_2 emission traces recorded on the storage oscilloscope, it was first necessary to run a calibration. This was required because firstly insufficient information was available in the literature on C_2 emission intensities from lean methane-air flames and secondly other experimental factors such as the transmission factor of the collecting lens and the quantum efficiency of the photocathode were not known with adequate precision to enable absolute values for C_2 emission intensity to be calculated. This calibration was obtained by measuring the C_2 emission from a laminar spherically expanding flame kernel ignited by a low energy (approximately 50 mJ) spark. Simultaneous high speed cine shadow photographs were taken with the C_2 emission measurements and the total flame areas obtained from the photographs were then compared with the C_2 oscillograms.

An example of this is shown in Plate (9) which shows the sequence of events following a spark ignition of a methane-air mixture. Flame areas measured from these photographs were compared with the C_2 emission oscillogram also shown in Plate (9) to obtain the calibration curve shown in Fig.(25). The C_2 emission measurements against time for this spark ignition are also shown in Fig.(26) together with calculated flame areas against time, assuming a spherical combustion wave with Su = 16 cms/s (ϕ = 0.62) and $\frac{\rho_u}{\rho_b}$ = 6.1. The dotted line in this diagram shows the C_2 emission intensities (in units of mV) which correspond to the calculated flame areas assuming an emission intensity of 0.036 mV per cm^2 of flame area. This curve agrees with the experimental curve over the

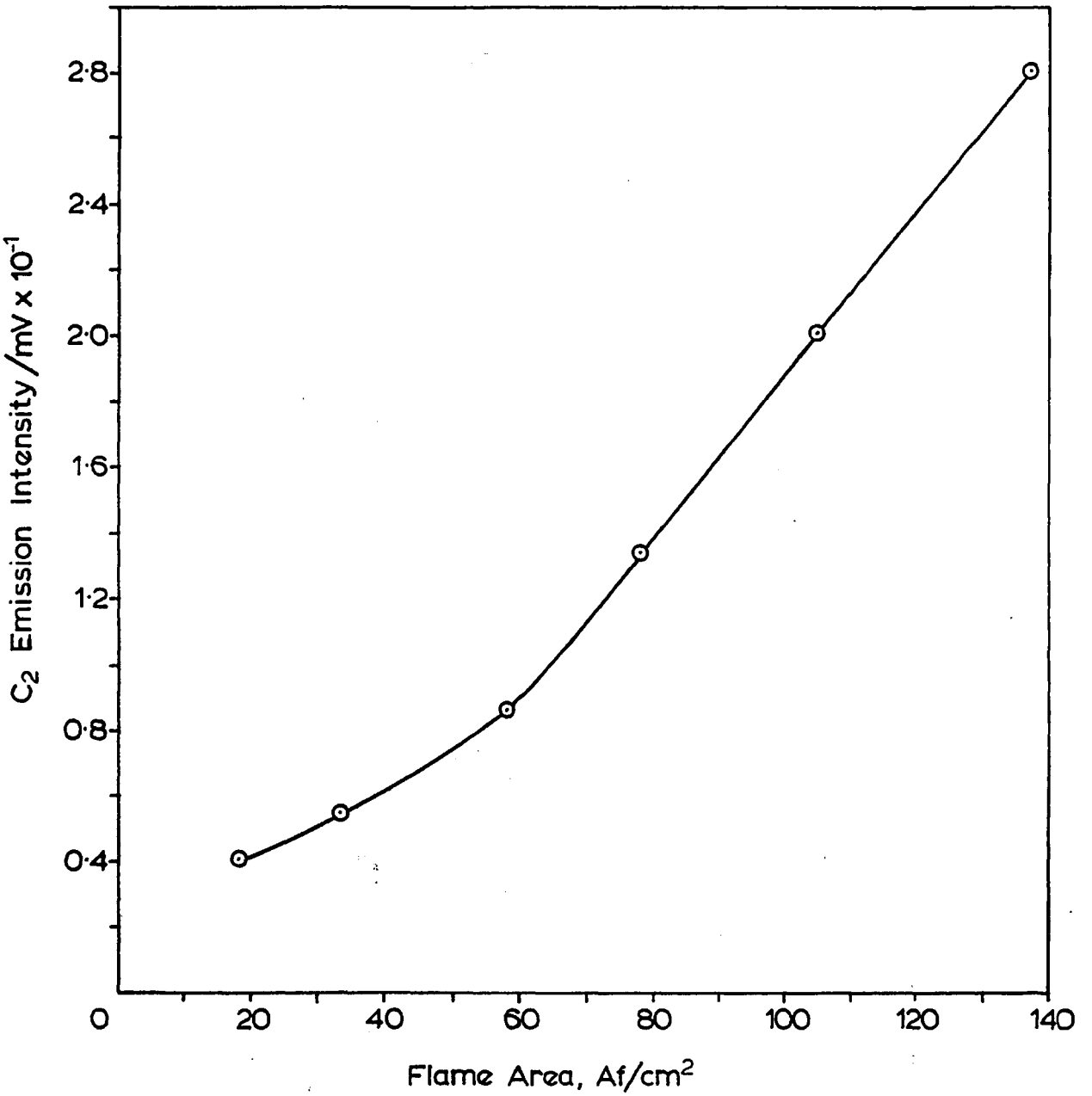


FIG. (25)

C_2 EMISSION INTENSITY CALIBRATION

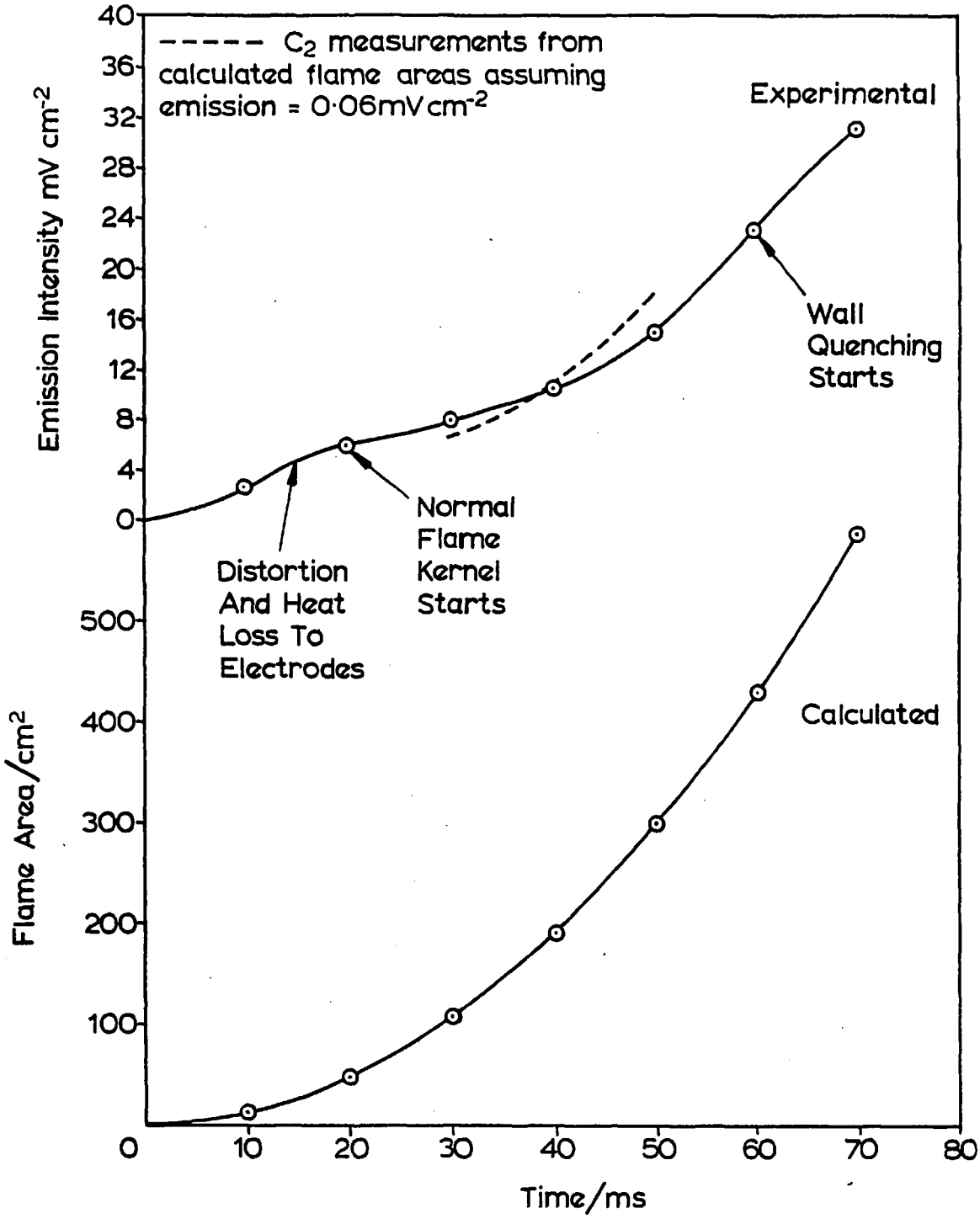


FIG. (26)

CALCULATED FLAME AREAS AND EXPERIMENTAL C_2 EMISSION MEASUREMENTS FOR SPARK IGNITED METHANE/AIR FLAMES WITH ϕ = 0·62

duration 20-50 mS, before and after which distortion of the flame by the electrodes or walls of the combustion vessel, respectively, occurs.

Clearly, it was necessary to run these calibration standards under absolutely identical conditions to those of the plasma ignited flames. For this reason, the calibrations were taken directly after the plasma ignited flames, thereby eliminating any possible error due to changing experimental conditions. In this way, the use of calibration curves enabled total flame areas of laminar or turbulent plasma ignited flames to be accurately measured.

(d) Limitations and Errors in the Method

The major limitation of the method was that due to light emission from the plasma. This continued up to about 5 mS after triggering the plasma jet and contributed a much larger voltage to the anode load of the photomultiplier than that due to the C_2 emission from the flame. For slowly igniting plasmas (e.g. Nitrogen and Argon), this presented no problem since this interference had diminished before a flame front formed, see Chapters 7 and 9. For hydrogen plasmas on the other hand (which were found to give rise to a flame in lean methane-air mixtures in less than 1 mS), the method could not be used successfully since the C_2 emission signal was swamped by that due to the light emission in the form of a strong continuum.

Attempts were made to prevent this intense plasma light reaching the photomultiplier (similar to the approach with the OH absorption method where an adequate distance between the plasma plug and the focussed beam was ensured) by blanking off parts of the image at the cathode surface. Although this certainly reduced the interference, it still did not make C_2 measurements of hydrogen plasmas igniting methane-air mixtures possible.

Comparisons were therefore made between nitrogen and argon plasmas igniting a methane-air mixture with an equivalence ratio, $\phi = 0.62$. For this equivalence ratio, the stored energy used for the nitrogen plasma

was 4.8 J. If higher energies were used a flame front formed too early and C_2 measurements became too inaccurate. Likewise if ϕ was increased (with a stored energy of 4.8 J), a flame front formed too early. In the case of argon, an energy equal to 8.6 J was required since plasmas with lower energies were unable to ignite a mixture with $\phi = 0.62$ (see Chapter 8). In summarizing, a comparison was made at a constant equivalence ratio of $\phi = 0.62$ between nitrogen plasmas (stored energy 4.8 J) and argon plasmas (stored energy 8.6 J) and the results are discussed in Chapter 9.

The errors in the method were again primarily due to the noise levels in the photomultiplier output (see Section 6.1(b) of this chapter). This caused fluctuations of about $\pm 1/2\%$ in the signal which was generally less than that corresponding to the OH resonance absorption technique, especially when the dual trace on the oscilloscope was used. Finally it can be seen by inspection of the C_2 oscillograms in Plates (10) and (11) that only the first part of the trace was used for the plasma jet ignitions. This was because the major section of the trace corresponded to the later stages of flame propagation, that is as the flame approached the walls of the combustion vessel.

CHAPTER 7

PLASMA JET IGNITION - AN EXAMINATION OF THE MECHANISMS

To assess the chemical effects associated with radical injection by plasma jets, a study was required of the other contributory effects causing ignition and rapid flame propagation in lean methane-air mixtures. These included primarily the fluid mechanical effects due to the turbulence and momentum of the jet, the radiation effects from the plasma and, in the case of a constant volume system, the effects associated with adiabatic compression of the reactants following rapid early flame expansion. This study involved both experimental and theoretical work which is described in the present chapter.

7.1 Effects due to Adiabatic Compression

In the preliminary experiments (4), enhanced rates of flame propagation were observed when the plasma cavity was filled with hydrogen or hydrocarbon feedstocks. These increases appeared to persist for the entire history of flame propagation through the test chamber which, in this case, was a constant volume bomb, (unlike the constant pressure combustion vessel used in the present experiments). Consequently, during the later stages of flame propagation, the reactant gases experienced increased pressure and temperature effects associated with the pressure rise due to combustion.

Calculations were made to assess the effects due to adiabatic compression using the following expressions for the temperature (112) and pressure (1) dependence of laminar burning velocity, Su:

(1) Temperature dependence (valid over the range 298 to 1000 K)

$$Su = 10 + 0.000371\ Tu^2 \text{ cm. } s^{-1} \qquad (7.1)$$

where Tu is the initial temperature (K).

(2) Pressure dependence

$$\frac{Su_{(a)}}{Su_{(b)}} = \left(\frac{P_a}{P_b}\right)^n \qquad (7.2)$$

where $Su_{(a)}$ and $Su_{(b)}$ are the burning velocities at pressures P_a and P_b and the exponent, n, is specified as a function of burning velocity at standard temperature.

The results of these calculations showed that the effects were very small except when the flame had nearly reached the vessel walls. In these later stages the values of Su could be more than doubled. For all other positions of the flame, the effects were small; e.g. even when the radius of the flame near the lean limit was 0.7 x vessel radius, the increase in Su due to adiabatic compression of the unburnt mixture was < 20%.

It was concluded from these calculations that the effects of adiabatic compression were not the main factor responsible for the enhanced rates of flame propagation observed in the preliminary experiments. Consequently, the results from the earlier study should be comparable to those obtained in the present experiments.

7.2 Effects of Long-Range Ultraviolet Radiation

The effects of any long-range vacuum ultraviolet radiation from the plasma were examined using the following set of preliminary experiments (39). Firstly, the plasma plug was used to ignite approximately stoichiometric methane-air and ethylene-air mixtures issuing from a porous plug burner at atmospheric pressure. After confirming that the plasma would readily ignite these mixtures even with the smallest amounts of energy that would form a plasma, some experiments were performed with a lithium fluoride window (chosen for its transparancy to vacuum ultraviolet radiation) separating the plasma from the reactants. In this

case no plasmas produced ignition in the stoichiometric methane and ethylene-air mixtures even though the plasma cavity was filled in turn with air, hydrogen and methane and the highest energies available ($\frac{1}{2}CV^2$ = 12 Joules) were dissipated in the discharge. In these experiments, the plasma jet plug was kept in an identical position to the previous experiments (i.e. those without a LiF window) and the position of the window was varied between 1 mm and 15 mm from the plasma plug orifice.

A further set of experiments were then carried out to check whether radiation of shorter wavelength (higher energy) than that transmitted by the LiF window ($\lambda \simeq 1350$ Å) could be responsible for the ignitions. The apparatus (shown in Fig.(27)) was designed to refocus almost all of the plasma radiation into an ethylene-air mixture. This was achieved using a pair of aluminized (> 90% reflectivity in the range thought relevant) parabolic headlamp mirrors which touched at their periphery and accommodated the plasma jet, argon inlet tube, flammable gas inlet tube and flammable gas outlet tube as shown in the diagram. The foci were located by both calculation and by the "no parallax" method. The flammable mixture at the focus of one mirror was discharged from an inlet tube (6 mm I.D.) and aspirated via a small funnel. The flow rate through the funnel was arranged to be faster than from the inlet tube thereby preventing the mixture spreading. Near the focus of the other mirror, the plasma plug and argon inlet tube were positioned. The purpose of the argon was to purge the volume enclosed by the two mirrors and in doing so reduce the absorption of radiation below 200 nm (i.e. absorption by the Schumann-Runge oxygen bands). In spite of several plasma plug "firings" each one being followed by minor changes in positioning of the inlet tube or plasma plug, again no ignition of the mixture could be achieved.

The results of these experiments indicate the absence of any long

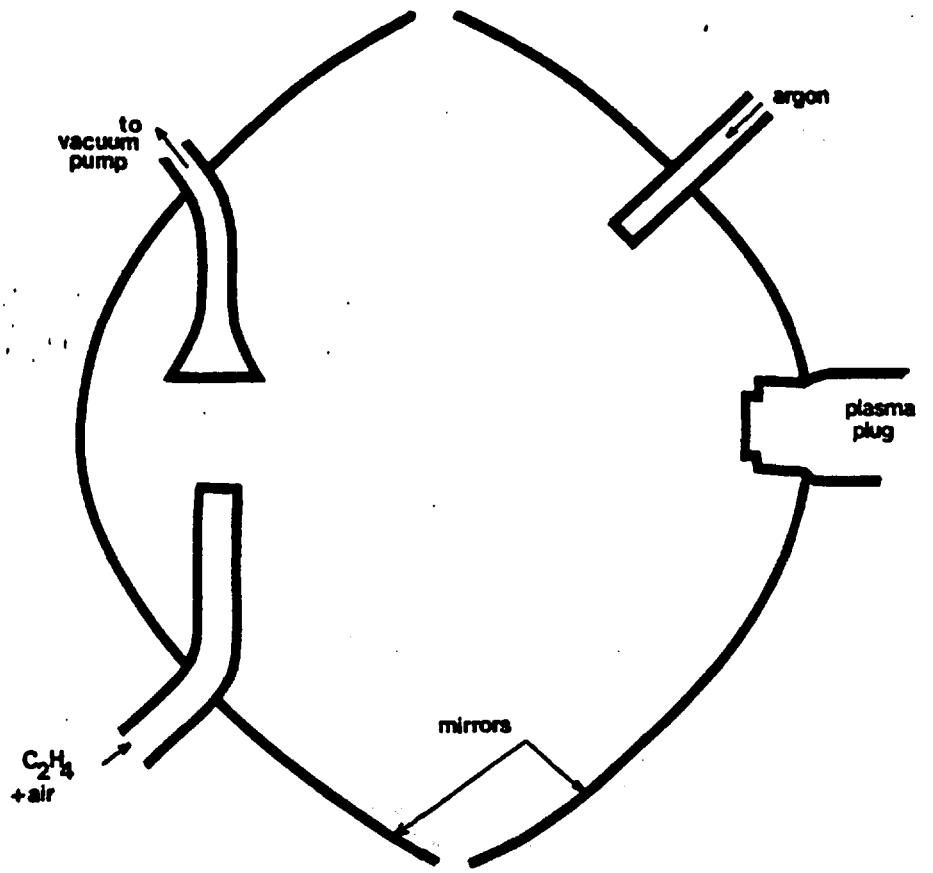


FIG.(27)

THE FOCUSSING
SYSTEM

range (i.e. > 3 to 4 mm) photochemical effects produced by this particular plasma plug. Thus it is possible that significant effects might occur at higher power inputs or different wavelengths. Moreover, the results do not rule out possible short-range effects of UV (e.g. effects confined to the vicinity of the zone of heat release) but then the design of a practical ignition plug based on short-range effects would be independent of whether these effects were diffusion or radiation controlled. However, it is possible to conclude from these experiments that at the input energies examined, long-range radiation effects make no significant contribution to the large improvements in flame initiation observed during ignition by hydrocarbon plasmas.

7.3 The Fluid Dynamic Properties of the Plasma Jet

The fluid dynamic properties of a plasma jet discharging into (1) air and (2) a flammable methane-air mixture were examined experimentally using mainly high speed schlieren photography. Apart from the necessity of assessing the importance of the jet fluid dynamics in causing ignition and increased rates of flame propagating this study became essential because the consistency of the spectroscopic measurements was found to depend on the reproducibility of the size and geometry of the expanding plasma jet plume.

The use of streak photography in previous experiments (15) in which a plasma plug (identical to that of the present research) was used, revealed that the length of the luminous plasma ejected from the cavity attained a maximum length of 17 mm with an orifice diameter of 2 mm and a discharge energy of 2.5 J. The light was emitted in two bursts each 200 to 300 μs in duration due to the oscillatory nature of the ignition circuit.

Schlieren flash photography, on the other hand, showed the formation of a turbulent plume embedded in a blast wave after 100 μs. This

turbulent plume continued to grow in size until 200 μS after the discharge when the blast wave formed as a single shock front. At a time of 1 mS, the plume had grown almost to full size with dimensions approximately 6 cms in length and 3 cms in diameter. Similar results to these were found in the present research and these are described in the following section.

(a) Results and Discussion

(1) Plasma jet discharging into air

The schlieren records for nitrogen, hydrogen and argon plasmas discharging into air are shown in Plates (6), (7) and (8) respectively. The reproducibility of the plasma plume size and geometry with respect to time was examined using measurements made on the axial length and maximun diameter (Fig.(28)) of several plasma plumes at two stored plasma energies of 4.8 J and 10.8 J. These are shown in Figs.(29), (30) and (31). From these graphs, it is seen that an argon plasma (stored energy of 4.8 J) attains a length of 5.3 cms in 1.6 mS; a nitrogen plasma requires 2.7 mS whilst a hydrogen plasma requires 5.4 mS to attain this length.

In the case of argon which is incapable of dissociation, the low specific heat would account for the high ejection velocity of this plasma although a similar explanation would not account for the large difference in ejection velocities of hydrogen and nitrogen. On the other hand, the curves of maximum diameter versus time are similar for argon and hydrogen over the time interval 0 to 2 mS, but not for nitrogen. It is quite likely that the cavity overpressures are in fact similar for both nitrogen and hydrogen plasmas but that the high diffusion coefficient of H atoms and H_2 molecules give high radial mass transport and consequently wider and shorter plasmas. This is certainly confirmed by visual observation of these plasmas discharging into air.

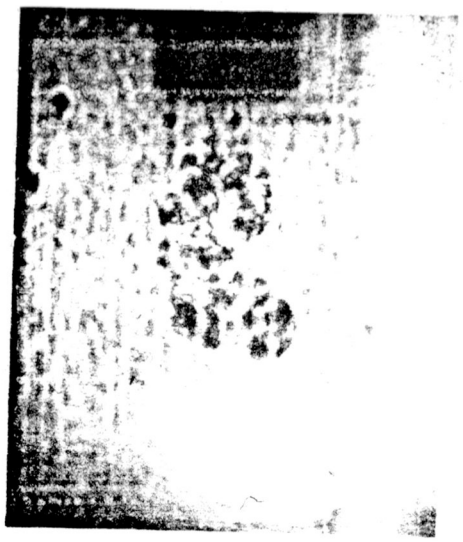
PLATE (6)

A Nitrogen Plasma Discharging Into Air

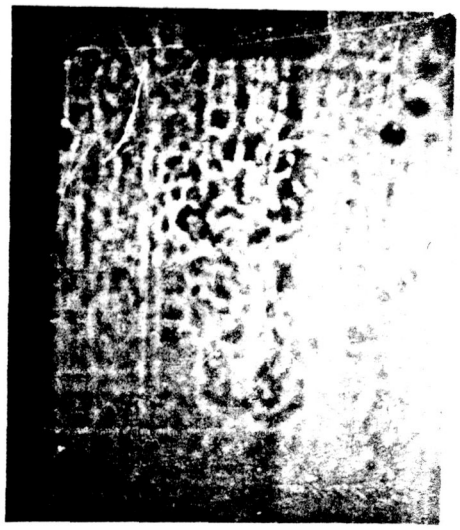
Stored Energy = 4.8 J



0.4 mS



1.0 mS



3.2 mS



6.0 mS

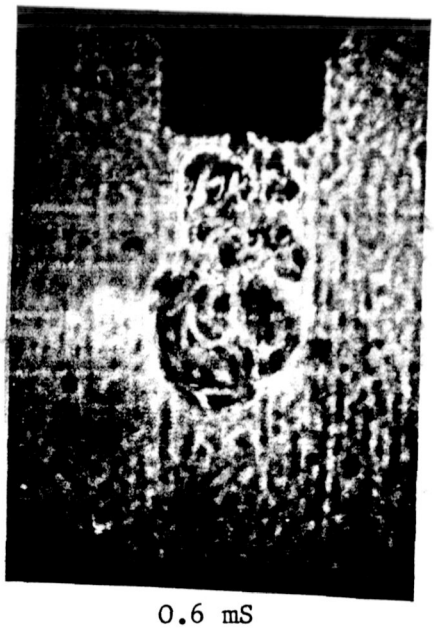
PLATE (7)

A Hydrogen Plasma Discharging Into Air

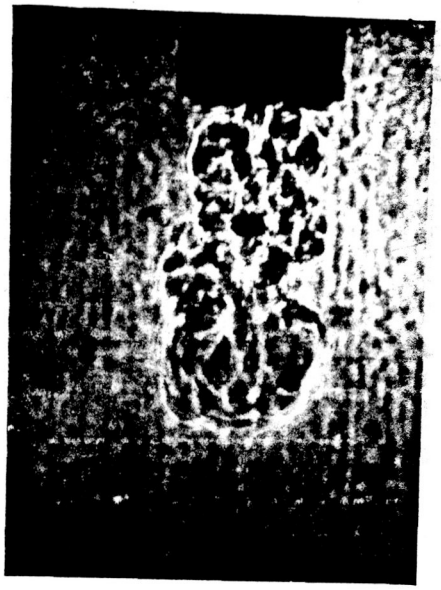
Energy = 4.8 J



0.4 mS



0.6 mS



1.0 mS



4.4 mS

PLATE (8)

An Argon Plasma Discharging Into Air

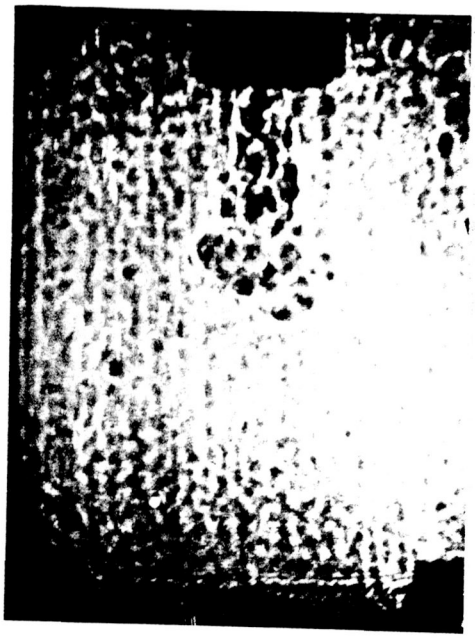
Stored Energy = 4.8 J



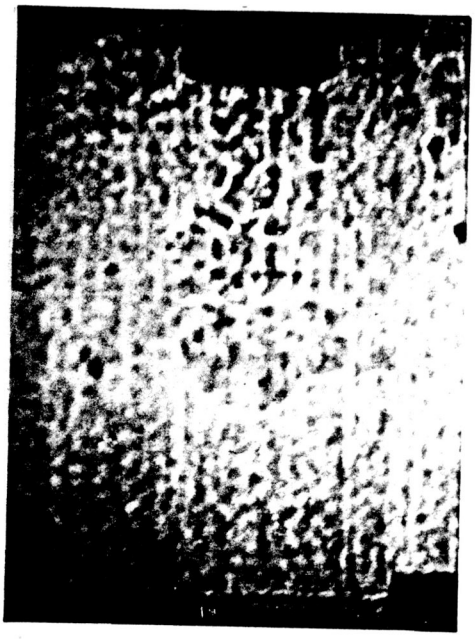
0.4 mS



0.6 mS



0.8 mS



1.8 mS

FIG. (28)

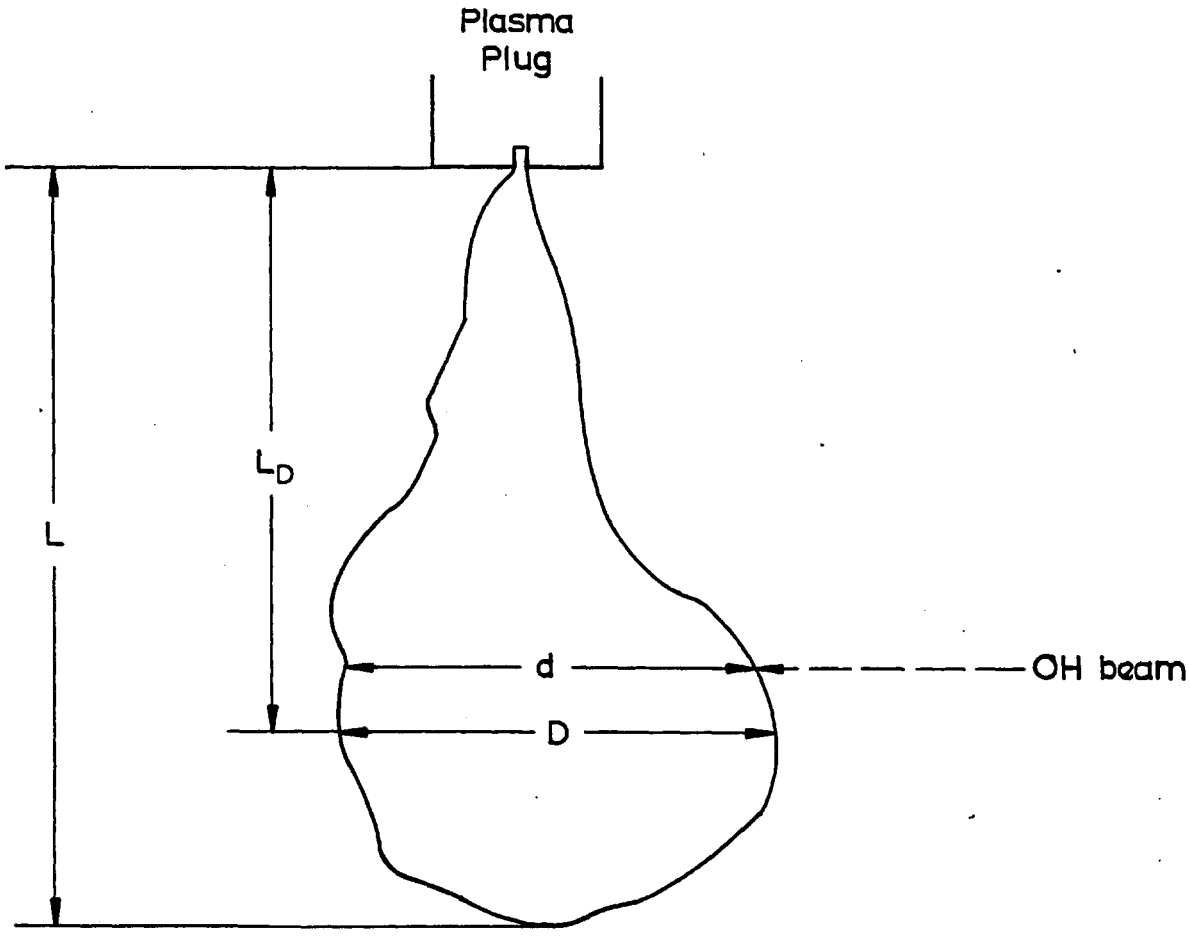
DEFINITION OF SYMBOLS

L - Axial Length Of Jet

D - Maximum Diameter Of Jet

L_D - Length Of Jet Corresponding To Maximum Diameter

d - Path Length Of Spectroscopic Beam



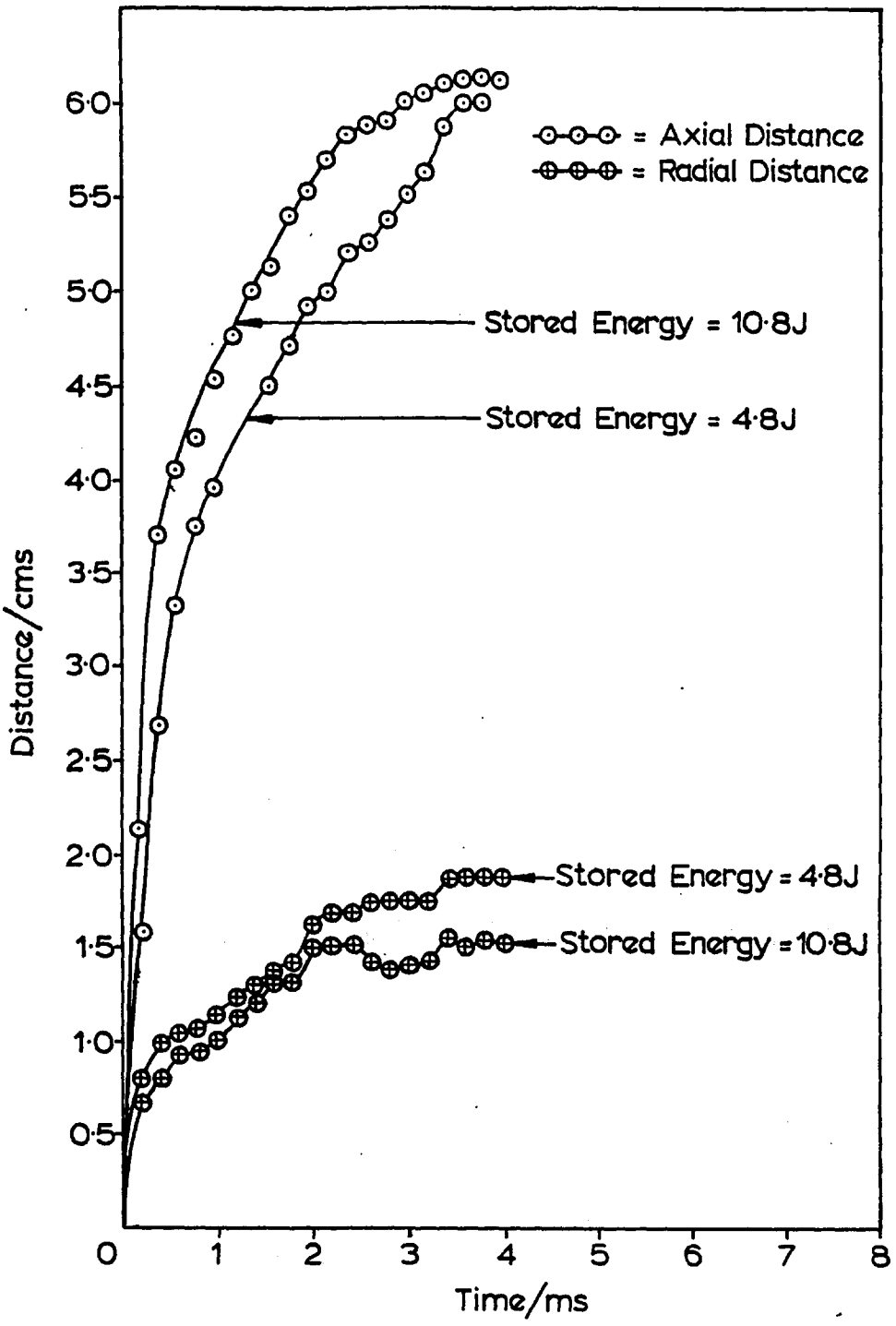


FIG. (29)

AXIAL AND RADIAL DISTANCE vs. TIME FOR A NITROGEN PLASMA JET DISCHARGING INTO AIR

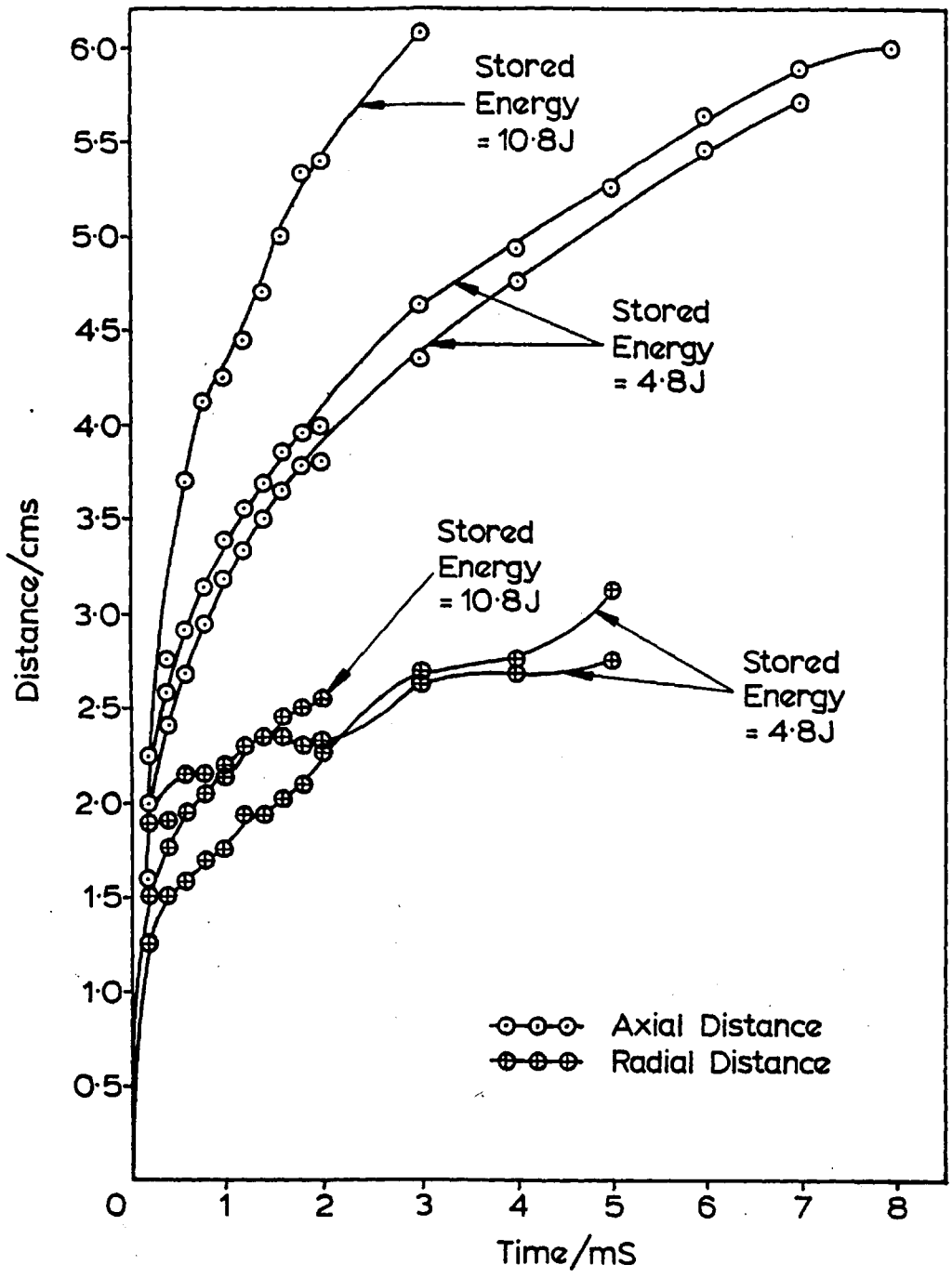


FIG. (30)

AXIAL AND RADIAL DISTANCES vs. TIME FOR A HYDROGEN PLASMA DISCHARGING INTO AIR

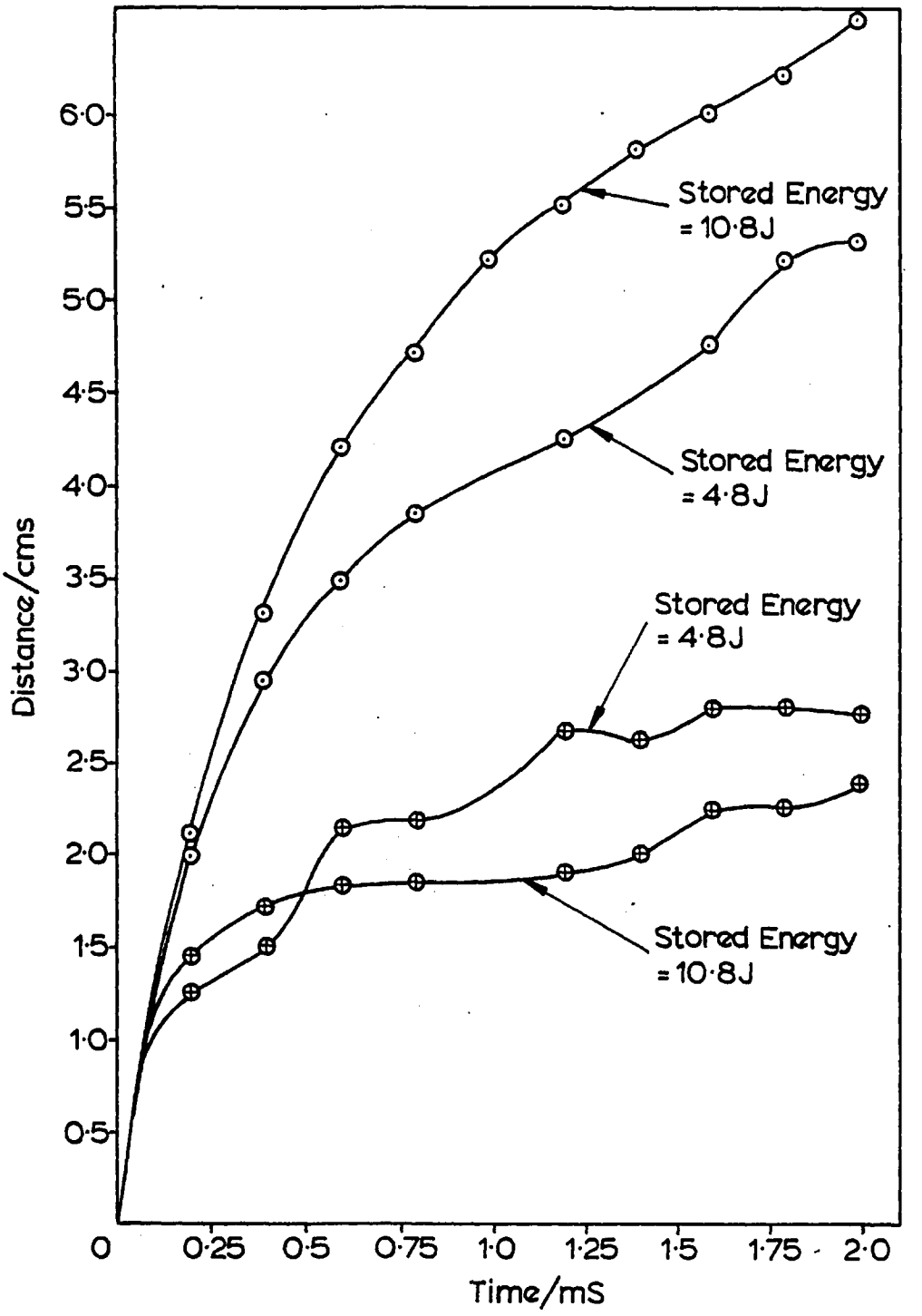


FIG. (31)

AXIAL AND RADIAL DISTANCES vs. TIME FOR AN ARGON PLASMA JET DISCHARGING INTO AIR.

Another feature that was observed was that the markings on the shadowgrams faded at different times for different plasmas. For example, measurements on argon plasma plumes became difficult to discern after 2 mS whilst for nitrogen, measurements can be made up to 14 mS and for hydrogen up to 68 mS (with a heavily over-exposed film). This may be partly a consequence of the difference in ejection velocities although primarily a result of the heat release due to recombination of H and N atoms (for hydrogen and nitrogen plasmas respectively) in the plume which is absent in the case of argon.

(2) Plasma Jet Igniting a Methane-Air Mixture

The sequence of schlieren photographs for nitrogen, argon and hydrogen plasma jets igniting a methane-air mixture are shown in Plates (11), (10) and (12) respectively. For the period of time up to 1 mS after the discharge, the structures of the plumes are almost identical to those discharging into air. The high temperature plasma ejected from the cavity entrains large volumes of methane-air mixture producing the plasma plumes shown in the photographs. This momentarily forms a stirred-high temperature reacting system within the boundaries of the plume and the formation of hot combustion products retards the temperature decrease of the plume whilst increasing its volume above that of an identical plasma discharging into air. After this period, (in the case of a successful ignition), a flame kernel is established on the outside of the original plasma plume which propagates outwards into the unburnt gas.

This is illustrated in the case of an argon plasma in Plate (10). As mentioned above, for an argon plasma discharging into air, the schlieren records begin to fade at a time of 3 mS. With an identical plasma discharging into a methane-air mixture, the markings on the records are still visible at a time of 10 mS indicating that some combustion has occurred at times $\leq$ 10 mS. This could not be detected by the C_2 emission

method since, during this early time period, the signal was masked by interference caused by light emission from the plasma. After about 12 mS, a flame kernel was formed reluctantly on one section of the plasma plume (Plate (10)) giving an overall ignition delay time equal to 12 mS.

A similar process occurred with nitrogen plasmas giving an overall ignition delay time of about 10 mS. Measurements of the effective OH absorption path length of 2 identical nitrogen plasmas, one discharging into air and the second into methane-air mixture are shown in Fig.(32). These indicate an expansion of the nitrogen plasma plume due to combustion within this "stirred" plasma plume volume. Simultaneous OH absorption measurements which show the growth and decay of the hydroxyl concentration during this pre-ignition period (lower curve on Fig.(32)) support this conclusion. Both these "pre-ignition" and "true ignition" processes are again illustrated by the two OH absorption oscillograms shown in Plate (13).

Hydrogen plasmas igniting methane-air mixtures behave quite differently to those of nitrogen and argon. The overall ignition delay time ($<$ 1 mS) is too short for the "stirred reaction" stage to be isolated. Fig.(33), which shows the axial lengths and maximum diameters of identical plasma jets discharging into (1) air and (2) methane-air mixtures, illustrates this situation. In the case where combustion occurs, the downward propagation of the jet is retarded compared to a jet discharging into air. This starts at time $<$ 1 mS and becomes progressively more important with time. In contrast, the maximum diameter increases more rapidly with combustion than without and again this becomes progressively more important with time after a time of 0.4 mS. These measurements therefore suggest that for hydrogen plasmas, a single ignition delay occurs which is $\leq$ 0.4 mS.

(3) Summary

As regards the fluid dynamic properties, the following observations

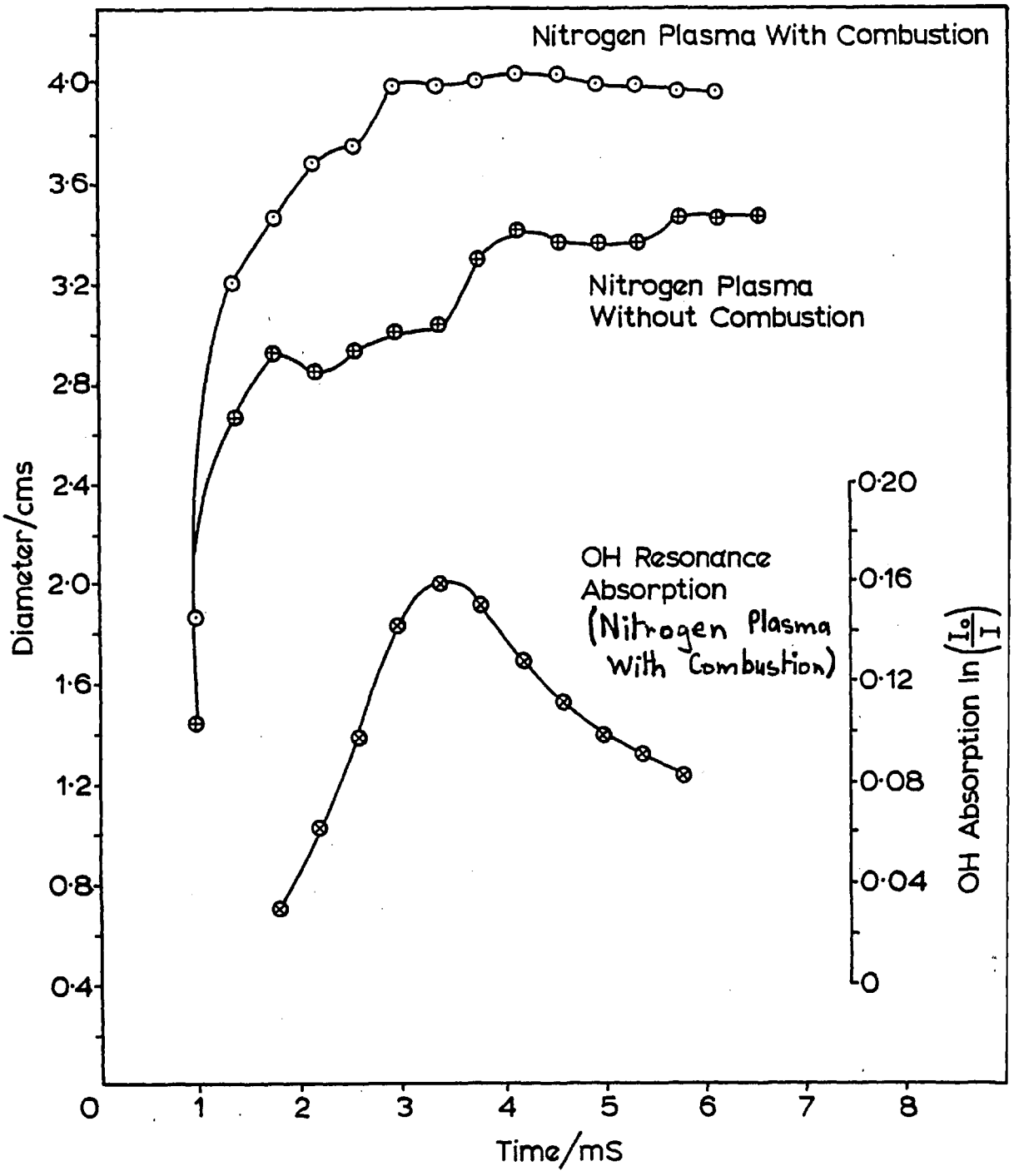


FIG. (32)

A NITROGEN PLASMA IGNITING A METHANE-AIR MIXTURE. OH RESONANCE ABSORPTION AND PLASMA DIAMETER ALONG AXIS OF OH DIAGNOSTIC BEAM. (OH beam focussed 4·0cms below plug with no horizontal displacement). $\emptyset$ = 0·54, Stored Plasma Energy = 10·8J, Plasma Flow rate = $5cm^3min^{-1}$.

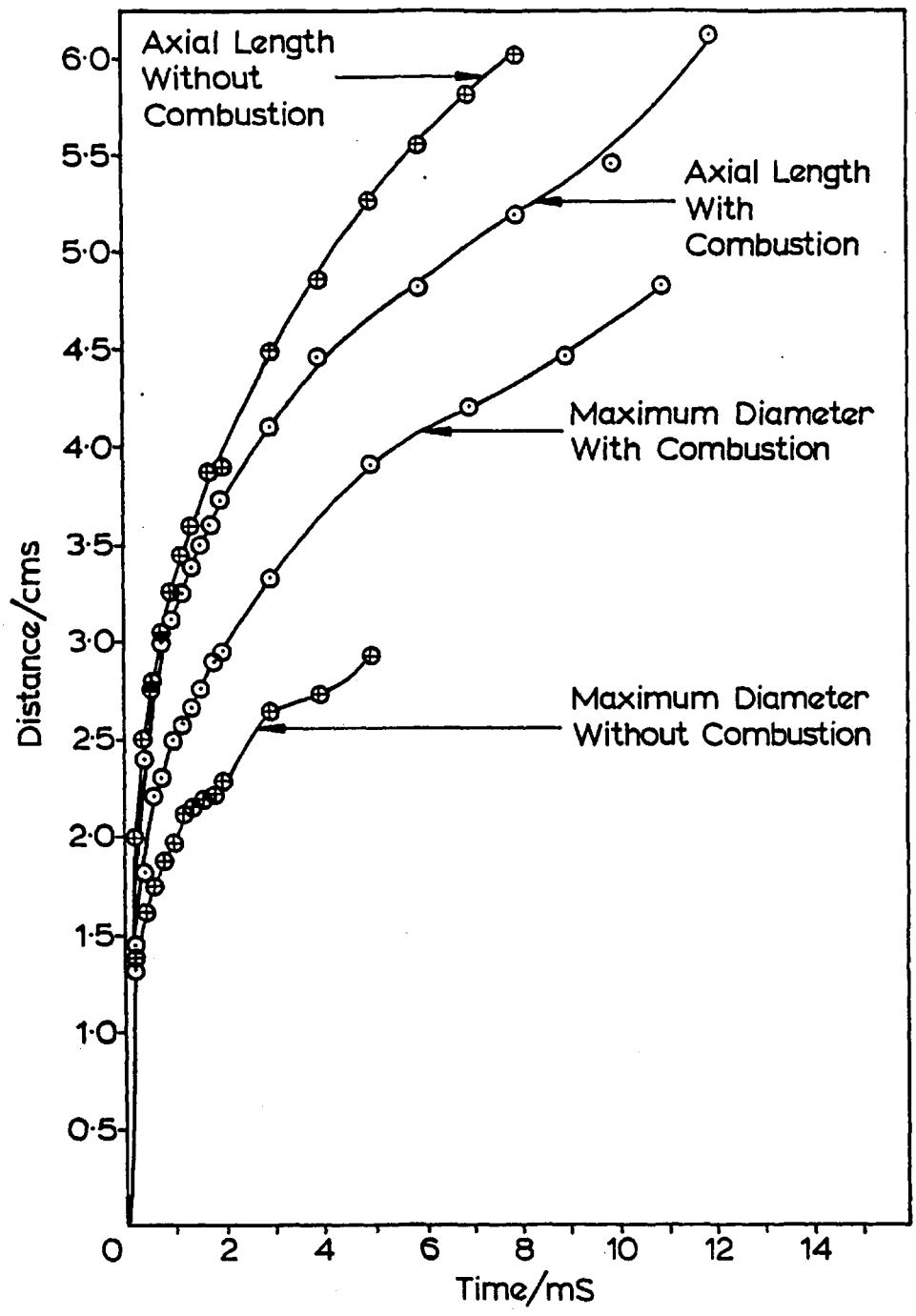


FIG. (33)

HYDROGEN PLASMA

(1) DISCHARGING INTO AIR

(2) IGNITING A METHANE AIR MIXTURE WITH $\phi = 0{\cdot}62$

have beem made.

Plasma Jet Discharging into Air

(1) For identical plasma firings, measurements of axial lengths and maximum diameters show that the growth of size and shape of the plasma plume is reasonably consistent from run-to-run.

(2) The ejection velocities were found to be a function of energy and plasma media as would be expected. The order of increasing ejection velocities for different plasma media was found to be argon > nitrogen > hydrogen. This could have some bearing (probably small though) on the observed dependence of combustion characteristics on plasma media.

Plasma Jet Igniting Methane-Air Mixture

(1) For nitrogen and argon plasmas, a 2-stage ignition has been identified. The 1st stage ignition ("the stirred reaction system") was found to occur during the period of about time = 1 mS to 6 mS for a nitrogen plasma. The second stage ignition (establishment of a flame kernel) was found after a time of about 10 mS (Nitrogen) and time $\simeq$ 12 mS (Argon). For hydrogen, a single ignition occurs immediately at time $\leq$ 0.4 mS.

7.4 Conclusions on the Contributory Mechanisms

The experimental and theoretical work described in the present chapter has shown that the effects of (1) long-range ultraviolet radiation from the plasma and (2) adiabatic compression of the reactants in a constant volume system on ignition and flame propagation are small.

In contrast, the fluid dynamic properties determine the size, geometry and turbulence of the jet and hence the initial location and surface area of the flame kernel. In the absence of any major chemical effects (e.g. with argon plasmas), the fluid dynamics

govern the ignition delay times and the overall burning rates. When chemical effects are present (e.g. in the case of hydrogen plasmas) they override the fluid dynamic properties in determining the combustion characteristics (e.g. limits of ignitability, ignition delay times and burning velocities) which are described in subsequent chapters.

CHAPTER 8

THE INCEND IVITY OF THE PLASMA JET

Some of the first more detailed experimental studies on plasma jet ignition involved an examination of the leanest methane-air mixtures (ϕ_{min}) which could be ignited by a plasma of a given initial energy and gas fed to the plug. Although at first, this was regarded as an essential preliminary to a spectroscopic analysis of the ignition process, the results became of sufficient interest to warrant further examination.

The ignition phase cannot be entirely separated from flame propagation since a small proportion of the total reactants will be burnt even for ignition energies smaller than that required for complete burning of the charge. Also due to the statistically random nature of the ignition process, a criterion was required with which to define ignition. This could have been based on the % volume of reactants burnt as determined by chemical analysis of the product gases or, in the case of a constant volume system, the measured rate of pressure rise associated with combustion. However, for the results described in the present thesis, the criterion was chosen such that, if out of every 5 plasma firings, at least 4 resulted in the flame propagating all the way to the walls of the vessel, the plasma was regarded as capable of igniting the mixture.

The dependence of ϕ_{min} on stored plasma energy, plasma medium and flow rate of plasma medium was investigated. The results are discussed in terms of the theory relating to spark ignition of lean limit mixtures and the importance of the chemical effects associated with hydrogen plasmas is illustrated.

8.1 Experimental

For all the data points obtained several sets of 5 plasma firings were made (in the region of 50) for each plasma condition to establish

the correct value of ϕ_{min}. During each set, all the external conditions were kept constant. For example, the time between plasma firings was kept to one minute during which time the storage capacitors (C2 in Fig.(20)) had adequate time to recharge and for the combustion vessel to refill with methane-air mixture. Also a continuous flow of plasma gas to the cavity was maintained throughout the set of firings thereby maintaining a steady state equilibrium gas composition. Finally, the methane-air input valves (Fig.(18)) were closed momentarily before firing the jet to ensure that the flammable mixture in the vessel was stationary during firing. This did not cause the pressure to rise within the combustion vessel during combustion since the surplus combustion products escaped via the gauze at the top of the vessel.

Corrections were made to the equivalence ratio of the methane-air mixture within the vessel to account for the overflow of plasma feed gas from the cavity. These corrections were extremely small (i.e. altered the equivalence ratio of the main charge by about 0.01) if it was assumed that the plasma gas mixed uniformly throughout the entire vessel.

The dependence of ϕ_{min} on plasma media, stored plasma energy and plasma gas flow rate was examined and the results are described in the next section.

8.2 Results

(a) Variation of Incend ivity with Applied Energy

The results on the variation of ϕ_{min} with applied energy for the 3 plasma media - hydrogen, nitrogen and argon, are shown in Figs. (34), (35), (36) and (37). These were obtained using a 25 μF capacitance (C2 in Fig.(20)) charged in the region of 500-980 V. Generally, no plasmas were formed when this storage capacitor, C2, was charged to less than about 430 V, presumably because of the very high energy losses which occurred in the plasma jet power supply circuit. The orifice plate

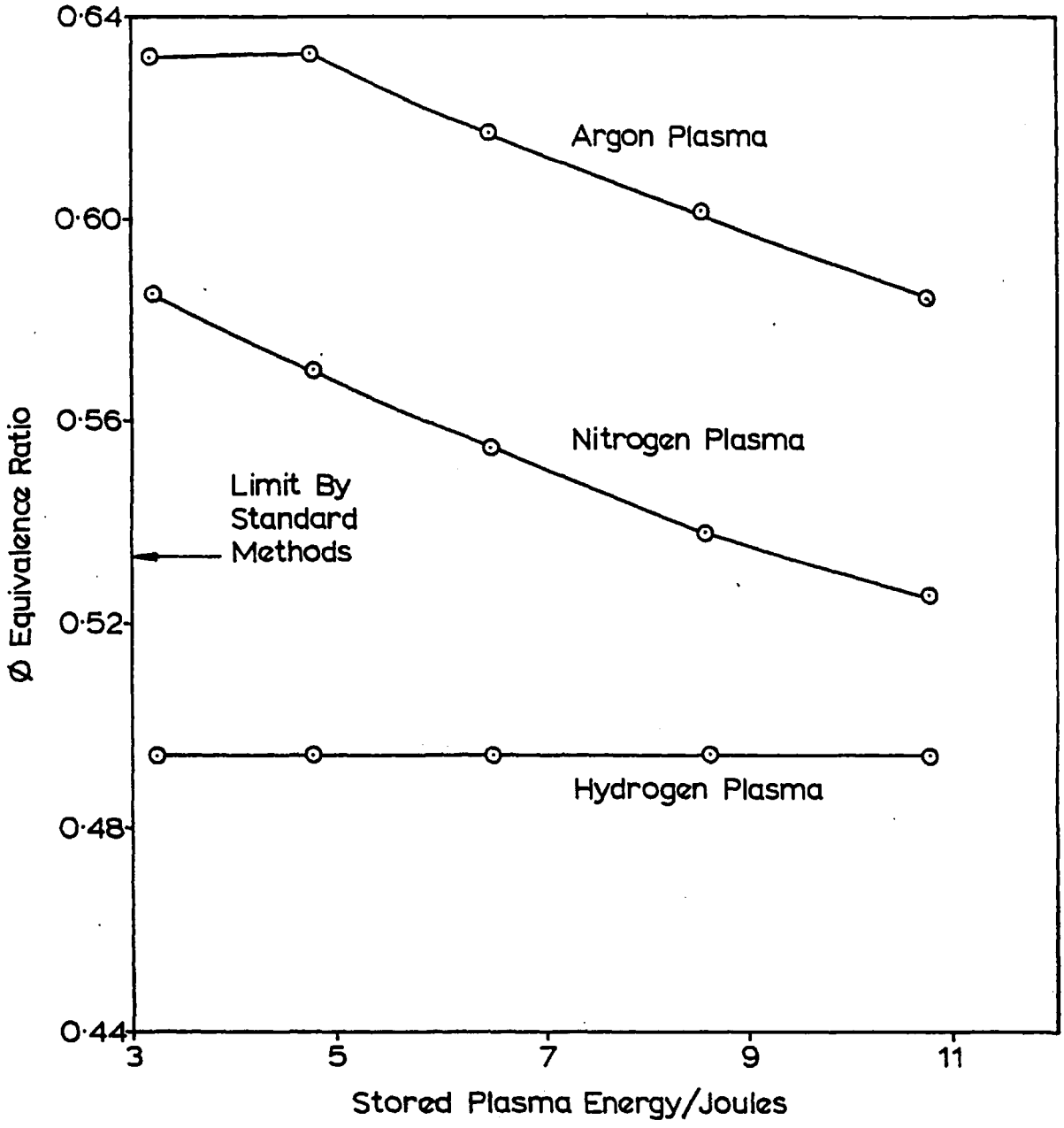


FIG. (34)

VARIATION OF Ø WITH STORED PLASMA ENERGY
Plasma Gas Flow Rate = $5cm^3min^{-1}$

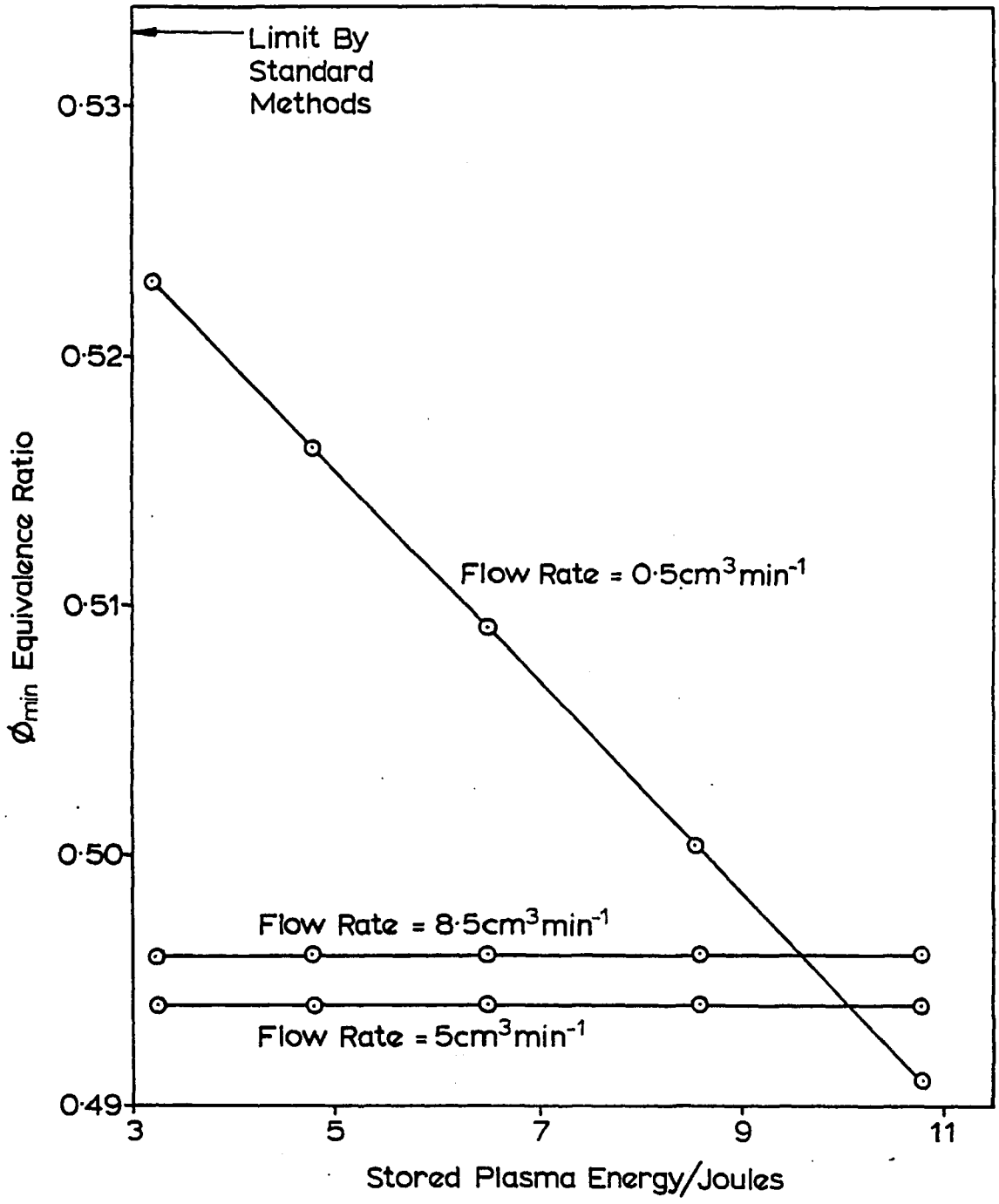


FIG. (35)

VARIATION OF Ø WITH STORED PLASMA ENERGY.
PLASMA GAS: HYDROGEN (DRIED).

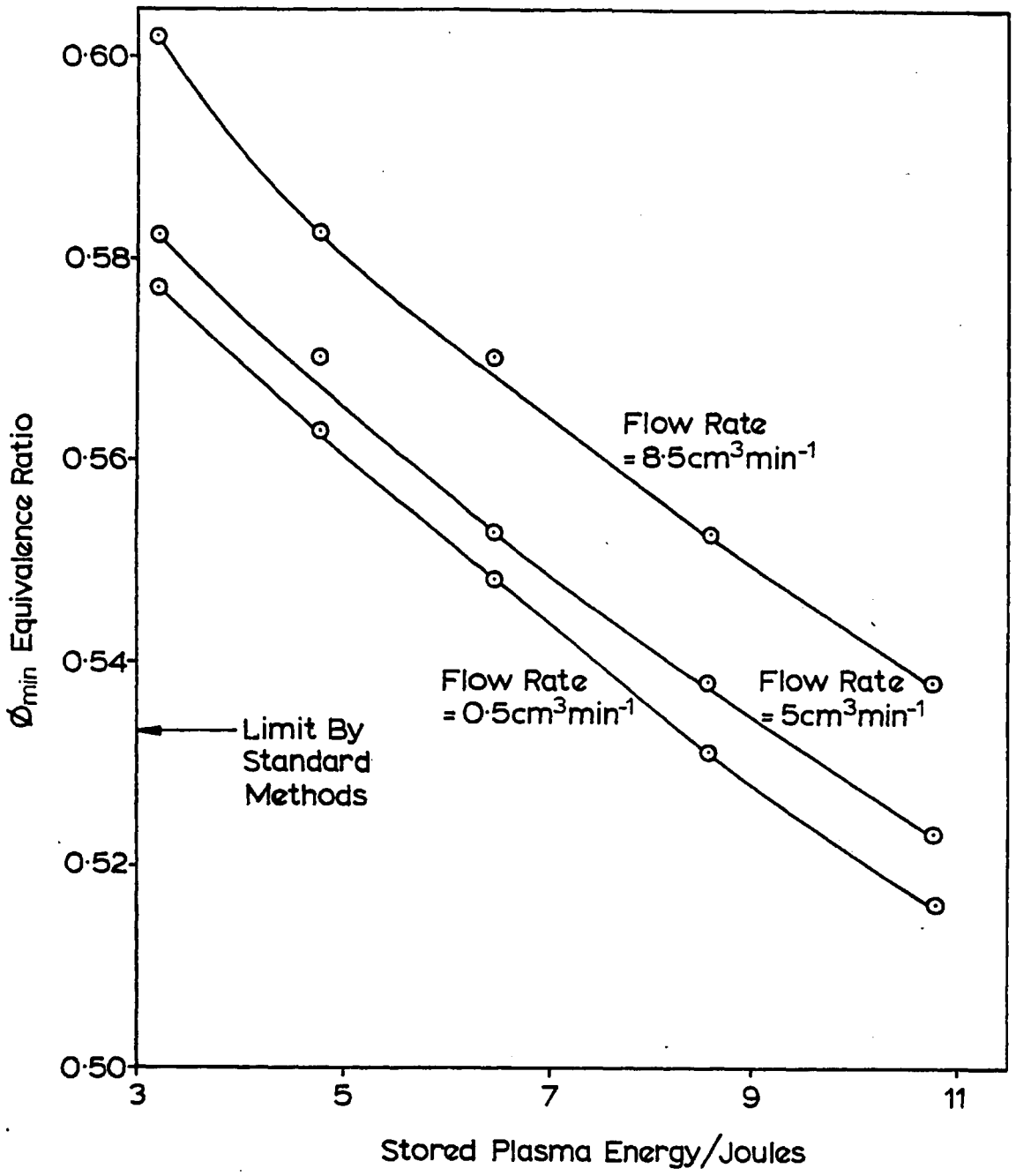


FIG. (36)

VARIATION OF ϕ_{min} WITH STORED PLASMA ENERGY
PLASMA GAS: NITROGEN (DRIED)

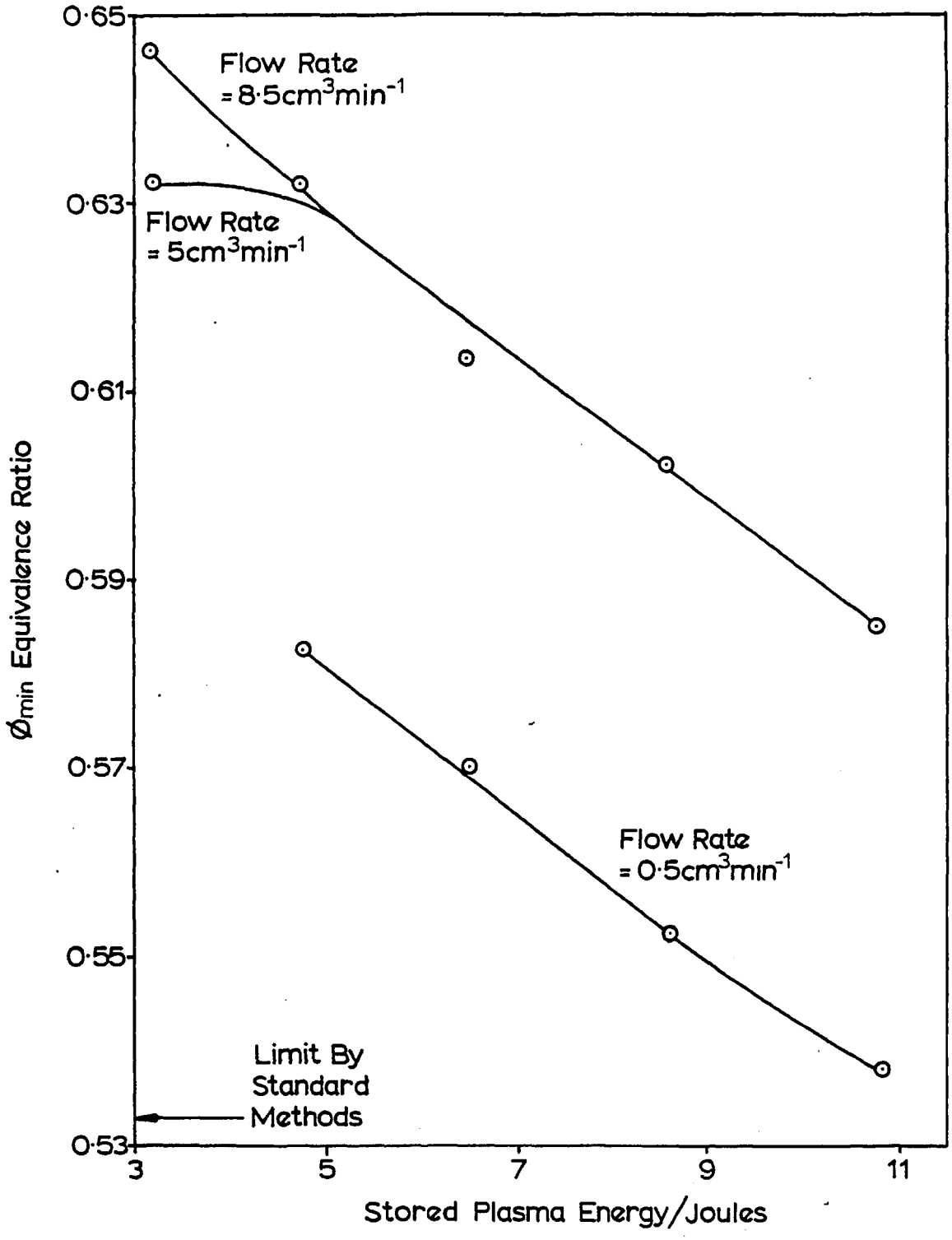


FIG. (37)

VARIATION OF $\emptyset_{min}$ WITH STORED PLASMA ENERGY.
PLASMA GAS: ARGON (DRIED).

attached to the base of the plasma spark plug was of 2 mm diameter.

The most interesting feature found during this study is shown in Fig.(34). Values of ϕ_{min} obtained for both nitrogen and argon plasmas have a strong dependence on the electrical energy supplied to the cavity whereas hydrogen plasmas (over the range of energies studied) had no such dependence. In fact, the entire ignition process for the 2 cases (i.e. nitrogen/argon and hydrogen) seemed different and will therefore be described separately.

(1) Nitrogen and Argon Plasmas

For nitrogen and argon plasmas with low values of applied energy (i.e. high values of ϕ_{min}), the equivalence ratio was high enough for a flame, once formed, to travel undisturbed through the entire vessel (i.e. as if initiated by a normal spark). For high applied energies (low values of ϕ_{min}), the flame which was formed at the boundary of the plasma plume seemed to proceed in a more erratic fashion, sometimes travelling through the entire vessel and sometimes through only 3/4 of the vessel. On some occasions several separate flamelets were formed, some travelling to the edge of the vessel while others were engulfed back into the expanding plume. On all occasions with low values of ϕ_{min}, the flame seemed to be formed reluctantly at the edges of the expanding plume.

(2) Hydrogen Plasmas

A quite different method of ignition was encountered when studying hydrogen plasmas. For all values of applied energy, a flame (or sometimes flamelets) was readily formed in the vicinity of the plasma plume which was more consistent in behaviour than with either nitrogen or argon plasmas. At values of ϕ slightly lower than ϕ_{min}, a yellowish flame (similar in appearance to a hydrogen flame coloured with sodium impurities) was seen to traverse part of the vessel with the size and

shape of an enlarged plasma plume. As ϕ was increased slightly, streaks of blue flame became superimposed on the yellowish plume flame.

(b) Variation of Incend ivity with Plasma Gas Flow

The variation of incend ivity with plasma gas flow rate for each plasma is shown in Figs.(35), (36) and (37). The increase of ϕ_{min} for increased plasma gas flow rates for nitrogen and argon suggests that a localised dilution of flammable gas in the vicinity of the plug occurs at the higher flow rates. For argon plasmas with high values of plasma flow rate, a limiting value for this dilution effect is reached since curves for plasma gas flow rates of 5 and 8.5 $cm^3\ min^{-1}$ are identical for all but the smallest energies.

For hydrogen plasmas, the opposite effect is observed. Increased flow rates produced a localised richening of the flammable mixture below the plug which reduced ϕ_{min}. Again this appeared to reach a critical value since an increase in ϕ_{min} was observed when increasing the flow rate from 5 $cm^3\ min^{-1}$ to 8.5 $cm^3\ min^{-1}$. On reducing the flow rate to 0.5 $cm^3\ min^{-1}$, an energy dependence of ϕ_{min} was found suggesting that at this flow rate, the plasma cavity was insufficiently filled with plasma gas and thus partially filled with methane-air mixture. A similar effect may be important with argon and nitrogen plasmas at the low flow rate of 0.5 $cm^3\ min^{-1}$.

8.3 Discussion of Results

(a) General

The lean limit of ignitability, ϕ_{min}, has been related to the conventional lower flammability limit. This is not strictly correct since the limits of flammability are defined in terms of flame propagation over a fixed distance which is many orders of magnitude larger than the dimensions of the combustion vessel used in these experiments.

The factors which cause the existence of very sharp, well defined

limit compositions are somewhat uncertain (1,85). Natural convection appears to play an important role in determining the limit for downward propagation whereas the upward limit of propagation can be explained in terms of gas-phase and wall quenching mechanisms (108). Since the flame thickness and quenching distance become very large (comparable to the dimensions of the vessel) as the lower limit is approached, it seems unlikely that flame propagation would continue in these sub-limit mixtures without the additional source energy and reactive species diffusional fluxes from the plasma. Although these effects continue for several cms from the source origin (see later chapters), the results have been regarded as "ignition limits" rather than "limits of flammability".

Calculations were made based on a simple thermal analysis of plasma jet ignition which neglects the effects of mass diffusion and these are described in section (8.3.3). These were only applicable to non-reactive plasmas for which comparisons could be made with normal spark ignition in lean mixtures.

(b) Hydrogen Plasmas

The results showed that hydrogen plasmas could consistently ignite sub-limit mixtures irrespective of the plasma energy within the range of approximately 3 to 11 J. This indicates that ignition in lean mixtures is facilitated when the ignition energy is employed to generate H atoms rather than just to increase the overall source temperature.

A complete analysis of the role of H atoms in plasma jet ignition would require the solutions of the time-dependent conservation equations governing flame propagation. This could be undertaken when more experimental data becomes available (i.e. simultaneous temperatures and reactive species concentrations) and is mentioned in the final chapter.

(c) Nitrogen and Argon Plasmas

(1) Calculation of the Fractional Plasma Energy Content

Fig.(38) shows the proportion of energy contributed by the plasma

HYDROGEN PLASMA : $\phi_{mm} = 0.494$ for $\frac{\Gamma E}{\Delta H} = 0.08 - 0.28$

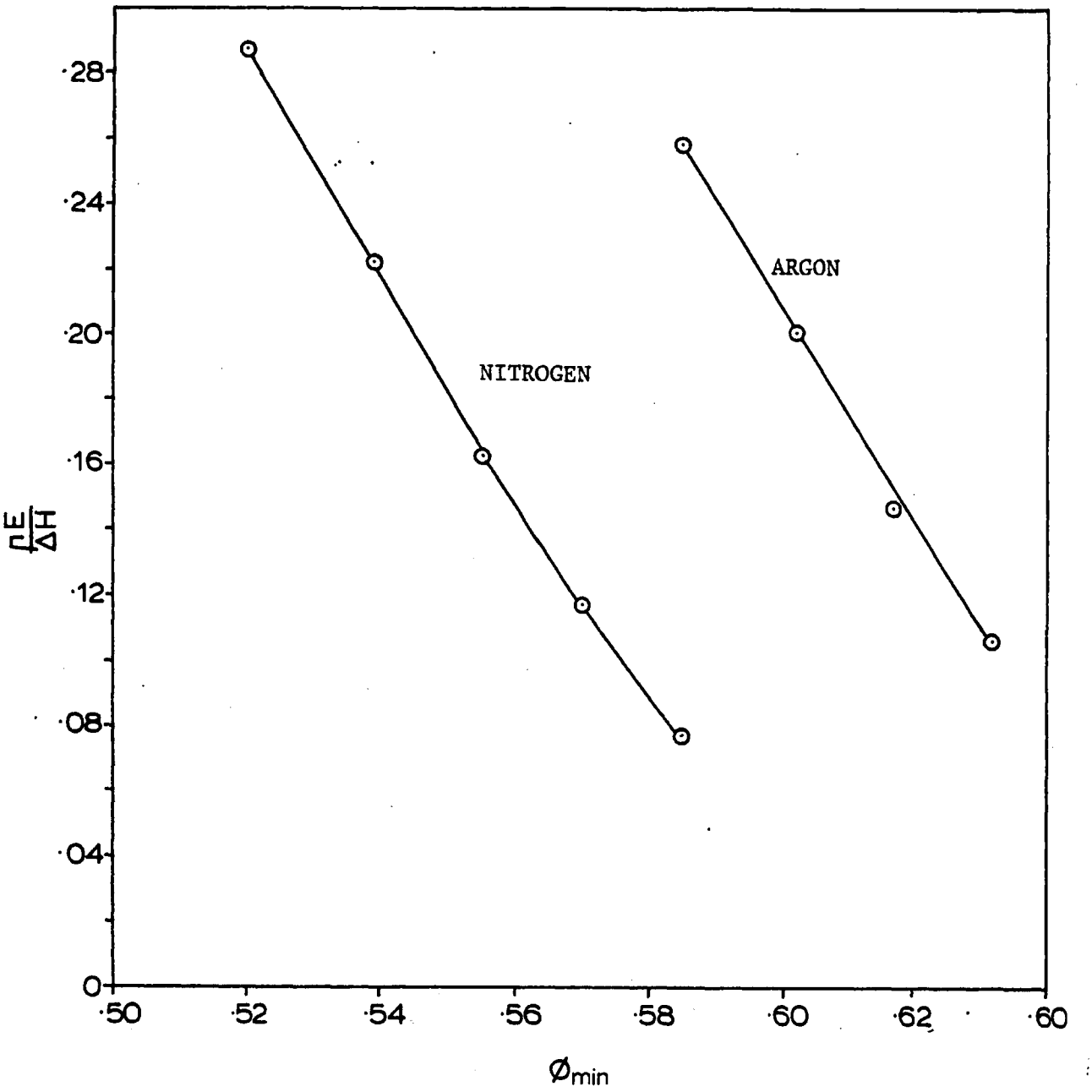


FIG. (38)

FRACTIONAL PLASMA ENERGY CONTENT

(Π E where E is the stored energy on the capacitor, C2) compared to the total enthalpy of combustion of the mixture in the vessel (Δ H) at the limits of ignitability. The value of Π was taken as 0.25 (see Fig.(39)) since it was anticipated that high energy losses would occur in the plasma plug power supply. These curves for chemically non-reactive plasmas illustrate the high plasma energies required for burning limit mixtures in contrast to chemically reactive plasmas such as hydrogen.

(2) Extension of Limits by Turbulence

An extension of the lower limit of flammability by a nitrogen plasma of high energy may have been caused by the turbulence imparted by the jet (see later). Thus as the nitrogen plasma plume expands and the jet velocity decreases, a series of individual flamlets are formed on the surface of the plume which later coalesce to form a wrinkled flame surface. Flame stretch occurs within this wrinkled flame surface at the crests of the undulations which point towards the unburnt gas and leads to extinction when the stretch exceeds a critical value (1). Re-ignition is affected by adjacent folds in the flame surface where convergent heat flow and diffusion effects exist. These folds preserve ignition and enable combustion to proceed slightly below the conventional limit of flammability.

The alternative mechanism for the lowering of the conventional flammability limit (or more strictly the ignitability limit) is that associated with the increased enthalpy content of the plume over that of a normal low energy spark. The discussion in the following section attempts to examine the thermal contribution of the plasma to ignition although it should be remembered that a nitrogen plasma would generate a lower concentration of direct initiating radicals (e.g. H) per unit of spark energy than the corresponding normal electrode spark in a methane-air mixture.

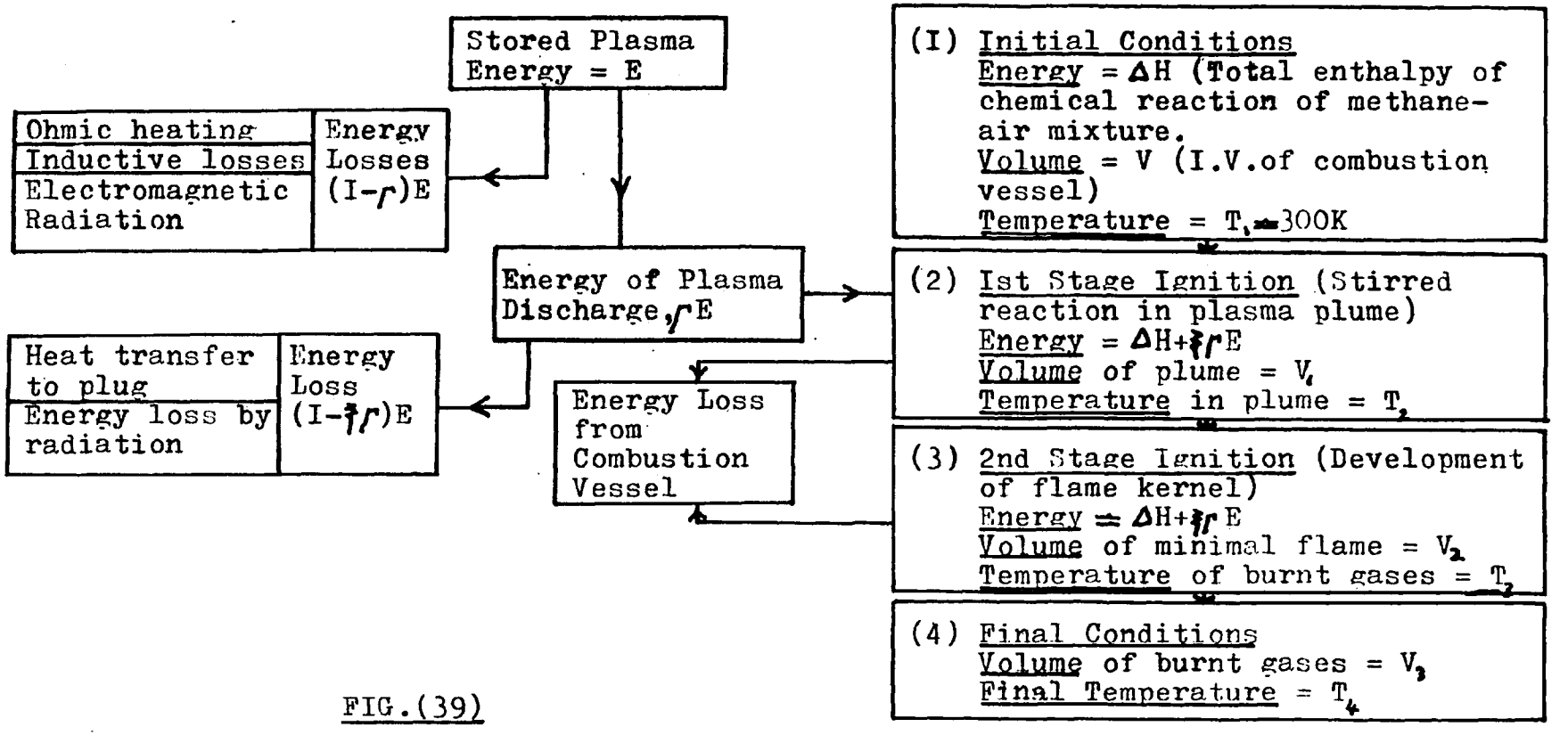


FIG.(39)

Energy Balance for a Nitrogen or Argon Plasma Igniting a Methane - Air Mixture.

(3) Energy Balance during Ignition

The total enthalpy of a plasma ignited flame is illustrated by the flow chart shown in Fig.(39). The accuracy of a thermal analysis is limited by the uncertainties in (1) the fraction of the total stored energy liberated in the plasma and (2) the lack of uniformity of energy (temperature) within the plasma plume or flame. The former could be ascertained by the use of a suction calorimeter (109) and the latter by simultaneous temperature measurements within the plume which will be mentioned in the final chapter.

The following discussion outlines briefly (a) the theory relating to spark ignition and (b) its application to plasma jet ignition. Although the ignition energies and the dimensions of the initiating hot gas kernel are an order of magnitude different for the two cases, similarities were observed which are described in section (b).

(a) Theory - Spark Ignition

From energy considerations, it has been suggested (1) that for spark ignition, a stable combustion wave can only be formed if the volume of heated gas associated with the spark has grown to a size such that when the temperature at the origin equals the flame temperature, the temperature gradient between the heated gas and the outer unburnt gas has approximately the same slope as a steady state combustion wave. If the gradient is too large (volume too small), the loss of heat to the unburned gas will exceed that released by chemical reaction until the temperature falls to a value at which the combustion wave cannot be maintained (i.e. the unburnt gas quenches the flame). This quenching can be associated with divergent flame propagation or flame stretching described by the Karlovitz number (or critical flame stretch number), K, where

$$K = 4 \frac{\ell_o}{d} \frac{\rho_u}{\rho_b} \qquad (8.1)$$

where

$$\eta_o = \frac{k}{Cp\ \rho_u\ Su}$$

k = thermal conductivity, Cp = specific heat,

ρ_u = unburnt gas density, and Su = burning velocity relative to the unburnt gas.

ρ_b = burnt gas density, d = critical minimum flame diameter.

The chemical enthalpy, H', resident in the critical minimum flame of unburnt gas is given by

$$H' = \frac{\Pi}{6} d^3\ Cp\ \rho_b\ (Tb - Tu)$$

where Tu and Tb are the temperatures of the unburnt and burnt gases respectively, and the heat conducted from the minimal flame, H'', is given by :

$$H'' = \Pi\ d^2\ \frac{k}{Su}\ (Tb - Tu) \qquad (8.2)$$

Values of $\frac{H''}{H'}$ have been calculated for spark ignition and have been found to be consistent over a wide range of minimal flames. As expected, for most flames, H'' was found to be smaller than H' although this was not found to be so for lean methane-air flames. The cause of this was attributed to the high diffusivity of methane over oxygen causing preferential diffusion within the strongly curved minimal flames. This gave higher concentrations of the deficient component, methane in the main reaction zone which gave higher values of Su than those used for evaluation H'' (i.e. from planar flames). Finally, the ratio $\frac{H''}{H'}$ is related to the stretch factor, K, by:

$$\frac{H''}{H'} = 1.5\ K \qquad (8.3)$$

Also reported (1) are values of $\frac{H}{H'}$ and $\frac{H}{H''}$ where H is the minimum ignition energy. These are compared with the corresponding values for plasma jet ignition using H equal to Γ E and d equal to the plasma plume diameter at the onset of 2nd stage ignition.

(b) Nitrogen Plasma Jet Ignition

The volume of the smallest plasma plume on which a stable combustion wave was formed (minimal flame volume) was measured from the schlieren photographs of a nitrogen plasma (stored energy 4.8 J) igniting a methane-air mixture of equivalence ratio, ϕ = 0.62. The correct photograph which referred to the minimal flame (i.e. development of the flame front) was found by measuring the time after the discharge which corresponded to the start of the C_2 emission signal.

For a nitrogen plasma (stored energy 4.8 J) igniting a methane-air mixture (ϕ = 0.62), the measured volume of the minimal flame at a time of 10 mS was found to be 151 cm^3. This value was used for the calculation of H' and H'' and the ratios $\frac{H}{H'}$, $\frac{H}{H''}$ and $\frac{H''}{H'}$ given below, which are compared with the corresponding values for spark ignition.

	Spark Ignition	Nitrogen Plasma Jet Ignition
H	0.756 mJ (ϕ = 0.7)	1.2 J (ϕ = 0.62)
H'	5.04 mJ (ϕ = 0.7)	48.3 J (ϕ = 0.62)
H''	7.56 mJ (ϕ = 0.7)	7.48 J (ϕ = 0.62)
H/H'	0.15	0.025
H/H''	0.10	0.16
H''/H'	1.5	0.155

The value of H/H' for the nitrogen plasma is six times that of the normal spark whereas the ratio H/H'' for the two cases is of similar magnitude. This indicates that the minimal volume taken for the evaluation of H' for the nitrogen plasma is six times too large whereas the flame area (for a plasma energy of 1·2J) is approximately correct. Thus if only the outer 1/6th volume of the plume (corresponding to approximately 4 mm from the edge of the plume) is regarded, the values are fairly consistent with those of spark ignition. This would mean that the temperature approximately 4 mm from the extreme edge of the plume is at flame temperature (at the onset of 2nd stage ignition) and would either (1) remain constant, (2) continue to rise or (3) decrease as the centre of the plume was approached. The results of the hydroxyl concentration measurements (see Chapter 10) seem to suggest that the temperature continues to rise as the centre of the plume is approached (for times $\geqslant$ 10 mS) although it would be necessary to use results from simultaneous temperature measurements to examine this further.

Clearly an additional complication encountered during the comparison described above is that associated with the jet velocity. A minimal flame is not formed earlier (i.e. of smaller volume) because the velocity of the expanding plume is higher than the characteristic burning velocity of the flame. This does not occur in the case of chemically reactive plasmas such as hydrogen since the rate of initiation of chemical reactions can "keep pace" with the expanding plume during the early stages of plasma growth.

The mean plasma plume temperatures above those of the final flame temperatures for a nitrogen plasma have been calculated from values of the plasma source energy densities. This assumes that the energy derived from the arc is distributed evenly throughout the plasma plume and that energy losses are small. Both these assumptions are not too drastic since

during the early stages, the plasma plume is almost perfectly stirred due to the high turbulence and heat losses which would only occur primarily by conduction to the plug and ahead of the plasma plume to the unburnt gases.

Calculation of Plasma Source Energy Densities and Mean Plasma Plume Temperatures for a Nitrogen Plasma

Plasma source energy densities, (E_D), as a function of time were calculated from plasma plume volumes (V_T), and the energies dissipated in the plasma plug cavity, (ΓE). These plasma energies excluded the enthalpy of combustion since in assessing the thermal effects of the plasma on the ignitability limits, only the excess plasma energies needed to be considered.

The plasma plume volumes were measured indirectly from the schlieren photographs and the plasma energies were calculated assuming that the fraction 0.25 (Γ) of the total stored energy on the capacitor, (E), was dissipated in the plasma arc, Thus,

$$E_D = \frac{\Gamma E}{V_T} \qquad (8.4)$$

The variation of E_D for a nitrogen plasma ($\Gamma E = 1.2$ J) igniting a methane-air mixture ($\phi = 0.62$) is shown in Fig.(40). Also shown are the corresponding rise in temperatures of the plume associated with the plasma energy which were calculated assuming a mean specific heat of the unburnt methane-air mixture.

From Fig.(40), an average plasma plume temperature of about 34K above the adiabatic flame temperature was found at a time of 10 mS corresponding to the development of the flame front. As described in the previous section, the temperature would probably not be uniform but increase steadily as the centre of the plume was approached.

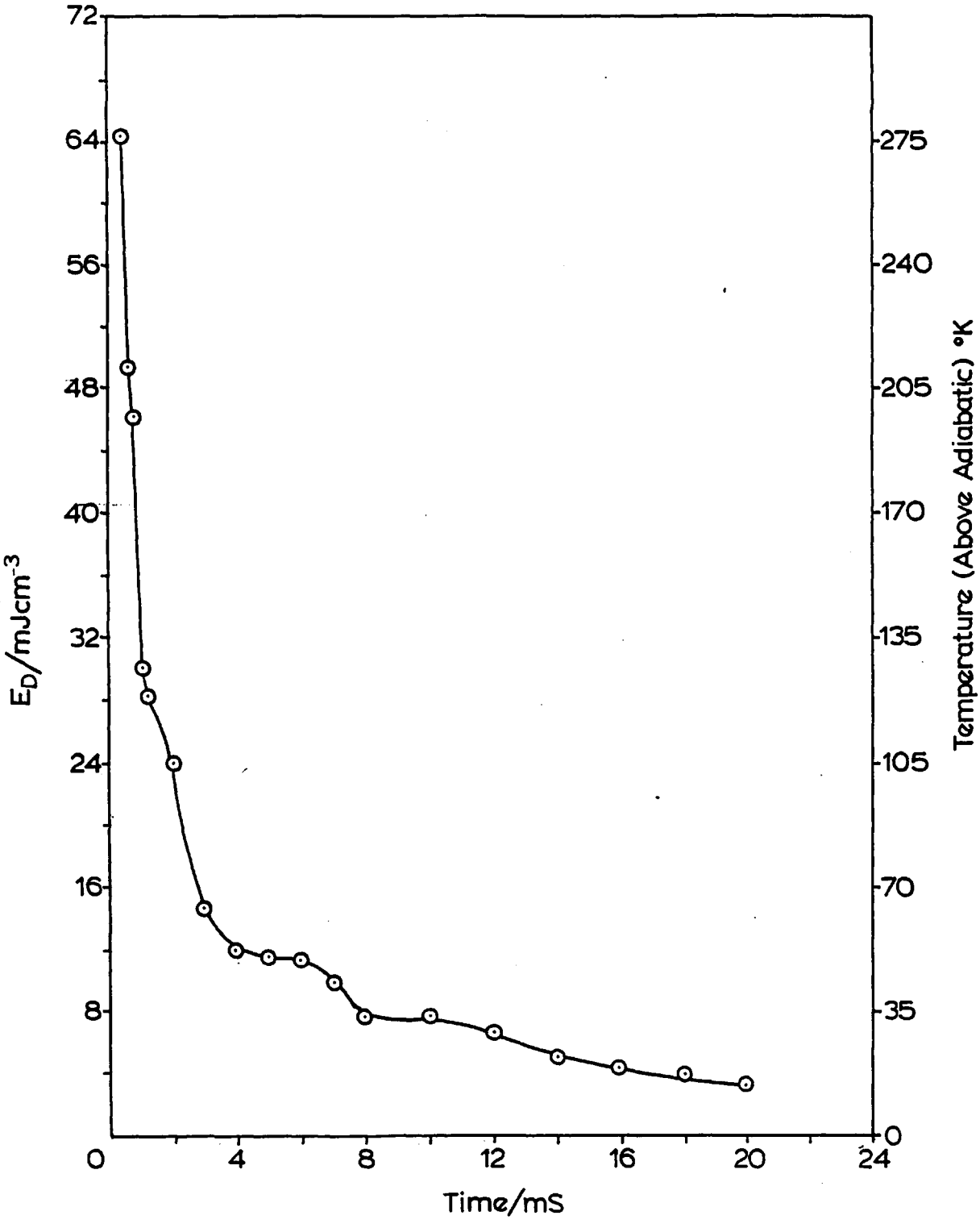


FIG. (40)

PLASMA PLUME ENERGY DENSITIES AND MEAN PLASMA PLUME TEMPERATURES (ABOVE ADIABATIC) FOR A NITROGEN PLASMA IGNITING A METHANE-AIR MIXTURE WITH $\phi = 0{\cdot}62$

Finally, it is interesting to compare the increased temperature (34 K) of the plasma plume with the influence of initial temperature on the lower flammability limit of methane-air (110). A value of

$$\frac{dL}{d\Theta} \simeq 4.6 \times 10^{-3}$$

over the range Θ = 25 to 200°C

where L is the lower flammability limit (% methane) and Θ is the initial temperature (°C).

An increase of 34 K in the initial temperature would lower the flammability limit by about 0.16% in the methane concentration which is of similar magnitude to the extension of the ignitability limits observed in this research (for example, see Fig.(34)).

8.4 Conclusions on the Incend ivity of the Plasma Jet

The results have shown that hydrogen plasmas are consistently more effective in igniting lean methane-air mixtures than nitrogen plasmas which in turn are more effective than argon plasmas. Over the range of energies studied (approx. 7 to 11 J of stored plasma energy), the incend. ivity of the hydrogen plasma was found to be independent of plasma energy whereas for nitrogen and argon plasmas, the lower ignitability limits could be extended by using higher initial stored plasma energies.

Argon plasmas were found to be very ineffective ignition sources in spite of their much higher translational temperatures at any given energy input. This was due to their complete lack of chemical reactivity.

For nitrogen plasmas, similarities were found to spark ignition using a thermal analysis only. This shows that for this plasma media there are no major chemical effects since this would be expected to give a large additional improvement.

In the case of hydrogen plasmas, the high level of chemical reactivity of the hydrogen atom produced a marked extension of the lean ignitability limit. Thus, even though the volume of the plasma plume was forced to expand very rapidly by entrainment, the increased rates of flame propagation due to augmentation by hydrogen atoms enabled the flame front to initiate and propagate rapidly away from the ignition source.

CHAPTER 9

RATES OF FLAME PROPAGATION

It was concluded from the study of the fluid dynamic characteristics described in Chapter 7 that two quite separate ignition stages occurred following the injection of a high temperature, high velocity plasma into a flammable mixture. The 1st stage ignition was associated with the growth of the plasma plume in which combustion reactions proceeded within a high temperature, perfectly stirred reacting system. This ignition stage always occurred to a greater or lesser degree even though the equivalence ratio of the mixture was below the ignitability limit defined in Chapter 8 for the particular plasma in question.

The second stage ignition corresponded to the development of a stable combustion wave and it is this stage with which we are concerned in the present chapter. Burning velocity measurements were taken only after the plasma jet velocities had fallen below the measured flame front velocities. The possible exceptions to this were those of the hydrogen plasmas in which the combustion reactions proceeded so rapidly as to keep pace with the fluid dynamics and therefore the 1st measurements were taken after the time duration of only 2 mS.

As described in Chapter 7, the transition from 1st to 2nd stage ignition was readily identified by all the diagnostic methods, i.e. from the characteristic change in the shape of the schlieren image, the change in the OH oscillograms and in some cases (see Chapter 6), from the C_2 emission results. Both with the reactive and non-reactive plasmas, the rates of flame propagation were found to be considerably higher than normal spark ignited spherically expanding laminar flames and the reasons for this are discussed.

9.1(a) Burning Velocities in Methane-Air Mixtures following Spark Ignition

The predicted (111) and experimental (112) laminar burning velocities of methane-air flames as a function of equivalence ratio, and initial temperature and pressure are reported in the literature. For an equivalence ratio of 0.62, a value of approximately 18 cm s^{-1} is given corresponding to an initial temperature of 298 K and an initial pressure of 1 atmosphere. This is larger than the value of about 7 cm s^{-1} obtained experimentally in this research and the reasons for the difference are given in Section 9.3.

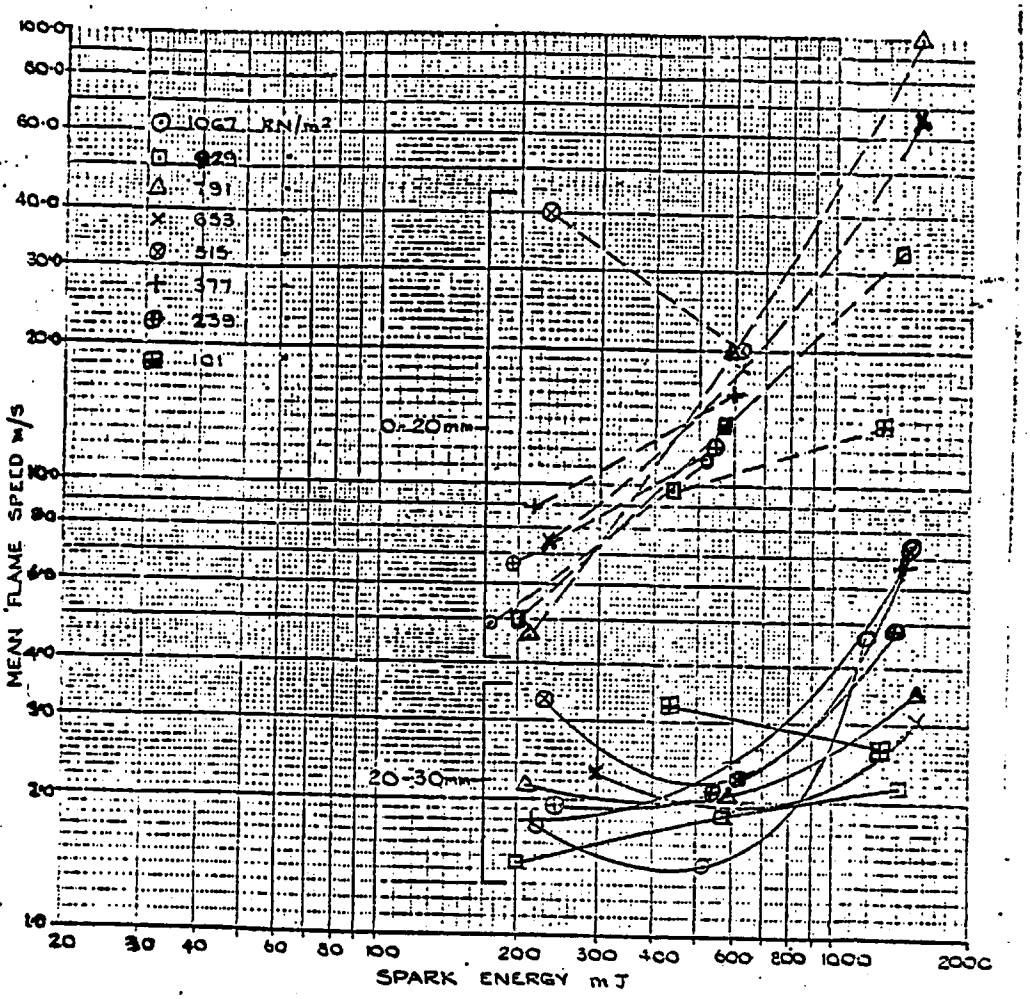
For spark ignited, expanding flame kernels at constant pressure, the burning velocities generally remain constant and independent of spark energy since this is soon exceeded by the energy liberated by combustion reactions. This contrasts with the behaviour of plasma ignited flames in which the fluid dynamic and chemical effects continue to enhance the burning velocity which decreases with time from a maximum shortly after the initiation of the flame front.

(b) Burning Velocities in Methane-Air Mixtures following Plasma Jet Ignition

Increased rates of flame propagation of methane-air flames ignited by plasma jet have been reported (113) and are shown in Fig.(41A). These were obtained using a plasma cavity gas indentical to that of the main charge (i.e. methane-air) producing a plasma of relatively low chemical reactivity. In spite of the low concentration of specific radicals generated, enhanced flame speeds were observed in comparison with a surface discharge igniter over the two distances, 0-20 mm and 20-30 mm from the plug.

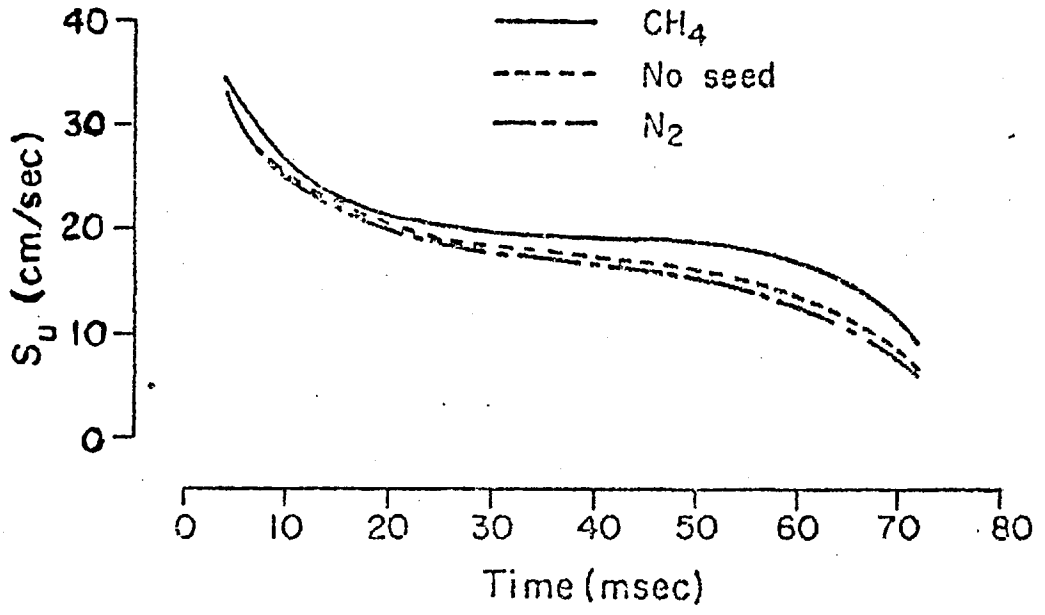
The results obtained more recently by Teichman (58) using a plasma plug identical to that used in this research are shown in Fig.(41B).

FIG.(41)



A

MEAN FLAME SPEED / SPARK ENERGY FOR PLASMA PLUG IGNITION OF 0·8 STOICHIOMETRIC METHANE / AIR MIXTURE



B

In this study, the plasma cavity was filled in turn with methane, nitrogen and methane-air immediately prior to discharge. Measurements were taken using a constant volume bomb although, as described earlier, the effects due to adiabatic compression of the reactant gases were found to be small.

To obtain burning velocities, measurements were made on the effective radius of a spherical volume of burned gas, V_b, at different times during its evolution. For each time interval, three different radii were measured and averaged, thereby minimizing inaccuracies due to wall effects and departures from spherical symmetry. Measurements were taken only after the turbulent cloud had transformed into a nearly spherical flame and before major departures from a spherical geometry were encountered. This meant that measurements were taken up to the position where about 60% of the total viewing volume of the initial charge had been consumed.

Analytical functions were then found to match the growth of V_b with time whilst pressure corrections to the calculated burning velocity were made by simultaneously using a pressure transducer for P(t). The laminar flame speed, Su, was then given by :

$$Su = (4\,\Pi)^{-1/3} (3V_b)^{-2/3} \frac{V_o - V_b}{Pe - P} \frac{dP}{dt}$$

where V_o = initial volume

Pe = pressure of burnt gases at equilibrium.

Maximum values for Su occurred at the beginning of flame propagation (at a time of 4 mS) and decreased steadily with time. These were found to be as follows:

Methane	$Su_{max} = 34.7$ cm s^{-1}
Methane/air	$Su_{max} = 33.4$ cm s^{-1}
Nitrogen seed	$Su_{max} = 33.0$ cm s^{-1}

The results of the present experiments for hydrogen, nitrogen and argon plasmas show a wider variation of burning velocities than those described above. For hydrogen plasma ignited flames, the values of Su at a time of 4 mS compare well with the corresponding value found previously (58) for the methane plasma. As described earlier, for the nitrogen plasma, a flame was not initiated until a time of 10 mS after the discharge at which time the measured burning velocity was of similar magnitude to that reported by this author (58).

9.2 The Methods used to Measure Flame Areas

The measurement of flame areas as a function of time were made indirectly using both the schlieren records and the C_2 emission results. In the case of flames ignited by hydrogen plasmas, interference from the plasma light prevented accurate measurements of C_2 emission and therefore the results were obtained exclusively from the schlieren records.

The method of interpretation of the schlieren records is described below and the numerical values obtained experimentally are given in Section 9.3.

(a) The Use of Schlieren Records

The correct method of data reduction required detailed consideration since the final values obtained depends on the method chosen to interpret the flame expansion. This is especially important for the more turbulent flames since convoluted flame areas associated with turbulent flame propagation were particularly difficult to measure accurately.

Firstly, in examining the method of interpretation, an important property in the theory of the schlieren image can be invoked which is that the flame propagates entirely in the plane of the record perpendicular to the parallel schlieren beam. This is a consequence of deflexions due to parts of the flame front which are tangential to the beam being very much greater than those at any other incidence (114).

Secondly, ignition would be expected to occur initially as a series of turbulent flames within and on the surface of the expanding turbulent plume. The transition from a plume to a turbulent flame could be distinguished by the appearance of cusps which are characteristic of turbulent flame propagation as opposed to the more wave-like appearance of a turbulent jet. At later times, the convolutions due to turbulence are consumed since flame propagation tends to flatten these indentations which smooths the flame front. This is the result of flame propagation orthogonal to the convoluted flame surface which tends to broaden "peaks" by the advancement of their foothills whilst narrowing their "valleys" by advancement of their sides (see Ref.115).

The rate at which this occurs depends on the magnitude of the laminar burning velocity which in the case of flames ignited by non-reactive plasmas will remain largely unchanged. For this reason, some flame corrugation persists for the entire travel of the flame towards the vessel walls and the measured velocities will be either turbulent burning velocities, S_T, or laminar burning velocities, S_L, depending on the method of interpretation of the schlieren records. Fitting contours to the nearest circle around a convoluted flame surface will tend to underestimate the total flame area, A_f, giving measured values closer to S_T than Su.

It was therefore decided to make use of an equivalent radius, r, defined by

$$r = \frac{L}{2\Pi}$$

where L is the length of the outermost continuous schlieren trace taken around all the indentation and assumes only that on average the spread is isotropic. In the absence of small scale turbulence (small in comparison to the flame front thickness), use of the equivalent radius will yield values closer to Su than S_T whereas by "short-circuiting"

these corrugations, values of S_T are obtained. Increased values of Su would indicate increased chemical reaction rates caused by larger enthalpy or species diffusional fluxes from the plasma. On the other hand, the turbulent burning velocity, S_T, based on mean flame area will depend on the turbulence, geometry and momentum of the initiating jet.

For these reasons, the additional method of measuring total flame areas based on C_2 emission spectroscopy was used to evaluate laminar burning velocities independently of the fluid dynamics.

(b) The Use of C_2 Emission Spectroscopy

This method has been described in Chapter 6, Section 6.2 , and provides a measure of the total flame area as a function of time independent of flame shape and corrugations so long as the flame structure is not modified by chemical effects associated with the plasma.

The flame areas measured using the two methods - schlieren and C_2 emission - were almost identical for flames ignited by argon plasmas whereas in the case of nitrogen plasmas, measured flame areas using the C_2 emission method, were somewhat lower than the corresponding values obtained from the schlieren records.

9.3 Calculation of Burning Velocities from Measured Flame Areas

Burning velocities, Su, relative to the unburnt gas were calculated using the equation for spherical flame propagation at constant pressure:

$$\frac{dm_b}{dt} = \rho_u \, Su \, A_f \qquad (9.1)$$

or

$$Su = \left(\frac{dr_b}{dt}\right) / \varepsilon \qquad (9.2)$$

where

where m_b = mass of burnt products = $\frac{4}{3}\pi r_b^3 \bar{\rho}_b$

A_f = flame area = $4\pi r_b^2$

r_b = radial distance to the boundary of the unburnt gas of density ρ_u

ϵ is the expansion ratio = $\frac{\rho_u}{\rho_b}$

and $\bar{\rho}_b$ is the mean density of the burnt gas which strictly (116) is given by :

$$\bar{\rho}_b = \frac{3}{r_b^3} \int_0^{r_b} \rho_b r^2 dr \qquad (9.3)$$

For the present purpose, the values of $\bar{\rho}_b$ were calculated based on the adiabatic flame temperature corresponding to the equivalence ratio of the unburnt mixture.

For a convoluted flame, the exact expression for Su is :

$$Su = \frac{1}{\epsilon A_f} \frac{dV_b}{dt} = \frac{1}{3\epsilon} \left(\frac{r_v}{r_A}\right)^2 \frac{dr_v}{dt} \qquad (9.4)$$

where V_b is the volume of burnt products, r_A = area mean radius and r_v = volume mean radius.

Consequently, the use of Equation (9.2) assumes that $r_A \equiv r_v$, whereas in fact, rough calculations show that r_A is a few percent greater than r_v depending on the geometry. However, as described in the following section, the difference in the calculated burning velocities of various plasma ignited and spark ignited flames is of such magnitude that small changes in the absolute values do not affect the overall conclusions.

9.4 Results and Discussion

The mean radii and burning velocities as a function of time and position for flames ignited by (1) a low energy ($\simeq$ 50 mJ) spark and (2) hydrogen, nitrogen and argon plasmas (stored energies of 4.8 J, 4.8 J and 8.6 J respectively) are shown in Figs.(42) to (44) inclusive. All of these were obtained using a static methane-air mixture with an equivalence ratio of 0.62.

The immediate observation from these results is that all of the plasma ignited flames had somewhat higher burning velocities than that recorded for the spark ignited flame. Even for the least chemically reactive plasma - argon (which was used as a convenient standard), the measured burning velocities were over twice those originating from spark ignition due to the highly convoluted flame front providing a large area of contact between the flame and the unburnt gases.

The results for the separate ignition sources are described in more detail and the conclusions drawn from some preliminary calculations to evaluate the magnitude and duration of turbulence are mentioned.

(a) Spark Ignition

The sequence of cine photographs showing the development of a spark ignited laminar spherical flame kernel is shown in Plate (9). It can be seen that a large proportion of the gas in the vessel is burnt only after the relatively long time period of 60 mS which contrasts with the behaviour of a hydrogen plasma (see Plate (12)), in which the same proportion is burnt after a time of about 20 mS.

The burning velocity for the spark ignited flame remains fairly constant at about 7 cm s^{-1} which is lower than the accepted value of approximately 18 cm s^{-1} reported in the literature. This value of 7 cm s^{-1} was calculated using Eqn.(9.2) on the basis of a mean burnt gas density at the adiabatic temperature of 1700 K (ϕ = 0.62) and neglecting the flame thickness which would tend to make the actual value slightly

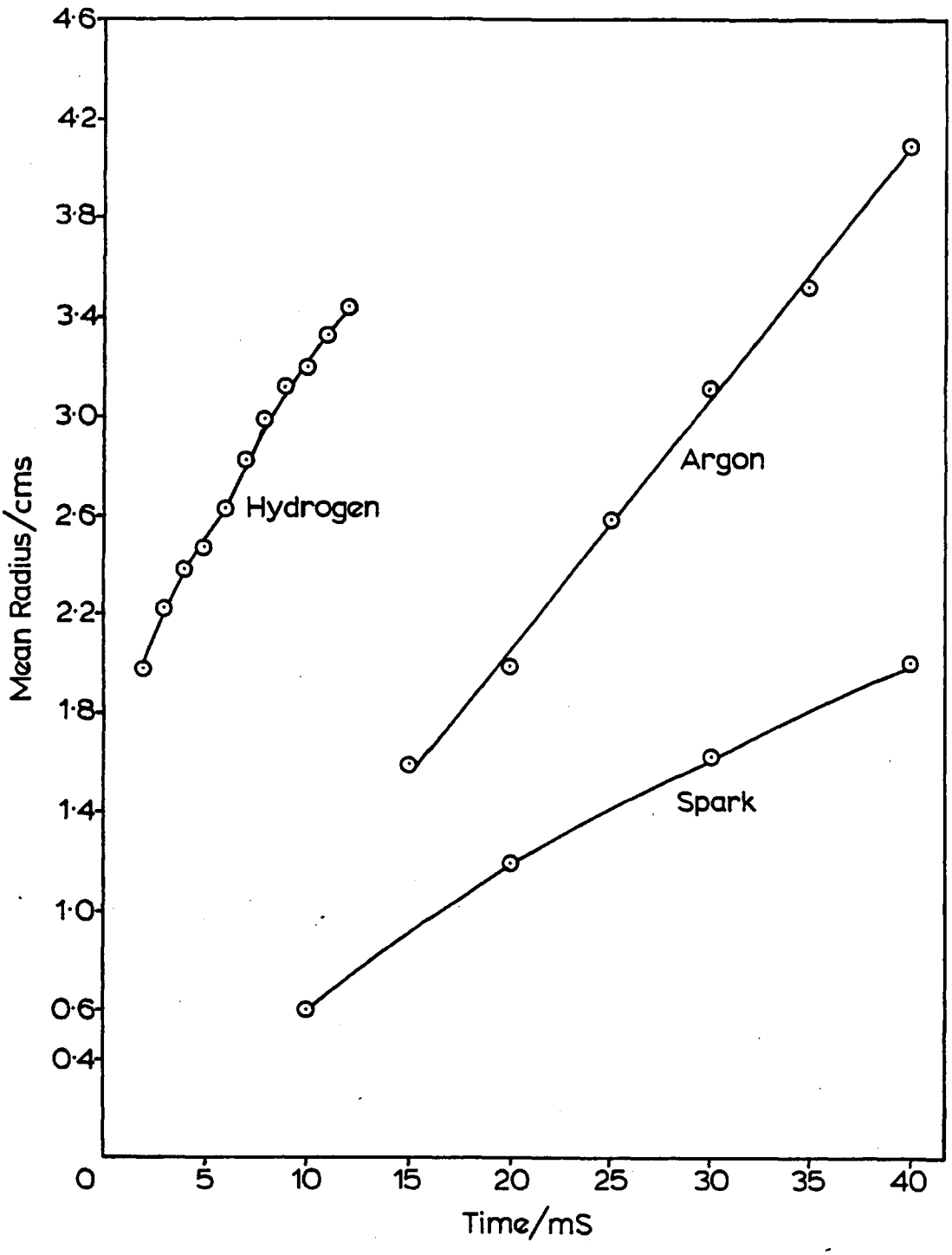


FIG. (42)

MEAN RADIUS vs. TIME FOR HYDROGEN AND ARGON PLASMAS AND SPARK IGNITION OF A METHANE-AIR MIXTURE WITH $\emptyset = 0{\cdot}62$

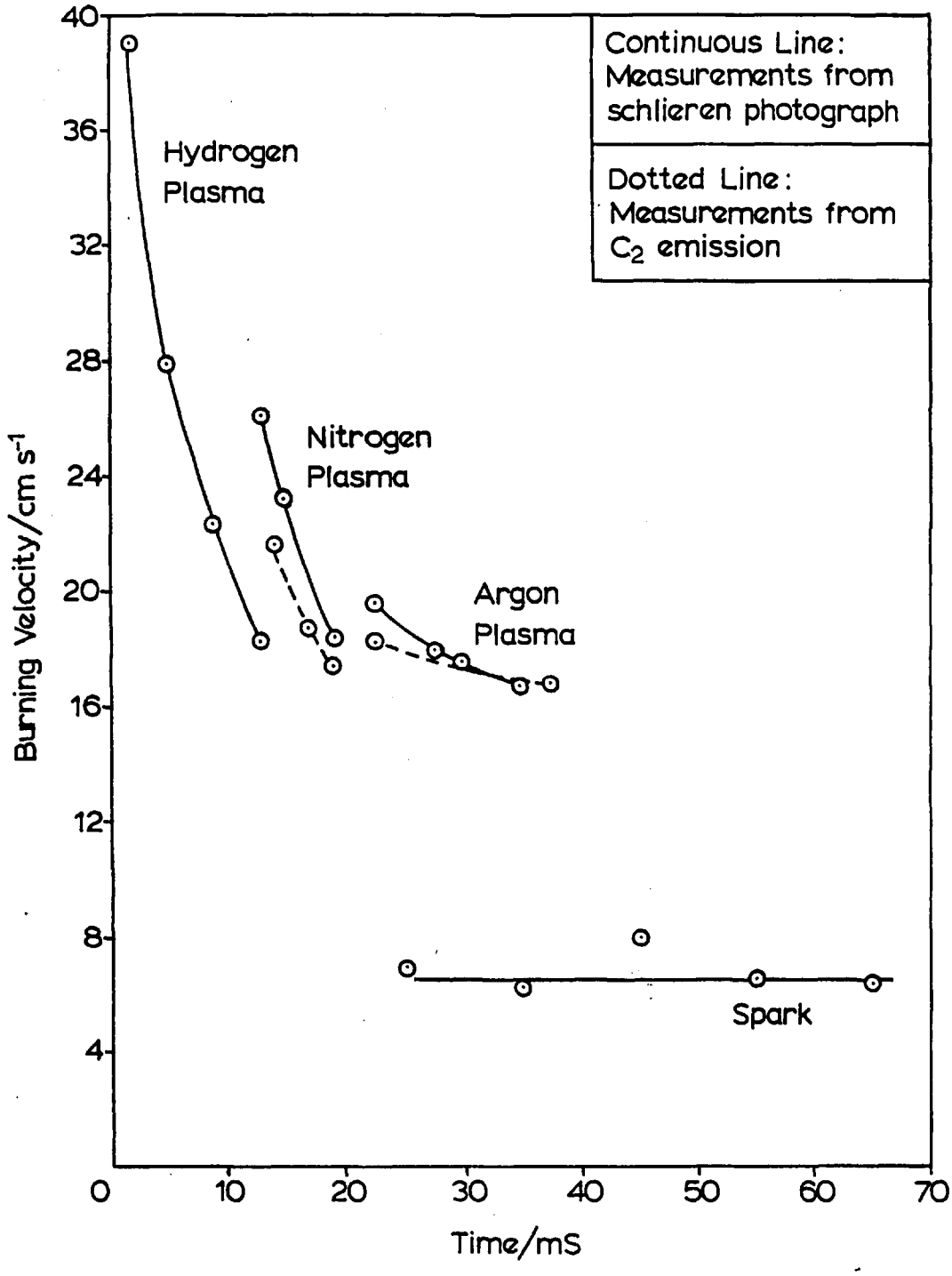


FIG. (43)

BURNING VELOCITY MEASUREMENTS FOR PLASMAS IGNITING A METHANE-AIR MIXTURE WITH $\phi = 0{\cdot}62$

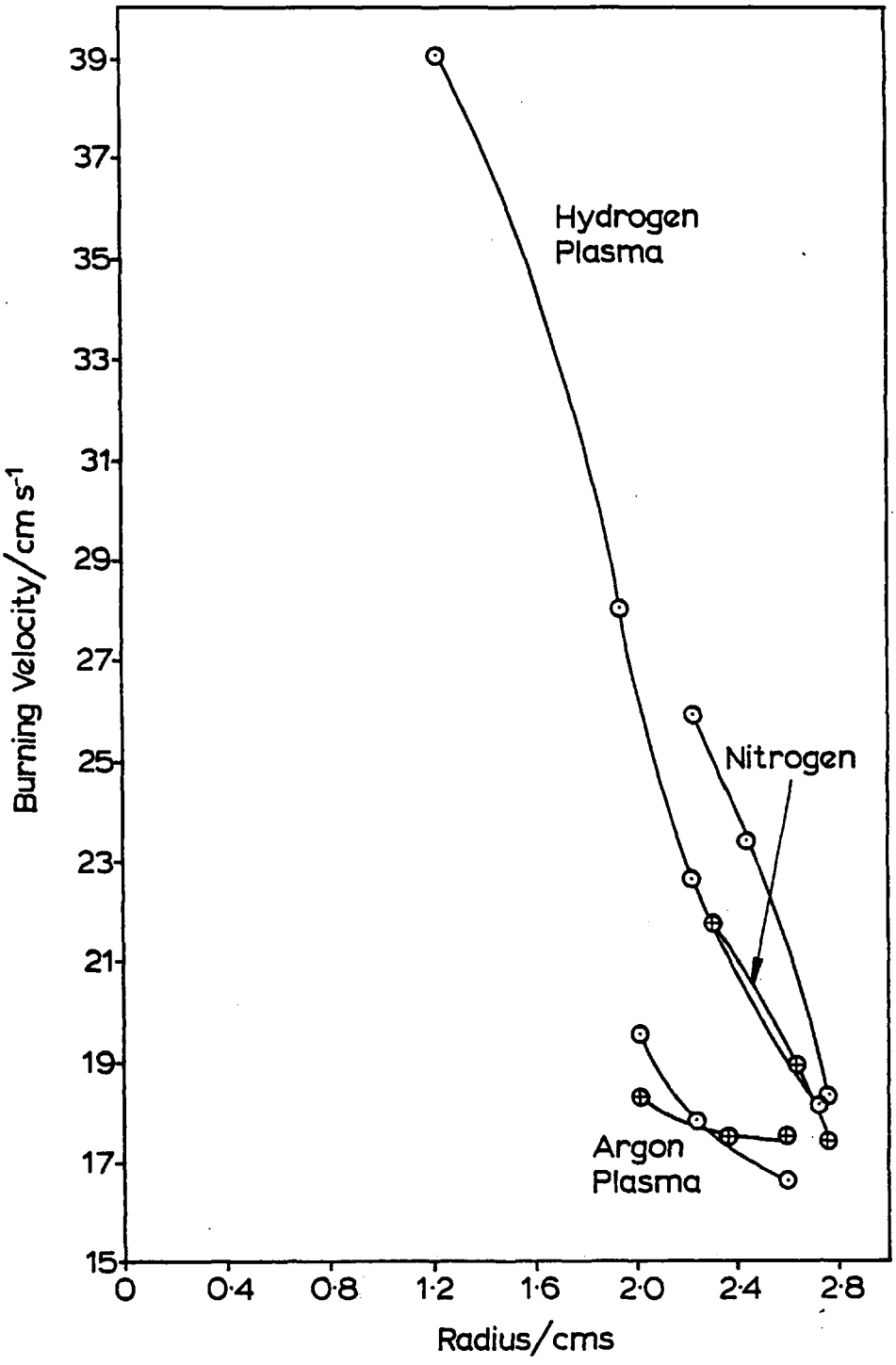


FIG. (44)

BURNING VELOCITY AGAINST FLAME RADIUS

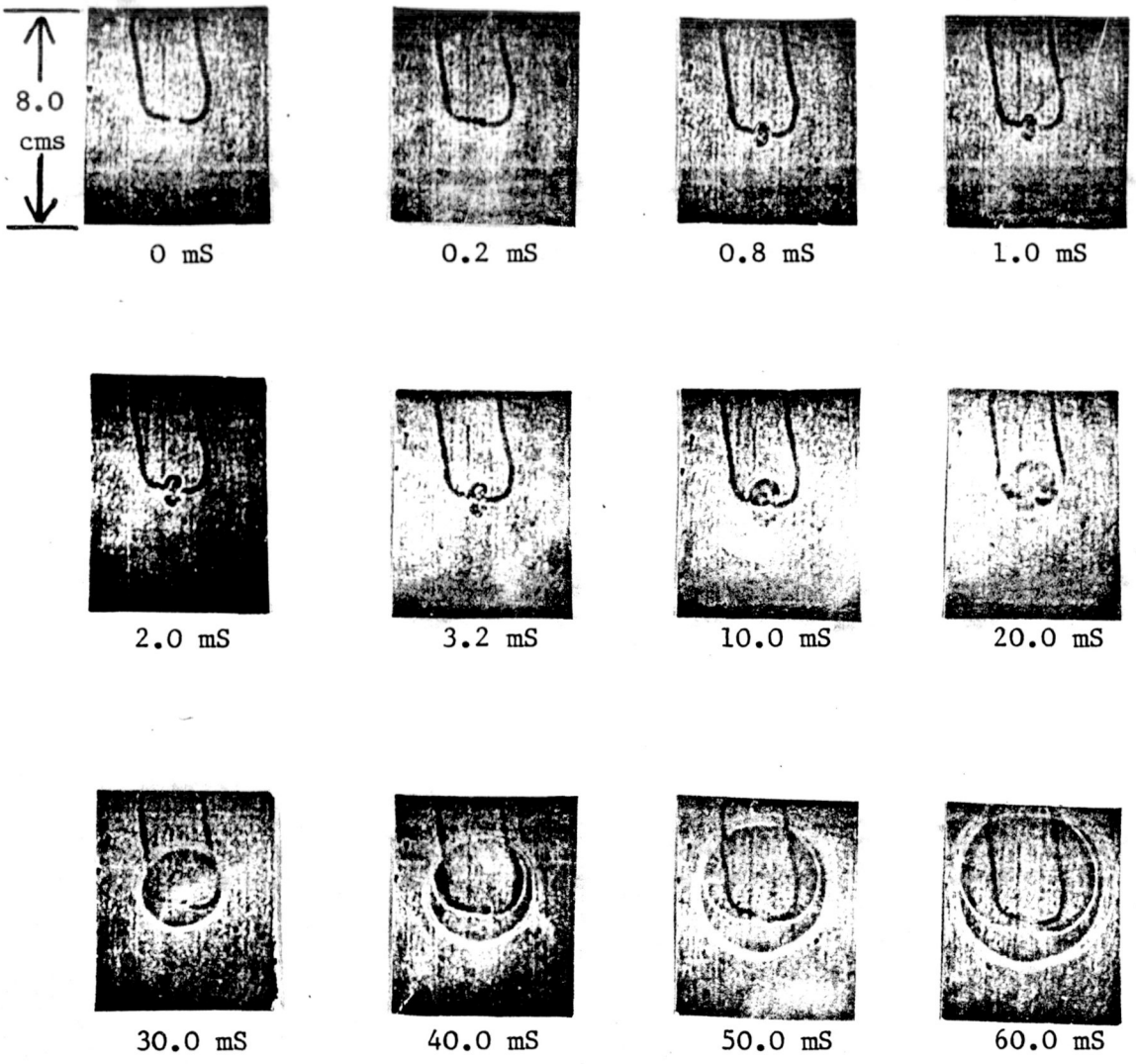
Measurements From Schlieren Photographs

Measurements From C_2 Emission

PLATE (9)

Spark Ignition for C_2 Emission Calibration

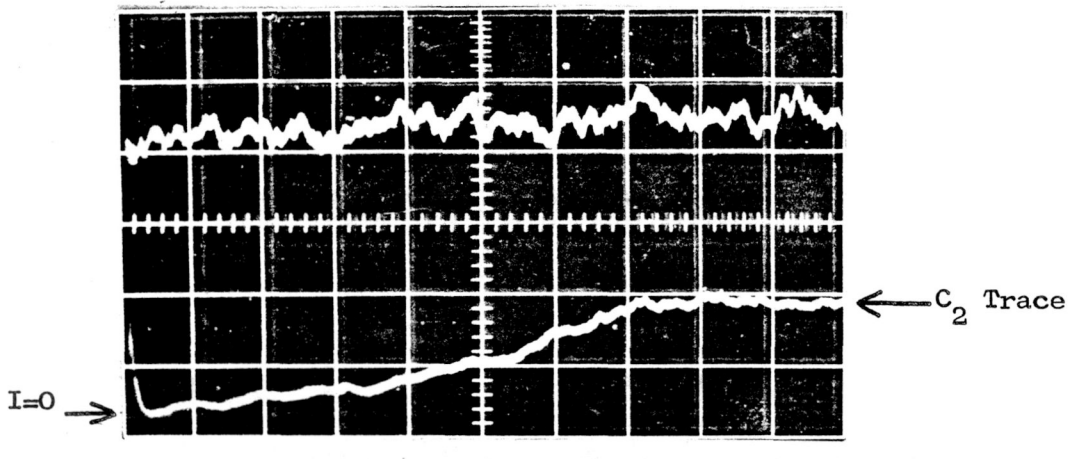
ϕ = 0.62 Spark Energy Approximately 80 mJ



C_2 Emission

Horizontal Scale : 10 mS/Division

Vertical Scale : 20 mV/Division



higher. The latter can be allowed for by using the following corrected expression (112) for the mean burnt gas density, $\bar{\rho}_b$:

$$\frac{\bar{\rho}_b}{\rho_u} = \frac{n\,T_u}{T_b}\,I \qquad (9.5)$$

where n is the mole ratio which is unity at $\phi = 0.62$, and

$$I = \frac{1}{r_b^3}\left[(r_b - x)^3 + 3T_b \int_{r = r_b - x}^{r = r_b} \frac{r^2}{T_r}\,dr\right] \qquad (9.6)$$

$$\simeq 1.4 \quad \text{at} \quad \phi = 0.62$$

Use of Eqn.(9.5) with Eqn.(9.2) gave the higher value of about 10 cm s^{-1} compared with the accepted value of about 18 cm s^{-1} and it was assumed that the difference was primarily due to possible variations and inaccuracies in the unburnt gas composition.

(b) Argon Plasmas

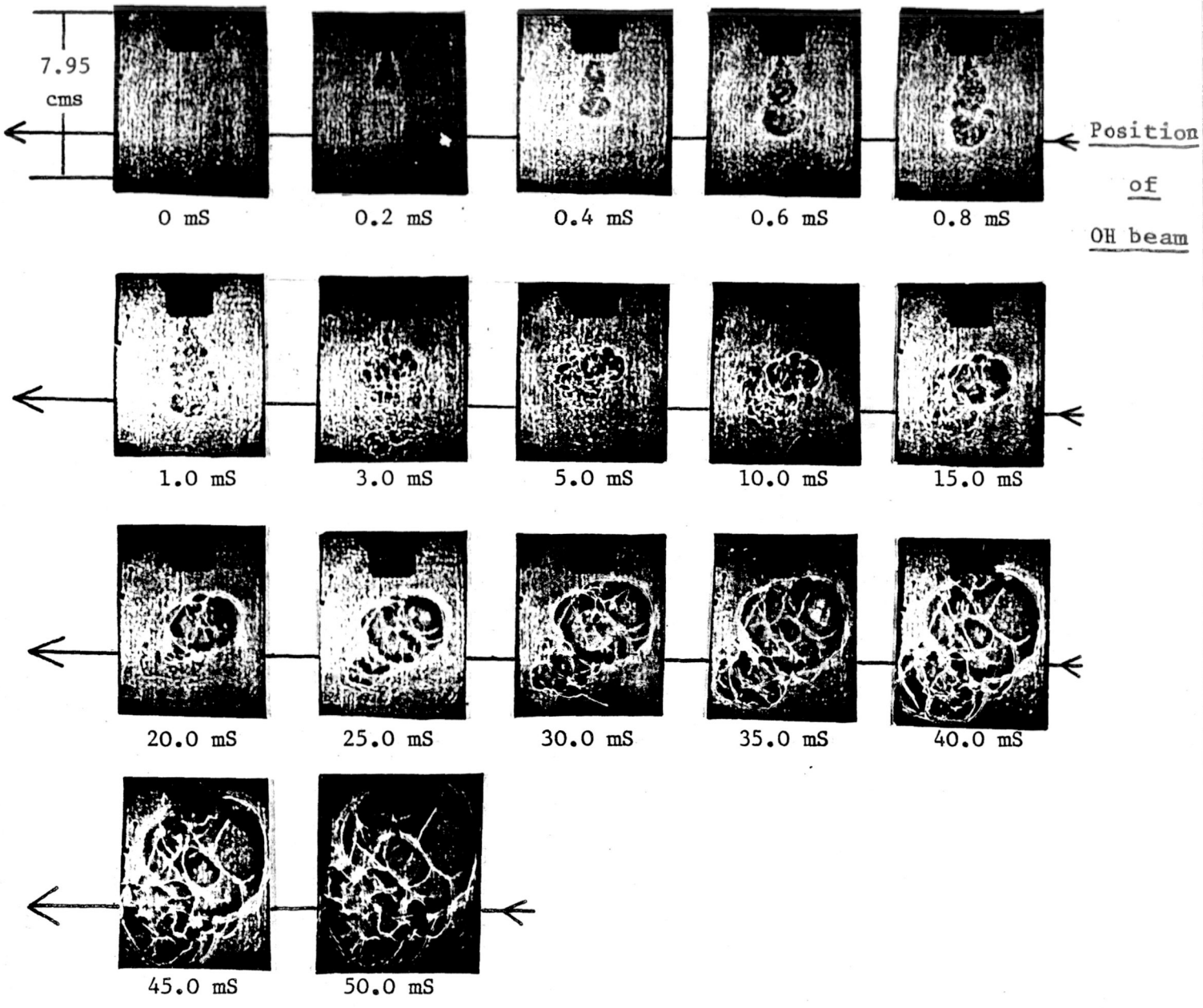
A maximum burning velocity of about 19 cm s^{-1} was recorded for an argon plasma (energy = 8.6 J) at a time of 22.5 mS after the discharge. This decayed with time to give an ultimate extrapolated value of about 16 cm s^{-1} (uncorrected) which is over twice that observed for the uncorrected spark ignited flames discussed above. As previously mentioned, due to the complete lack of chemical reactivity of this plasma, the enhanced rates of flame propagation are thought to be a consequence of the convolutions of the flame front which can be seen in Plate (10).

PLATE (10)

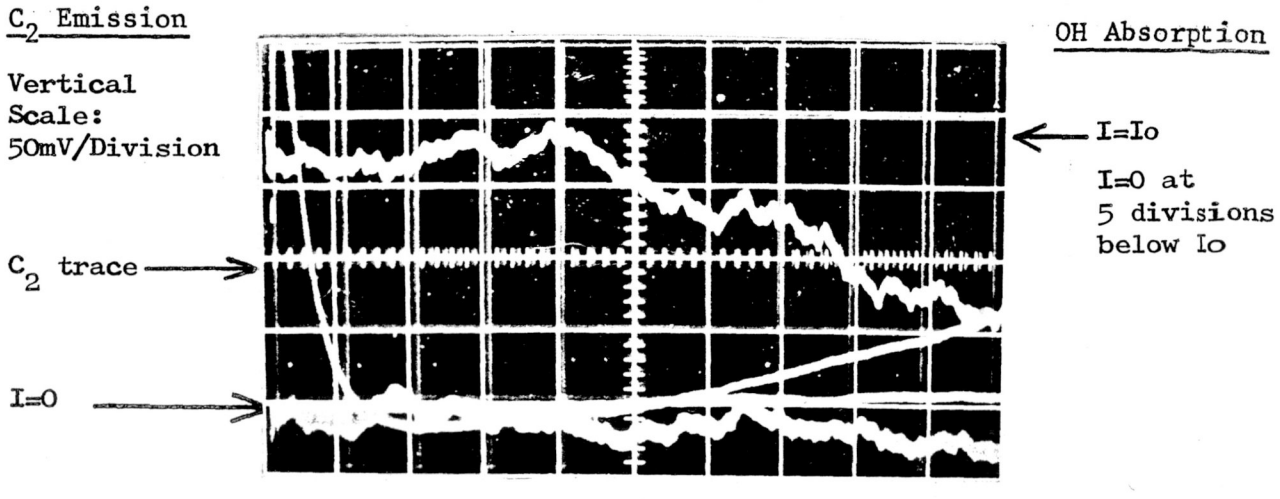
An Argon Plasma Igniting a Methane-Air Mixture

ϕ = 0.62 Stored Plasma Energy = 8.6 J Plasma Gas Flow Rate = 5 cms min^{-1}

OH beam focussed 4 cms below plug with no horizontal displacement (ie. On Axis)



OH Resonance Absorption and C_2 Emission. Horizontal Scale : 5 mS/Division



(c) Nitrogen Plasmas

This plasma generated a larger instantaneous flame area at the time of initiation of the flame front than either the hydrogen or argon plasmas. This was achieved by providing a highly convoluted and extended flame front which gave measured (turbulent) burning velocities at a radial distance > 2.2 cms of similar magnitude to those initiated by hydrogen plasmas (see Fig.(44)). In spite of the high overall burning rates after the relatively long time delay of 10 mS, the time required for the flame to reach the vessel walls was longer than that required for the hydrogen plasmas. Also due to the possible non-uniformity of temperature within the original plasma plume, it may not be entirely correct to assume that the entire proportion of the reactants within the expanding plume (before ignition of the flame front) had been burnt.

(d) Hydrogen Plasmas

Due to their high chemical reactivity, these plasmas gave higher measured burning velocities in lean mixtures than the highly turbulent nitrogen or argon plasma ignited flames. The maximum values recorded (56.8 cm s^{-1} (ϕ = 0.51))for a plasma of stored energy 10.8 J and 39 cm s^{-1} (ϕ = 0.62) for stored energy = 4.8 J) occurred at a time of 2.5 mS shortly after the initiation of the flame front (see Fig.(43) and Fig.(45)). These then decayed (for plasma energy = 4.8 J) to approximately half the maximum value over a period of 10 mS. As shown in Fig.(44), this corresponded to almost the entire length of travel through the combustion vessel.

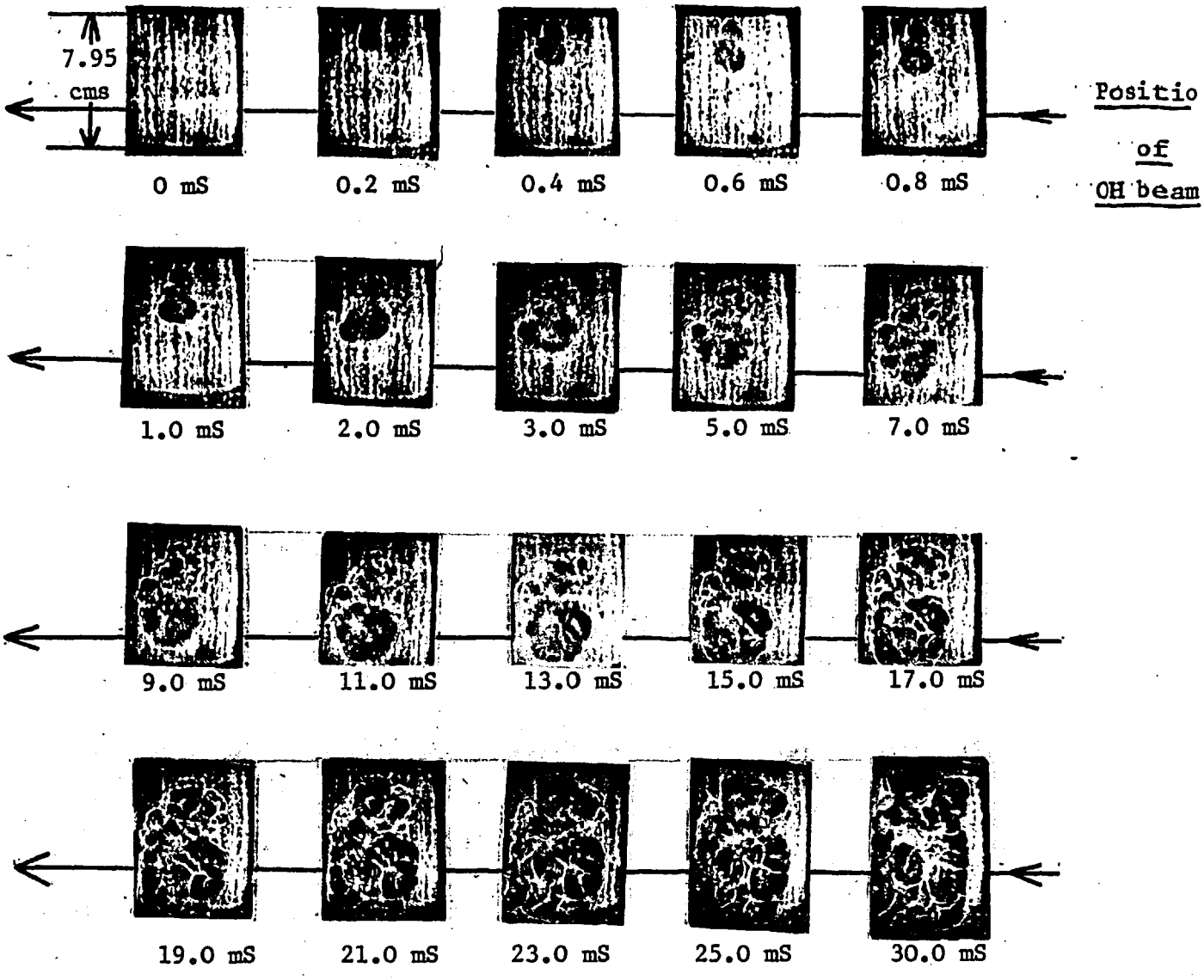
The sequence of schlieren photographs of a hydrogen plasma (energy = 4.8 J) igniting a methane-air mixture is shown in Plate (12). The very high initial laminar burning velocities caused by the high H atom concentrations within the plume result in the convoluted flame surface being smoothed out at a very early stage of the flame growth.

PLATE (11)

A Nitrogen Plasma Igniting a Methane-Air Mixture

ϕ = 0.62 Stored Plasma Energy = 4.8 J Plasma Gas Flow Rate = 5 cm^3 min^{-1}

OH beam focussed 5.6 cms below plug with no horizontal displacement (ie. On Axis)



OH Resonance Absorption and C_2 Emission

Horizontal Scale : 10 mS/Division

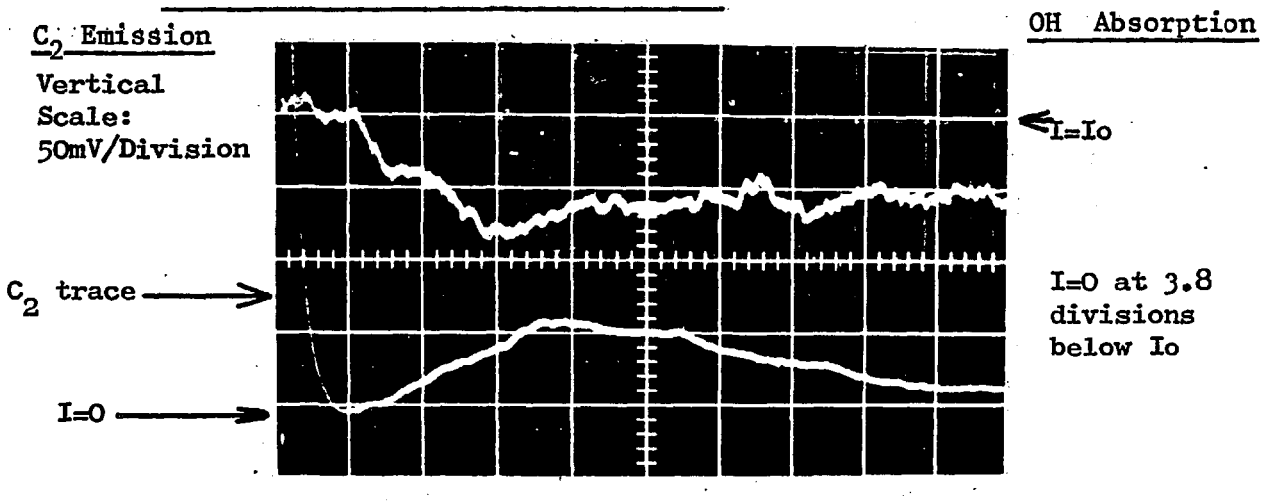
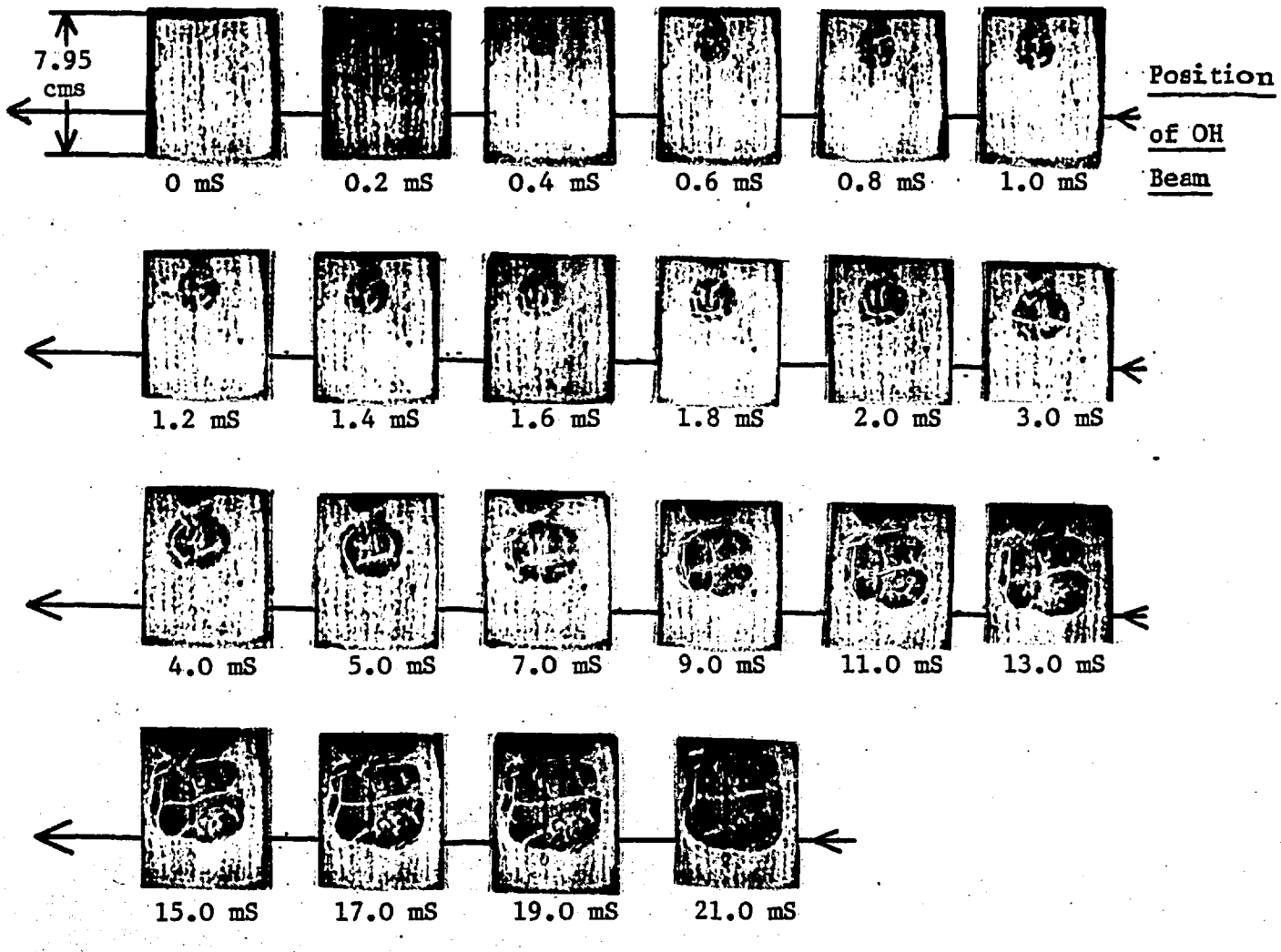


PLATE (12)

A Hydrogen Plasma Igniting a Methane-Air Mixture

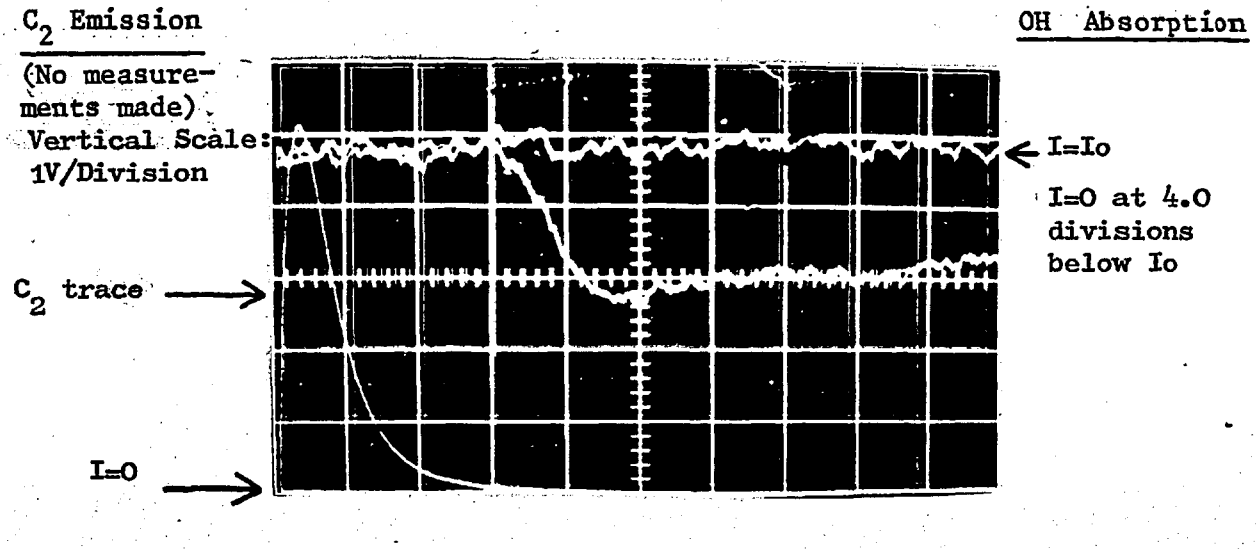
ϕ = 0.62 STored Plasma Energy = 4.8 J Plasma Gas Flow Rate = 5 cm^3 min^{-1}

OH beam focussed 5.6 cms below plug with no horizontal displacement (i.e. On Axis)



OH Resonance Absorption and C_2 Emission

Horizontal Scale : 5 mS/Division



This contrasts the behaviour of the nitrogen and argon plasmas in which the initial laminar burning velocity is virtually unchanged and the plasma plume has generated a highly convoluted flame area by the time the flame front has developed. This results in high (turbulent) burning velocities which are of comparable magnitude to the falling laminar burning velocities initiated by hydrogen plasmas.

The results from a study of the variation of burning velocity with plasma energy shown in Fig.(45) also illustrate this behaviour. Flames in methane-air mixtures (ϕ = 0.62) ignited by a plasma of higher stored energy (10.8 J) show higher initial laminar burning velocities than the flames ignited by lower energy (E = 4.8 J) plasmas. However, due to the high initial values of Su for the higher energy (10.8 J) plasma ignited flames, the rate of decay of Su was faster and it was found that at 4 mS, the laminar burning velocity had decreased to a value almost that of the constant value observed with spark ignited flames.

The chemical effects associated with reactive plasmas such as hydrogen are discussed in more detail in Chapter 10, and the increases in flame propagation due to turbulence are examined in the following section.

Calculations to Evaluate the Importance of Turbulence

Some preliminary calculations were carried out on a simplified model to study the effect of perturbations on the growth of flame area. These were based on equal numbers of convex and concave perturbations superimposed on the surface of a sphere. Close packing was achieved by construction of regular polyhedra such that each hemisphere was centred on a face and touching the edges. The entire surface was then expanded normal to itself at every point.

Calculations on five separate polyhedra showed that the results were surprisingly insensitive to the numbers and consequent size of

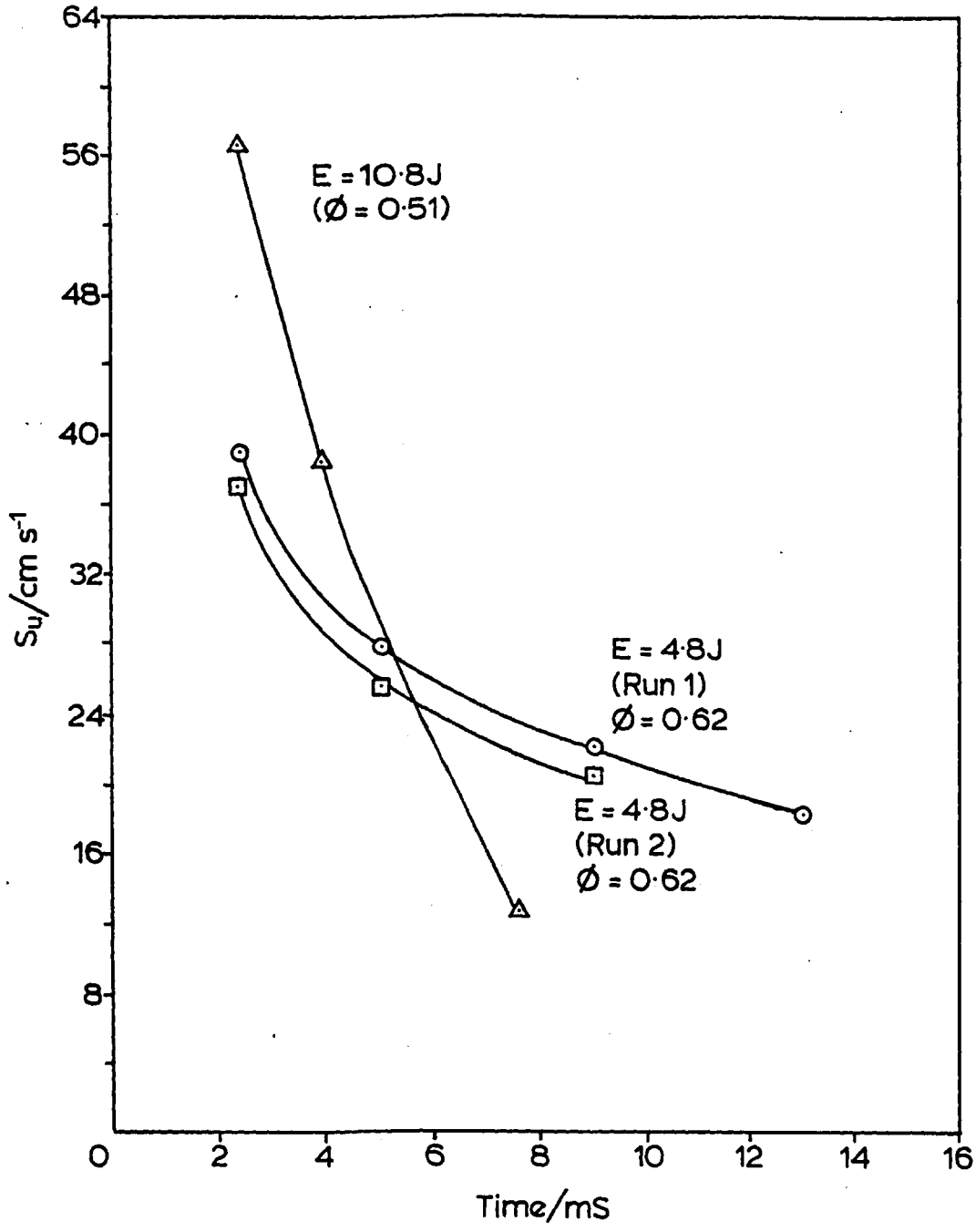


FIG. (45)

BURNING VELOCITIES FOR HYDROGEN PLASMAS IGNITING A METHANE-AIR MIXTURE WITH Ø = 0·62 AND Ø = 0·5

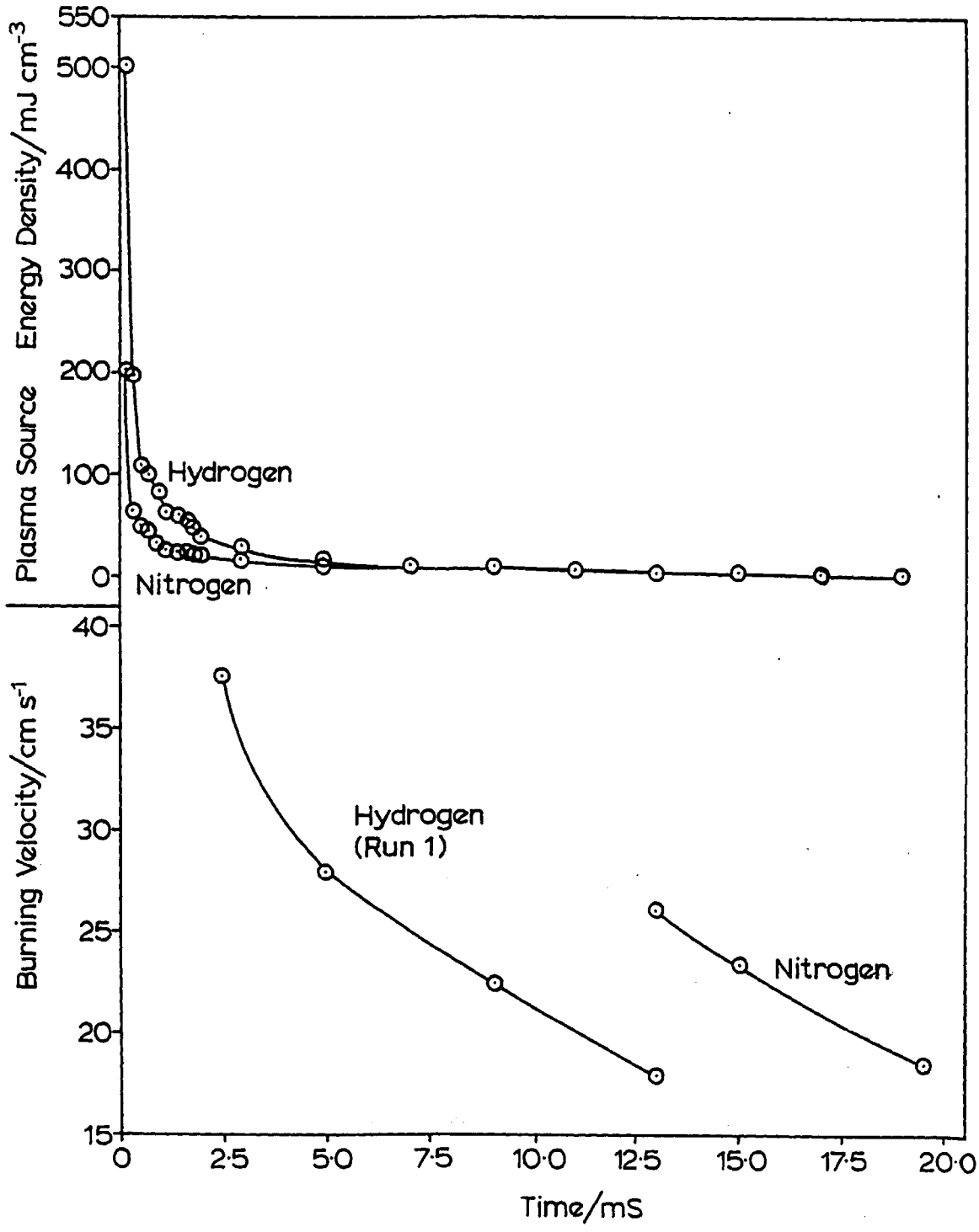


FIG. (46)

PLASMA SOURCE ENERGY DENSITIES AND BURNING VELOCITIES AGAINST TIME FOR A HYDROGEN AND NITROGEN PLASMA IGNITING A METHANE-AIR MIXTURE WITH $O = \phi \cdot 62$

the perturbation especially once the initial radius was doubled. Although the calculations did not allow for the effects of gas expansion, the rate of flame growth was found to be smaller than that observed experimentally.

Finally some results (117) using air plasmas igniting methane-air mixtures at equivalence ratio 0.6 in constant volume systems show a convoluted:laminar flame area of approximately 3 persisting for most of the flame travel. A number of plugs with variable cavity geometry were used and the ratio was found to be higher for a larger critical length of the cavity but only during the initial stages (no difference observed above 15 mS).

CHAPTER 10

RESULTS AND DISCUSSION OF THE OH RESONANCE ABSORPTION MEASUREMENTS

In the previous chapters, the change in combustion characteristics (limits of ignitability and burning velocities) compared with standard (e.g. spark ignited) flames have been described and the contributory mechanisms responsible for these changes have been discussed. In this chapter, an assessment is made of the chemical effects of plasma jet ignition using the OH resonance absorption measurements obtained with the apparatus described in Chapters 4 and 6. During this study, argon has again been used for the plasma feed gas as a standard because of its lack of chemical reactivity.

Since two quite distinct plasma ignition stages have been isolated (Chapter 7), the OH resonance absorption measurements relating to each stage will be discussed separately.

10.1 Flame Growth (1st Stage Ignition)

(a) Results

As previously mentioned in Chapter 7, the early stage of flame growth in which the plasma entrains large volumes of reactant gases were generally characterised by a low or zero concentration of OH within the expanding plume. Although this applies to nitrogen and argon plasmas, it may not be strictly true for hydrogen plasmas for the reasons given below.

(1) Hydrogen Plasmas

Due to the high chemical reactivity of hydrogen plasmas, the transition to the development of the flame front occurred extremely rapidly and under the conditions used in the present experiments, no hydroxyl concentration measurements were possible. This was because

the transition to 2nd stage ignition required times of less than 1 mS and for the plasma energies (e.g. stored energy = 4.8 J) and plasma plug orifice plates (orifice diameter 2 mm) used for these experiments, the flame was initiated too close to the plasma plug (see Plate (12)). This meant that for measurements to be obtained during these early stages (for times less than 1 mS), the OH diagnostic beam also had to be situated near to the plug(e.g. within 1 to 2 cms). However, at this position, the OH resonance absorption signal became severely affected by the light emission from the plasma.

This could probably be overcome by taking several measurements to ascertain the required plasma energy and plasma plug origice plate to produce an ejected plasma plume about 4 cms from the plug in a time of less than 1 mS. In this way OH resonance absorption measurements could be taken without interference from the plasma light.

This very fast transition by a hydrogen plasma to 2nd stage ignition can be easily understood with reference to the branching chain reaction:

$$H + O_2 \rightleftharpoons OH + O$$

This would become very important for ignition of lean mixtures (i.e. high $[O_2]$) due to the direct availability of H atoms which would reduce the overall chemical induction time for a given plasma temperature.

(2) Argon Plasmas

The hydroxyl concentration was found to be zero (or at least below the detection limits of the method) throughout the duration of the 1st stage ignition for all of the argon plasmas examined. Only after the much longer time period of about 12 mS (for plasma energy = 8.6 J - see Plate (10)) corresponding to the development of the true flame (or 2nd stage ignition) did the hydroxyl concentration begin to rise. This would probably be expected since translationally "hot" argon atoms

from the plasma would have to transfer energy to other molecules collisionally to generate radicals by dissociation. A typical sequence of reactions could be

$$Ar + O_2 \xrightarrow[\text{Energy Transfer}]{} O + O + Ar$$

then $$O + CH_4 \longrightarrow CH_3 + OH$$

or $$Ar + CH_4 \longrightarrow CH_3 + H + Ar$$

These reactions require higher activation energies (higher plasma temperatures) and are generally slower than those following the direct injection of radicals. For this reason, the hydroxyl concentration during the 1st stage ignition would be extremely small and consequently argon plasmas (in spite of their high translational temperatures) would be expected to be poor ignition sources - as found in the present research.

(3) Nitrogen Plasmas

In the case of nitrogen plasmas a particularly interesting result was encountered which has been mentioned previously in Chapter 7. During the early time period of about 1 to 5 mS for a nitrogen plasma (E = 10.8 J) discharging into a methane-air mixture (ϕ = 0.54), the hydroxyl concentration in the plume was found to increase then decay as shown in Fig.(32). This rise and fall of OH was characteristic of the 1st stage ignition which was also associated with an expansion of the plume compared with an identical plasma discharging into air. This was because entrainment of methane-air mixture into the initial hot plasma produced a high hydroxyl concentration which then decayed rapidly as the temperature fell due to further entrainment and continued expansion of the plume.

A second larger increase in hydroxyl concentration then occurred at later times which corresponded to the 2nd stage ignition or development of the flame front. As shown in Fig.(47), for a nitrogen plasma with initial conditions: E = 4.8 J and ϕ = 0.62, the second increase was found at a time of about 12 mS. Although the hydroxyl concentrations shown in Fig.(32) and Fig.(47) refer to the 1st and 2nd stage ignitions respectively (the corresponding OH oscillograms from which measurements were taken were shown in Plates (13) and (11)), it should be noted that a direct comparison is not possible due to the difference in initial conditions of plasma energy and equivalence ratio of the two nitrogen plasmas. In fact it was usually not possible to obtain the entire hydroxyl concentration profile of the pre-ignition and true ignition in a single plasma firing because of the different time scales required in the two cases. However, the general trend of this phenomenon can be seen from the results.

Plate (13) shows an OH oscillogram of a "true" ignition in which the "pre-ignition" phase can just be identified at a time of about 5 mS. Occasionally, a "true" ignition developed from a "pre-ignition" stage at a time of about 5 mS. This suggests that in the majority of cases, the concentration of specific radicals (and temperarure) was slightly below that required to maintain a stable combustion wave for the particular plasma ejection velocities and plasma plume dimensions. Consequently, the concentration of radicals fell as the rates of the chain termination reactions exceeded those of chain branching and the plasma plume continued to grow to a size required for the initiation of a stable combustion wave. In some cases, due to the statistical variations in plasma ejection velocities, plasma temperatures and N atom concentrations, the concentration of specific radicals (and temperatures) exceeded that required for the initiation of a flame which coincided with the "pre-ignition" stage.

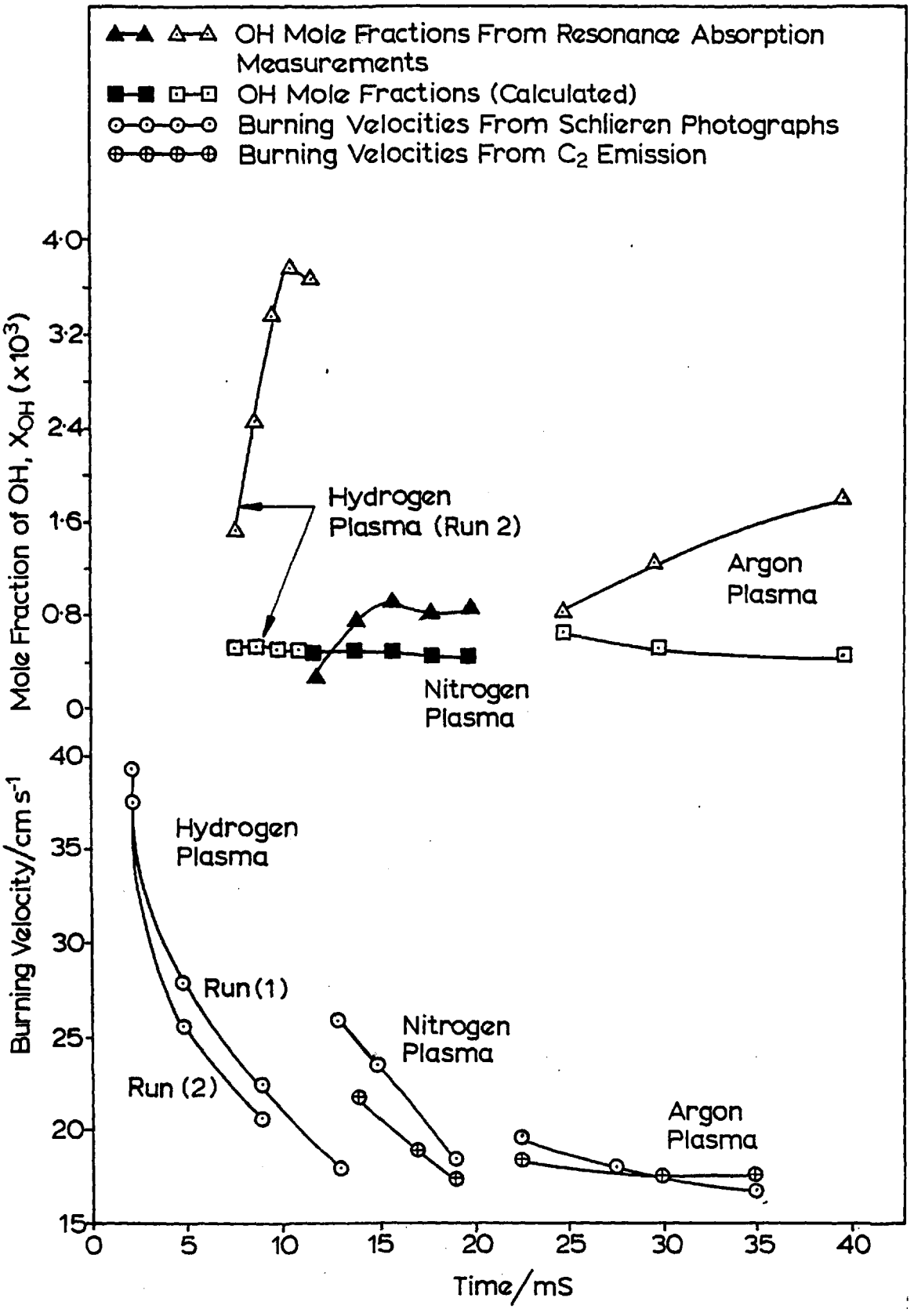


FIG. (47)

BURNING VELOCITIES AND HYDROXL CONCENTRATION FOR PLASMAS IGNITING A METHANE-AIR MIXTURE WITH $\emptyset = 0{\cdot}62$.

PLATE (13)

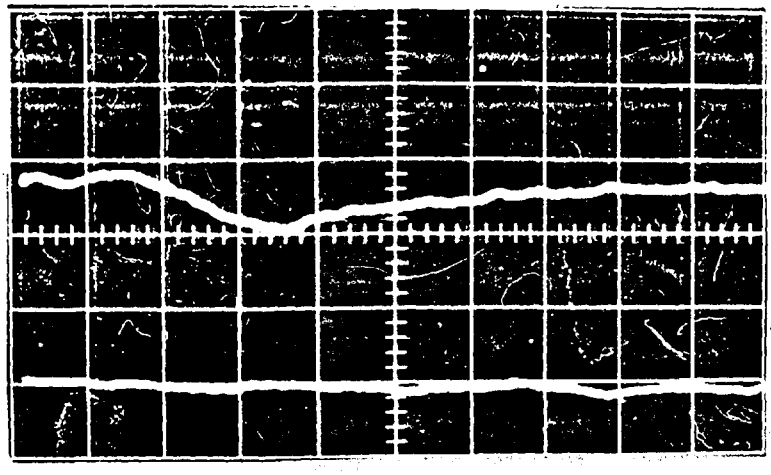
OH Resonance Absorption Oscillograms for a Nitrogen Plasma Jet Igniting A Methane-Air Mixture

A. Stored Plasma Energy = 10.8 J

ϕ = 0.54. Plasma Gas Flow Rate = 5 cm^3 min^{-1}

Horizontal Scale : 1 mS/Division

OH beam focussed 4 cms below plug with no horizontal displacement

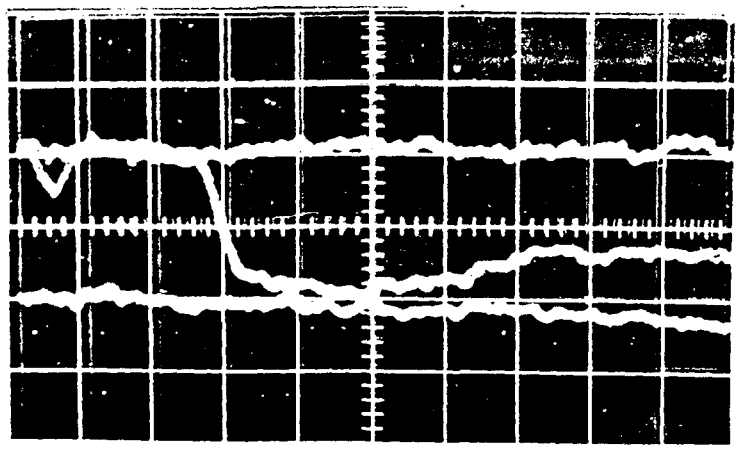


B. Stored Plasma Energy = 4.8 J

ϕ = 0.60 Plasma Gas Flow Rate = 5 cm^3 min^{-1}

Horizontal Scale : 10 mS/Division

OH beam focussed 4 cms vertically below plug and 0.4 cms horizontally displaced from axis.



The growth of the hydroxyl concentration during the "pre-ignition" period was not easily quantified since the initial conditions of radical concentrations and temperatures were not known with any degree of precision. However a comparison was attempted between the measured peak OH values (based on an assumption for the plasma plume temperature) and the decay of hydroxyl radicals during the pre-ignition period with that of normal methane-air flames.

(b) Kinetic analyses of the peak values and decay of Hydroxyl concentration during the pre-ignition stage of a nitrogen plasma

(1) Peak hydroxyl concentration, $[OH]_{max}$

A peak value of $[OH]_{max} = 3.2 \times 10^{15}$ molecules cm^{-3} was found during the pre-ignition stage of a nitrogen plasma (stored energy = 10.8 J) igniting a methane-air mixture ($\phi = 0.54$). As shown in Fig.(48), this occurs at a time of 3.4 mS and compares with the lower calculated peak value at this time (assuming a perfectly stirred system) of slightly less than 1×10^{15} molecules cm^{-3} (calculated from values given in reference (104)).

The difference in the two values was due to the increased temperature of the plasma plume caused by the higher energy content ($\Delta H + \Gamma E$) compared with a perfectly stirred flame of the same equivalence ratio. From calculations of plasma source energy densities (see Fig.(48)), the temperature of the plume was approximately 110 K above that of the adiabatic flame temperature (1550 K with $\phi = 0.62$) at the time of 3.4 mS when the peak hydroxyl concentration was measured.

(2) Decay of Hydroxyl Concentration from the Peak Value

The decay of hydroxyl concentration in a nitrogen plasma plume during the "pre-ignition" stage described in the preceding section was examined in more detail. This was made possible by a comparison of

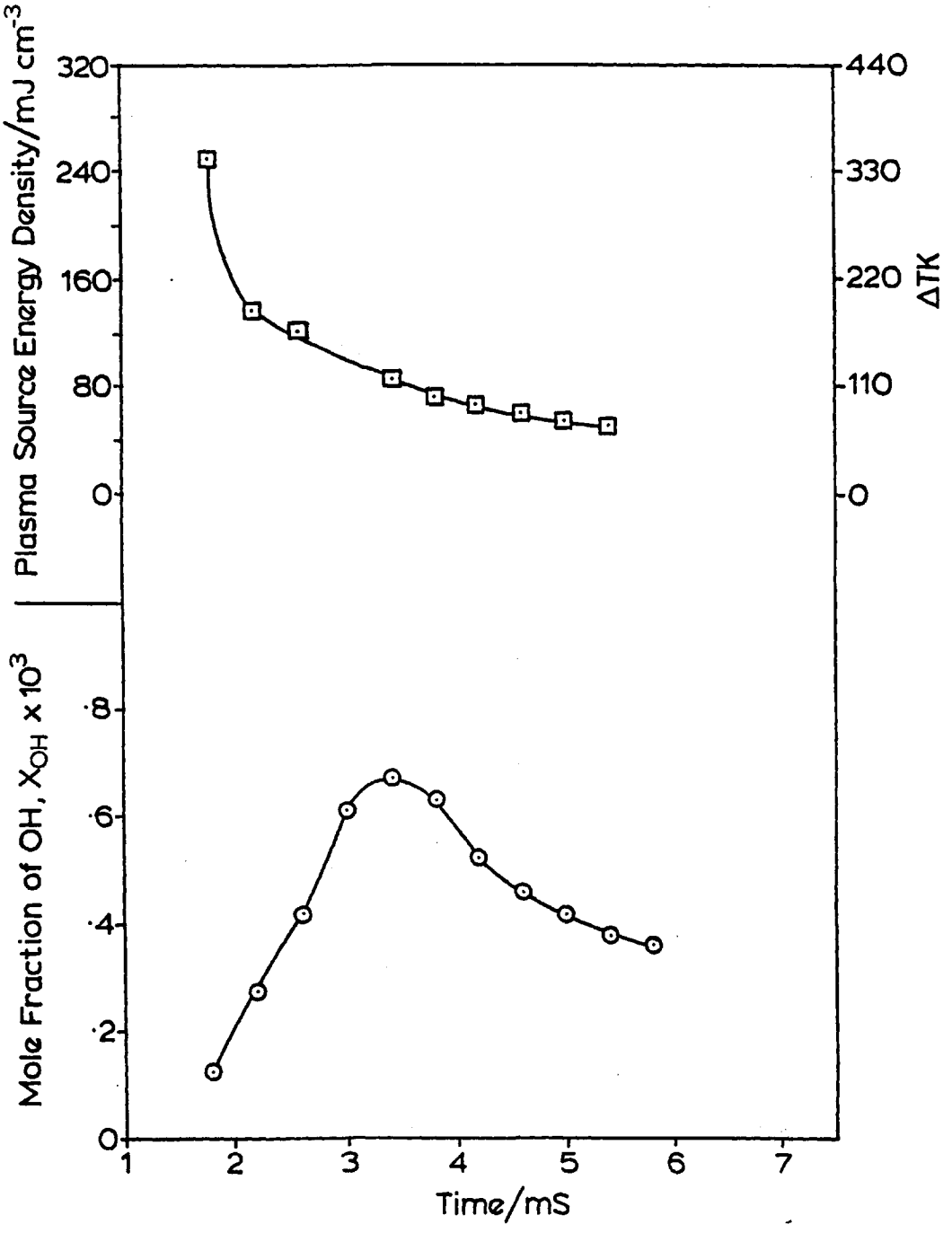


FIG. (48)

OH CONCENTRATIONS, PLASMA SOURCE ENERGY DENSITIES AND TEMPERATURES FOR A NITROGEN PLASMA (Stored Energy = 10·8J) PRE-IGNITING A METHANE-AIR MIXTURE WITH Ø = 0·54

experimental and predicted $[OH]$ decay rates in methane-air flames reported by previous authors (104, 103, 102).

The inverse of the measured hydroxyl concentrations were plotted against time as shown in Fig.(49). The almost linear relationship (Fig.(49)) indicates a second order dependence of the hydroxyl decay rate on OH given by :

$$\frac{d\,[OH]}{dt} = - k_{OH}\ [OH]^2$$

k_{OH} is indicative of an effective global reaction rate constant involving only the elementary reactions with the hydroxyl radical since during the early "pre-ignition" stage, the plasma plume could be regarded as a perfectly stirred system. This is not so with some flames (to which the present system was compared) since the influence of transport phenomena such as the diffusion of H and OH severely affect the overall decay rates of the hydroxyl radical.

Since the rate of decay of OH within the plume was controlled by termolecular elementary reactions, the decay constant, k_{OH} should be normalised by the total number density, M to give a decay rate constant α

$$\text{where} \qquad \alpha = \frac{k_{OH}}{M}$$

Although M was a function of temperature, for the sake of simplicity, the temperature of the plume during the pre-ignition stage was assumed constant at 1660 K (Tadiabatic + Δ T) giving a constant value for $M = 4.4 \times 10^{18}$ molecules cm^{-3}. Taking k_{OH} from the gradient of the straight line in Fig.(49), a value of $\alpha = 2.95 \times 10^{-32}$ cm^6 $molecules^{-2}$ s^{-1} was obtained which is slightly higher than that reported (see reference (104)) of about 0.8×10^{-32} cm^6 $molecules^{-2}$ s^{-1}

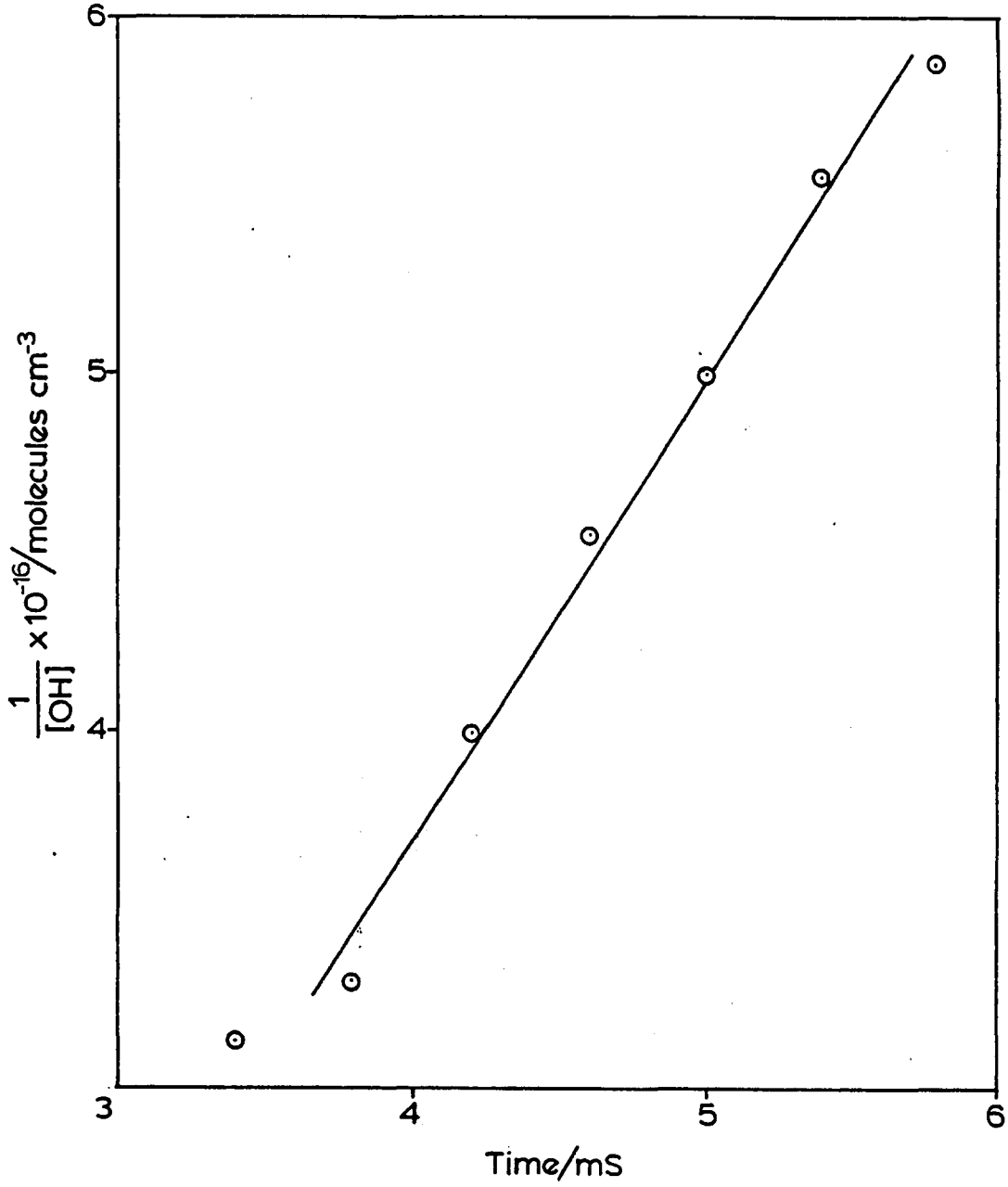


FIG. (49)

1/[OH] vs. TIME FOR THE DECAY DURING THE PRE-IGNITION PERIOD BY A NITROGEN PLASMA.

for methane-air flames (extrapolated to ϕ = 0.51). It is however very much lower than the value quoted by one author in reference (104) of about 11 x 10^{-32} cm^6 $molecules^{-2}$ s^{-1} (extrapolated to ϕ = 0.51).

It would be expected that the decay rates would be higher in the nitrogen plasma plume than in the methane-air flames with which the decay rates were compared. This would be due to the effects of diffusion from the main reaction zone of the flame which would tend to counteract the chemical decay rate of the hydroxyl radical. In the case of the stirred nitrogen plasma plume, these effects would be accounted for and the measured decay rate constant would be independent of diffusional transport phenomena.

10.2 Development of the Flame Front

It was only after the development of a stable combustion wave that the measured hydroxyl concentration was found to rise significantly. This can be seen in Fig.(47) which shows the rise and decay of hydroxyl concentration with time for plasma ignited methane-air flames (ϕ = 0.62) with the OH diagnostic beam orthogonal to the direction of travel along the central axis of the flame front. As explained in more detail below, for hydrogen and argon plasmas, the results refer to the combustion wave overtaking the diagnostic beam whereas for the nitrogen plasma, the plume had already overtaken the beam before hydroxyl radicals were detected (i.e. after the pre-ignition stage).

Although it would be expected that the hydroxyl concentration in an unperturbed methane-air flame would be at a maximum when the flame front overtook the diagnostic beam at tangential incidence (i.e. when the OH per unit path length was at its highest), this was not found to be strictly correct for plasma ignited flames. This was realised when a comparison was made between measured $[OH]$ for plasma ignited flames and calculated $[OH]$ values assuming that the plasma

ignited flames were normal methane-air flames. It was shown (see below) that the [OH] profile was modified in comparison to the reported (104, 103, 102) [OH] profiles for normal methane-air flames which would suggest that other species concentration profiles (e.g. H, O and N), the temperature profile and therefore the flame structure is different for the plasma ignited flames compared to normal methane-air flames at the same equivalence ratio.

This would be expected for two reasons. Firstly, the plasma ignited flames would enclose a volume of reacting gas resulting from the original high temperature and (in the case of hydrogen, and possibly nitrogen) chemically reactive plasma plumes. The reactive species concentrations in the post flame gases of any flame front formed on the plume would be modified by the presence of the plume until the flame had grown to a sufficient size to be unaffected by the diminishing ignition source. This would result in higher measured hydroxyl concentrations when the beam traversed a relatively large portion of the post flame gases than the calculated values based on normal methane-air flames.

The second reason why the measured hydroxyl concentrations for plasma ignited flames are higher than the calculated values for normal flames is connected with the primary aim of this research. For plasmas generating chemically reactive species with high diffusion coefficients (especially the H atom) it would be expected that the region immediately ahead of the plasma plume would be enriched in these species. This would tend to modify the [OH] profile compared to that for a similar unperturbed methane-air flame. Both of these explanations will be discussed further in the present chapter.

The most important result obtained in this study was that the hydroxyl concentration in hydrogen plasma ignited flames was found to be considerably higher than that corresponding to nitrogen or argon plasma

flames. This was not immediately apparent from the OH resonance absorption measurements because of the different geometry of the flames ignited by different plasma media. For example, the large radius of curvature of the hydrogen plasma ignited flame (see Plate 12) would provide a greater volume of flame with high $[OH]$ than a different shaped flame kernel with a smaller radius of curvature measured from the position of the diagnostic beam at tangential incidence to the centre of the expanding flame. For this reason, OH concentrations for each measured plasma ignited flame value were calculated (see below) and from values of $[OH]_{Experimental} - [OH]_{Calculated}$ it was observed that higher hydroxyl concentrations existed in hydrogen plasma ignited flames than those of nitrogen or argon.

(1) Calculated Hydroxyl Radical Concentrations

(i) The Method

For each experimentally measured hydroxyl concentration within a plasma ignited flame, the corresponding $[OH]$ value based on the assumption that the plasma ignited flame was a normal (e.g. spark ignited) methane-air flame was calculated. As shown in the example in Plate (14), the calculated value was obtained by enlarging the schlieren photograph and marking the position of 7 zones (of different hydroxyl concentration) relative to the OH diagnostic beam. The boundaries of each zone and the mean mole fraction of OH, X_{OH} within the zone which were used in the calculations are given in Table (2). These values were derived from reported hydroxyl concentration profiles for methane-air flames, examples of which are shown in Table (1).

(ii) The Results

Some of the calculated values using this procedure are shown in Fig.(47) and Table (3). It can be seen more clearly in Table (3) that the mean calculated value of OH, $X_{OH(calc.)}$ does not change

PLATE (14)

An example of the "zone" method for measurement of calculated hydroxyl values.
Plasma: hydrogen, time 8.0mS, magnification = X 5.1

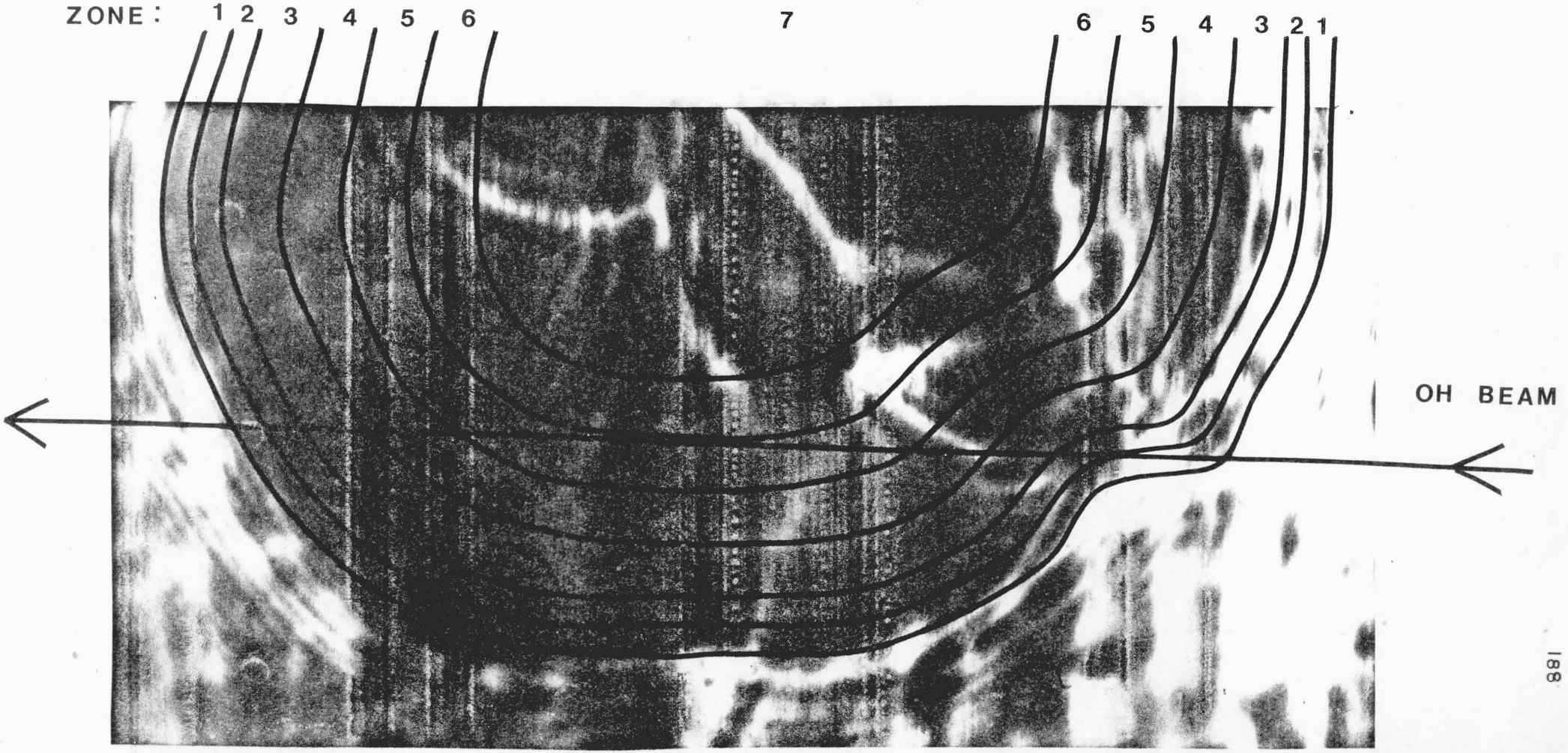


TABLE 1

Mole Fractions of OH Through A

Methane-Air Flame with ϕ = 0.62

(A) Peak OH Concentrations

Reference	Peak X_{OH}
Smoot (11)	2.4×10^{-3}
Tsatsaronis (Extrapolated) (118)	2.8×10^{-3}
Cattolica, R.J. (104) (Extrapolated)	2.5×10^{-3}
Value Chosen	2.6×10^{-3}

(B) OH Concentration Profile

Distance from beginning of temperature rise (mm)	OH Mole Fraction, X_{OH} ($\times 10^3$)
1 mm (Peak)	2.6
2 mm	1.6
4 mm	0.6
6 mm	0.4
8 mm	0.3
10 mm	0.2
> 10 mm	0.2

TABLE 2

Mole Fractions of OH Through A Methane-Air Flame with $\phi = 0.62$

Zone	Start	Finish	Mean X_{OH}
1	0	1	1.3
2	1	2	2.1
3	2	4	1.1
4	4	6	0.5
5	6	8	0.35
6	8	10	0.25
7	10	-	0.2

Definitions:

(1) Start and Finish : Distance from beginning of temperature rise.

Units mm.

(2) Mean X_{OH} : Mean value for the mole fraction of OH (X_{OH}) over the range studied.

Units 1×10^{-3}.

TABLE 3

Mole Fraction of OH Through Plasma Ignited

Methane-Air Flames with ϕ = 0.62

Plasma Gas	Time (mS)	Total Distance x 2 (mm)	Mean X_{OH}
N_2	12.0	21.2	.492
N_2	14.0	21.1	.494
N_2	16.0	23.7	.462
N_2	18.0	26.7	.432
N_2	20.0	27.2	.428
H_2 (Run 1)	17.0	4.82	1.3
H_2	19.0	12.05	1.59
H_2	21.0	18.07	1.41
H_2	23.0	24.09	0.75
H_2 (Run 2)	8.0	17.3	.558
H_2	9.0	18.1	.543
H_2	10.0	19.5	.518
H_2	11.0	20.5	.502
H_2	12.0	21.1	.494
Ar	25.0	14.5	.628
Ar	30.0	21.1	.494
Ar	40.0	27.7	.424

significantly with time for a given plasma, unlike the experimentally measured values (Fig.(47)). This illustrates the higher hydroxyl concentrations found in plasma ignited flames (especially hydrogen plasmas) compared with normal flames due to the increased temperature and radical concentrations.

The results (experimental and calculated hydroxyl values) are discussed below in more detail in relation to each plasma medium.

(a) Argon Plasmas

The measured rise in hydroxyl concentration as the stable flame front overtook the OH diagnostic beam at tangential incidence is shown in Fig.(47). As seen in Plate (10), which shows the sequence of high speed cine schlieren photographs referring to these messurements, the development of a flame front occurred only after a long time delay of about 12 mS. After this long time delay the flame kernel appeared to form on one side of the original plasma plume; unlike the situation for the hydrogen and nitrogen plasmas.

This would be expected due to the high ejection velocity associated with an argon plasma (Chapter 7) and the slow initiation of combustion reactions by hot argon atoms. As explained in Section 10.1 of this chapter, the slow initiation is caused by the energy transfer and dissociation processes required before radicals can be generated from translationally "hot" argon atoms. The thermal dissociation step (i.e. of O_2, N_2, CH_4, etc.) would be a relatively slow and inefficient step in terms of the plasma plume temperature unlike that of chemically active plasmas. For this reason, the initiation of flame reactions "lags behind" the expansion of the jet, the latter being relatively high (for example, see Fig.(31) - graphs of axial and radial distances vs. time for an argon plasma discharging into air). Consequently, the flame front is not formed at the interface of the unburnt gas and plasma

plume furthest from the plasma plug but downstream of this position in a higher temperature environment which is nearer the original plasma. This, of course, contrasts with the behaviour of a hydrogen plasma in which the initiation of combustion reactions occurs so fast that the ejected plasma has reached only a fraction of its final dimension before combustion reactions commence.

The calculated values for the hydroxyl concentration show a maximum at a time of 25 mS (with the beam at tangential incidence) and decaying with increasing time. The trend for the measured values is the reverse of this (minimum at 25 mS and increasing with time) and one of two possible explanations could account for this. Firstly, the higher temperature of the plasma plume would modify the actual hydroxyl concentration profile through the expanding flame kernel giving higher values for the mean hydroxyl concentration than those based on standard methane-air flames of the same equivalence ratio. Secondly, due to the slow initiation, distributed reaction within the flame kernel might still be occurring (i.e. the stirred reaction) which would undoubtedly modify the average hydroxyl concentrations which were obtained experimentally through the plume. However, it was not possible in this case to calculate the plasma source energy densities during ignition because of the separation of the original plume into 2 segments and therefore the relative importance of these two phenomena could not be examined further.

(b) Nitrogen Plasmas

The main rise and decay of the hydroxyl concentration during the development of a nitrogen plasma ignited flame front is shown in Fig.(47). This change in hydroxyl concentration occurred some 10 mS after that corresponding to the earlier "pre-ignition" stage which has been described in Section 10.1 of this chapter. The sequence of high speed cine schlieren photographs which were taken simultaneously with the hydroxyl concentration measurements are shown in Plate (11) and

these show that, unlike the argon and hydrogen plasma ignited flames, the first change in the measured hydroxyl concentration did not correspond to the plume overtaking the OH diagnostic beam. This is a particularly interesting result since it shows the absence of any chemical reactions occurring even though the plasma plume has expanded to an appreciable size.

(c) Hydrogen Plasmas

The growth of the hydroxyl concentration with time within a hydrogen plasma ignited flame is shown in Fig.(47). As expected, the hydroxyl concentrations were found to be higher than than those of nitrogen or argon plasma ignited flames and this was confirmed using calculated values for the hydroxyl concentrations based on normal methane-air flames (see Section (i)). The calculated values of $[OH]_{Exp.} - [OH]_{Calc.}$ for each plasma is shown in Fig.(50) and, as explained earlier, these are indicative of the overall radical concentration level within the flame.

2. Evidence for the Change in Flame Structure

There is evidence that the flame structure is altered by the effects of additional radicals supplied by the plasma, in hydrogen plasma ignited flames, quite apart from the higher measured hydroxyl concentrations and increase in burning velocities.

This was most readily seen from the general form of the OH oscillograms of hydrogen plasma ignited flames compared with those of nitrogen or argon. For the hydrogen plasma ignited flames, the initial detection of hydroxyl radicals was followed by a steep rate of increase of light absorption which reached a maximum value at an early time period (e.g. see oscillogram A in Plate (15)). This maximum value of light absorption then persisted throughout the duration of the measurements (e.g. approximately 90 mS as shown in oscillogram A, Plate (15)).

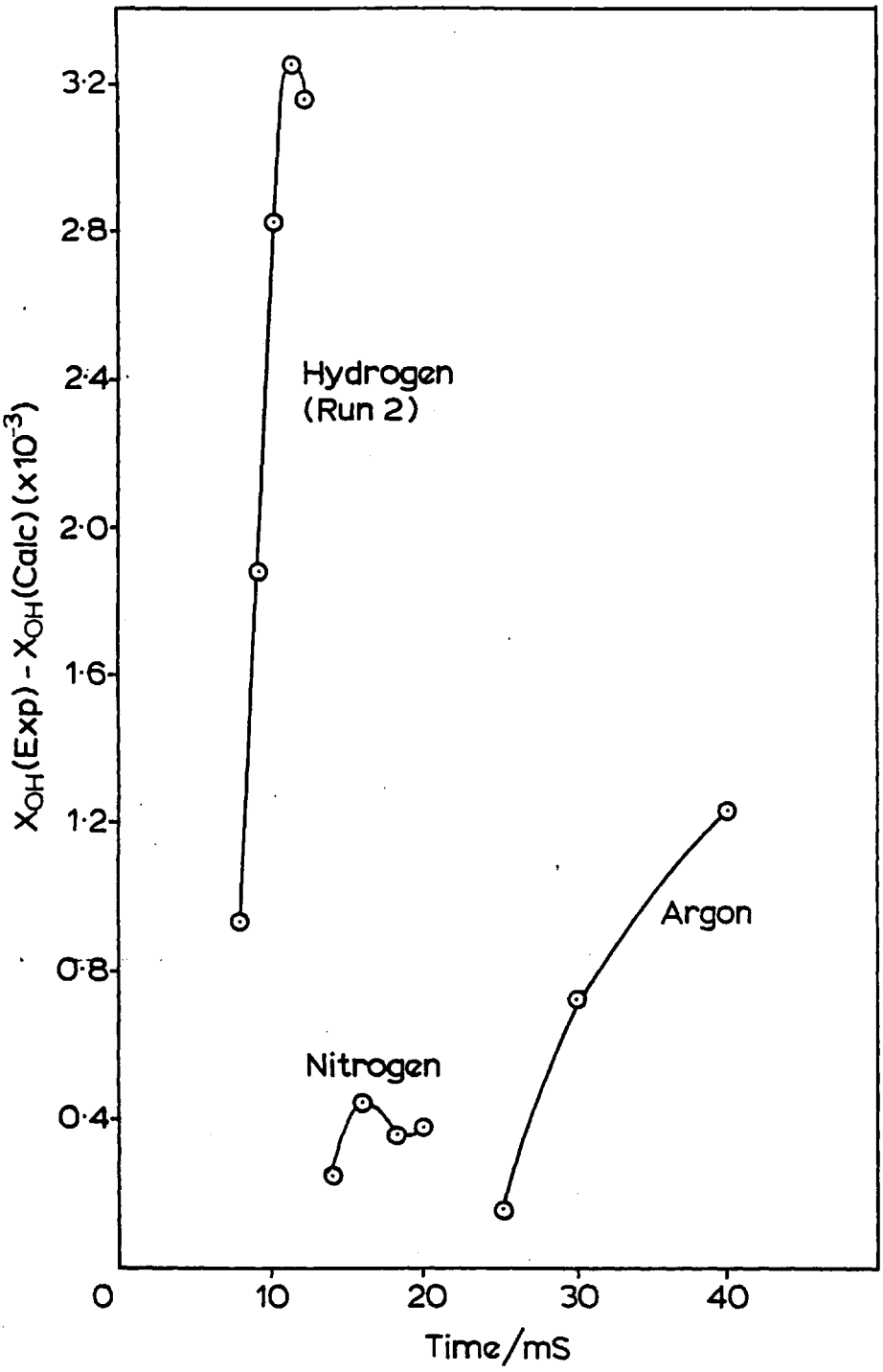


FIG. (50)

$[OH]_{EXPERIMENTAL} - [OH]_{CALCULATED}$ FOR PLASMAS IGNITING A METHANE-AIR MIXTURE WITH $\phi = 0{\cdot}62$.

PLATE (15)

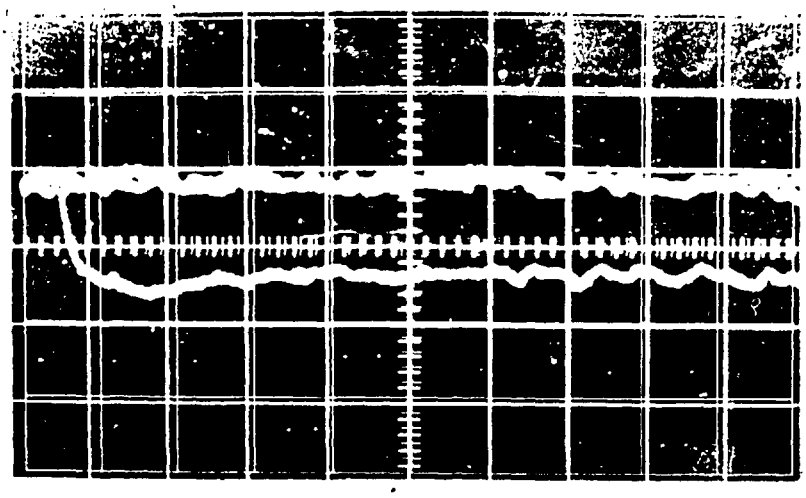
OH Resonance Absorption Oscillograms for a Hydrogen Plasma Igniting a Methane-Air Mixture

A. Stored Plasma Energy = 4.8 J

ϕ = 0.60 Plasma Gas Flow Rate = 5 cm^3 min^{-1}

Horizontal Scale : 10 mS/Division

OH beam focussed 4 cms below plug with no horizontal displacement (i.e. On Axis)



B. Stored Plasma Energy = 4.8 J

ϕ = 0.60 Plasma Gas Flow Rate = 5 cm^3 min^{-1}

Horizontal Scale : 10 mS/Division

OH beam focussed 4 cms below plug and 3.6 cms horizontally displaced from axis.

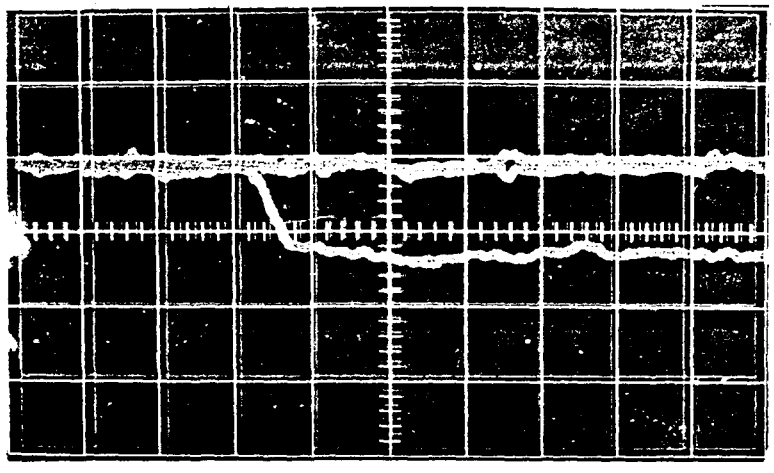


PLATE (16)

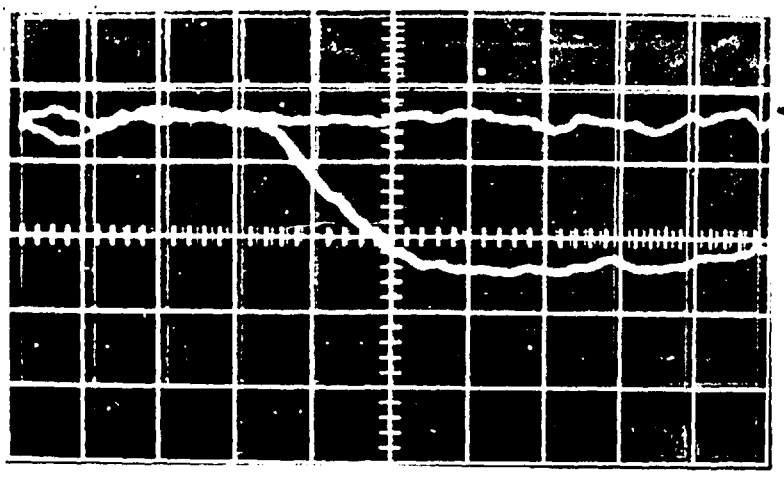
OH Resonance Absorption Oscillograms for a Hydrogen Plasma Igniting a Methane-Air Mixture

A. Stored Plasma Energy = 4.8 J

ϕ = 0.60 Plasma Gas Flow Rate = 5 cm^3 min^{-1}

Horizontal Scale : 2 mS/Division

OH beam focussed 4 cms below plug with no horozintal displacement (i.e. On Axis)

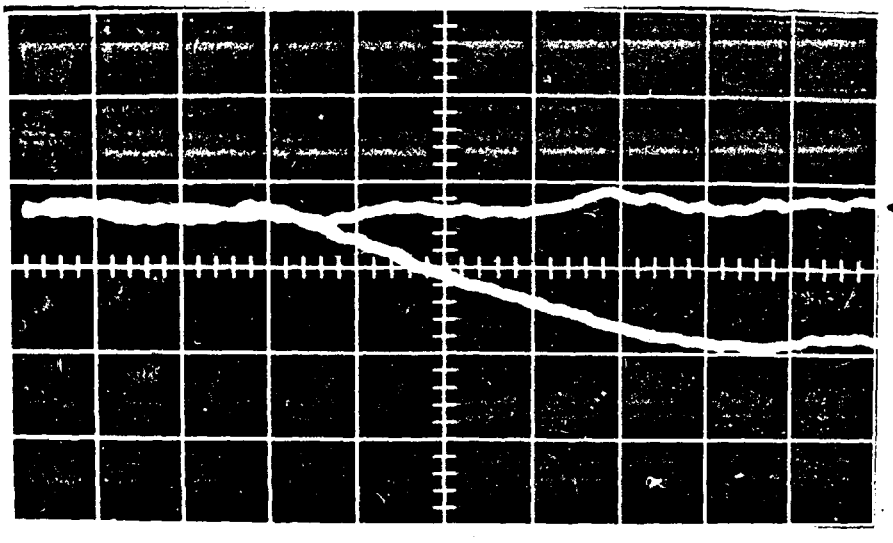


B. Stored Plasma Energy = 10.8 J

ϕ = 0.51 Plasma Gas Flow Rate = 5 cm^3 min^{-1}

Horizontal Scale : 1 mS/Division

OH beam focussed 4 cms below plug with no horizontal displacement (i.e. On Axis)



For the majority of nitrogen plasma ignited flames, the rate of increase in light absorption was not as steep as that corresponding to hydrogen plasmas. Also, the light absorption fell soon after the maximum value had been reached (e.g. see oscillogram B in Plate (13)) and as discussed in a later section, it appeared that the maximum value of light absorption was higher for nitrogen plasma ignited flames than for those of hydrogen plasmas.

This does not contradict the finding that higher hydroxyl concentrations were found in hydrogen plasma ignited flames than those of nitrogen or argon since firstly the light absorption values were not corrected for changes in path length and secondly the maximum values in these experiments correspond to the situation where the flame had reached the sides of the combustion vessel. However, the findings do illustrate that the flame structure is different for the two cases examined - hydrogen and nitrogen/argon.

(3) Variation with Position of OH Beam

(a) Vertical distance from plug

Fig.(51) shows the change in hydroxyl concentration with time as the flame overtook the OH diagnostic beam for 2 different distances of the beam vertically below the plasma plug. The schlieren records and OH oscillogram for one of these positions (run (1) - 5.6 cms below plug) is shown in Plate (12).

The calculated values of X_{OH}(Experimental) - X_{OH}(Calculated) for each of the 2 positions of the OH beam are shown in Fig.(52). The initial and maximum values of X_{OH}(Experimental) - X_{OH}(Calculated) shown in Fig.(52) are very slightly higher in run (2) than run (1). This would be expected since the radicals generated by the plasma would have slightly less time to recombine before measurements were taken. Finally, the gradient corresponding to run (2) is steeper than that of run (1) due to the higher values of the burning velocity of the expanding flame

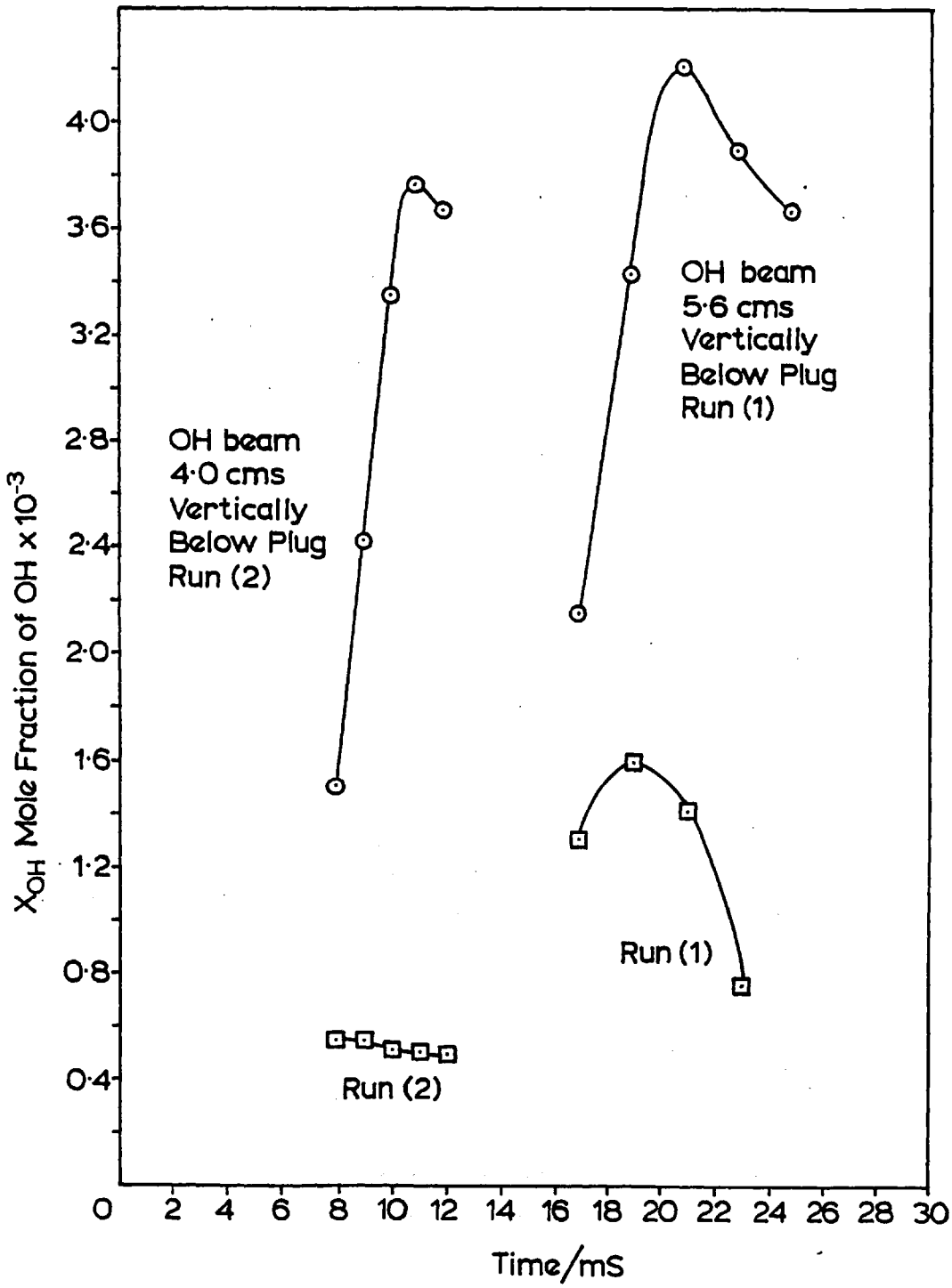


FIG. (51)

OH CONCENTRATIONS FROM RESONANCE ABSORPTION MEASUREMENTS FOR A HYDROGEN PLASMA IGNITING A METHANE-AIR MIXTURE WITH $\phi = 0{\cdot}62$

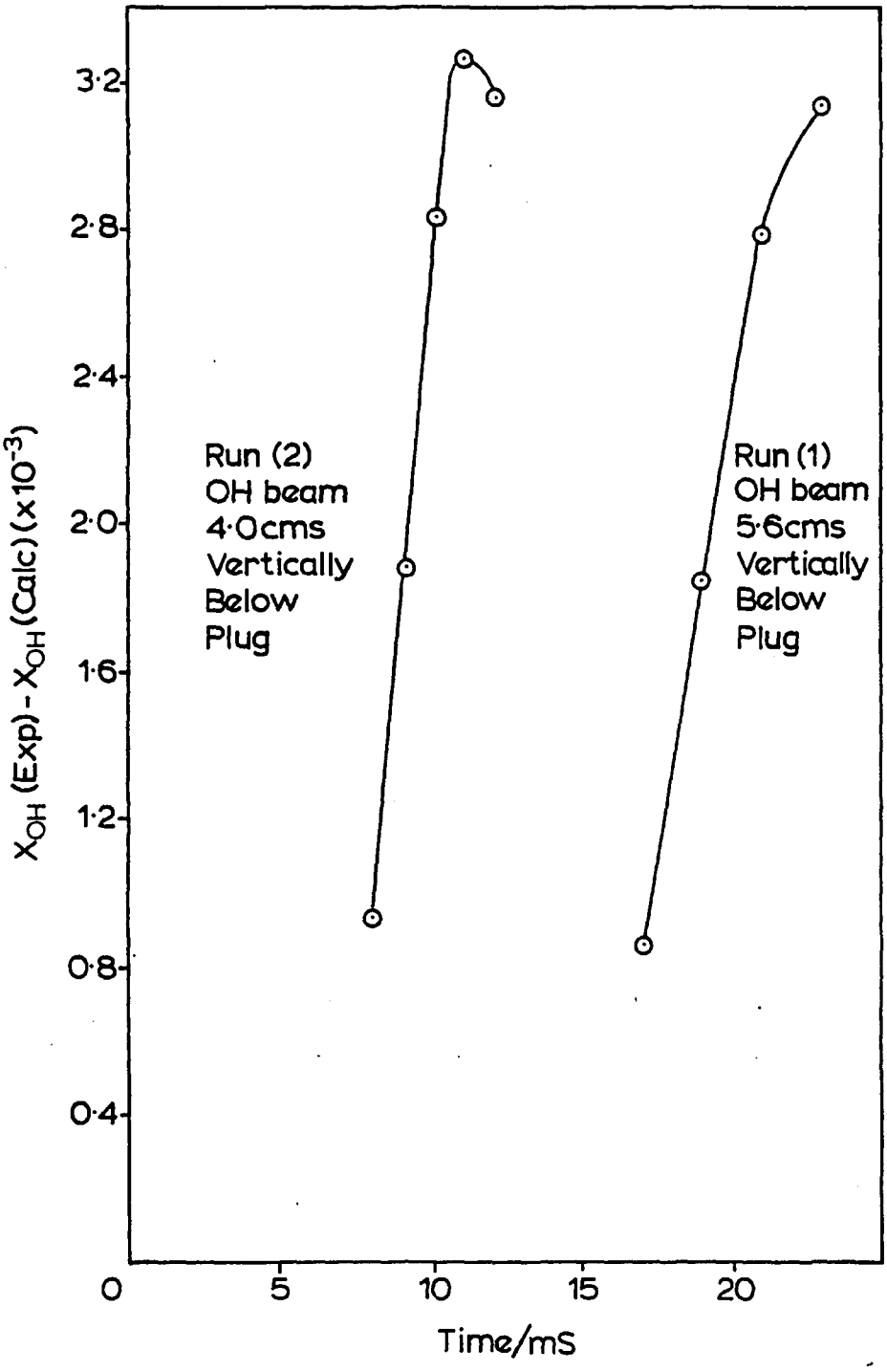


FIG. (52)

VARIATION OF $[OH]_{EXPERIMENTAL}$ - $[OH]_{CALCULATED}$ WITH POSITION FOR HYDROGEN PLASMAS IGNITING A METHANE-AIR MIXTURE WITH $\phi = 0{\cdot}62$

when the measurements were taken.

(b) Horizontal distance from plug

The results for the maximum light absorption recorded and for the time for the initial detection of hydroxyl radicals for hydrogen and nitrogen plasma ignited flames are shown in Fig.(53) and Fig.(54) respectively. These were taken for a fixed vertical distance of 4 cms below the plug whilst the x axis refers to the distance of the position of the focussed OH beam from the vertical axis below the plug. Each point in Fig.(53) and Fig.(54) was the average from 30 plasma "firings" taken over 3 separate experiments.

As shown in Fig.(53), the maximum light absorption for near axis measurements was higher for nitrogen plasma ignited flames than for those of hydrogen. Although the measurements were not corrected for path length and refer to the last stages of flame propagation, the results do indicate the different nature of the 2 types of flame. For example, due to the very long induction times and high convoluted flame areas associated with nitrogen plasmas, high rates of burning would be expected as the flame approached the walls of the vessel. On the other hand, for hydrogen plasmas, the very short induction times would lead to a steady increase in the mass burnt (i.e. similar to a normal expanding flame kernel) in which the maximum values for light absorption were generally lower than those corresponding to nitrogen plasmas.

The time for the initial detection of hydroxyl radicals is shown in Fig.(54) and this again illustrates the much longer induction times observed with nitrogen plasmas than with hydrogen plasmas. In this, the linear section of nitrogen plasma curve (between distance = 0.4 and 1.2 cms) corresponds to the situation described earlier in which, even though the plasma plume had overtaken the beam, the hydroxyl radical concentration remained zero. Lastly, for distances greater than about 2 cms, the change in gradient between that of nitrogen plasmas and that

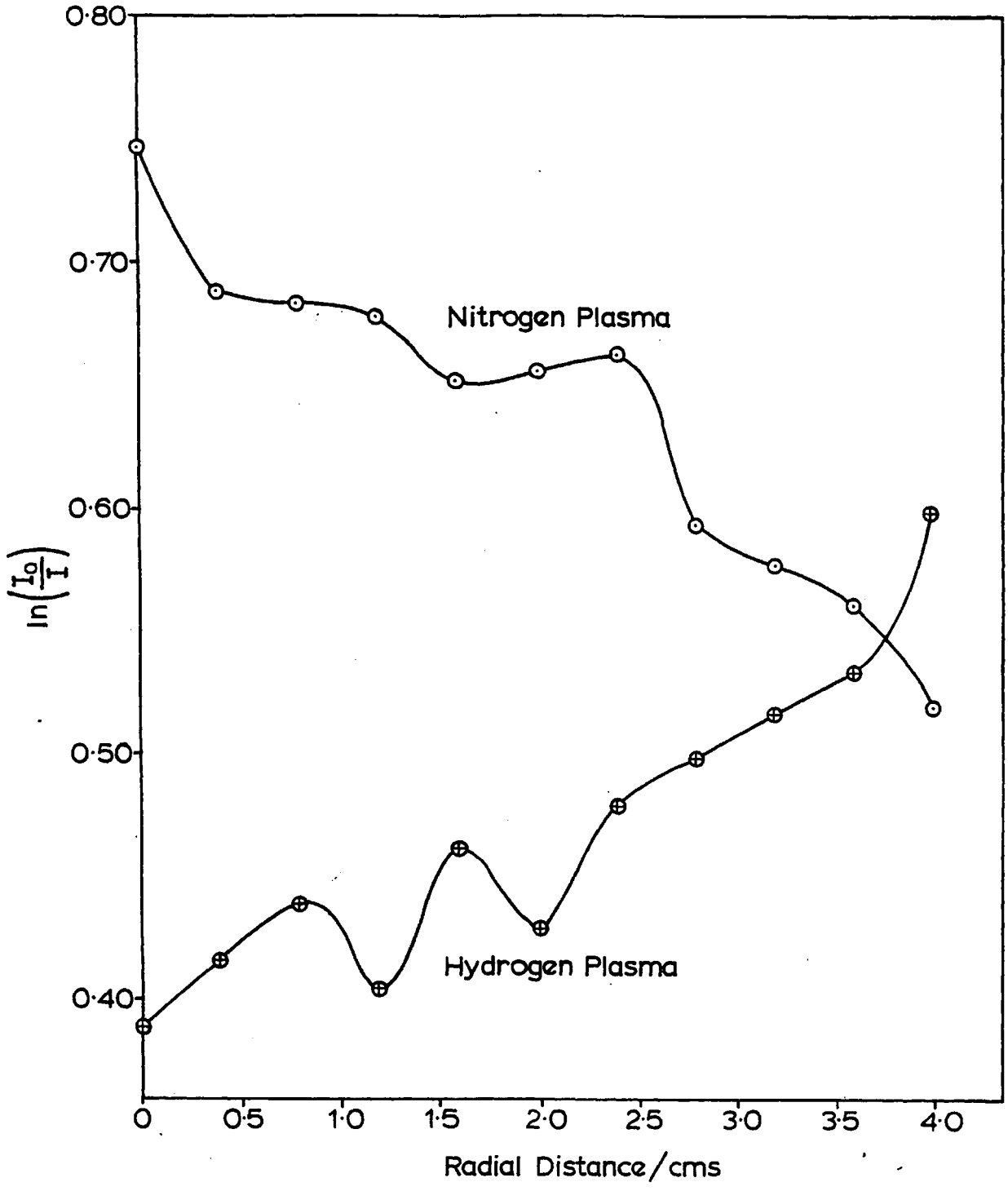


FIG. (53)

MAXIMUM OH RESONANCE ABSORPTION vs. RADIAL DISTANCE FOR HYDROGEN AND NITROGEN PLASMA JETS IGNITING A METHANE-AIR MIXTURE WITH $\phi = 0{\cdot}6$.

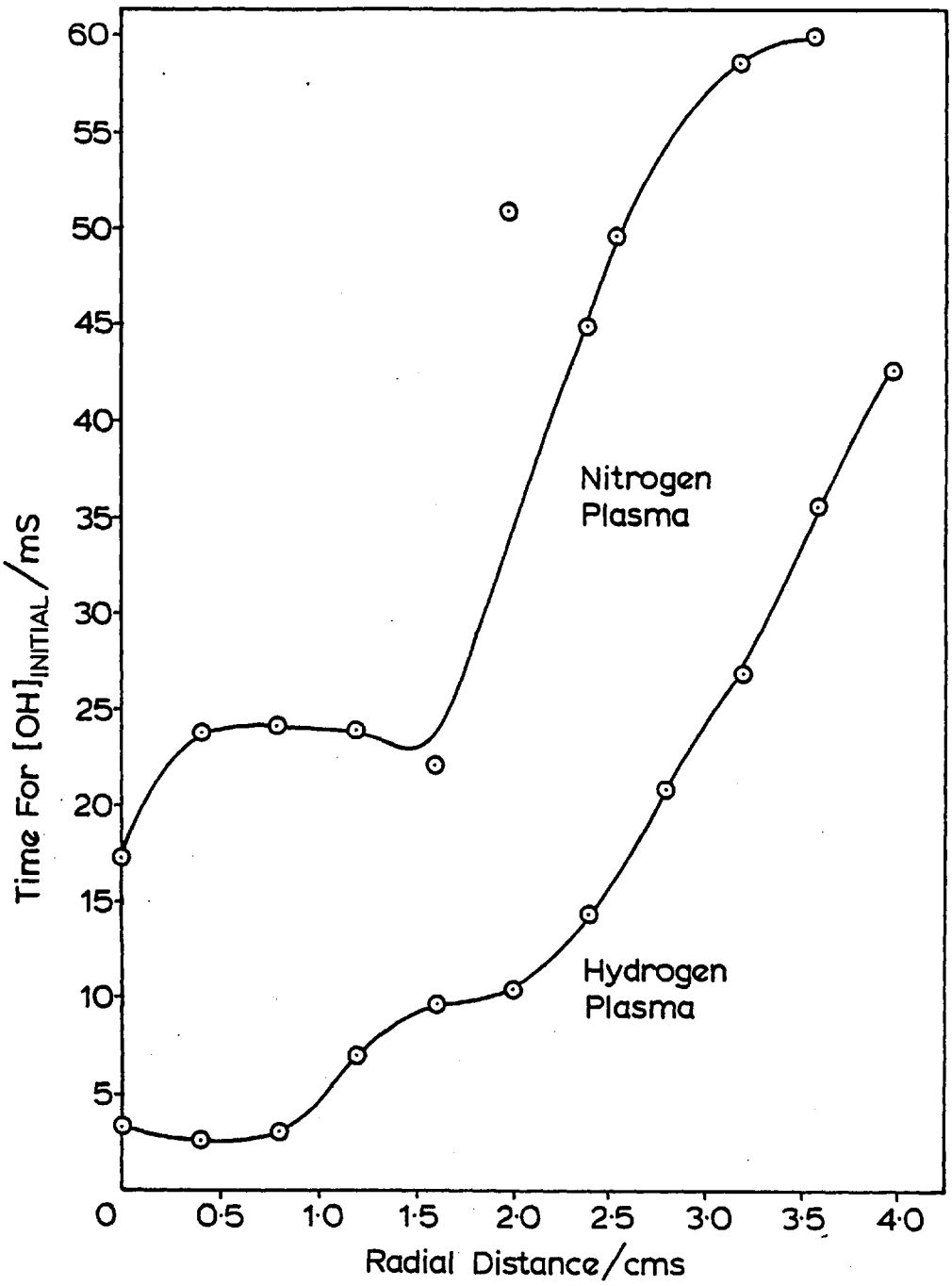


FIG. (54)

TIME FOR $[OH]_{INITIAL}$ AGAINST RADIAL DISTANCE OF OH DIAGNOSTIC BEAM.

of hydrogen plasmas illustrates the different flame propagation rates for the two cases.

(c) Hydroxyl Radical Concentrations and Plasma Source Energy Densities

The calculated plasma source energy densities and corresponding values for X_{OH}(Experimental) - X_{OH} (Calculated) for the time duration of 8 to 11 mS are shown in Fig.(55). It can be seen from Fig.(55) that even though the mean energy density (and therefore temperature) of the flame was decreasing, the observed hydroxyl concentration above that which could be expected for a normal flame was increasing. It should be noted however that the position of the beam with increasing time was moving towards the centre of the expanding flame. However, it does illustrate the higher hydroxyl concentrations above those based on calculations for a normal flame as the position of the original plume was approached.

10.3 Relationship between Hydroxyl Concentration and Flame Properties

It has been predicted (103) that flame properties such as burning velocity depend strongly on the radical concentrations, H, OH and O within the flame. Since these radicals are in quasi steady state equilibrium (91), it was possible to gain an insight into the chemical effects of plasma jet ignition by relating the measured flame properties to the hydroxyl concentrations (measured and calculated) obtained during this study.

For plasma ignited flames, it is immediately obvious that injection of radicals could have a very profound effect on burning velocity, for example, through hydrogen atom diffusion ahead of the flame. This is along the same lines as the Tanford and Pease concept in which H atom diffusion competes strongly with the transfer of heat by conduction ahead

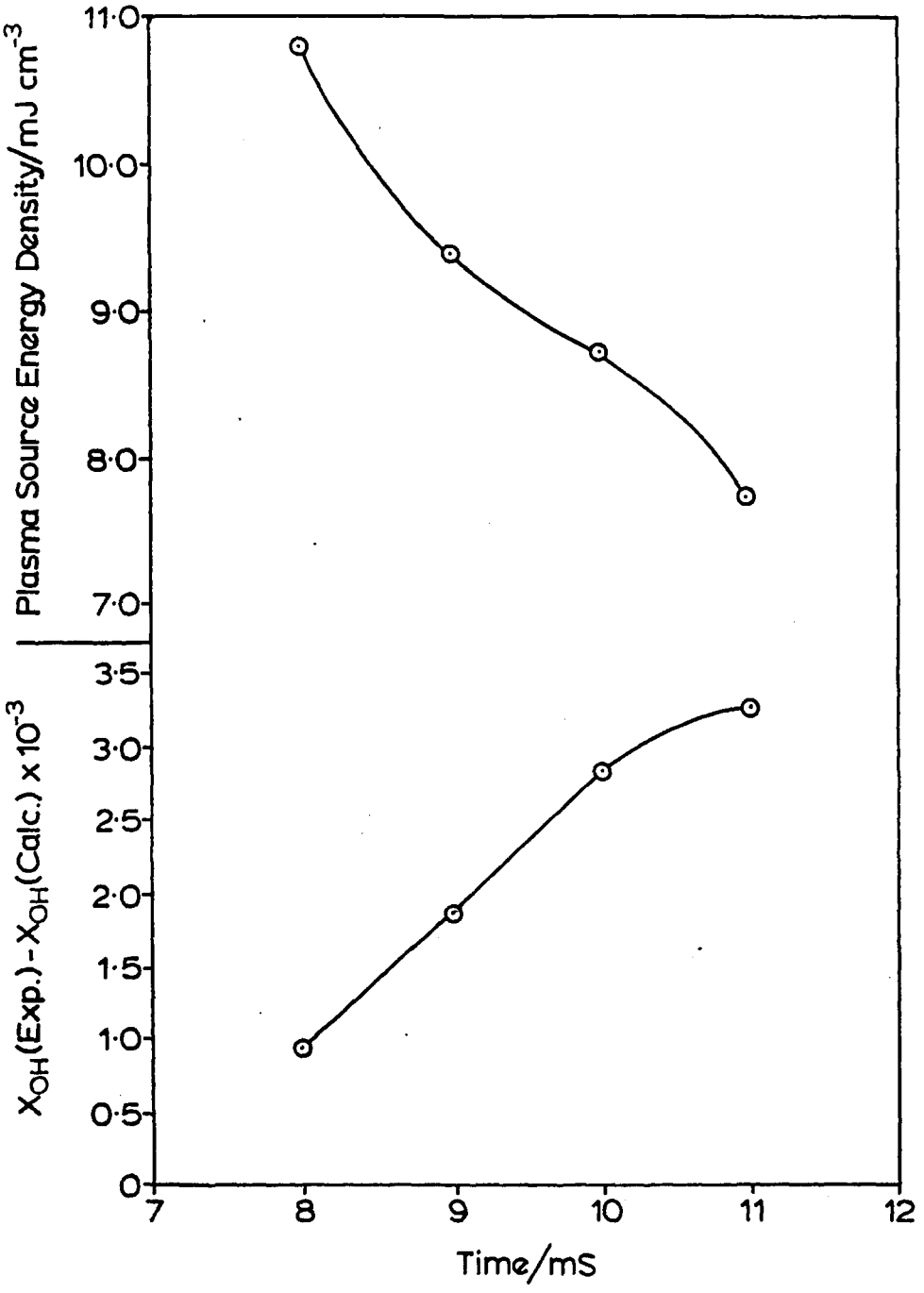
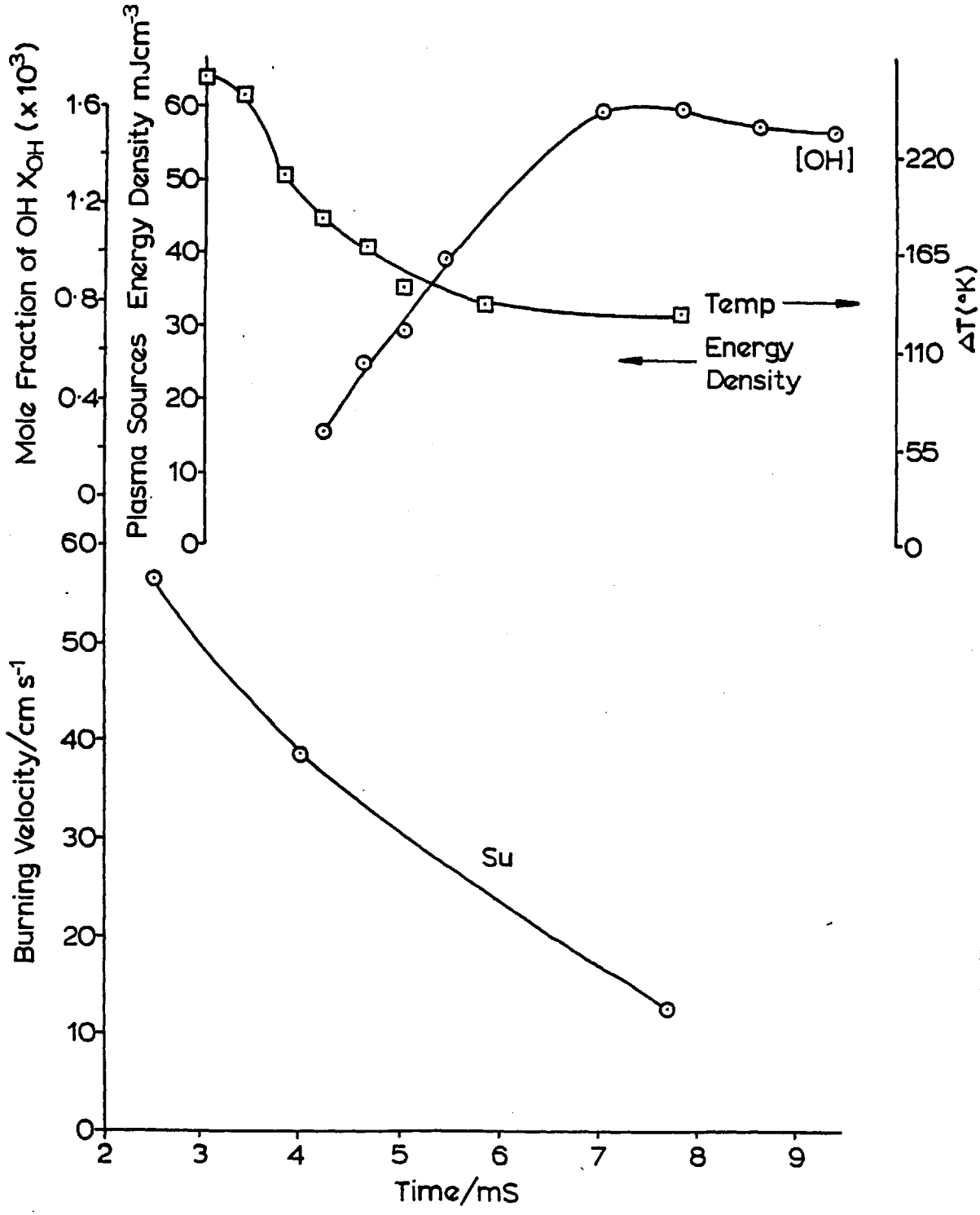


FIG. (55)

PLASMA SOURCE ENERGY DENSITIES AND X_{OH} (Experimental) - X_{OH} (Calculated) AGAINST TIME FOR A HYDROGEN PLASMA ($\int E$ = 1·2J) IGNITING A METHANE-AIR MIXTURE WITH ϕ = 0·62 (RUN 2).

FIG. (56)

BURNING VELOCITIES AND OH CONCENTRATIONS FOR A HYDROGEN PLASMA (Stored Energy = 10·8J) NEAR THE LOWER IGNITABILITY LIMIT (ϕ = 0·51).



of the flame front. Even moderately low rates of hydrogen atom diffusion from the plume into spatially adjacent unburnt gases would trigger combustion reactions in a relatively low temperature environment thereby altering the flame structure.

Hydrogen atom injection would not act only through preparing the gas ahead but could in fact also "push the flame from behind". As one example of a plausible mechanism by which this could occur involves an increase in the rate of CO oxidation downstream of the main reaction zone. Normally, in hydrocarbon flames, OH is depleted so long as any hydrocarbon remains and therefore the CO oxidation doesn't take place until after all the hydrocarbon molecules are consumed. Injection of hydrogen atoms would provide a source of OH in the tail of the flame thereby moving the zone of heat release due to CO oxidation forward. This would increase the temperature and rate of heat transfer at the interface with the hydrocarbon stage and effectively push the main reaction zone of the flame from behind.

Computer Studies on the Effects of H Atom Injection from the Plasma

Rather than do approximate calculations to test the hypotheses referred to above, it was decided to persuade Dr. C.K. Westbrook of Lawrence Livermore Laboratory to use computer studies involving a time-marching iterative procedure with 86 elementary reactions among 26 species to simulate plasma injection.

For a normal methane-air flame with $\phi = 0.5$, the computations gave a value for $S_u = 5$ cm s^{-1} with the species concentrations shown in Fig.(57). The injection of H atoms from the plasma was then simulated by, at some point in the computation, increasing the mole fractions of H and H_2 in the burnt gases at the peak of the chemical heat release rate (marked P in Fig.(57)) from the values of H:10^{-7}, H_2 : 10^{-6},

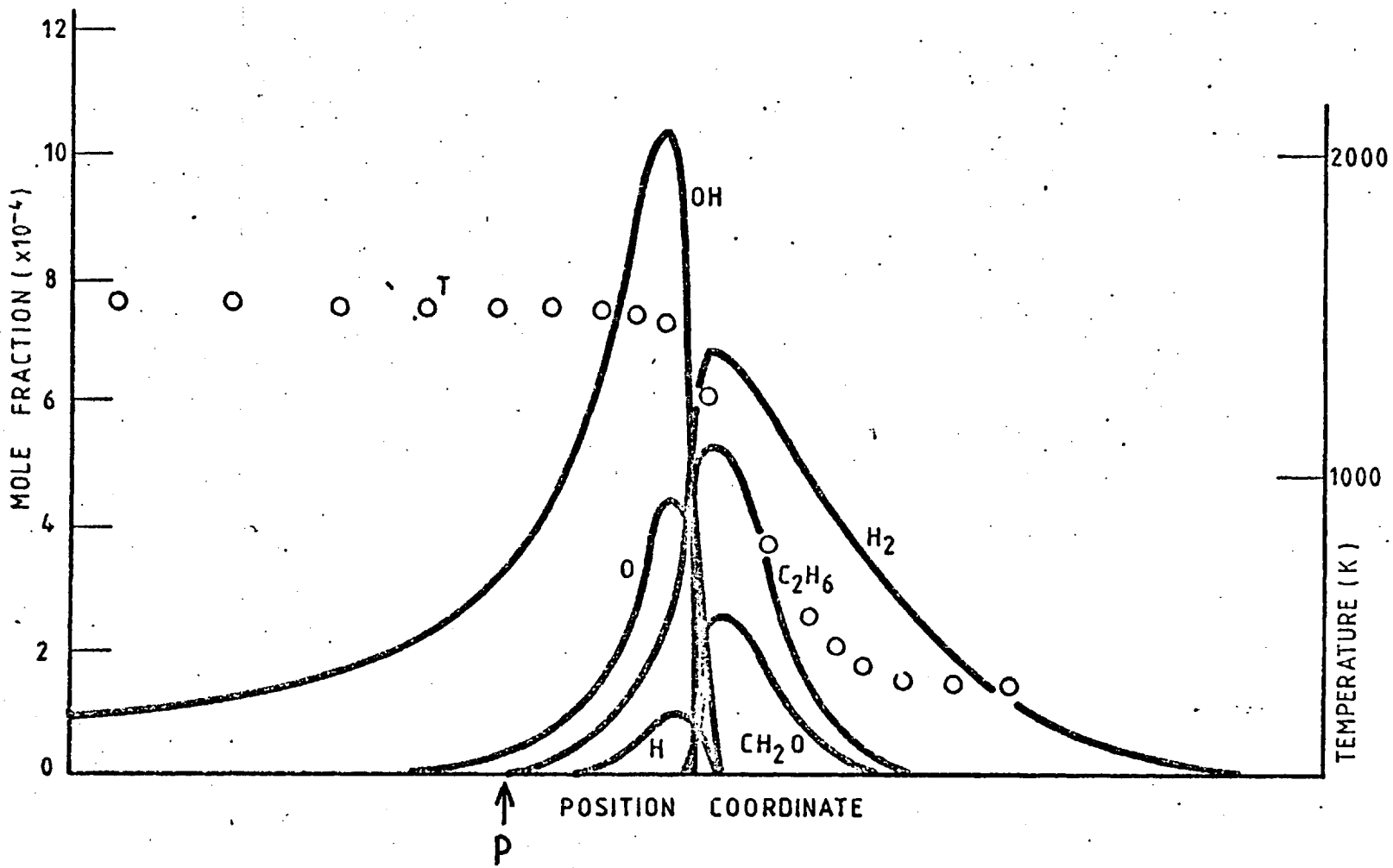

12
10
8
6
4
2
0
MOLE FRACTION (x10⁻⁴)
OH
T
O
H
H₂
C₂H₆
CH₂O
2000
1000
TEMPERATURE (K)
POSITION COORDINATE
P

FIG. (57)

O : 10^{-6}, O_2 : 10^{-1} to the values of H : 10^{-4}, H_2 : 10^{-1}, O : 10^{-6}, O_2 : 10^{-6}. The computer runs was then allowed to continue. Following a transient phase during which the flame readjusted to the suddenly modified species distribution, the flame settled down to a new steady propagation rate of about 10 $\pm$ 2 cm s^{-1}, approximately twice the original value.

The modified species distribution and temperature profile of the flame shown in Fig.(58) was taken at a time of 22 ms after the perturbation. During this time the flame had travelled a distance of 1.4 cms or more relevant, a distance of 1 cm in 20 ms after the initial transient phase which lasted 2 ms. This corresponded to a value of S_u = 10 cm s^{-1} over the 20 ms time period which is a surprisingly high value persisting over a long time period. This is similar to the behaviour of hydrogen plasma ignited flames which has been described in Chapter 9.

Also it is interesting to attempt to relate the hydroxyl concentration profile of the modified computed flames to the mean values obtained experimentally at ϕ = 0.62. For this equivalence ratio, the flame thickness would be smaller and the 2 separate maxima for OH in Fig.(58) would not be so well resolved. For this reason, the two peaks inthe OH profile would not be easily identified from the experimental [OH] values as the beam moved downstream of the position corresponding to the main reaction zone of a normal flame. However due to the change in flame structure, the mean hydroxyl value would continue to rise as the flame overtook the OH absorption beam which was shown to occur experimentally.

In these computational studies, the only approximation or uncertainty was the arbitrarily postulated high concentration of H and H_2 which was added to the flame. The amount of H_2 was approximately 5 x 10^{-6} moles cm^{-2} corresponding to a mole fraction in the burned gas of about 0.1

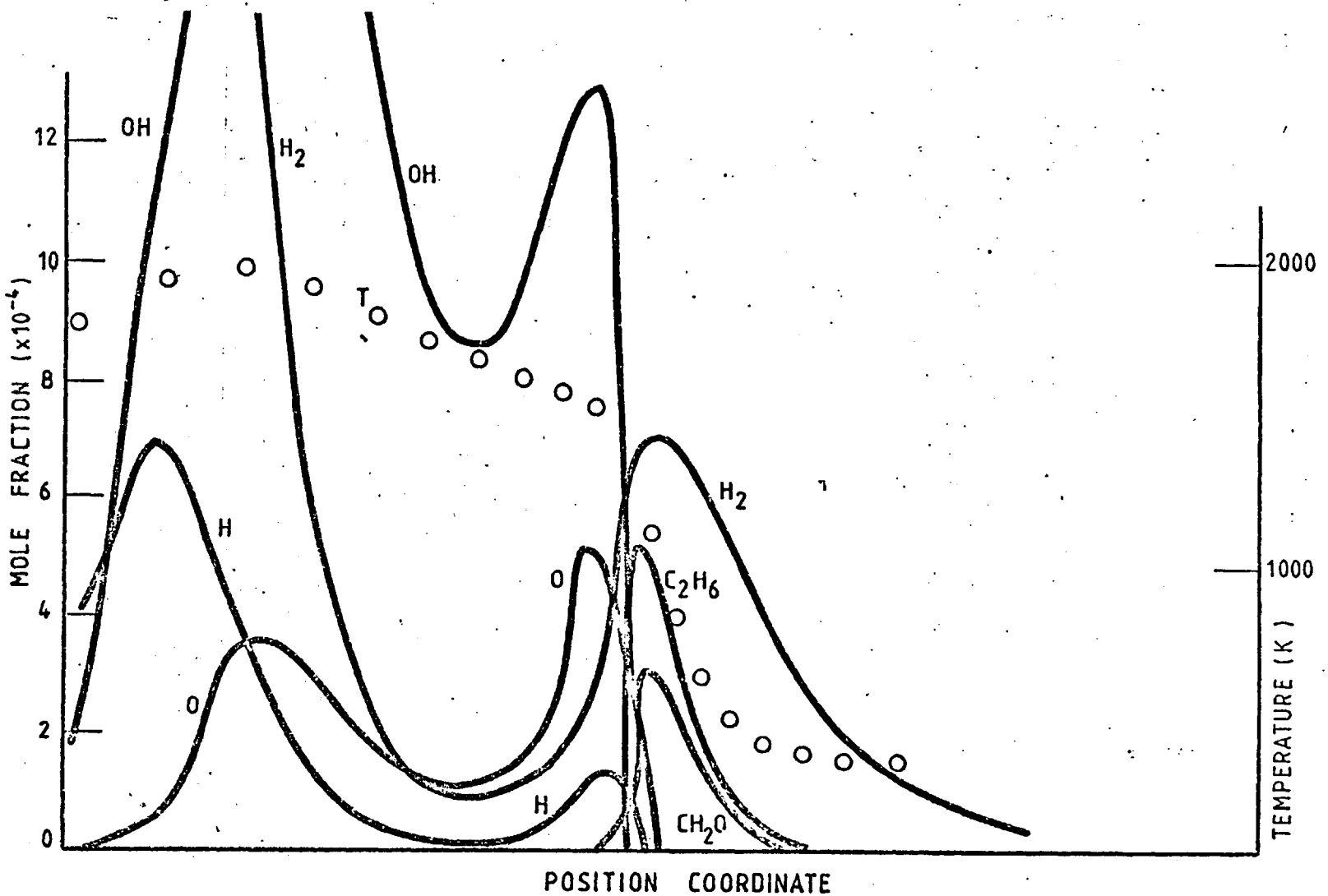

OH
H2
OH
T
H
O
H2
C2H6
O
H
CH2O
12
10
8
6
4
2
0
MOLE FRACTION (x10⁻⁴)
2000
1000
TEMPERATURE (K)
POSITION COORDINATE

FIG.(58)

and during the 25 mS only about 25% of this had been burnt. In spite of this, the general trends described are very similar to those observed experimentally throughout the present research.

CHAPTER 11

CONCLUSIONS AND SUGGESTIONS FOR FUTURE WORK

A plasma plug has been used in the present work to study ignition and the enhancement of flame propagation rates in lean methane-air mixtures. The most important contributory mechanisms were found to be those due to the chemical effects following the injection of radicals from the plasma and those associated with the fluid dynamic properties of the jet. Either of these effects could be fostered by the design of the plasma jet, and the choice of the plasma medium.

The results have indicated major contributions from both chemical and fluid mechanic effects and that the mechanisms are in fact complementary. The relative importance of each depended on the chemical reactivity of the plasma.

For non reactive plasmas, it was concluded that the fluid dynamics due to the turbulence, momentum and enthalpy of the jet dominated. This was based on the following observations:

(1) The lower limits of ignitability were found to be a function of the plasma energy and in all cases were higher than those of chemically reactive plasmas.

(2) The delay times for the development of the flame front were considerably longer for non reactive plasmas than for reactive plasmas. This could be inferred from the schlieren records, the C_2 measurements and the OH absorption measurements.

(3) Increased values for burning velocities compared with spark ignited flames in the same mixture were measured. These were a consequence of the very large, convoluted boundary which was generated between the plasma plume and the unburnt gases. This led to high burning rates

corresponding to high turbulent burning velocities even though, unlike for the case of chemically reactive plasmas, the laminar burning velocity did not change appreciably. This can be seen from the schlieren records for nitrogen and argon plasmas which show the high levels of turbulence persisting throughout the flame's travel to the walls.

(4) The measured hydroxyl concentration profiles through nitrogen and argon plasmas were found to be different from those of standard (e.g. spark ignited) spherical flames. The difference was not as large as those originating from chemically reactive plasmas and was thought to be due to the plasma enthalpy producing higher equilibrium radical concentrations. An analysis based on the variation of plasma source energy densities with time was attempted to examine this contribution.

For chemically reactive plasmas such as hydrogen, the chemical effects on ignition and flame propagation dominated the fluid dynamics. This became evident from the following observations:

(1) The lower limit of ignitability was found to be independent of plasma energy over the range studied. Very lean mixtures (ϕ = 0.488) could be ignited using relatively low stored plasma energies (3.25 J) unlike the case of non reactive plasmas.

(2) Extremely short delay times for the development of the flame front were observed compared with the much longer delay times for non reactive plasmas. This was due to the high radical concentrations existing within the plume enabling the formation of a flame front in spite of the high jet velocities and high rates of heat loss from the flame associated with its small volume and low radius of curvature.

(3) Very high laminar burning velocities were measured during the initial stages of flame growth. These rapidly smoothed out the convolutions due to the turbulence of the jet which gave the flame a lower effective flame area in contact with the unburnt gas as seen in the

schlieren records. Although, the high laminar burning velocities persisted for most of the duration of the flame's travel to the vessel walls, the overall flame propagation rate during the later stages became comparable to that of the non reactive plasmas (especially nitrogen). This was due to the loss of the turbulent flame corrugations which gave high turbulent burning velocities for non reactive plasmas even though laminar burning velocities were low in these mixtures (ca 10 cm s^{-1}).

(4) The difference between the measured hydroxyl concentrations of flames ignited by reactive plasmas and those of standard (e.g. spark ignited) flames were larger than the difference corresponding to non reactive plasmas. This originates from the high radical concentrations generated by the plasma which gave the extended ignitability limits, enhanced laminar burning velocities and short delay times described above. As in the case of the non reactive plasmas, part of the difference could be accounted for by the higher equilibrium radical concentations as a direct consequence of the plasma plume enthalpy. This contribution is however small compared to the hydroxyl concentration resulting from the injection of radicals from the plasma.

In comparing the numerical values which were obtained for the properties of plasma ignited flames with those found in the literature, the following values are reported :

(1) Ignitability Limits

	Reference	ϕ min
(a)	Teichman (15) Plasma Jet Ignition (Energy = 2.5 J, orifice diameter = 2.4 mm, plasma medium : methane/air).	Methane-air mixture of ϕ = 0.5 ignited.

	Reference	ϕ min
(b)	This Work;	
	(Orifice diameter = 2.4 mm, plasma gas flow rate = 5 $cm^3 min^{-1}$)	
	Hydrogen (Energy 10.8 J - 3.25 J) :	ϕ min = 0.494
	Nitrogen (Energy 10.8 J) :	ϕ min = 0.523
	Argon (Energy 10.8 J) :	ϕ min = 0.585

(2) Delay Time to Combustion

(a)	Cetegen et al. (117) Plasma Jet Ignition Energy = 2.5 J Characteristic length of cavity, L^+ = 0.765, 1.042 and 1.675. ϕ = 0.6. Plasma medium : methane/air.	Time delay between discharge and moment when the amount of burned gas became sufficiently large to cause a definite response of the pressure transducer = 3 to 4 mS.

(b) This Work :

	Delay Time
(Orifice diameter = 2.4 mm) = 0.62.	
Argon Plasma (Energy = 8.6 J) :	Approx. 12 mS.
Nitrogen Plasma (Energy = 4.8 J) :	Approx. 10 mS.
Hydrogen Plasma (Energy = 4.8 J) :	$\leqslant$ 0.4 mS.

(3) Burning Velocities

	Reference	Burning Velocity
(a)	Waterson (113) See Fig.(41) Plasma Energy Approx. 1 J ϕ = 0.8. Plasma medium: methane/air.	Laminar (Su) Turbulent (S_T) Approx. 2 m/s.
(b)	Teichman (58)	
	(Orifice diameter = 2.4 mm) ϕ = 0.6.	
	Methane	Su_{max} = 34.7 cm s^{-1}
	Methane/air	Su_{max} = 33.4 cm s^{-1}
	Nitrogen seed	Su_{max} = 33.0 cm s^{-1}

(c) Cetegen et al. (117)

Plasma Energy = 2.5 J $S_T \simeq 100$ cm s^{-1}

$\phi = 0.6$.

Characteristic length of cavity, $Su \simeq 25$ cm s^{-1}

$L^+ = 1.675$.

Plasma medium : methane/air.

(d) This Work

(Orifice diameter = 2.4 mm)

Plasma medium :

Hydrogen (E = 10.8 J, $\phi = 0.50$) : $Su_{max} \simeq 57$ cm s^{-1}

Hydrogen (E = 4.8 J, $\phi = 0.62$) : $Su_{max} \simeq 38$ cm s^{-1}

Nitrogen (E = 4.8 J, $\phi = 0.62$) : $S_{T_{max}} \simeq 26$ cm s^{-1}

$Su_{max} \simeq 22$ cm s^{-1}

Argon (E = 8.6 J, $\phi = 0.62$) : $S_{T_{max}} \simeq 19$ cm s^{-1}

$Su_{max} \simeq 18$ cm s^{-1}

(4) [OH] decay rates during pre-ignition period by nitrogen plasma

Value of decay constant k_{OH}

(a) Catolica, R.J. Reference (104).

$k_{OH} \simeq 0.8 \times 10^{-32}$ cm^6 $molecules^{-2}$ s^{-1}

(b) This Work

$k_{OH} = 2.95 \times 10^{-32}$ cm^6 $molecules^{-2}$ s^{-1}

The following conclusions on the effect of additional radicals on ignition and flame propagation can be drawn from the results presented in this thesis. With reference to the characteristics of flames ignited by chemically reactive plasmas such as hydrogen, much higher hydroxyl concentrations were measured than for non reactive plasma ignited flames.

These persisted throughout the entire flame profile and indicated that the concentrations of other atoms and radicals in equilibrium with the hydroxyl radical would consequently be higher. These flames with artificially high radical concentrations were also observed to have a correspondingly extended lower limit of ignitability and higher burning velocities than those with lower overall radical concentrations. Also, as described above, ignition was facilitated and occurred after much shorter delay times than when initiated by non reactive plasmas.

In broad outline, the results described agree well with the detailed computational analysis by Dr. Westbrook on simulated plasma jet ignition. Further computations to eliminate the uncertainty in the analysis of excluding all the oxygen would clearly be a starting point for any future work done on this subject. This could be followed by the construction (from experimental data) of complete temperature and reactive species concentration profiles which could be compared to those of the computational analysis. This would then provide a further insight into the observed chemical effects by reactive plasmas. For example, by using the existing experimental set-up, it should be possible to obtain several different hydroxyl concentration profiles as a function of the vertical distance from the position of the OH diagnostic beam to the plasma plug orifice. In this way, measurements could be taken at the shortest limiting distance between the plug and the beam which were unaffected by interference caused by light emission from the plasma. This would enable OH measurements to be taken during the initial stages for a hydrogen plasma corresponding to the highest values for the burning velocity. Although it might be too difficult to make OH resonance absorption measurements on a hydrogen plasma before and during the transition to the 2nd stage ignition (because the time duration is extremely short) it should be possible to record the change in hydroxyl concentration with time (and position) of the flame at a fixed position

relative to the flame front. This would be an extremely important result since it would be possible to examine the change in hydroxyl concentration with the changing magnitude of the burning velocity (i.e. with time or position) at fixed positions relative to the flame front. This would require a large number of plasma firings to eliminate statistical variations in the size and shape (at any given time) of the ejected plasma.

To enable more accurate calibrations to be made for the OH resonance absorption technique, measurements could be taken on spark ignited spherically expanding laminar flame kernels similar to those taken for the C_2 emission calibrations. These calibrations could be taken immediately prior to those for plasma ignited flames without an interruption of the methane-air flow to the combustion vessel thereby minimizing inaccuracies due to changes in equivalence ratio.

The next major step would be to record temperatures simultaneously with the hydroxyl concentration measurements for plasma ignited flames. This could be done in theory with the present apparatus by using the absorption measurements of at least two OH rotational lines although a very large number of plasma firings would be required to achieve the required accuracy. More suitable would be to construct temperature probes such as the ionization or hot wire anemometry methods. The measured temperatures together with the hydroxyl concentration measurements could be related to the instantaneous values of burning velocity at any fixed time for the plasma ignited flames.

The recorded temperature values which should be slightly higher than the normal flame temperatures could thus be correlated with the plasma source energy densities calculated from the initial plasma energies and from measurements taken from the schlieren records. In the present research, only approximate values for the initial plasma energies (calculated as 25% of the stored energy of the capacitors) were used for calculating

the plasma source energy densities. This would be improved with the use of high voltage and high current probes to measure the total energy dissipated within the arc.

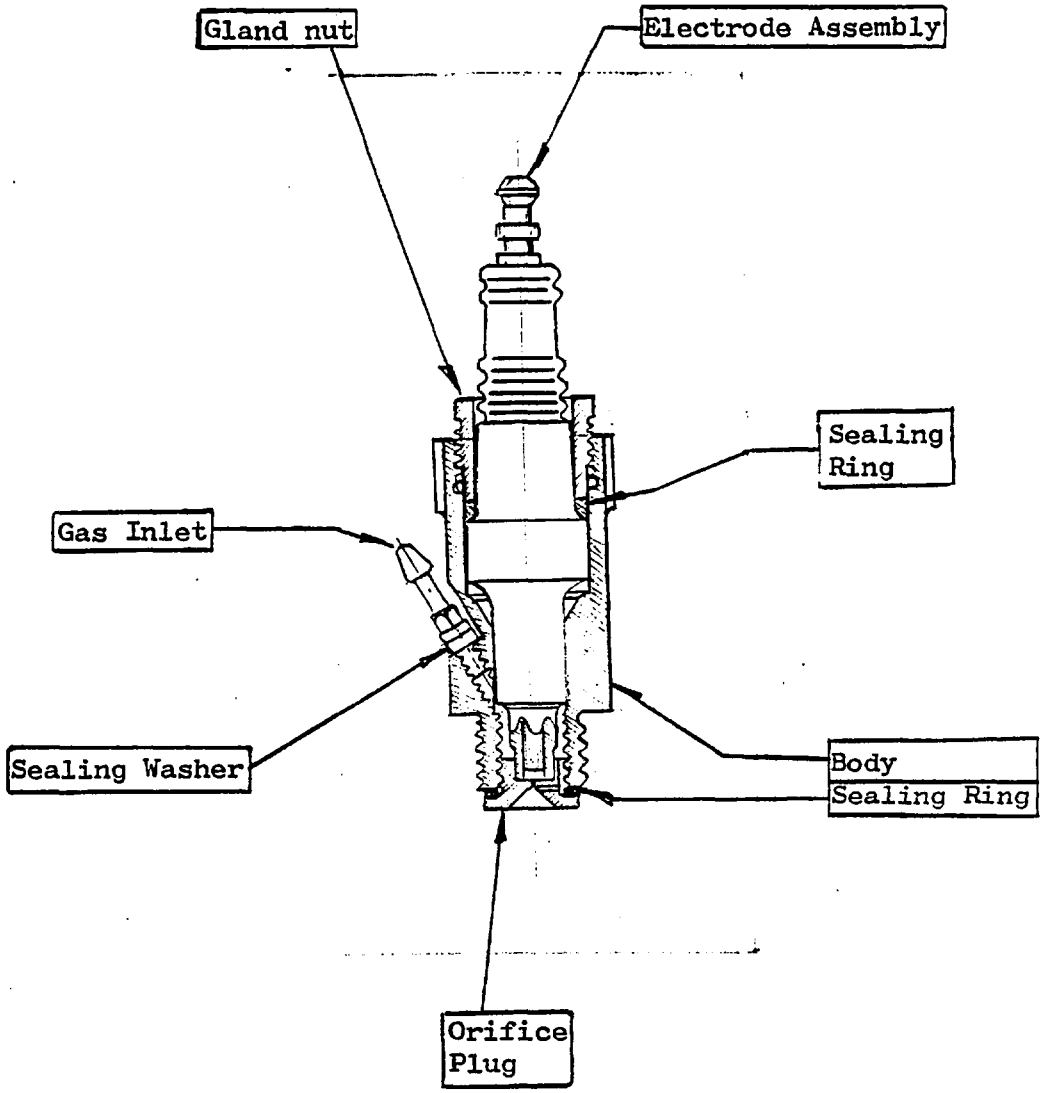
Two further variations could be made which although being of little practical value, would provide basic information on the kinetics of ingition and flame propagation reactions. The first would be to use oxygen as a feed gas to the plasma plug for the examination of the role of oxygen atoms in the initiation of hydrocarbon combustion reactions. Due to the severe electrode erosion in the presence of oxygen, only a few plasma firings would be possible. The second variation would be to use a lean hydrogen-air mixture in place of the lean methane-air mixtures used in the present experiments. This would provide a system which would enable quantitative measurements to be made on the chemical mechanisms of plasma jet ignition.

All of the suggestions for future work described above would open the way to further improvements in the understanding of the chemical and fluid dynamic mechanisms of plasma jet ignition. By alteration of the plasma feed gas, the relative importance of the contributions of each to ignition and enhanced rates of flame propagation can be controlled and studied separately.

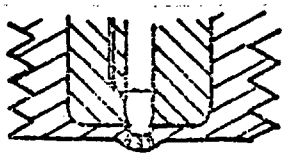
Finally, future work would be required for the achievement of the practical objectives outlined in the introductory chapters. The intermittent plasma jet spark plug described throughout this thesis would be most suitable for the ignition and enhancement of flame propagation rates of leaner mixtures in internal combustion engines. For these reasons, work is currently being undertaken on the design and development of plasma jet igniters for practical applications. Fig.(59) shows the designs of some of the plugs under investigation. The pepper pot (B) and simple nozzle configurations were aimed at modifying the fluid dynamics of the jet whilst not being adapted for use at high pressure in an engine.

FIG. (59)

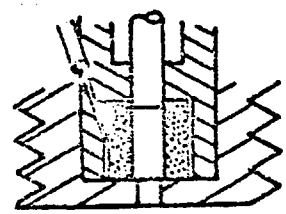
(A) HIGH PRESSURE "FUNNEL" DESIGN



(B) "PEPPER POT" DESIGN



(C) "CAPILLARY LIQUID FEED" DESIGN



This is because the effect of the advancing piston would be to compress the gas within the cavity thereby diluting the intended plasma medium. This problem was overcome in the funnel design (Fig.(59A)) and capillary liquid feed (Fig.(59C)) by two separate means. In the funnel design, an external resevoir is provided which is filled with the plasma gas together with the cavity sometime before the end of the compression stroke. During compression, gas is transferred from the resevoir to the cavity thus preventing dilution of the cavity gas by the cylinder gases.

In the capillary liquid feed plug (Fig.(59C)), use is made of the incompressibility of a liquid feedstock. A liquid hydrocarbon (e.g. petrol) continuously wets a porous sleeve (e.g. a ceramic) surrounding the discharge channel and is vapourised in the required amounts by the arc itself. This type of plug is particularly suitable because of the very small amounts of liquid hydrocarbon required and the availability of the feedstock. Ultimately, it is with this type of plug that it is hoped to achieve the practical objectives of increasing the thermodynamic efficiency and lowering pollutant emissions of internal combustion engines since it is towards this goal that the present research was directed.

REFERENCES

(1) Lewis and von Elbe. "Combustion, Flames and Explosions of Gases", Academic Press, New York, 1967.

(2) Spiers, H.M. "Technical Data on Fuel", Sixth Edition, 1962.

(3) Steiner, J.C. and Mirsky, W. S.A.E. 660346.

(4) Morgan, J.D. "Principles of Ignition", Sir Isaac Pitman and Sons, Ltd., London, 1942.

(5) Kono, M, Kumagai, S. and Sakai, T. Combustion and Flame 27, 85-98 (1976).

(6) Maly, R. and Vogel, M. 17th International Symposium on Combustion, 1978.

(7) Gussak, L.A. S.A.E. 750890.

(8) Creighton, J.R. S.A.E. 790249.

(9) Westbrook, C.K. S.A.E. 790248.

(10) Westbrook, C.K. Acta.Astronautica, Vol.5, pp.1185-1198, 1978.

(11) Harrison, A.J. and Weinberg, F.J. Proc.Roy.Soc. London A.321, 95-103 (1971).

(12) Hilliard, J.C. and Weinberg, F.J. Nature, Vol.259, No.5544, pp.556-557 (1976).

(13) Khoshnoodi, M. Ph.D. Thesis, University of London, 1978.

(14) Jones, A.R., Lloyd, S.A. and Weinberg, F.J. Proc.Roy.Soc.London. A360, 97-115 (1978).

(15) Teichman, K.Y. Ph.D. Thesis, University of California, Berkeley, 1978.

(16) Dixon-Lewis, G. and Shepherd, I.G. 15th Symposium (International) on Combustion, p.1483 (1975).

(17) Dixon-Lewis, G. Combustion and Flame, 33, 319-321 (1978).

(18) Gaydon, A.G. "Dissociation Energies and Spectra of Diatomic Molecules", Chapman and Hall, London. Third Edition, 1968.

References (Continued)

(19) Gaydon, A.G. and Hurle, I.R. "The Shock Tube in High Temperature Chemical Physics", Reinhold, New York, 1963.

(20) Schott, G.L. and Kinsey, J.L. J.Chem.Phys. 29, 1177 (1958).

(21) Miyama, H. and Takeyama, J. J.Chem.Phys. 41, 2287 (1965).

(22) Meyer, J.W. and Oppenheim, A.K. 13th International Symposium on Combustion, p.1153, 1971.

(23) Brokaw, R.S. 10th International Symposium on Combustion, p.269, 1965.

(24) Hendrie, J.M. J.Chem.Physics, Vol.22, No.9 (1954).

(25) Langmuir, I. J.Am.Chem.Soc. 37, 417 (1915).

(26) Brennan, D. and Fletcher, P.C. Proc.Roy.Soc. A250 (1959), p.389.

(27) Hickmott, T.W. J.Chem.Phys. Vol.32, No.3 (1959).

(28) Doty, P.M. J.Chem.Phys. Vol.11, No.12 (1943).

(29) Lockwood, G.J., Helbig, H.F. and Everhart, E. J.Chem.Phys. Vol.14, No.12 (1964).

(30) Tollefson, E.L. and Le Roy, D.J. J.Chem.Phys. Vol.16, No.11 (1948).

(31) Bennett, J.E. and Blackmore, D.R. 13th International Combustion Symposium, (1971).

(32) Norrish, R.G.W. Plenary Lecture Tenth Symposium (International) on Combustion, pp.1-18, (1965).

(33) Kinbara, T. and Noda, K. Fourteenth Symposium (International) on Combustion, pp.321-327, (1973).

(34) Kinbara, T. and Noda, K. Fifteenth Symposium (International) on Combustion, pp.993-1001, (1974).

(35) Morley, C. and Smith, I.W.M. J.Chem.Soc. Faraday Transactions, 5, 1016-1030 (1972).

(36) Wolfrum, J. Chapter 9, Atom Reactions in Physical Chemistry, An Advanced Treatise, Volume VIB, Academic Press, New York.

References (Contd.)

(37) Hertzberg, G. Molecular Spectra and Molecular Structure. I. Spectra of Diatomic Molecules. 2nd Edition, 1950. Van Nostrand Reinhold Company.

(38) Cerkanowicz, A.E. and McAlevy, R.F. III, Photochemical Ignition and Combustion Enhancement. In High Speecd Flows of Fuel Air Mixtures, 11th Aerospace Sciences Meeting, AIAA, paper No.73-216, January 1973.

(39) Orrin, J.E., Vince, I.M. and Weinberg, F.J. Ignition by Radiation from Plasmas. Brief Communication, Combustion and Flame (Forthcoming Issue) (1979).

(40) Weinberg, F.J., Hom, K., Oppenheim, A.K. and Teichman, K. Nature, 272, p.341 (1978).

(41) Meek, J.M. and Craggs, J.D. Electrical Breakdown of Gases (1977). John Wiley and Sons, New York.

(42) Somerville, J.M. The Electric Arc (1959). Methuen and Co.Ltd. London.

(43) Phelps, A.V. Advan.Chem.Ser. 80, 18-28 (1969).

(44) Steacie, E.W.R. Atomic and Free Radical Reactions. 1954. Reinhold Publishing Corporation, New York.

(45) Shaw, T.M. in Formation and Trapping of Free Radicals by Bass, A.M. and Broida, H.P. 1960. Academic Press, New York.

(46) Gaydon, A.G. The Spectroscopy of Flames, Second Edition; 1974. Chapman and Hall, London.

(47) Kimura, I. and Imajo, M. Sixteenth Symposium (International) on Combustion, pp.809-815, (1976).

(48) Chen, D.C.C., Lawton, J. and Weinberg, F.J. Tenth Symposium (International) on Combustion, pp.743-754 (1965).

(49) Fells, I., Gawen, J.C. and Harker, J.H. Combustion and Flame, 11, 309-319, (1967).

References (Contd)

(50) Lawton, J. and Weinberg, F.J. Electrical Aspects of Combustion, Clarendon Press, Oxford, 1969.

(51) Harrison, A.J. and Weinberg, F.J. Proc.Roy.Soc.Lond. A321, 95-103, (1971).

(52) Vidaud, P.H., Wayne, R.P., Yaron, M. and von Engel, A. J.Chem.Soc. Faraday Transactions II, Vol.72, pp.1185-1193, (1976).

(53) Asik, J.R., Piatkowski, P., Foucher, M.J. and Rado, W.G. Paper 770355, presented at S.A.E. Annual Meeting, Michigan, 1977.

(54) Wyczalek, F.A., Frank, D.L. and Neuman, J.G. Paper 750349, presented at S.A.E. Automotive Engineering Congress and Exposition, Michigan, 1975.

(55) Topham, D.R., Smy, P.R. and Clements, R.M. Combustion and Flame, 25, 187-195 (1975).

(56) Dale, J.D., Smy, P.R. and Clements, R.M. Combustion and Flame, 31, 173-185 (1978).

(57) Oppenheim, A.K., Teichman, K., Hom, K. and Stewart, H.E. S.A.E. paper 780637 (1978).

(58) Teichman, K.V. Ph.D. Thesis, "Study of Jet Ignition for Lean Mixtures", University of California, Berkeley. (1979).

(59) Garvin, D. and Broida, H.P. Ninth Symposium (International) on Combustion, p.678 (1963).

(60) Del Greco, F.P. and Kaufman, F. Disc. Faraday Soc. 33, 128 (1962).

(61) Clyne, M.A.A. and Thrush, B.A. Trans.Faraday Soc. 57, 1305 (1961).

(62) Wightman, J.P. Proceedings of the IEEE, Vol.62, No.1 (1974).

(63) Reed, T.B. J.Appl.Physics, Volume 32, No.5 (1961) pp.821-824.

(64) McCarthy, R.L. J.Chem.Phys. Volume 22, No.3 (1954) pp.1360-1365.

(65) Currie, S.J. and Thrush, B.A. Trans.Faraday Soc., Volume 64, pp.390-395 (1968).

References (Contd)

(66) von Engel, A. Ionized Gases (1955). Clarendon Press, Oxford.

(67) Massey, H.S.W., Burhop, E.H.S. and Gilbody, H.B. Electronic and Ionic Impact Phenomena, Volume II (1969). Clarendon Press, Oxford.

(68) von Engel, A. Symposium on Electrochemical Engineering, Colume 2. Held in Newcastle-upon-Tyne, 1971. Published in 1973 by I.Chem.E. Services.

(69) Lawton, J., Payne, K.G. and Weinberg, F.J. Nature, London 193, 736 (1962).

(70) Fells, I., Gawen, J.C. and Hawker, J.H. Nature, London 210, 1149 (1966).

(71) Jaggers, H.C. and von Engel, A. Combustion and Flame, 16, 275-285 (1971).

(72) Ward, M.A.V. and Wu, T.T. Combustion and Flame, 32, 57 (1978).

(73) Bradley, D. and Ibrahim, S.M.A. Combustion and Flame, 27, 353-362 (1976).

(74) Wood, B.J. and Wise, H. J.Chem.Phys. 65, 1976-1983 (1961).

(75) Smith, W.V. J.Chem.Phys. Vol.11, pp.110-125 (1943).

(76) Kent, J.H. Combustion and Flame, 14, 279-282 (1970).

(77) Foner, S.N. APL Technical Digest,pp.2-7 (1970).

(78) Barber, M., Cuthbert, J., Farren, J. and Linnett, J.W. Proc.Roy.Soc. A274, 285-292 (1963).

(79) Jenkins, D.R. and Voisey, M.A. J.Phys.E: Scientific Instruments, Vol.6, pp.827-832 (1973).

(80) Greene, F.T., Brewer, J. and Milne, T.A. J.Chem.Phys. Vol.40, No.6 (1964).

(81) Westenberg, A.A. and Fristrom, R.M. Tenth Symposium (International) on Combustion, pp.473-487 (1965).

(82) Clyne, M.A.A. and Down, S. J.Chem.Soc. Faraday Transactions II. pp.253-266 (1974).

References (Contd)

(83) Anderson, J.G. and Kaugman, F. Chemical Physics Letters, Volume 16, No.2 (1972).

(84) Atkinson, R., Hansen, D.A. and Pitts, J.N. J.Chem.Phys. 62, (1975).

(85) Gaydon, A.G. and Wolfhard, H.G. "Flames", Third Edition, 1970.

(86) Pungor, E. Flame Photometry Theory. Von Nostrand Company Ltd. London (1967).

(87) Fenimore, C.P. and Jones, G.W. J.Phys.Chem. 65, 2200-2203 (1961).

(88) Fenimore, C.P. and Jones, G.W. J.Phys.Chem. 63, 1834-1838 (1959).

(89) Kaskan, W.E. Combustion and Flame, 2, 229-243 (1958).

(90) Kaskan, W.E. Combustion and Flame, 2, 286-304 (1958).

(91) Creighton, J.R. J.Phys.Chem. 81, 2520-2526 (1977).

(92) Harvey, R. and Jessen, P.F. Nature Physical Science, Vol.241, No.109, pp.102-103 (1973).

(93) Mitchell, A.C.G. and Zemansky. "Resonance Radiation and Excited Atoms". The University Press, Cambridge (1961).

(94) Kirkbright, G.F. and Sargent, M. Atomic Absorption and Fluorescence Spectroscopy. New York, Academic Press, 1974.

(95) Mavrodineanu, R. and Boiteux, H. "Flame Spectroscopy", Wiley, New York. 1965, Chapter 14.

(96) Dieke, G.H. and Crosswhite, H.M. "The Ultraviolet Bands of OH - Fundamental Data". J.Quant.Spectrosc.Radiat.Transfer. Vol.2, (1962).

(97) Jessen, P.F. Ph.D. Thesis, University of London, 1968.

(98) Botha, J.P. and Spalding, D.B. Proc.Roy.Soc. A225, 71 (1954).

(99) Kaskan, W.E. Sixth Symposium (International) on Combustion, p.134 (1957).

(100) Barker, J.R. and Michael, J.V. J.Opt.Soc.Am. 58, 1615 (1968).

(101) Jessen, P.F. and Gaydon, A.G. 12th International Combustion Symposium, p.481 (1969).

(102) Tsatsaronis, G. and Luck, K.C. J.Non-Equilib.Thermodynamics, Vol.4 (1979), pp.193-200.

(103) Smoot, D.L., Hecker, W.C. and Williams, G.A. Combustion and Flame, 26, pp.323-342 (1976).

(104) Cattolica, R.J. Paper No.79-54. Presented at the 1979 Fall Combustion Meeting (Western States Section), Lawrence Berkeley Laboratory, Berkeley, Ca., October 15-16,(1979).

(105) Janif Thermochemical Tables, Second Edition U.S. Department of Commerce, National Bureau of Standards.

(106) Hurle, I.R., Price, R.B., Sugden, T.M.,FRS., and Thomas, A. Proc.Roy.Soc. A303, 409-427 (1968).

(107) Fox, M.D. and Weinberg, F.J. Thirteenth Symposium (international) on Combustion, p.641 (1954).

(108) Andrews, G.E. and Bradley, D. Fourteenth Sympsoium (International) on Combustion (1973), p.1119.

(109) Kingdon, R.G. and Weinberg, F.J. Sixteenth Symposium (International) on Combustion (1977), pp.747-756.

(110) Coward, H. and Hones, G. "Limits of Flammability of Gases and Vapours". Washington, D.D., U.S. G.P.O. (1952),(U.S. Bureau of Mines Bulletin 503).

(111) Smoot, D.L., Hecker, W.C. and Williams, G.A. Combustion and Flame, 26, 323-342, (1976).

(112) Andrews, G.E. and Bradley, D. Combustion and Flame, 19, 275-288, (1972).

(113) Waterson, K. Ph.D. Thesis. "Some Operating Characteristics of Novel Ignition Devices for Hydrocarbon/Air Mixtures". Oxford University, 1973.

(114) Weinberg, F.J. "Optics of Flames". (1963), Butterworths, London.

(115) Fox, M.D. and Weinberg, F.J. Proc.Roy.Soc. A268, (1962), 222.

(116) Andrews, G.E. and Bradley, D. Combustion and Flame, 18, 133-153, (1972).

(117) Cetegen, B., Teichman, K.Y., Weinberg, F.J. and Oppenheim, A.K. S.A.E. 800042 (1980).

(118) Tsatsaronis, G. Combustion and Flame, 26, pp. 217-239 (1978).

APPENDIX 1

Spectral Coincidences of Metallic Lines With the $^2\Sigma^+ - {}^2\Pi$ Transition of OH

Absorption measurements were made on an approximately stoichiometric methane-air flame with path length 1.5 cms.

Hallow Cathode Lamp	Metallic Emission Line	Wavelength (nm)	Absorbance %
Bi	Bi	306.7	15
Al	Al	309.3	None
Multi-element (Cu,Co,Mn,Mo,Fe)		309.3	40
Fe	Fe	309.2	None
Fe	Fe	306.7	None
Cu	Cu	309.4	None
Mo	Mo	308.9	None
V (old lamp)	V	309.3	40

APPENDIX 2

INCENDITIVITY OF HYDROCARBON PLASMAS

